

# The Relationship Between Intergalactic HI/O VI and Nearby ( $z < 0.017$ ) Galaxies

B.P. Wakker<sup>1</sup>, B.D. Savage<sup>1</sup>

## ABSTRACT

We analyze intergalactic HI and O VI absorbers with  $v < 5000 \text{ km s}^{-1}$  in HST and FUSE spectra of 76 AGNs. The baryons traced by HI/O VI absorption are clearly associated with the extended surroundings of galaxies; for impact parameters  $< 400 \text{ kpc}$  they are  $\sim 5$  times more numerous as those inside the galaxies. This large reservoir of matter likely plays a major role in galaxy evolution. We tabulate the fraction of absorbers having a galaxy of a given luminosity within a given impact parameter ( $\rho$ ) and velocity difference ( $\Delta v$ ), as well as the fraction of galaxies with an absorber closer than a given  $\rho$  and  $\Delta v$ . We identify possible “void absorbers” ( $\rho > 3 \text{ Mpc}$  to the nearest  $L_*$  galaxy), although at  $v < 2500 \text{ km s}^{-1}$  all absorbers are within  $1.5 \text{ Mpc}$  of an  $L > 0.1 L_*$  galaxy. The absorber properties depend on  $\rho$ , but the relations are not simple correlations. For four absorbers with  $\rho = 50\text{--}350 \text{ kpc}$  from an edge-on galaxy with known orientation of its rotation, we find no clear relation between absorber velocities and the rotation curve of the underlying galaxy. For  $\rho < 350 \text{ kpc}$  the covering factor of Ly $\alpha$  (O VI) around  $L > 0.1 L_*$  galaxies is 100% (70%) for field galaxies and 65% (10%) for group galaxies; 50% of galaxy groups have associated Ly $\alpha$ . All O VI absorbers occur within  $550 \text{ kpc}$  of an  $L > 0.25 L_*$  galaxy. The properties of three of 14 O VI absorbers are consistent with photoionization, for five the evidence points to collisional ionization; the others are ambiguous. The fraction of broad Ly $\alpha$  lines increases from  $z=3$  to  $z=0$  and with decreasing impact parameter, consistent with the idea that gas inside  $\sim 500 \text{ kpc}$  from galaxies is heating up, although alternative explanations can not be clearly excluded.

*Subject headings:* IGM

## 1. Introduction

Intergalactic gas has been detected in optical spectra of QSOs since the 1970s. At ultraviolet wavelengths, the low redshift HI Lyman  $\alpha$  forest of absorption lines was initially

---

<sup>1</sup>Department of Astronomy, University of Wisconsin, 475 N. Charter St, Madison, WI 53706.

detected at moderate and low resolution with the *Goddard High Resolution Spectrograph* (GHRS) and the *Faint Object Spectrograph* (FOS) aboard the Hubble Space Telescope (HST) (Morris et al. 1991; Bahcall et al. 1991). Data from the HST QSO absorption-line Key Project (Januzzi et al. 1998 and references therein), allowed a comparison between the properties of the high- and low-redshift absorption lines and revealed evidence for the evolution of the gas (Weymann et al. 1998). The realization that the low column density portion of the low-redshift HI absorption lines is tracing very highly photoionized gas in the intergalactic medium (IGM) (containing  $\sim 30\%$  of the baryons at low  $z$ ) followed from more extensive observational studies (Penton et al. 2004), combined with theoretical insights about the very large corrections required to convert measures of the observed HI column densities into total (HI+HII) column densities (Schaye 2001). More recent work has revealed that the low  $z$  Ly $\alpha$  forest includes both narrow and broad absorption lines and that many of the broad lines are probably tracing gas  $\sim 3$ – $10$  times hotter than expected for gas in photoionization equilibrium (Richter et al. 2004; Lehner et al. 2007). The detection of the relatively high line density of intergalactic O VI absorption at low redshift (Tripp et al. 2000) provided additional information about the highly-ionized state of some of the low redshift IGM. The most recent studies (Tripp et al. 2008; Danforth & Shull 2008; Thom & Chen 2008) revealed that the O VI is tracing a complex mixture of highly photoionized and warm-hot collisionally ionized gas. The combination of results from the narrow Ly $\alpha$ , broad Ly $\alpha$  and O VI absorption line studies suggests that  $\sim 40$ – $50\%$  of the baryons at low  $z$  probably resides in photoionized gas and the cooler part of the warm-hot IGM predicted by cosmological hydrodynamical simulations (Cen & Ostriker 1999; Davé et al. 2001). This implies that the baryonic content of the detected low redshift IGM is  $\sim 6$  times larger than the baryonic content of galaxies, which is estimated to be  $\sim 8\%$  (Fukugita & Peebles 2004). Four percent of the baryons are in the hot plasmas found in galaxy clusters while the hydrodynamical simulations suggest most of the remaining  $\sim 50\%$  of the baryons may reside in the hotter portions of the warm-hot IGM with  $T > 3 \times 10^5$  K. The hotter gas has been detected through Ne VIII absorption (Savage et al. 2005b; Narayanan et al. 2008). However, the reported X-ray detections of O VII absorption in the WHIM at  $z > 0$  toward Mrk 421 (Nicastro et al. 2005) are not supported by the independent studies of the X-ray spectrum of this object (Kaastra et al. 2006; Rasmussen et al. 2007).

At low redshift it is possible to study the relation between the intergalactic gas and galaxies. In high column density HI systems the very strong Mg II  $\lambda\lambda 2796.352, 2803.531$  absorption lines are observable from the ground at redshifts above about  $z=0.25$ , and with HST at lower redshifts. They have been associated with galaxies at impact parameters  $< 100$  kpc (Bergeron 1991; Steidel et al. 1995). Steidel et al. (1995) inferred that all  $L > 0.05 L_*$  galaxies are surrounded by spherical halos with sizes on the order of 100 kpc, having 100%

covering fraction in MgII, but later work suggested that the MgII halos are patchy, with covering fraction about 50% (Churchill et al. 2007; Kacprzak et al. 2008).

The first studies of the relation between galaxies and Ly $\alpha$  absorbers were done near the 3C 273.0 sightline (Morris et al. 1993). This study suggested that Ly $\alpha$  clouds did not strongly associate with galaxies. Later, Lanzetta et al. (1995), Tripp et al. (1998), Impey et al. (1999), Chen et al. (2001), Bowen et al. (2002), Penton et al. (2002), Côté et al. (2005), Aracil et al. (2006) and Prochaska et al. (2006) studied this question. These authors typically started with observations of 5–15 UV-bright AGNs, identified the absorbers and then complemented this with a survey of the galaxies near the sightline, where “near” typically means within  $1^\circ$ , or even within  $10'$ . In a few cases the study started with a search for sightlines to bright AGNs passing within about 200 kpc of a nearby galaxy (Bowen et al. 1996, 2002; Côté et al. 2005). We discuss the parameters of these studies in Sect. 4.3, and compare the detailed results to ours in many of the subsections of Sects. 3, 4 and 5. Generally, these authors concluded that Ly $\alpha$  absorbers at low impact parameters ( $<350$  kpc or so) originate in galaxy halos, even though there are many Ly $\alpha$  absorbers far from galaxies, in the general intergalactic medium. Penton et al. (2002) in particular argued that about 20% of the Ly $\alpha$  absorbers are “void absorbers”, which they defined as absorbers occurring more than 3 Mpc from the nearest  $L_*$  galaxy.

For the low redshift intergalactic O VI absorption, a number of papers associated particular O VI absorbers with galaxies (Danforth & Shull 2008; Tripp et al. 2008). Comparing the locations of O VI absorbers with galaxy catalogs, Stocke et al. (2006) found that most O VI absorbers originate relatively close to galaxies. Oppenheimer & Davé (2008) used theory to conclude that O VI absorbers consist of photoionized gas within 300 kpc from  $L>0.1 L_*$  galaxies. On the other hand Ganguly et al. (2008) used modeling to predict that collisionally ionized O VI should occur relatively far from galaxies. Thus, the general relation between O VI absorbers and galaxies requires additional observational and theoretical work.

Theoretically (e.g. Oort 1970; Sommer-Larsen 2006; Fukugita & Peebles 2006), galaxies are predicted to be surrounded by hot ( $10^5$ – $10^6$  K) coronae with sizes on the order of several hundred kpc. These coronae may contain as much or more matter as is present inside the galaxies. Some of the hot gas may condense and rain down onto the galaxies, becoming visible as neutral high-velocity clouds. UV absorption line studies show strong evidence for the presence of  $3\times 10^5$  K gas around the Milky Way (Sembach et al. 2003). The most likely origin of this phase of the gas is in interfaces between cool ( $10^3$ – $10^4$  K) condensations that are embedded in  $10^6$  K gas at distances of a few to 100 kpc (Fox et al. 2005). Direct evidence for  $10^6$  K coronal gas is ambiguous, however. Pedersen et al. (2006) claimed to have found the associated X-ray emission for the case of NGC 5746, but Yao et al. (2008) compared

Galactic O VII and Ne IX X-ray absorption in several different sightlines and concluded that the hot gas is confined to the Galactic thick disk only.

In this paper we analyze the relation between galaxies and absorbers by concentrating on the nearest examples, i.e., galaxies and absorbers with recession velocities above 400 and below 5000 km s<sup>-1</sup> (with the exception of three O VI lines at  $v < 400$  km s<sup>-1</sup> that are included in the tables and figures, though not in statistical calculations). At these velocities the galaxy sample is basically complete down to 0.5 L<sub>\*</sub>. We also analyze a subsample, using only absorbers with  $v < 2500$  km s<sup>-1</sup>, where the galaxy sample is complete down to 0.1 L<sub>\*</sub>. We look at Ly $\alpha$  (using 52 sightlines observed with HST), and at Ly $\beta$  and O VI (using 63 sightlines observed with the *Far Ultraviolet Spectroscopic Explorer*, FUSE). Our galaxy sample combines the “Third Reference Catalogue of Galaxies” (de Vaucouleurs et al. 1991) with all galaxies within 5° of each AGN sightline listed in the *NASA Extragalactic Database* (NED: <http://nedwww.caltech.ipac.edu>). We also use the group catalogues of Geller & Huchra (1982, 1983) and Garcia (1993) to classify galaxies as either field or group galaxies.

By concentrating on the very nearest galaxies and absorbers we can address questions such as (1) What fraction of absorbers has a galaxy above a certain luminosity near them? (2) What fraction of galaxies has associated HI and/or O VI absorption, as function of impact parameter? (3) Do group and field galaxies have the same or a different relation with the absorbers? (4) Is there a relation between impact parameter and the parameters of the absorbers (equivalent width, linewidth, difference in velocity with associated galaxy)? (5) Are the properties of the lowest-redshift O VI absorbers similar to those at higher redshift, and if so, what does this imply for the association of O VI with galaxies?

We describe our data and measurement methods in Sect. 2. In Sects. 3, 4 and 5 we present our analyses. In the first of these (Sect. 3), we study just the absorbers, without reference to the galaxies near them. In Sect. 4 we discuss the statistics of the galaxies that can be found near the absorbers, as well as individual galaxy-absorber associations. In Sect. 5 we look at the galaxies first and then determine the properties and statistics of the absorbers found near them. In Sects. 6 and 7 we discuss and summarize the results.

## 2. Observations

### 2.1. Absorption Line Data Origin

The background targets were selected in the following manner. First, we retrieved the data for the 421 extragalactic targets that were observed by the *Far-Ultraviolet Spectroscopic Explorer* (FUSE) (excluding stars in the SMC, LMC, M31 and M33). In this sample, 106



targets have an S/N ratio per resolution element  $>8$  near  $1031 \text{ \AA}$ . The 53 of these that have recession velocity  $>7500 \text{ km s}^{-1}$  ( $z>0.025$ ) were selected for the study in this paper. Second, we searched the *Hubble Space Telescope* (HST) archive for targets observed with the *Goddard High Resolution Spectrograph* (GHRS) or the *Space Telescope Imaging Spectrograph* (STIS) with spectrograph settings that produce data with velocity resolution better than  $30 \text{ km s}^{-1}$ . There are 24 targets with good STIS-E140M data (S/N $>5$  per  $6.5 \text{ km s}^{-1}$  resolution element). For 20 of these there is also good FUSE data, while for four targets the FUSE data only has S/N $\sim 4$  near  $1031 \text{ \AA}$ . There are 29 sightlines with good (S/N $>5$ ) STIS-G140M or GHRS-G140M data, with a velocity resolution of 30 or  $20 \text{ km s}^{-1}$ , respectively. For 15 of these FUSE data with S/N $\sim 8$  also exist, while for 7 targets the FUSE data have low S/N. Eleven targets were only observed using STIS-G140M. Four final targets were added to the sample, even though they only have FUSE spectra with S/N $<5$ . However, there are known galaxies with low impact parameter ( $<150 \text{ kpc}$ ) and clear detections of Ly $\beta$  and/or O VI absorption. These targets combine to make a sample size of 76.

We note that two targets are included that have redshifts below  $7500 \text{ km s}^{-1}$ . ESO 438-G09 has  $v=7200 \text{ km s}^{-1}$ , while  $v(\text{ESO } 185\text{-IG13})$  is  $5600 \text{ km s}^{-1}$ . The first of these is the only AGN observed with STIS-G140M that has  $v<7500 \text{ km s}^{-1}$ , and there are absorbers at  $1426$  and  $2215 \text{ km s}^{-1}$ . So, rather than excluding it based on its velocity, we decided to keep this target for some of the tables. However, for the statistical analyses the low S/N ESO 185–IG13 data were automatically excluded, as we apply strict selection criteria. ESO 185-IG13 is one of the targets with a low S/N FUSE spectrum, but there is an absorber at  $2635 \text{ km s}^{-1}$  with low impact parameter ( $62 \text{ kpc}$ ). Since Tripp et al. (2008) concluded that all absorbers with velocity differing by more than  $2500 \text{ km s}^{-1}$  from the redshift of the AGN are likely to be intergalactic, it is justified to include ESO 185-IG13 and ESO 438-G09 in our sample.

The processing of the FUSE data was described in detail by Wakker et al. (2003) and Wakker (2006), and therefore only a summary is given here. First, the spectra were calibrated using v2.1 or v2.4 of the FUSE calibration pipeline. To correct for residual wavelength shifts, the central velocities of the Milky Way interstellar lines were determined for each detector segment (LiF1A/1B/2A/2B, SiC2A/2B) of each individual observation. The FUSE segments were then aligned with the LSR interstellar velocities implied by the STIS-E140M, or if no E140M data were available, with the LSR velocity of the strongest component in the 21-cm HI spectrum. For targets with a STIS-E140M spectrum, the interstellar reference velocity was determined by fitting all Milky Way lines in that spectrum; the STIS wavelength calibration is accurate to about  $1 \text{ km s}^{-1}$  (Tripp et al. 2001, 2005). For sightlines with S/N $>10$  near  $1031 \text{ \AA}$ , the resulting shifts were given by Wakker (2006). Using these shifts, LiF1A and LiF2B data are added together to produce the final spectrum for each target.

Although the data were aligned using an LSR velocity scale, we shifted the spectrum to the heliocentric velocity scale to measure the intergalactic absorption lines, as that is the convention for extragalactic studies

For HST data, the calibrated fits files in the MAST archive were retrieved. This is the only step needed, except for observations with the *STIS*-G140M grating and central wavelength 1222 Å, where a 1-pixel shift seems necessary. That conclusion is based on fourteen sightlines with good data and relatively simple ISM absorption lines. For these sightlines the S II  $\lambda$ 1250.584, 1253.811 lines can be fit both in a G140M spectrum centered on 1222 Å and in one centered on 1272 Å, and sometimes also in an E140M spectrum. To align the lines in the 1222 Å-centered spectrum with those in the other spectra, an average redward shift of 12 km s<sup>−1</sup> is needed, which corresponds to one pixel.

Finally, for observations with the *STIS*-E140M echelle the MAST fits files give the data for each of the 42 orders separately. These orders were combined into a single spectrum by interpolating the photon counts and errors onto a common grid, adding the photon counts (weighted by the rms at each pixel), and converting back to a flux.

Using the final combined datasets, we measured the target flux and the S/N ratio of each spectrum near 977, 1031 and 1238 Å. Table 1 presents the observation IDs, exposure times, fluxes and S/N ratios for all the targets in the final sample. Table 2 gives the FUSE segment shifts for datasets that were not included in Wakker (2006).

Table 1. Target Exposure List

object	lon	lat	$z$	type	datasets <sup>1</sup>	$T_{\text{exp}}^2$	Flux <sup>3</sup>	S/N <sup>4</sup>	S/N <sup>4</sup>	S/N <sup>4</sup>
(1)	[°]	[°]	(4)	(5)	(6)	[ks]	[f.u.]	1031	977	1238
	(2)	(3)	(4)	(5)	(6)	(7)	(8)	(9)	(10)	(11)
1H0419–577	266.99	–42.00	0.1040	Sey1	D8080801, F0260101, F0260102	36.8	2.8	7	2	–
1H0707–495	260.17	–17.67	0.0411	Sey1	B1050101, B1050102, B1050103, E1190101	114.4	1.8	16	6	–
1H0717+714	143.98	28.02	0.5000	BLLac	Z9071301, F0260302	70.0	3.2	15	6	–
3C232	194.17	52.32	0.5305	QSO	O67002(Ga)	11.2	0.5	2	0	12
3C249.1	130.39	38.55	0.3115	QSO	P1071601, P1071602, P1071603, S6010901	246.5	1.1	15	3	8
					D1170101, D1170102, D1170103, U1027501					
					U1027502					
					O6E124–30(E)	68.8	1.1	15	3	8
3C263	134.16	49.74	0.6460	QSO	E8480701, D8081701, G0440201, G0440202	220.1	1.2	14	3	–
					G0440203, F0050101, F0050103, F0050104					
					F0050105					
3C273.0	289.95	64.36	0.1583	QSO	P1013501	43.2	26.9	31	19	27
					O5D301(E)	18.7	26.9	31	19	27
3C351.0	90.08	36.38	0.3719	QSO	O57901–04(E)	77.0	0.0	0	–0	8
ESO141–G55	338.18	–26.71	0.0360	Sey1	I9040104	40.6	5.2	16	8	20
					Z3E702	15.6	5.2	16	8	20
ESO185–IG13	343.64	–29.37	0.0187	HII	Z9091401, G0200201, G0200203, G0200204	19.9	1.5	5	2	–
ESO438–G09	277.55	29.36	0.0240	Sey1.5	O5EW06(Ga)	11.3	0.3	–	–	11
Fairall 9	295.07	–57.83	0.0470	Sey1	P1010601	33.9	1.5	6	3	19
					Z3E704	14.4	1.5	6	3	19
					Z26O02	8.1	1.5			
					Z3E704	6.9	1.5			
H1821+643	94.00	27.42	0.2844	QSO	P1016402, P1016405, C0950201, C0950202	276.5	3.0	29	8	13
					O5E703–04(E)	50.9	3.0	29	8	13
HE0226–4110	253.94	–65.77	0.4950	QSO	P2071301, P1019101, P1019102, P1019103	206.9	2.7	25	11	9
					P1019104, D0270101, D0270102, D0270103					
					O6E107–11(E)	43.8	2.7	25	11	9
HE0340–2703	222.68	–52.12	0.2830	QSO	O8E103(Ga)	4.9	0.6	–	–	10
HE1029–1401	259.33	36.52	0.0860	QSO	O4EC05(Ga)	4.1	5.1	–	–	28
					O4EC05(Gb)	3.4	5.1			
HE1143–1810	281.85	41.71	0.0329	Sey1	P1071901	7.2	6.1	8	4	–
HE1228+0131	291.26	63.66	0.1170	QSO	P1019001	4.0	4.9	5	2	5
					O56A01–02(E)	27.2	4.9	5	2	5
HS0624+6907	145.71	23.35	0.3700	QSO	P1071001, P1071002, S6011201, S6011202	113.5	1.0	11	3	7
					O6E112–16(E)	62.0	1.0	11	3	7
HS1543+5921	92.40	46.36	0.8070	QSO	O8MR01(Ga)	25.3	0.8	2	0	10
					O8MR02–04(Gb)	28.8	0.8			
IRAS09149–6206	280.61	–9.20	0.0573	Sey1	A0020503, S7011002, S7011003, U1072201	100.0	1.7	13	2	–
					U1072202, U1072203					
IRAS F22456–5125	338.51	–56.63	0.1000	Sey1	Z9073901, Z9073902, E8481401	41.5	1.9	9	3	–
MCG+10–16–111	144.21	55.08	0.0271	Sey1	O5EW02(Ga)	19.5	1.5	–	–	23
MRC2251–178	46.20	–61.33	0.0661	QSO	P1111010	51.4	2.1	12	3	30
					O4EC03(Ga)	5.9	2.1	12	3	30
					O4EC03(Gb)	4.6	2.1			

Table 1—Continued

object	lon	lat	$z$	type	datasets <sup>1</sup>	$T_{\text{exp}}^2$	Flux <sup>3</sup>	S/N <sup>4</sup>	S/N <sup>4</sup>	S/N <sup>4</sup>
(1)	[°]	[°]	(4)	(5)	(6)	[ks]	[f.u.]	1031	977	1238
Mrk 9	158.36	28.75	0.0399	Sey1.5	P1071101, P1071102, P1071103, S6011601	52.4	2.3	13	2	—
Mrk 106	161.14	42.88	0.1235	Sey1	C1490501	121.9	1.6	12	3	—
Mrk 110	165.01	44.36	0.0353	Sey1	O4N352(Ga)	2.2	0.3	1	1	11
Mrk 205	125.45	41.67	0.0708	Sey1	Q1060203, S6010801, D0540101, D0540102 D0540103, U1031102	223.8	1.2	17	6	8
Mrk 279	115.04	46.86	0.0305	Sey1.5	O62Q03–05(E)	62.1	1.2	17	6	8
					P1080303, P1080304, D1540101	181.8	10.2	45	21	32
					O6JM01(E)	13.2	10.2	45	21	32
					O8K101–05(E)	41.4	10.2			
Mrk 290	91.49	47.95	0.0296	Sey1	P1072901, D0760101, D0760102, E0840101 E0840102	90.6	3.2	19	6	12
					Z3KH01	7.1	3.2	19	6	12
Mrk 335	108.76	−41.42	0.0258	Sey1.2	P1010203, P1010204	83.7	7.1	27	11	11
					O8N504–05(E)	15.2	7.1	27	11	11
Mrk 421	179.83	65.03	0.0300	BLLac	P1012901, Z0100101, Z0100102, Z0100103	83.7	9.6	30	14	23
					Z2IA01	15.7	9.6	30	14	23
Mrk 477	93.04	56.82	0.0378	Gal	D1180101	146.3	1.0	10	2	—
Mrk 478	59.24	65.03	0.0791	Sey1	P1110909	14.0	3.5	8	5	37
					O4EC14(Ga)	7.9	3.5	8	5	37
					O4EC14(Gb)	6.3	3.5			
Mrk 501	63.60	38.86	0.0337	BLLac	P1073301, C0810101	29.8	3.1	10	3	11
					Z1A652	31.3	3.1	10	3	11
Mrk 509	35.97	−29.86	0.0344	Sey1.2	X0170101, X0170102, P1080601	114.3	6.7	30	7	14
Mrk 586	157.60	−54.93	0.1553	Sey1	D0550101, D0550102	63.6	2.1	12	4	—
Mrk 734	244.75	63.94	0.0502	Sey1	P1071702	4.9	4.0	6	3	—
Mrk 771	269.44	81.74	0.0630	Sey1	P1072301	6.3	2.2	5	2	25
					O4N305(Ga)	2.0	2.2	5	2	25
					O4EC07(Ga)	5.8	2.2			
					O4EC07(Gb)	5.2	2.2			
Mrk 817	100.30	53.48	0.0315	Sey1.5	P1080403, P1080404	161.5	9.6	44	20	43
					Z3E701	26.8	9.6	44	20	43
Mrk 876	98.27	40.38	0.1290	Sey1	P1073101, D0280203	127.4	6.3	34	11	11
					O8NN01–02(E)	29.2	6.3	34	11	11
Mrk 926	64.09	−58.76	0.0473	Sey1.5	O4EC12(Ga)	3.9	0.7	3	1	9
					O4EC12(Gb)	3.8	0.7			
Mrk 1095	201.69	−21.13	0.0323	Sey1	P1011201, P1011202, P1011203	55.8	2.0	11	4	18
					Z3E706	14.9	2.0	11	4	18
Mrk 1383	349.22	55.12	0.0865	Sey1	P1014801, P2670101	63.3	6.6	24	12	9
					O8PG01–02(E)	19.2	6.6	24	12	9
Mrk 1513	63.67	−29.07	0.0630	Sey1	P1018301, P1018302, P1018303, P1018304	58.6	3.9	16	6	20
					O4EC10(Ga)	7.3	3.9	16	6	20
					O4EC10(Gb)	6.2	3.9			
MS0700.7+6338	152.47	25.63	0.1530	Sey1	P2072701, S6011501, D0550501, U1021403 U1021404	181.9	1.6	16	4	—

Table 1—Continued

object	lon	lat	$z$	type	datasets <sup>1</sup>	$T_{\text{exp}}^2$	Flux <sup>3</sup>	S/N <sup>4</sup>	S/N <sup>4</sup>	S/N <sup>4</sup>
(1)	[°]	[°]	(4)	(5)	(6)	[ks]	[f.u.]	1031	977	1238
(1)	(2)	(3)	(4)	(5)	(6)	(7)	(8)	(9)	(10)	(11)
NGC985	180.84	−59.49	0.0431	Sey1	P1010903	50.6	3.4	11	5	29
					O4EC11(Ga)	3.7	3.4	11	5	29
					O4EC11(Gb)	3.8	3.4			
PG0804+761	138.28	31.03	0.1020	QSO	P1011901, P1011903, S6011001, S6011002	151.5	7.0	31	14	35
					O4N301(Ga)	2.4	7.0	31	14	35
					O4EC06(Ga)	4.9	7.0			
					O4EC06(Gb)	4.2	7.0			
PG0838+770	136.66	32.68	0.1310	Sey1	G0200104, G0200105, G0200106, G0200107	100.5	0.7	6	2	—
PG0844+349	188.56	37.97	0.0640	Sey1	P1012002, D0280301, D0280302, D0280303	81.2	3.7	20	7	—
					D0280304					
PG0953+414	179.79	51.71	0.2341	QSO	P1012201, P1012202	74.4	5.2	24	10	10
					O63G01−04(E)	26.9	5.2	24	10	10
PG1001+291	200.08	53.21	0.3297	QSO	P2073101	11.3	2.0	5	2	8
					O6E117−23(E)	48.4	2.0	5	2	8
PG1011−040	246.50	40.75	0.0580	Sey1	B0790101	85.3	2.6	17	7	—
PG1049−005	252.28	49.88	0.3599	QSO	O4N303(Ga)	1.5	1.0	—	—	7
PG1116+215	223.36	68.21	0.1765	QSO	P1013101, P1013102, P1013103, P1013104	76.7	5.7	25	12	12
					P1013105					
					O5E701−02(E)	26.5	5.7	25	12	12
PG1149−110	280.47	48.89	0.0490	Sey	O5EW05(Ga)	8.3	0.1	—	—	5
PG1211+143	267.55	74.32	0.0804	Sey1	P1072001	52.2	5.2	17	10	18
					O61Y01−08(E)	42.5	5.2	17	10	18
PG1216+069	281.07	68.14	0.3313	QSO	P1072101	12.4	1.4	5	2	7
					O6E131−39(E)	69.8	1.4	5	2	7
PG1259+593	120.56	58.05	0.4778	QSO	P1080101, P1080102, P1080103, P1080104	553.8	1.8	37	14	8
					P1080105, P1080106, P1080107, P1080108					
					P1080109, U1031801					
					O63G05−11(E)	95.8	1.8	37	14	8
PG1302−102	308.59	52.16	0.2784	QSO	P1080201, P1080202, P1080203	145.9	1.6	16	5	4
					O5BU61−02(E)	22.1	1.6	16	5	4
PG1341+258	28.71	78.15	0.0870	QSO	O5EW01(Ga)	8.1	0.9	—	—	16
PG1351+640	111.89	52.02	0.0882	Sey1	P1072501, S6010701	118.4	1.6	16	4	13
					O4EC54(Ga)	8.5	1.6	16	4	13
					O4EC54(Gb)	6.3	1.6			
PG1444+407	69.90	62.72	0.2673	QSO	P1072701	10.0	1.8	4	3	9
					O6E101−06(E)	48.6	1.8	4	3	9
PG1553+113	21.91	43.96	0.3600	BLLac	E5260501, E5260502, E5260503	47.1	2.7	12	4	—
PG1626+554	84.51	42.19	0.1330	Sey1	C0370101	90.9	1.5	14	0	—
PHL1811	47.47	−44.81	0.1920	QSO	P2071101, P1081001, P1081002, P1081003	75.7	4.9	17	0	11
					O8D901−04(E)	33.9	4.9	17	0	11
PKS0405−12	204.93	−41.76	0.5726	QSO	B0870101, D1030101, D1030102	140.3	2.2	19	7	8
					O55S01−02(E)	27.2	2.2	19	7	8
PKS0558−504	257.96	−28.57	0.1370	QSO	P1011504, C1490601	93.0	3.3	19	9	—
PKS2005−489	350.37	−32.60	0.0710	BLLac	P1073801, C1490301, C1490302	48.7	5.0	18	8	57

Table 1—Continued

object	lon	lat	$z$	type	datasets <sup>1</sup>	$T_{\text{exp}}^2$ [ks]	Flux <sup>3</sup> [f.u.]	S/N <sup>4</sup> 1031	S/N <sup>4</sup> 977	S/N <sup>4</sup> 1238
(1)	(2)	(3)	(4)	(5)	(6)	(7)	(8)	(9)	(10)	(11)
					O4EC09(Ga)	6.1	5.0	18	8	57
					O4EC09(Gb)	5.4	5.0			
PKS2155–304	17.73	–52.25	0.1160	BLLac	P1080701, P1080705, P1080703	121.5	12.8	31	12	12
					O5BY01–02(E)	28.5	12.8	31	12	12
RX J0048.3+3941	122.28	–23.18	0.1340	QSO	D1310101, D1310102, D1310103, D1310104	191.3	1.4	14	4	–
					D1310105, D1310106, D1310107					
RX J0100.4–5113	299.48	–65.84	0.0620	Sey1	D8060301, E8970201	23.0	3.1	10	3	14
					O8P802(Ga)	2.3	3.1	10	3	14
					O8P802(Gb)	1.1	3.1			
RX J1830.3+7312	104.04	27.40	0.1230	Sey1	G0200302	25.4	3.5	6	0	25
					O5EW09(Ga)	5.8	3.5	6	0	25
Ton S180	139.00	–85.07	0.0620	Sey1.2	P1010502, D0280101	26.9	6.3	13	6	32
Ton S210	224.97	–83.16	0.1160	QSO	P1070301, P1070302	52.7	6.2	20	8	4
					O6L001–02(E)	17.3	6.2	20	8	4
VIIZw118	151.36	25.99	0.0797	Sey1	P1011604, P1011605, P1011606, S6011301	129.8	2.0	18	6	19
					O4EC13(Ga)	9.5	2.0	18	6	19

Note. — 1: This column identifies the FUSE and HST datasets; FUSE datasets consist of an 8-character code giving the observing program, object id, and exposure number; HST datasets list a 4-character program id, followed by a 2-digit object id and a 3-digit observation id, which we omit; for HST *STIS* observations an extra identifier between parentheses shows whether the data were taken using the G140M grating centered at 1222 Å (Ga) or 1272 Å (Gb) or with the E140M echelle (E); datasets starting with “Z” were obtained with the *GHR*S. 2: Exposure time in kiloseconds, given separately for each FUSE exposure (which corresponds to several orbits); only a single value is given for each multi-orbit HST exposure. 3: Flux in units of  $10^{-14} \text{ erg cm}^{-2} \text{ s}^{-1} \text{ Å}^{-1}$ ; for FUSE datasets this is the flux at 1031 Å, while for targets with only HST datasets it is the flux at 1238 Å. 4: Signal-to-noise ratio per resolution element at 1031, 977 and 1238 Å; for FUSE data the resolution element is  $20 \text{ km s}^{-1}$ , while for HST data it depends on the instrument and grating:  $20 \text{ km s}^{-1}$  for *GHR*S spectra,  $30 \text{ km s}^{-1}$  for *STIS* grating (G140M) exposures, and  $6.5 \text{ km s}^{-1}$  for *STIS* echelle (E140M) data.

Table 2. FUSE Velocity Shifts for Exposures not in Wakker (2006)

object	dataset	Cal	T <sub>exp</sub>	shifts					
		FUSE	[ks]	LiF1A	LiF1B	LiF2A	LiF2B	SiC2A	SiC2B
(1)	(2)	(3)	(4)	(5)	(6)	(7)	(8)	(9)	(10)
1H 0419–577	D8080801	2.4	4.7	–22	–22	–22	–22	–48	–48
	F0260101	2.4	16.9			16	27	0	
	F0260102	2.4	15.2			16	27	0	
1H 0707–495	E1190101	2.4	48.2	–19	–19	–19	–19	–13	–13
3C 249.1	U1027501	2.4	13.2	14	14		58	0	
	U1027502	2.4	16.9	14	14		58	0	
3C 263	E8480701	2.4	7.1	9	9	42	42	42	42
	D8081701	2.4	3.3	9	9	42	42	42	42
	G0440201	2.4	14.7	9	9	42	42	42	42
	G0440202	2.4	14.7	9	9	42	42	42	42
	G0440203	2.4	20.1	9	9	42	42	42	42
	F0050101	2.4	79.2	25	25	54	54	42	42
	F0050103	2.4	17.3			54	54	42	42
	F0050104	2.4	40.1			54	54	42	42
	F0050105	2.4	20.7			54	54	42	42
ESO 185–IG13	Z9091401	2.4	12.8	0	0	0	0	0	0
	G0200201	3.2	2.1	0	0	0	0		0
	G0200203	3.2	2.6	0	0				
	G0200204	3.2	2.4	0	0	0	0		0
HE 1143–1810	P1071901	2.4	7.3	5	5	5	5	–2	–2
HE 1228+0131	P1019001	2.4	4.0	17	17	6	6	10	10
IRAS 09149–6206	A0020503	2.4	13.1	–6	–6	–19	–6		
	S7011002	2.4	13.6	–6	–6	–12			
	S7011003	2.4	14.1	–12	–12	–12			
	U1072202	2.4	39.1	7	7	35	43		
	U1072203	2.4	16.2	–12	–12	35	43	–5	–5
IRAS F22456–5125	Z9073901	2.4	5.7	–11	–11	–11	–11	20	20
	Z9073902	2.4	31.6	–11	–11	–11	–11	10	10
	E8481401	2.4	4.2	–1	10	10	–1	10	10
Mrk 205	U1031102	3.2	15.9	7	7	58	58		
Mrk 478	P1110909	2.1	14.0	34	34	34	34	34	34
Mrk 734	P1071702	2.4	4.9	–4	04	–9	–4	–31	–31
MS 0700.7+6338	U1021403	2.4	23.1	17	17	42	42	0	0
	U1021404	2.4	54.3	17	17	42	42	0	0
PG 0838+770	G0200101	2.4	5.9	29	29	67	67	29	29

## 2.2. Absorption Line Identification

For each background target, we began by identifying all intrinsic and intergalactic hydrogen and metal lines, looking for redshifted Lyman series lines and high-ionization lines such as those of O VI, O III, N V, N IV, N III, C IV, C III, Si III, S VI, as well as low-ionization lines, if appropriate. We also identified all high- and low-ionization Milky Way and high-velocity cloud (HVC) ionic and molecular absorption lines. For each background target, we modeled all H<sub>2</sub> absorption lines, using the method presented by Wakker (2006). A further complication is the contamination by the geocoronal O I\* emission lines near Ly $\beta$ , Ly $\gamma$ , O VI  $\lambda$ 1031.926 O VI  $\lambda$ 1037.617 and C III  $\lambda$ 977.020. The geocoronal lines are absent in FUSE data taken during the orbital night, but for many sightlines the orbital-night-only data have much lower S/N ratios.

Figure 1 shows the velocities of the interstellar lines relative to Ly $\alpha$ , Ly $\beta$  and the two O VI lines. The three panels are for three different levels of contamination by Galactic molecular hydrogen (H<sub>2</sub>): no H<sub>2</sub> with good night-only data, median contamination with just  $J=0$  and 1 H<sub>2</sub> lines, and strong H<sub>2</sub> (lines up to  $J=4$  are seen). A box that is 80 km s<sup>-1</sup> wide is drawn around each ISM line. This is a typical absorption width, though it will be different in detail for each sightline.

If there are no H<sub>2</sub> lines, both O VI lines are visible for velocities of about 500 to 1200 km s<sup>-1</sup> and above 2300 km s<sup>-1</sup> (except for a few regions contaminated by interstellar Ar I  $\lambda$ 1048.220 and Fe II  $\lambda$ 1063.176). More typical, however, is the situation in the middle panel, where some H<sub>2</sub> is present, but useful orbital-night-only data do exist. In that case, Ly $\beta$  can be seen over most of the velocity range between 500 and 7000 km s<sup>-1</sup>, except between about 3000 and 3700 km s<sup>-1</sup>, where C II  $\lambda$ 1036.337, O VI  $\lambda$ 1037.617 and O I  $\lambda$ 1039.230 interfere. The most-easily visible O VI line alternates between the 1031 and the 1037 line, with O VI  $\lambda$ 1031.926 mostly uncontaminated in the velocity ranges 500–1200 km s<sup>-1</sup> and 3000–7000 km s<sup>-1</sup>, while the O VI  $\lambda$ 1037.617 line is clear from 1300–3000 km s<sup>-1</sup> and above 4000 km s<sup>-1</sup>. The bottom panel represents the worst case. It is clear that in this case intergalactic lines will only be visible if they occur at just the right velocity.

With the intrinsic, interstellar and geocoronal contamination in mind, we checked whether any of the identified intergalactic absorbers occur near the systemic velocity of each galaxy with impact parameter  $\rho < 1$  Mpc. If we did not find intergalactic absorption, we measured equivalent width upper limits and noted these. If we did find intergalactic absorption having a small velocity difference with a galaxy, we measured the line(s) and decided whether or not to associate the galaxy with the absorber. These associations are discussed in more detail in Sect. 4.3. Between the lines from interstellar ions, interstellar H<sub>2</sub>, intrinsic lines and intergalactic absorption-line systems there are only a few marginally



Table 2—Continued

object	dataset	Cal	T <sub>exp</sub>	shifts					
		FUSE	[ks]	LiF1A	LiF1B	LiF2A	LiF2B	SiC2A	SiC2B
(1)	(2)	(3)	(4)	(5)	(6)	(7)	(8)	(9)	(10)
	G0200104	2.4	31.9	29	29	67	67	29	29
	G0200105	2.4	28.8	29	29	67	67	29	29
	G0200106	2.4	20.7	29	29	67	67	29	29
	G0200107	2.4	19.0	29	29	67	67	29	29
PG 1001+291	P2073101	2.4	11.3	36	36	36	36	36	36
PG 1444+407	P1072701	2.4	10.0	32	32	32	32	32	32
RX J0048.3+3941	D1310101	2.4	37.6	27	27	31	31	46	46
	D1310102	2.4	32.9	27	27	31	31	46	46
	D1310103	2.4	6.6	27	25	31	31	46	46
	D1310104	2.4	39.3	25	25	13	13	34	34
	D1310105	2.4	24.4	25	25	13	13	34	34
	D1310106	2.4	26.6	25	25	13	13	34	34
	D1310107	2.4	23.9	25	25	13	13	34	34
RX J0100.4–5113	D8060301	2.4	5.8	0	0	0	0	0	0
	E8970201	2.4	17.2	0	0	0	0	0	0
RX J1830.3+7312	G0200302	2.4	25.4			30	30		

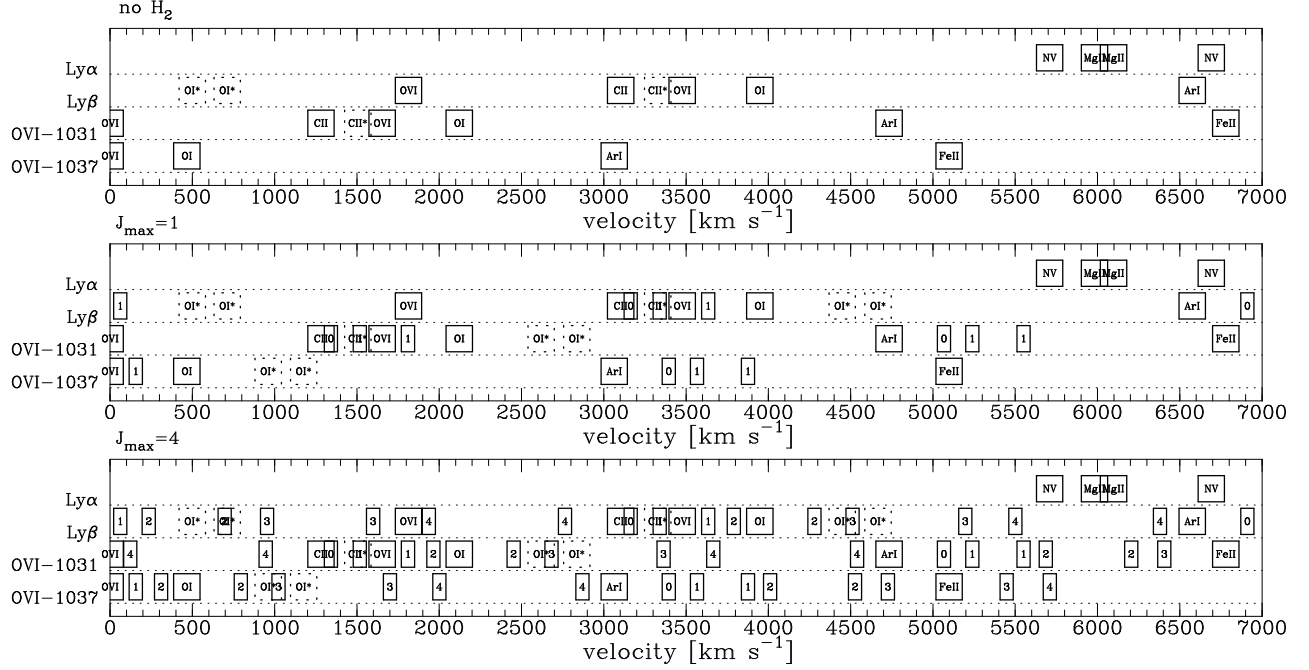


Fig. 1.— Plot showing the velocity ranges where intergalactic  $\text{Ly}\alpha$ ,  $\text{Ly}\beta$ , OVI  $\lambda 1031.926$  and OVI  $\lambda 1037.617$  absorption may be obscured, for three different levels of interstellar  $\text{H}_2$  absorption: none (top panel), medium ( $J=0$  and  $J=1$  lines only, middle panel) and strong (bottom panel). The square boxes enclose an  $80 \text{ km s}^{-1}$  velocity range around metal lines (with ion name given),  $40 \text{ km s}^{-1}$  around  $\text{H}_2$  lines (with  $J$ -value given). Boxes with dotted borders are given for the geocoronal OI\* lines, which are absent in orbital-night-only data.

significant features that have remained unidentified in the FUSE data. They do not match known Ly $\alpha$  lines, nor can they be Ly $\beta$  as no corresponding Ly $\alpha$  is seen.

### 2.3. Absorption Line Measurements

For each background target, we determined a continuum for each absorption line that we looked at by fitting a low-order (up to 4th) polynomial through line-free regions, using the method described by Sembach & Savage (1992). For most sightlines the velocity range of the fit is about  $5000 \text{ km s}^{-1}$ , but for complex spectra, the continuum fit is made in several pieces. In the case of Ly $\alpha$ , we fitted the continuum through the parts of the spectrum outside the damping wings of the Galactic Ly $\alpha$  line, and then we modeled the ISM Ly $\alpha$  Voigt profile. The detailed results of this effort will be reported in a future paper (Brown et al., in preparation).

To measure the absorption lines, we integrated over the velocity range where absorption is apparent, using the fitted continua as a reference. We also determined an error estimate, which consists of two parts, a statistical and a systematic error, listed separately in Cols. 11–14 of Table 3. The determination of these errors was described in detail by Wakker et al. (2003). The statistical error combines the random noise in the data with the uncertainty associated with the placement of the continuum. The systematic error combines the uncertainty associated with the choice for the minimum and maximum velocity of the absorption (i.e. the change in measured equivalent width when changing the velocity range by  $\pm 5 \text{ km s}^{-1}$ ) with the fixed-pattern noise (6 mÅ for FUSE data, 1.2 mÅ for *STIS*-G140M and 0.3 mÅ for *STIS*-E140M observations). In addition to measuring the equivalent width by straight integration, the central velocity and line width of the absorption line are estimated by fitting a gaussian to the observed absorption profile.

We also note non-detections associated with galaxies (see next subsection). For these we determined a  $3\sigma$  upper limit on the equivalent width as three times the quadrature sum of the statistical and fixed-pattern noise error obtained when integrating over  $60 \text{ km s}^{-1}$  around the systemic velocity of the galaxy. The  $60 \text{ km s}^{-1}$  figure corresponds to three resolution elements for FUSE spectra, two for *STIS*-G140M data, and nine for *STIS*-E140M. It is based on the median line width of detected features, discussed in Sect. 3.2. Previous authors used different widths for this estimate. Tripp et al. (2008) did integrate over the width of a typical detected line, but used 15 *STIS*-E140M pixels, corresponding to about  $55 \text{ km s}^{-1}$ . On the other hand, Penton et al. (2000a,b, 2002, 2004) and Danforth & Shull (2005, 2008), determined  $4\sigma$  detection limits by integrating over a single resolution element, i.e.  $20 \text{ km s}^{-1}$  for FUSE,  $40 \text{ km s}^{-1}$  for *STIS*-G140M,  $6.5 \text{ km s}^{-1}$  for *STIS*-E140M data. This leads to equivalent

width limits that are a factor  $\sqrt{60/20} * 3/4 \sim 1.3$  smaller for FUSE spectra, and a factor 2.3 smaller for *STIS*-E140M data. Since the narrowest absorption lines have an FWHM of about  $25 \text{ km s}^{-1}$ , integrating over a single resolution element yields detection limits that are generally optimistic, and most appropriate only for the small fraction of narrow lines. Thom & Chen (2008) used yet another method: they derived  $3\sigma$  limits assuming lines have  $b=10 \text{ km s}^{-1}$  (FWHM  $25 \text{ km s}^{-1}$ ), which gives values a factor  $\sqrt{60/25}=1.5$  lower than ours. When comparing results between these different papers, we have to correct for the differences in these definitions.

Figure 2 presents the  $\text{Ly}\alpha$ ,  $\text{Ly}\beta$ ,  $\text{O VI } \lambda 1031.926$  and  $\text{O VI } \lambda 1037.617$  spectra for all detected intergalactic systems. For each of these we list the galaxy that we associate with the detection. We discuss each  $\text{Ly}\alpha$ ,  $\text{Ly}\beta$  and  $\text{O VI}$  absorber and the galaxy association separately for each sightline in the Appendix. Figure 2 shows a total of 133 intergalactic absorption line systems, including 115 with  $\text{Ly}\alpha$ , 40 with  $\text{Ly}\beta$ , 13 with  $\text{O VI } \lambda 1031.926$ , and 5 with  $\text{O VI } \lambda 1037.617$ .  $\text{H I}$  (i.e.  $\text{Ly}\alpha$  or  $\text{Ly}\beta$  is seen in 129 systems),  $\text{O VI}$  (i.e. either line) in 14 systems. For two systems (at  $3073 \text{ km s}^{-1}$  toward Mrk 290 and at  $260 \text{ km s}^{-1}$  toward Ton S180) we only list the two  $\text{O VI}$  lines, while we identify two lines as uncorroborated  $\text{O VI } \lambda 1031.926$  – at  $3109 \text{ km s}^{-1}$  toward PG 1302–102 and at  $288 \text{ km s}^{-1}$  toward Ton S210.

## 2.4. Galaxy Data Origin

For each target, we searched for nearby galaxies with low impact parameter ( $\rho$ ), as described below. We started with the “Third Reference Catalogue of Galaxies” (de Vaucouleurs et al. 1991). This catalogue gives names and positions for 23011 galaxies, velocities for 16689 galaxies and angular diameters for 21605 galaxies. A distance estimate was made for each of these galaxies, using the following method.

Distances for Local Group galaxies were taken from Mateo (1998). For about 100 galaxies individually determined distances were taken from Sandage & Tammann (1975) and Freedman et al. (2001), though the distances of Sandage & Tammann (1975) were corrected to correspond to a Hubble constant of  $71 \text{ km s}^{-1} \text{ Mpc}^{-1}$ , rather than the value of  $50 \text{ km s}^{-1} \text{ Mpc}^{-1}$  used in the original paper. Next, the group catalogues of Geller & Huchra (1982, 1983) and Garcia (1993) were used. In these papers, galaxy groups were defined using automated algorithms. In the remainder of this paper, these groups will be identified by their GH (Geller & Huchra 1983) or LGG (Garcia 1993) number (LGG stands for “Lyon Galaxy Groups”). These papers listed the galaxies that are considered members of each of the 176 GH or 486 LGG groups. The GH catalogue only includes galaxies at declinations

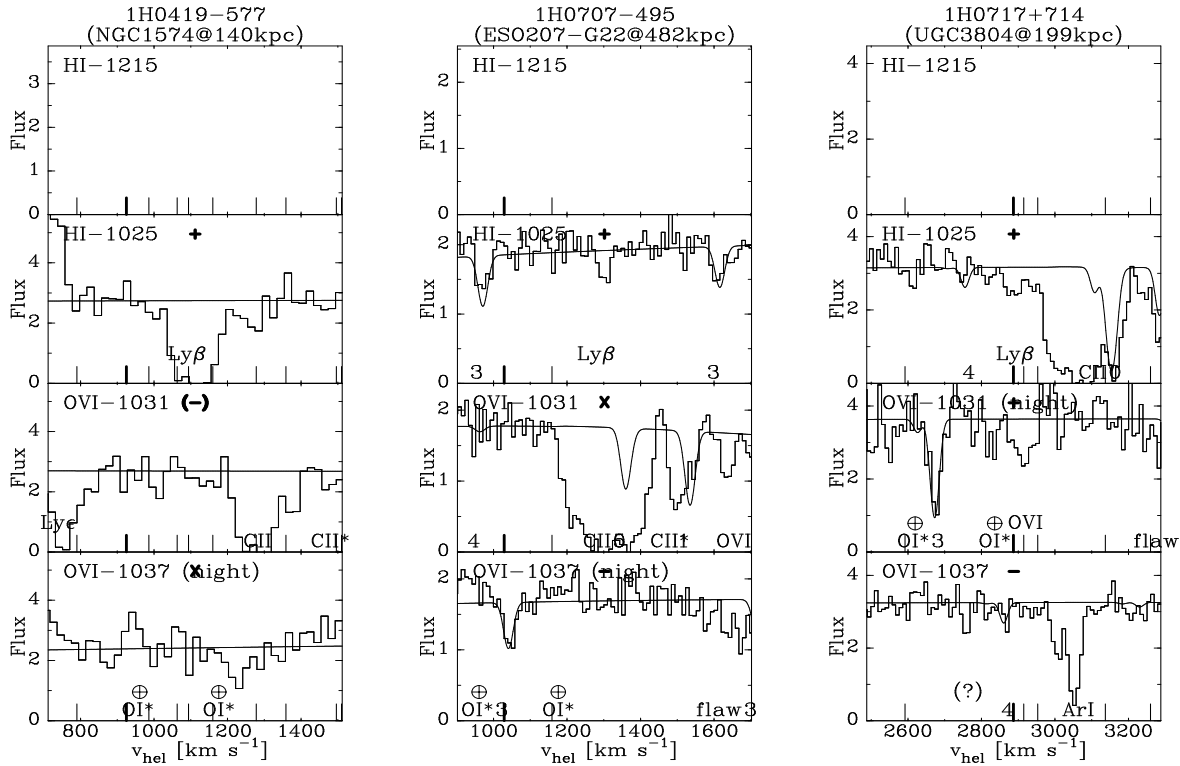
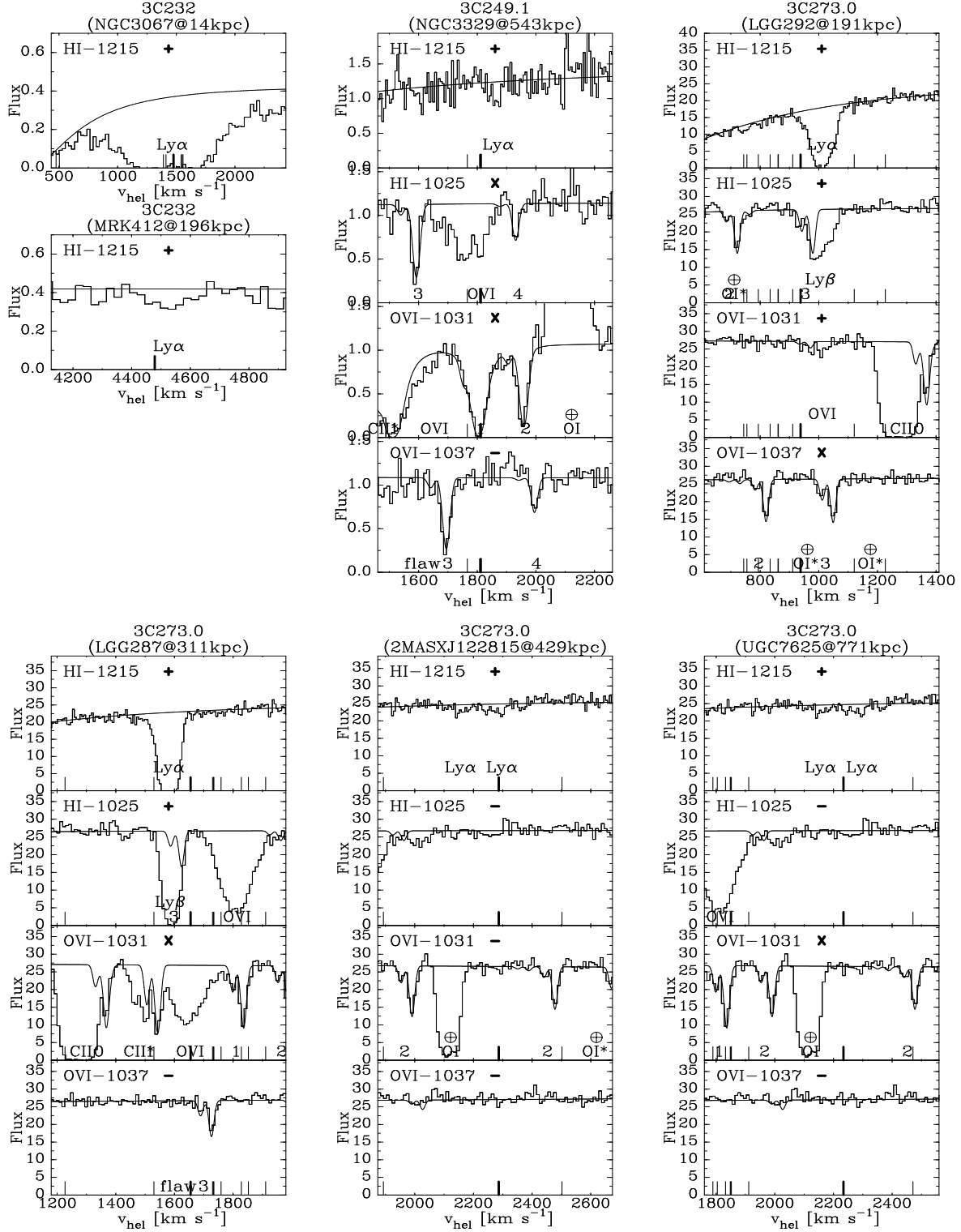


Fig. 2.— This figure shows the Ly $\alpha$ , Ly $\beta$  and O VI spectra for all of the detected intergalactic absorption lines. At the top of each panel, we give the AGN’s name, and within parentheses the galaxy with which the absorption is associated, as well as the impact parameter of that galaxy. The flux scale has units of  $10^{-14} \text{ erg cm}^{-2} \text{ s}^{-1} \text{ \AA}^{-1}$ . If orbital-night only data were used, the line-identification includes “(night)”. A velocity range of  $800 \text{ km s}^{-1}$  is shown, centered at the velocity of the absorber. Data are represented by the histogram, while the fitted continuum (including the H<sub>2</sub> model) is shown by the solid line. The dashed vertical line denotes the velocity of the intergalactic absorber. Solid vertical lines give the velocities of galaxies with impact parameter  $<1 \text{ Mpc}$ , with the thick line identifying the velocity of the galaxy associated with the absorber. At the bottom of each panel interstellar Milky Way absorption lines are identified, with single numbers given for the  $J$ -level of H<sub>2</sub> lines. An “earth” symbol is given at places where geocoronal Ly $\beta$  or OI\* emission is present. The word “flaw” near  $1043.2 \text{ \AA}$ , indicates a flaw in the FUSE detector, which makes any feature near this wavelength suspect. Intergalactic absorption lines are identified with the label raised relative to that identifying the Milky Way absorption. For each intergalactic detection a “+” is added. A “–” shows a non-detection. A “+” or “–” in parentheses shows uncertain detections and upper limits worse than  $50 \text{ m\AA}$ . Finally, an “x” means that we cannot measure the line, most often because of blending with Galactic absorption or geocoronal emission or sometimes because there is no data.



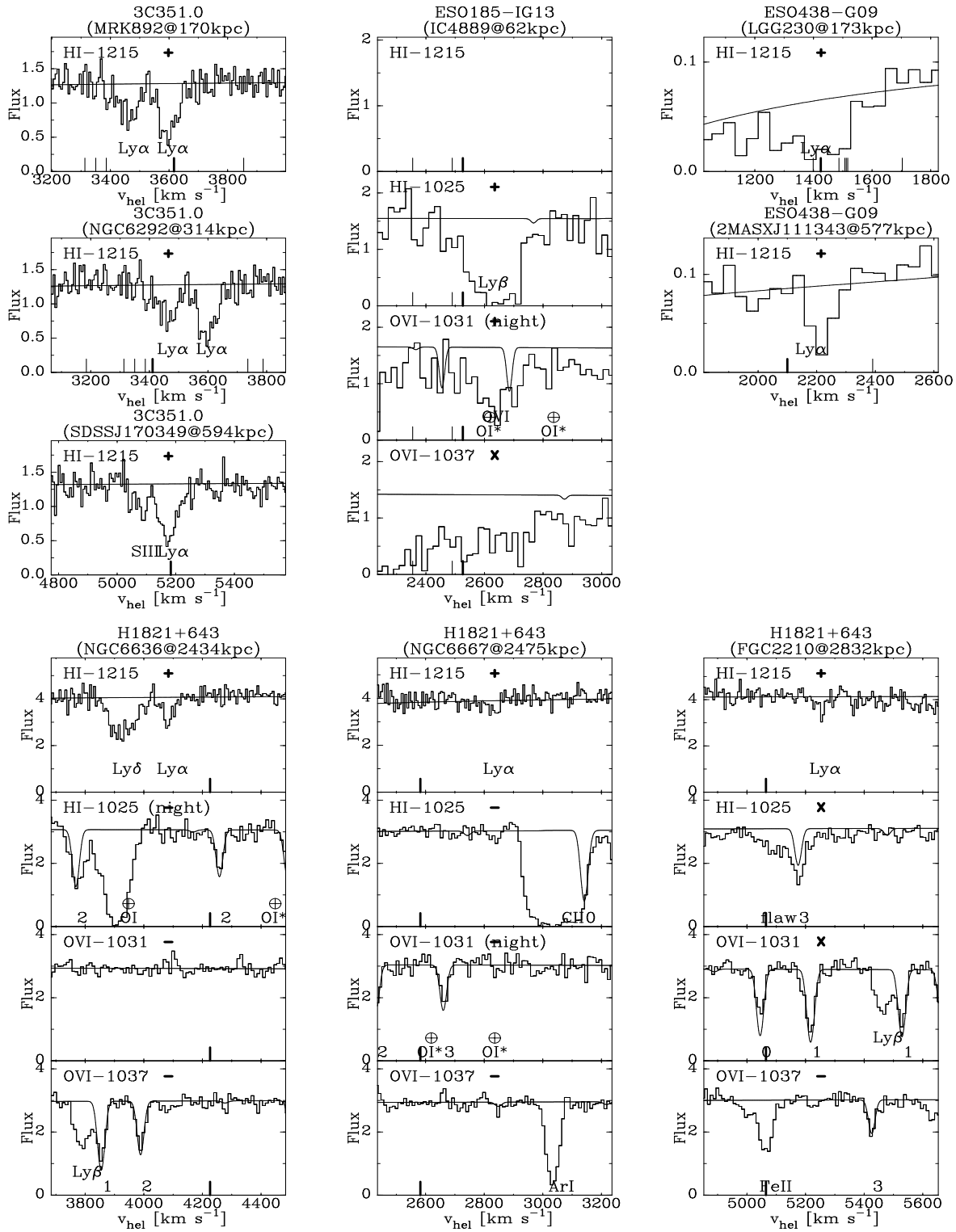


Fig. 2.— Continued.

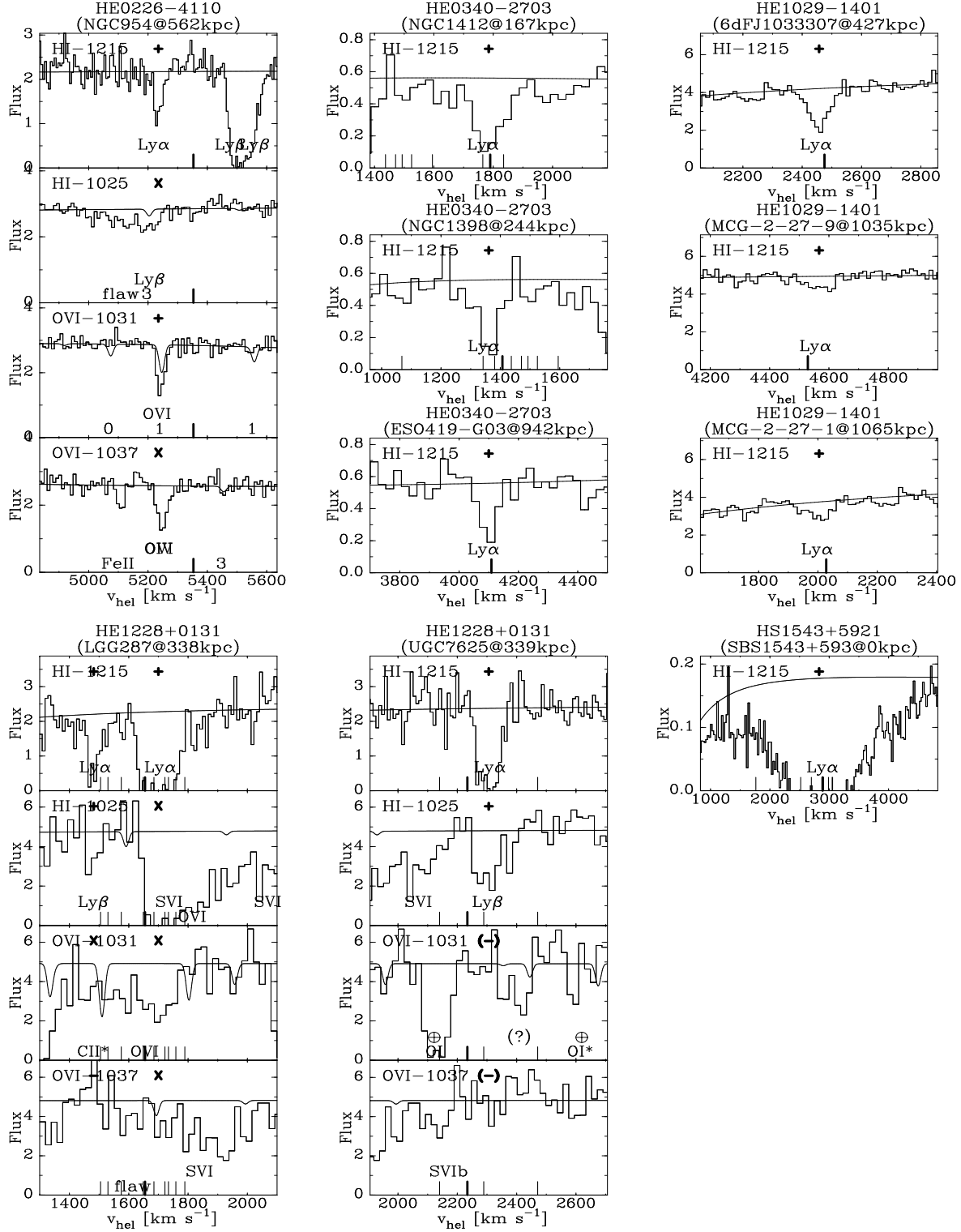


Fig. 2.— Continued.



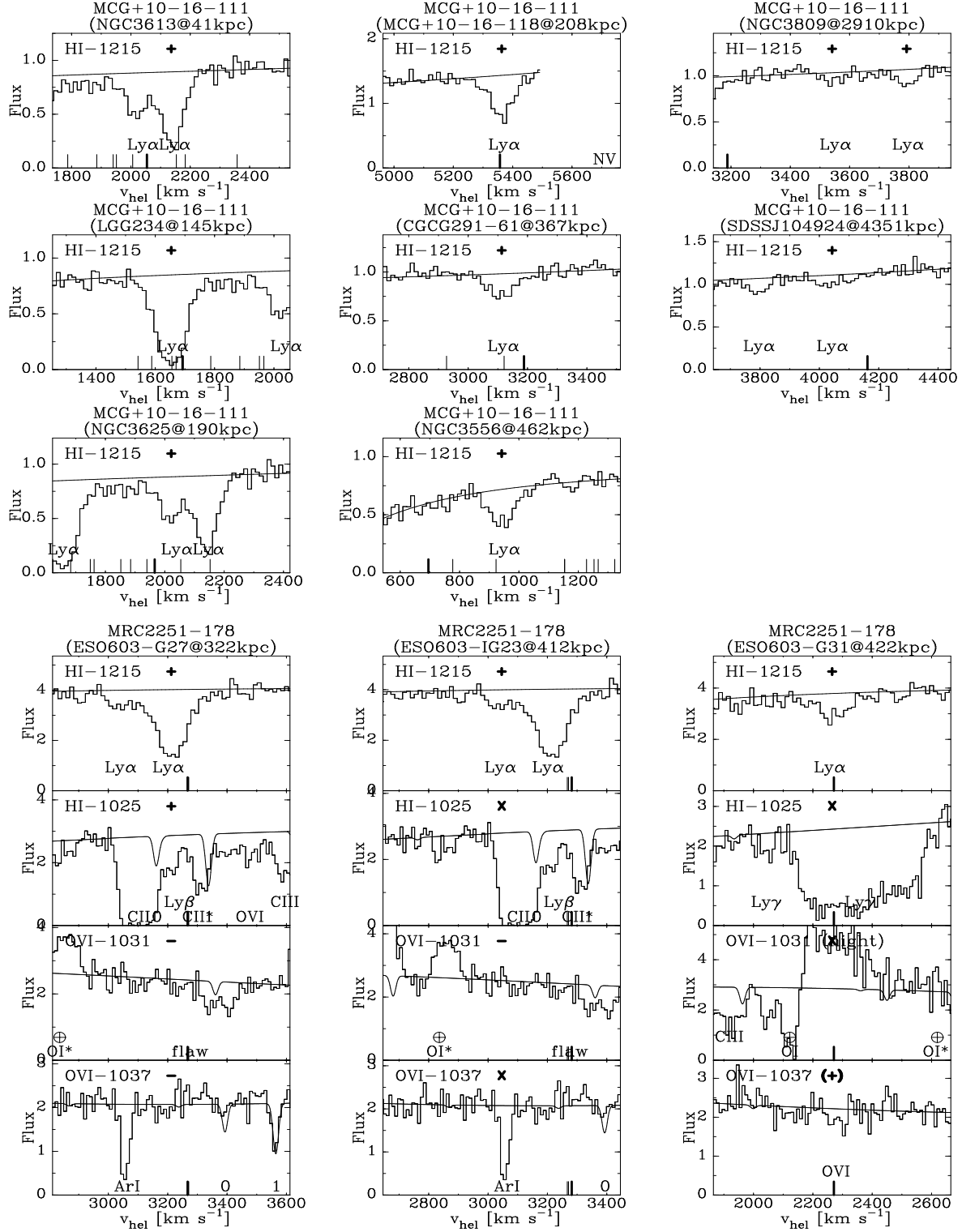


Fig. 2.— Continued.

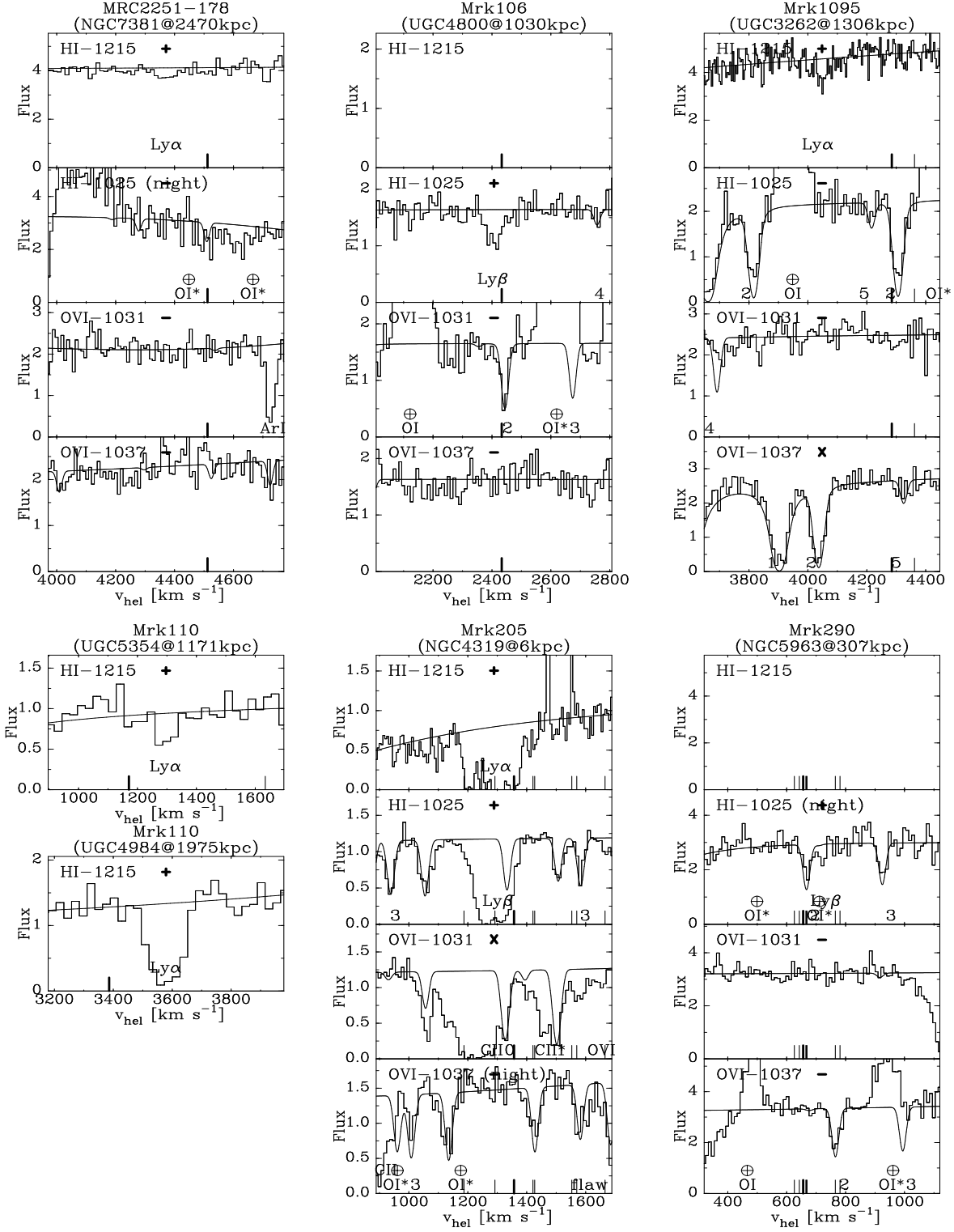


Fig. 2.— Continued.

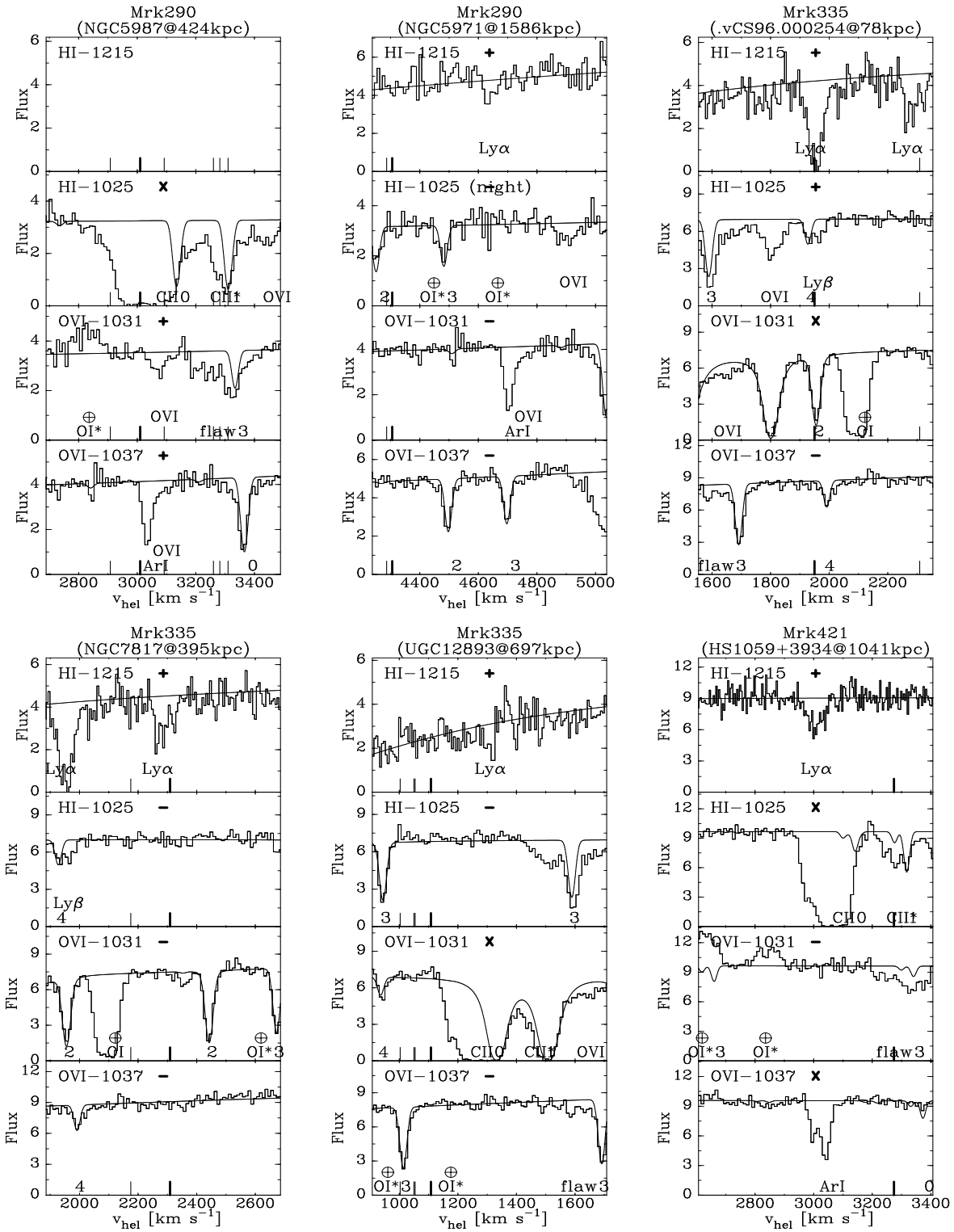


Fig. 2.— Continued.

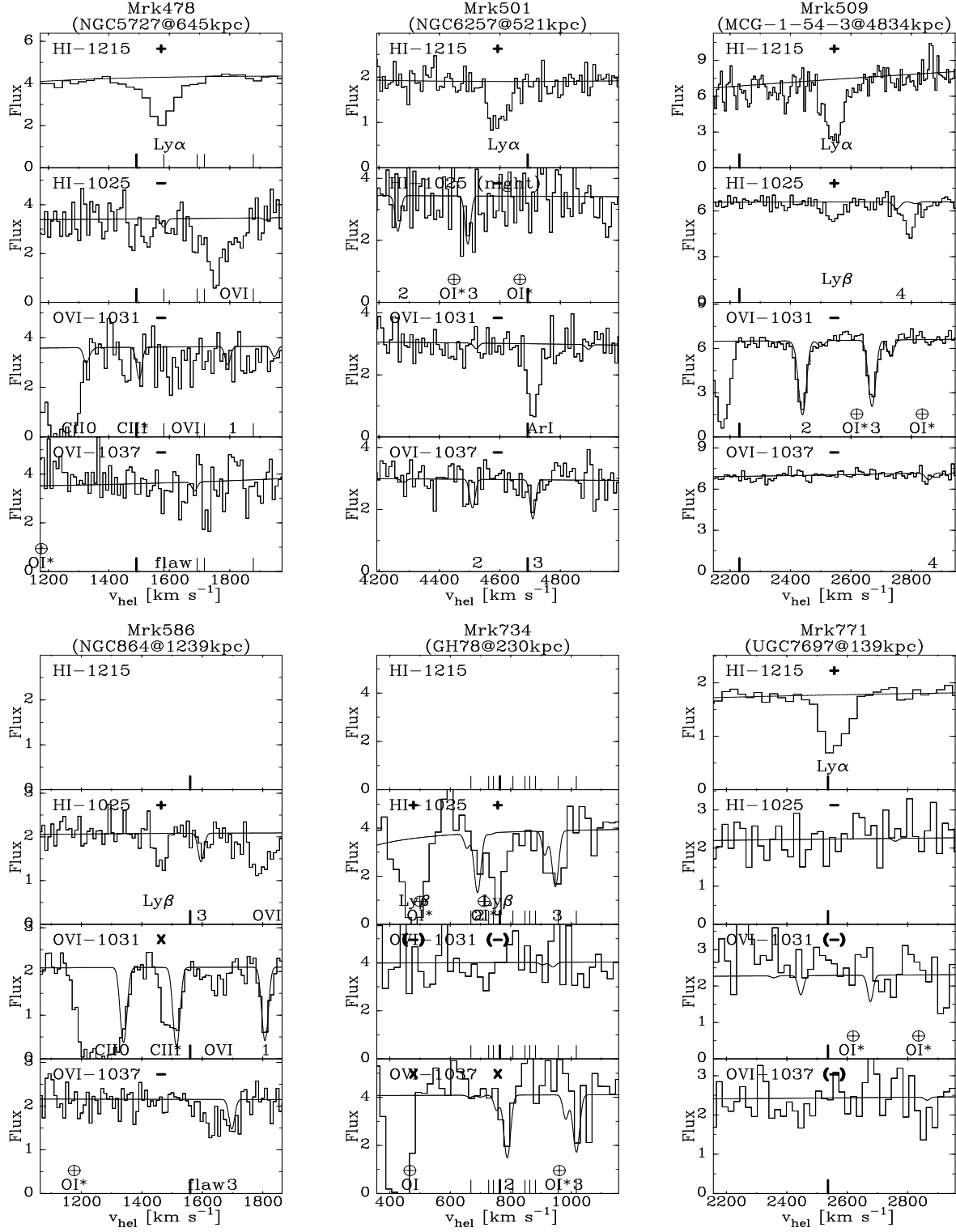


Fig. 2.— Continued.

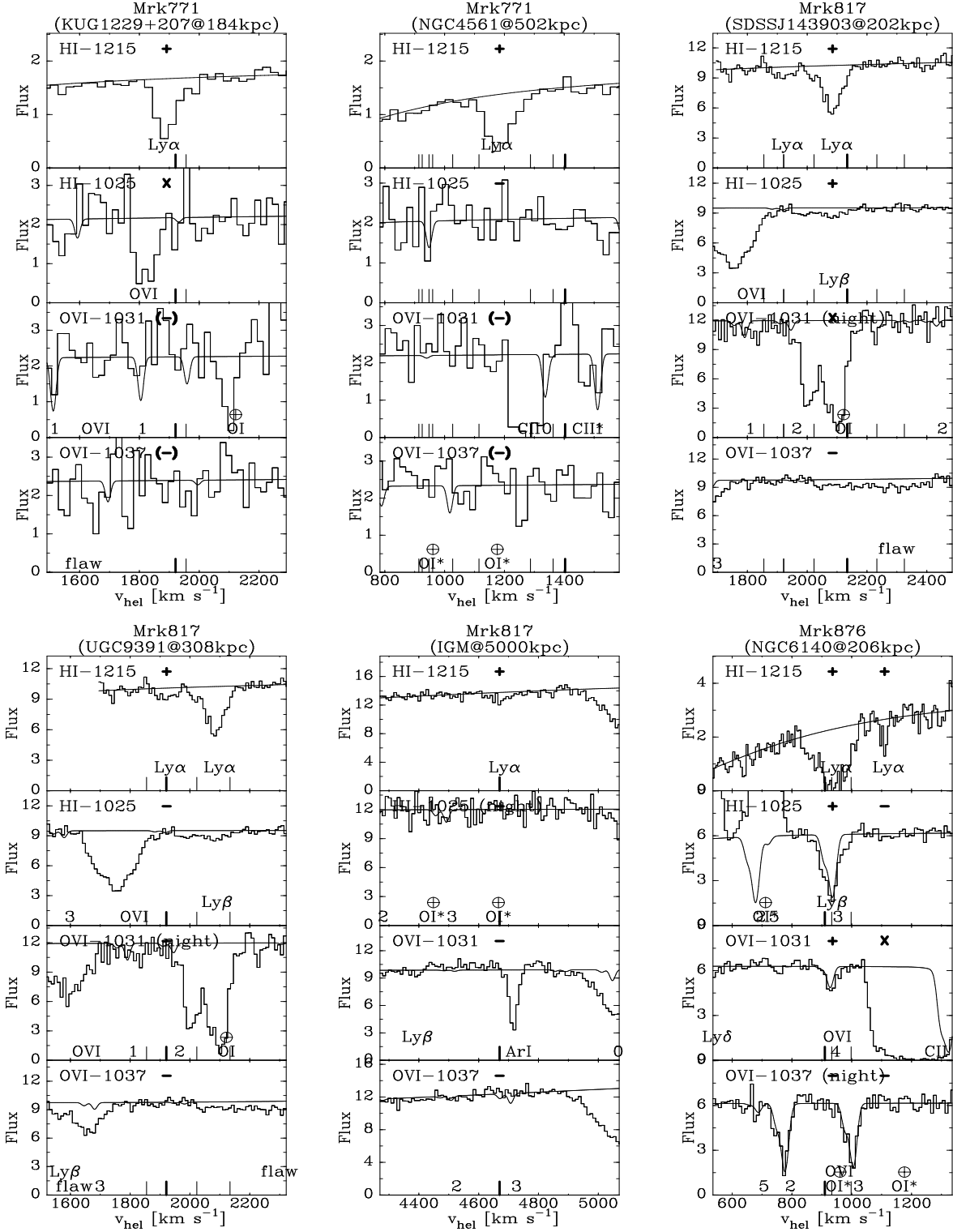


Fig. 2.— Continued.

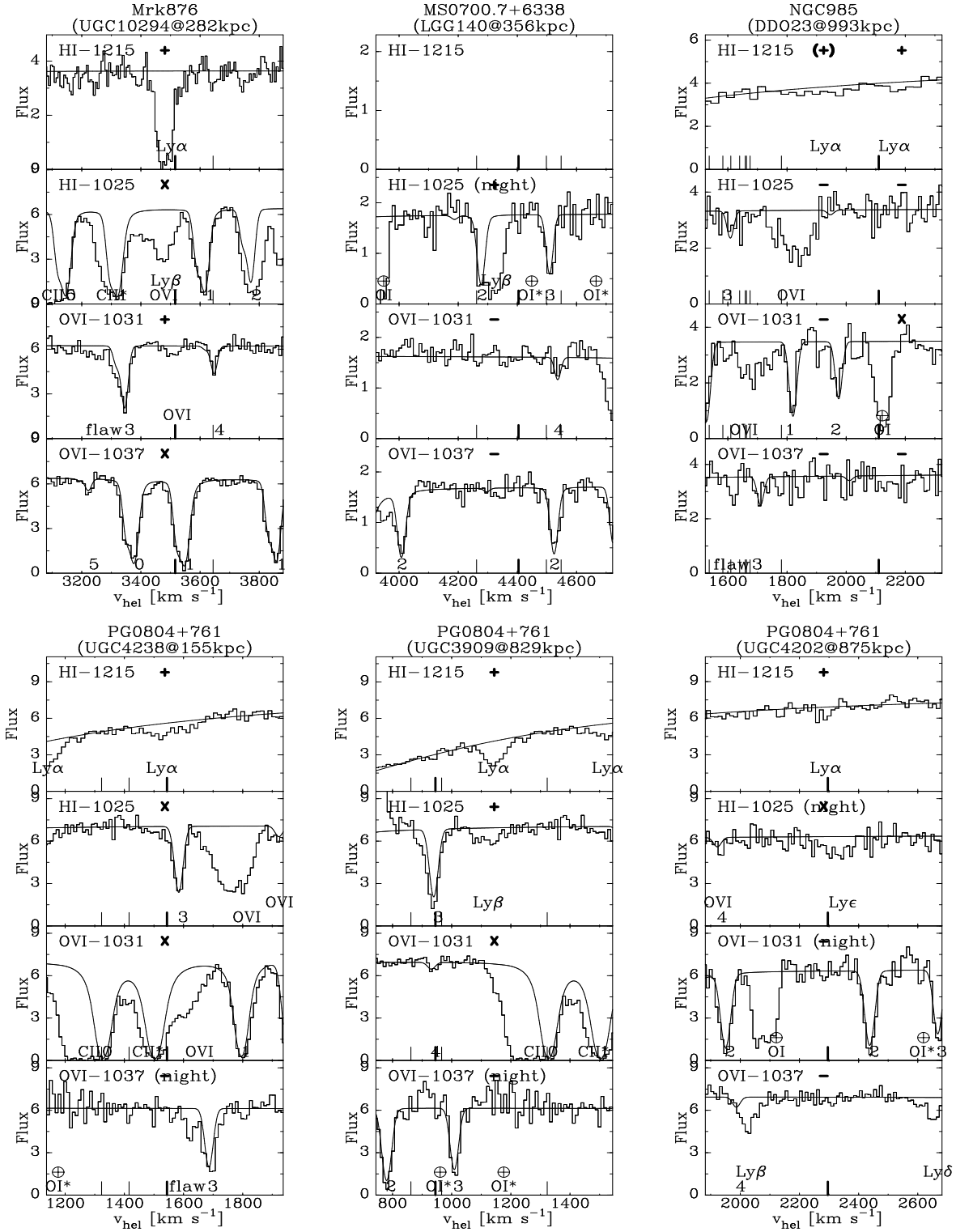


Fig. 2.— Continued.

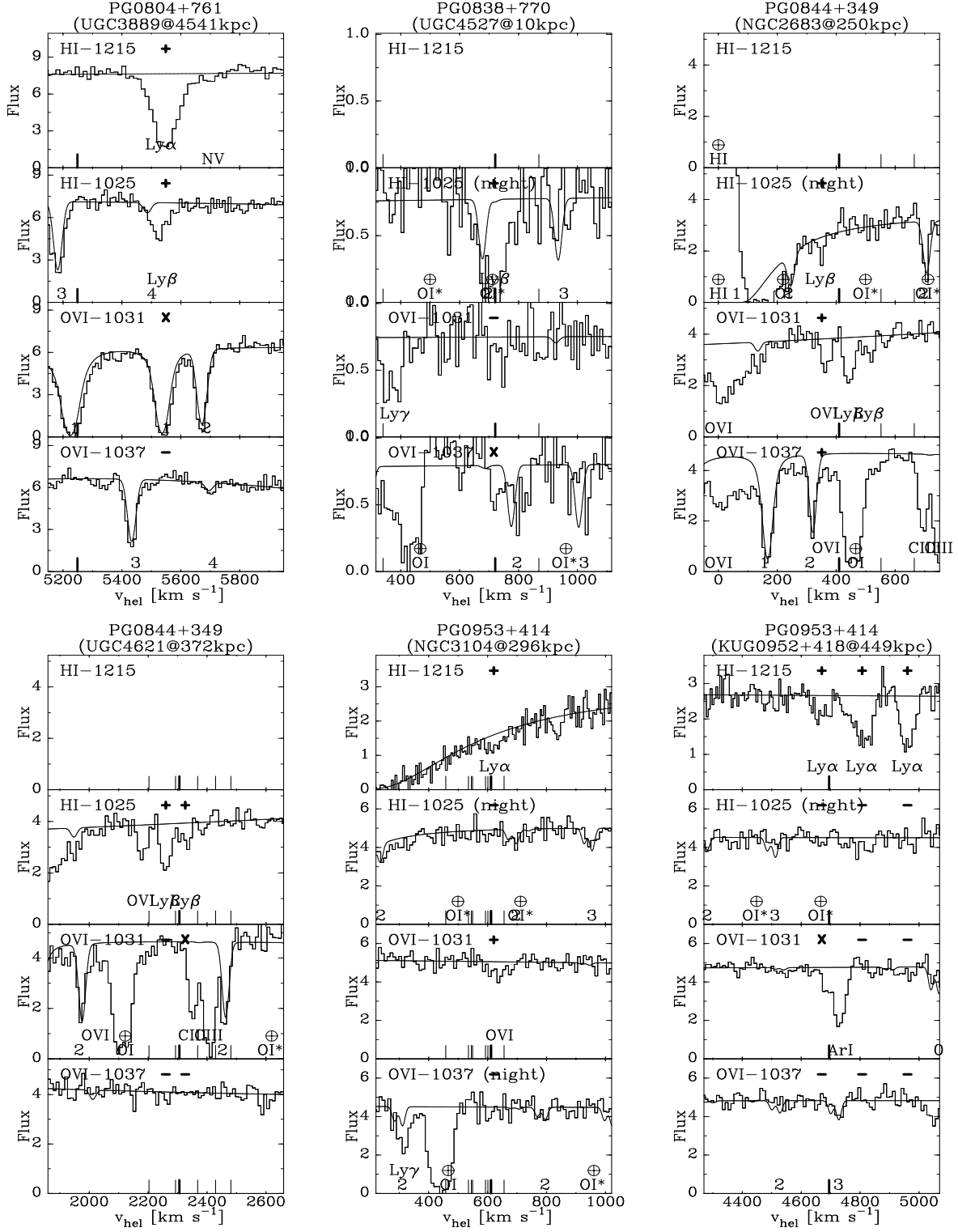


Fig. 2.— Continued.

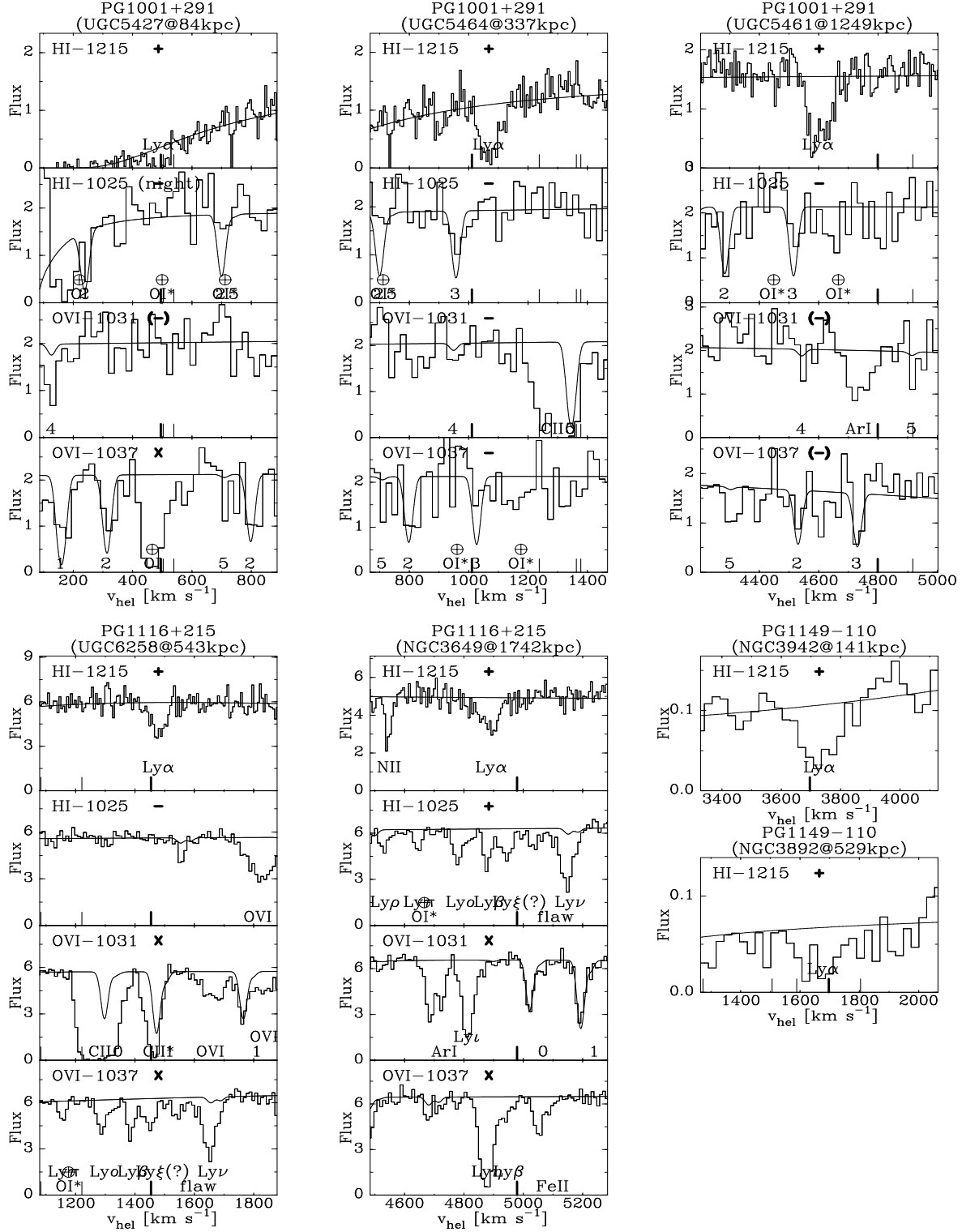


Fig. 2.— Continued.



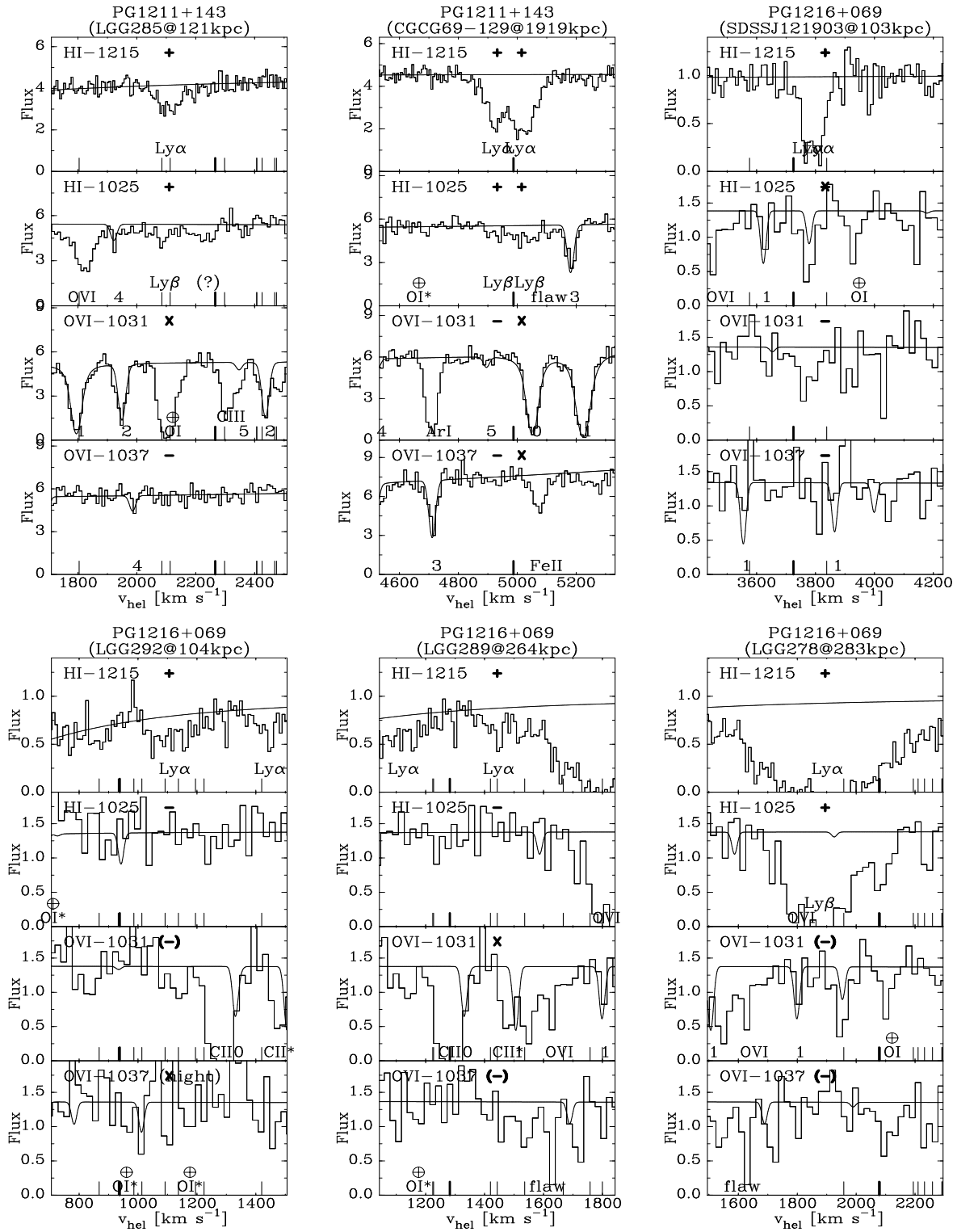


Fig. 2.— Continued.

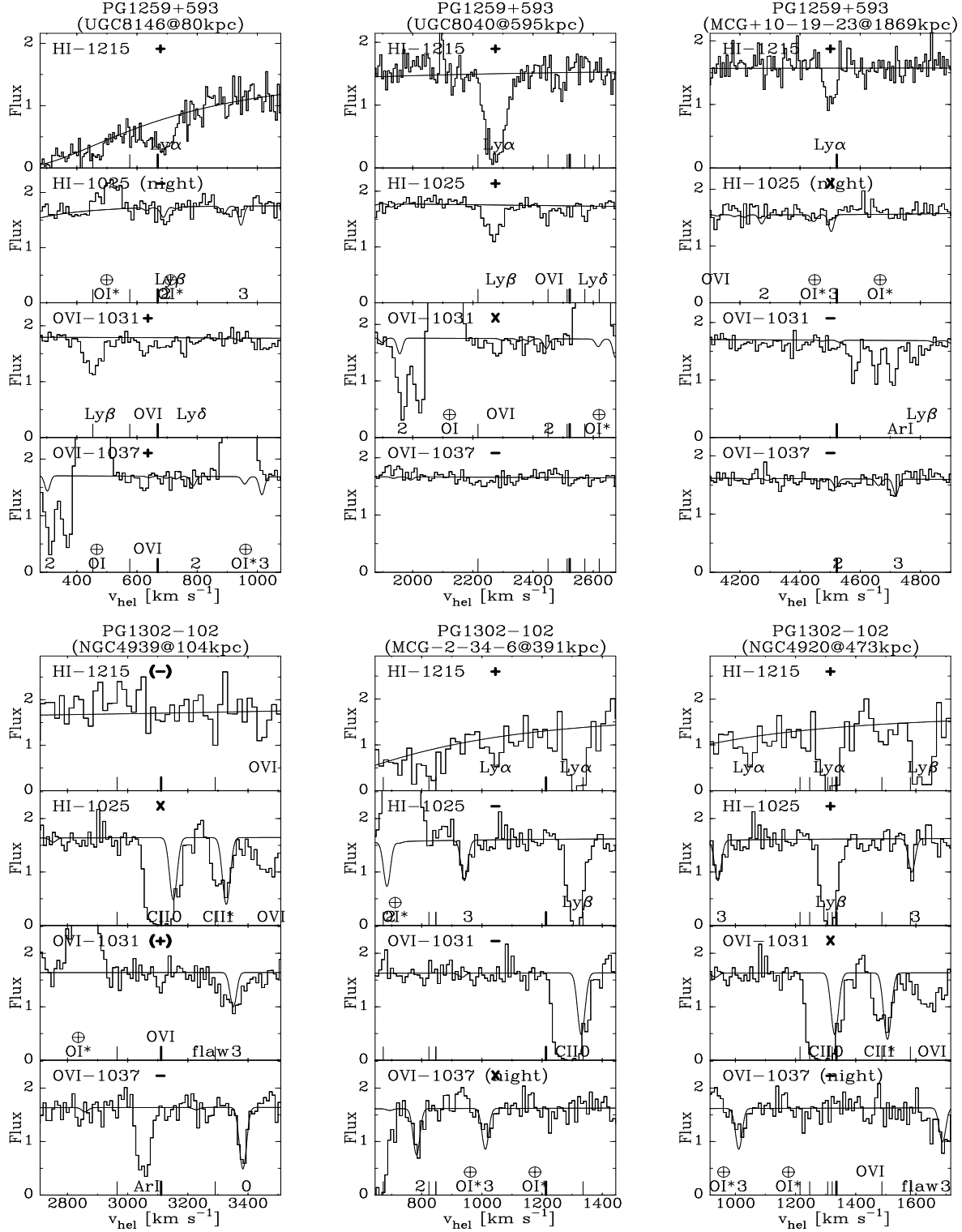


Fig. 2.— Continued.

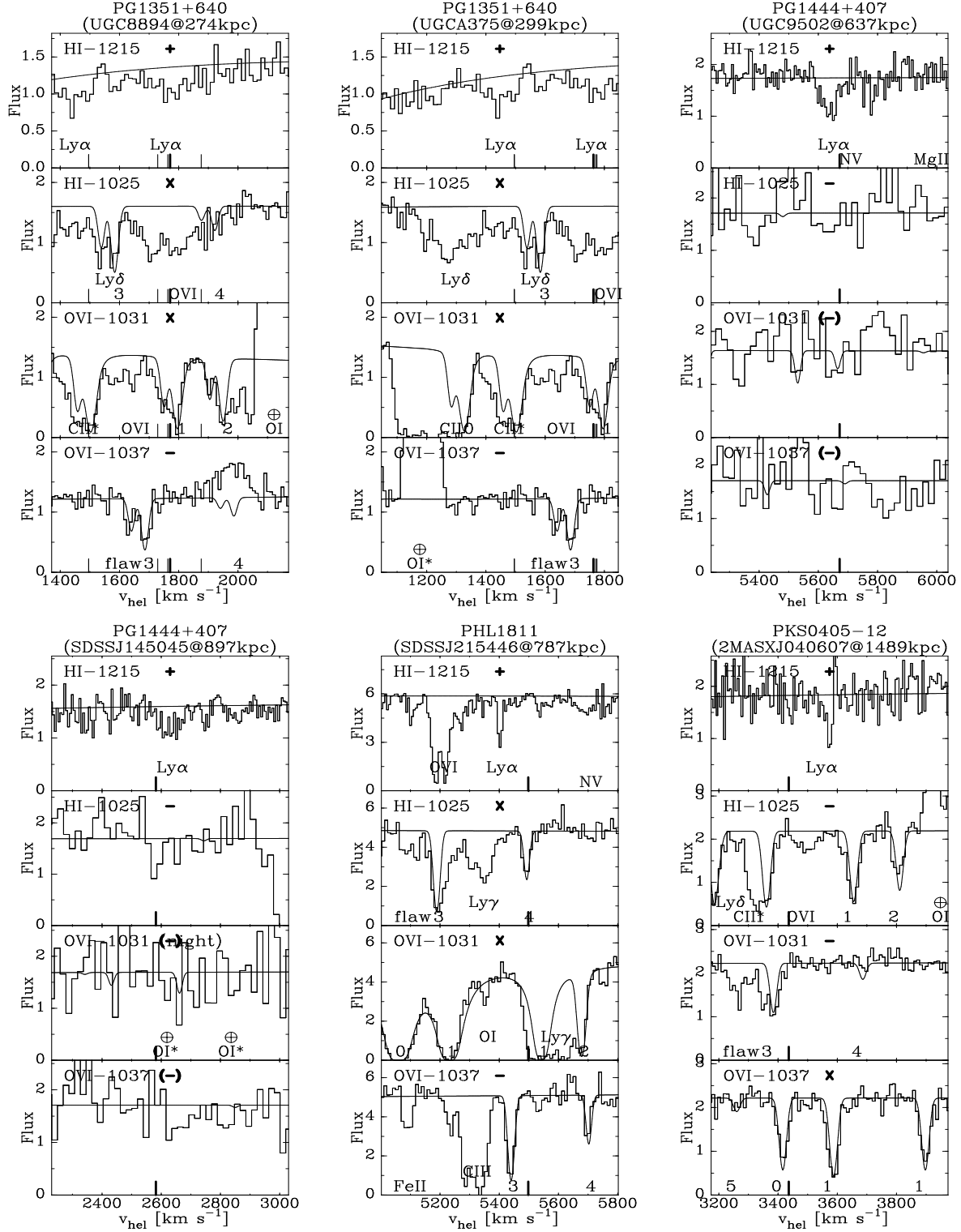


Fig. 2.— Continued.

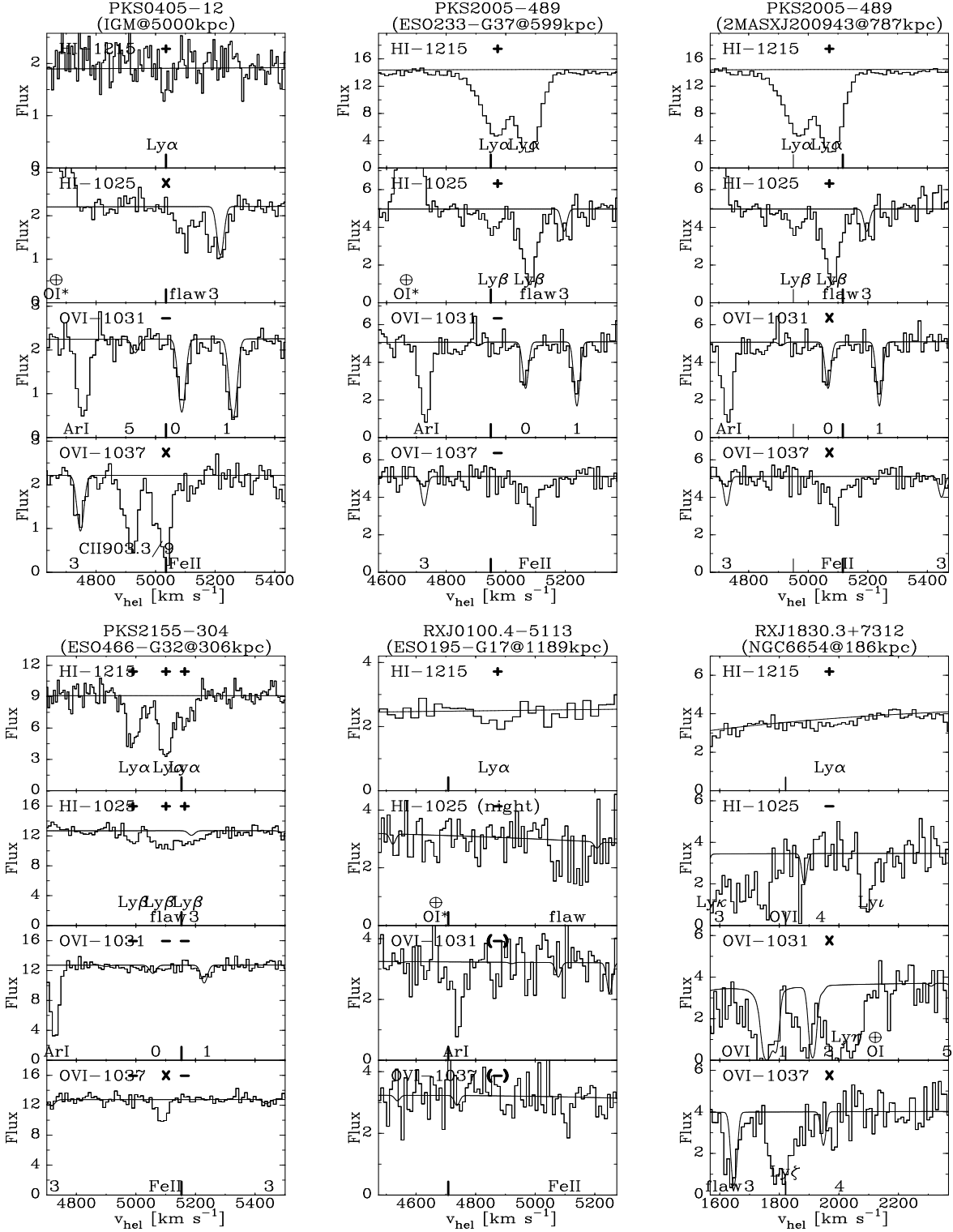


Fig. 2.— Continued.

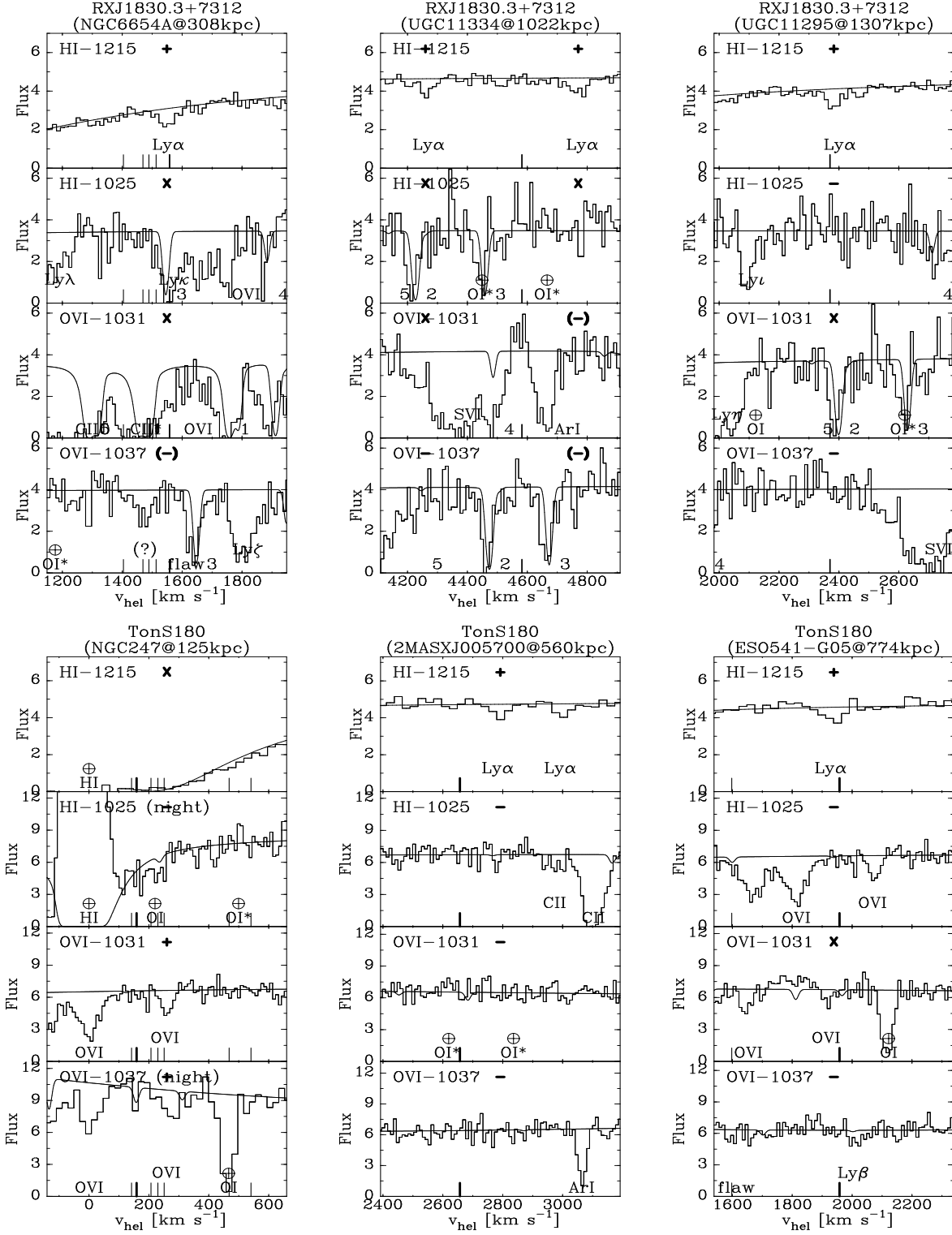


Fig. 2.— Continued.

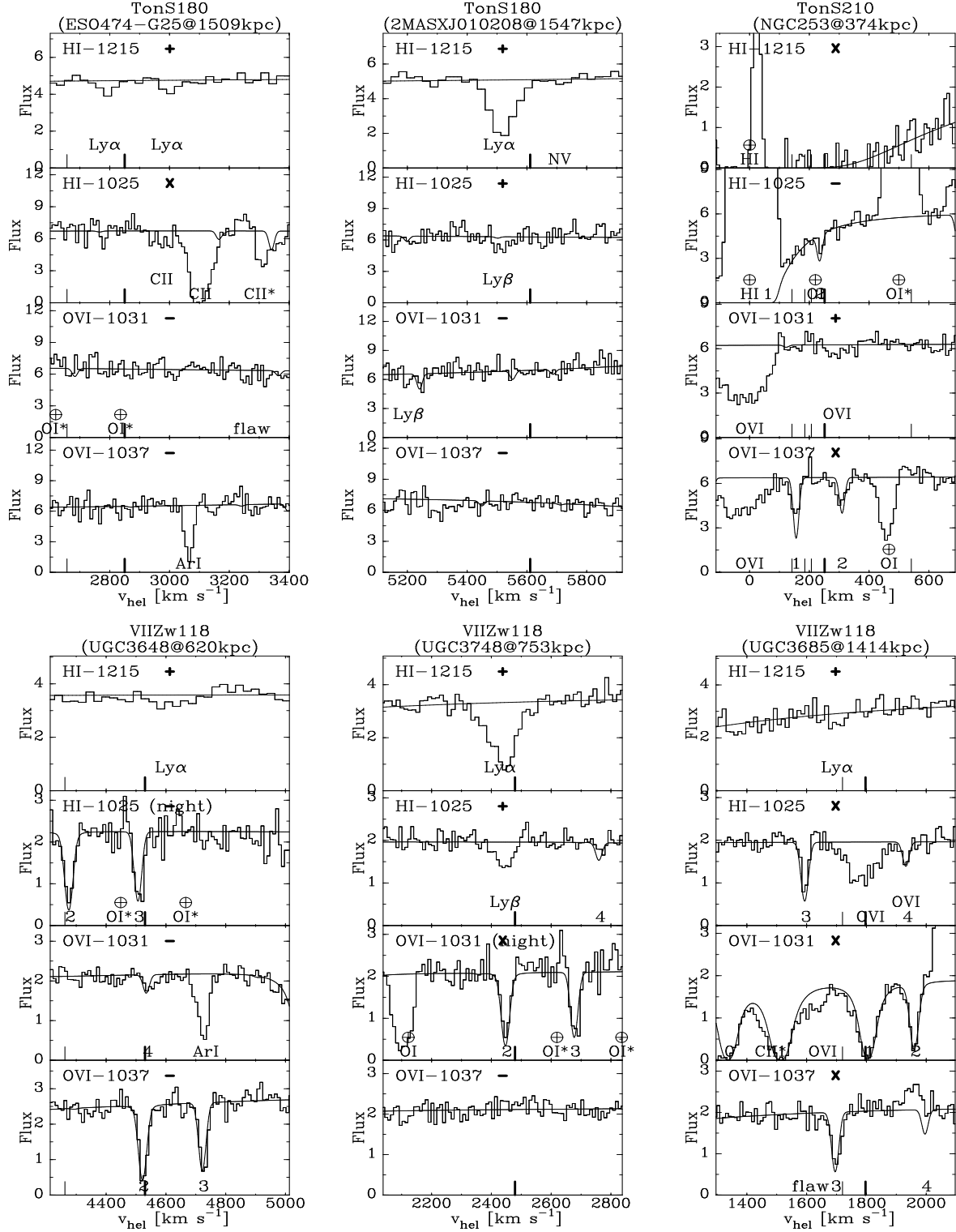


Fig. 2.— Continued.

$>-3^\circ$ , while the LGG catalogue covers the whole sky. There is overlap between the two catalogues, so that many GH groups have an LGG counterpart. However, rarely is the exact same set of galaxies used to define a group, mostly because the LGG catalogue is newer, so Garcia used more galaxies with known radial velocities, but also because he used slightly stricter criteria. In crowded areas, GH groups are often split into two or even more groups in the LGG list. We add two new groups to the ones listed in these two papers (see notes to 3C 351.0 and RX J1830.3+7312), as there are clear concentrations of galaxies, but no GH or LGG group, probably because not all radial velocities were measured before 1993.

For each galaxy listed as an LGG or GH group member, the galaxy’s heliocentric velocity was found from the RC3. An average velocity was then determined for each group using the velocities of its members. This was converted into a distance estimate after correcting for a Virgocentric flow (following Geller & Huchra 1982), which corresponds to a velocity of  $300 \text{ km s}^{-1}$  in the direction R.A.=186°7833, Dec=12°9333. All galaxies in a group were then assigned the distance corresponding to this corrected average group velocity, using a Hubble constant of  $71 \text{ km s}^{-1} \text{ Mpc}^{-1}$ . This procedure yields a distance for  $\sim 4800$  RC3 galaxies. In the remainder of the paper, we usually do not explicitly add the Hubble constant scale to each distance, but we use  $H_o=71 \text{ km s}^{-1}$  throughout.

The remainder of the galaxies in the RC3 are not considered a member of a GH or LGG group, so each galaxy’s individual velocity was corrected for a Virgocentric flow to obtain a distance estimate. For the  $\sim 5000$  RC3 galaxies without listed velocity measurement, a velocity of 2000 (usually) or  $4000 \text{ km s}^{-1}$  (for UGC galaxies) was assumed to continue the calculation (but see below). Finally, a distance of 2.8 Mpc was assigned to any galaxy for which the calculation gave distance smaller than 2.8 Mpc. None of these very nearby galaxies are included in the final sample of galaxies with small impact parameter.

As we were completing the study described in this paper, Tully et al. (2008) published a paper giving the most recent distance estimates for 1791 galaxies, derived from a variety of methods. We compared these distances to our earlier estimates and found that Tully et al. (2008) give values for 40 of the galaxies in our final sample. For many of the galaxies several different methods were used, and the different estimates usually agree (but not always). For 26 of the 39 overlapping galaxies our estimate is within 30% of the Tully et al. (2008) estimate. For the remaining 13 our value and the value given by Tully et al. (2008) differ by  $>30\%$ . In five cases the differences can sometimes be attributed to the fact that the galaxy was assigned to a GH group when it apparently should not have been (NGC 1398, NGC 2841, NGC 3067, NGC 3692, NGC 5963). In the other eight cases (NGC 1533, NGC 2671, NGC 4802, NGC 4939, NGC 5727, NGC 5981, UGC 10014, IC 2763) the Tully et al. (2008) value just differs from the value suggested by  $v_{gal}/D_{gal}$ .

The RC3 galaxy sample is more or less complete down to a B magnitude of 15.5, and angular diameter larger than about 1 arcmin. To complement this catalogue with fainter, smaller, lower surface brightness, and more recently discovered galaxies, we searched the *NASA Extragalactic Database* (*NED*: <http://nedwww.caltech.ipac.edu>) for all galaxies with  $v < 7000 \text{ km s}^{-1}$  lying within 5 degrees (the maximum distance allowed by *NED*) of each target. This yields  $\sim 6000$  galaxies with impact parameter  $< 3 \text{ Mpc}$ , including about 250 NGC/UGC and 100 IC galaxies that were not listed in the RC3, as well as  $\sim 1600$  low-redshift galaxies discovered by the *Sloan Digital Sky Survey* (SDSS),  $\sim 800$  from the *Two-Micron All-Sky Survey* (2MASS), and between 100 and 300 each from the *2-degree Field* (2dF) survey, the *Kiso Ultraviolet Galaxy* (KUG) survey, and the ESO, CGCG, MCG and VCC catalogues.

We estimated a distance for each of the additional galaxies found in *NED* using the same procedure described above for RC3 galaxies. Since an angular distance of 5 degrees corresponds to a linear distance  $< 1 \text{ Mpc}$  for galaxies with distance  $> 11.5 \text{ Mpc}$ , or velocity  $> 800 \text{ km s}^{-1}$ , it is unlikely that any target-galaxy pairs with impact parameter  $< 1 \text{ Mpc}$  have been missed. Of course, galaxies for which *NED* does not include a velocity are still not included in this sample.

Next, we calculated the angular distance between the extragalactic UV source and each RC3 and *NED* galaxy, and converted this into an impact parameter by multiplying with the galaxy’s distance. We kept all galaxies with impact parameter  $< 1 \text{ Mpc}$  and systemic velocity between 400 and 6000  $\text{km s}^{-1}$ . However, for some of the statistical work described below, we used a maximum velocity of 5000  $\text{km s}^{-1}$  (or even 2500  $\text{km s}^{-1}$  in some cases), as the galaxy sample becomes too incomplete at higher velocities. This velocity corresponds to a distance of  $5000/(H_0=71) = 70.4 \text{ Mpc}$ , or a distance modulus of 34.2. Since  $M_B = -19.57$  for an  $L_*$  galaxy (Marzke et al. 1994), an  $L_*$  galaxy with  $v=5000 \text{ km s}^{-1}$  has  $m_B=14.7$ . This means that for this velocity limit the RC3 should be more or less complete for galaxies brighter than  $0.5 L_*$ . For velocities  $< 3700 \text{ km s}^{-1}$ , the sample is complete above  $L > 0.25 L_*$ , and for velocities  $< 2500 \text{ km s}^{-1}$  above  $L > 0.1 L_*$ .

For several of the analyses we do in Sects. 4 and 5 we would like to apply a galaxy luminosity selection criterion. However, the RC3 includes a magnitude for only 17% of the listed galaxies, while the angular size at 25th magnitude surface brightness is given for 94%. The angular diameters are converted to linear diameter using the galaxy’s distance. We correlated linear diameter ( $D_{gal}$ ) and absolute magnitude when both are known and we use a galaxy’s diameter as a proxy for brightness in the remainder of the paper. This correlation is shown in Fig. 3, using the galaxies in the RC3 with both diameter and absolute magnitude given. The correlation yields a diameter  $D_{gal}=20.4 \text{ kpc}$  for an  $L_*$  galaxy,  $D_{gal}=14.6 \text{ kpc}$  for  $0.5 L_*$ ,  $D_{gal}=11.2 \text{ kpc}$  for  $0.25 L_*$ , and  $D_{gal}=7.5 \text{ kpc}$  for a  $0.1 L_*$  galaxy. Using this



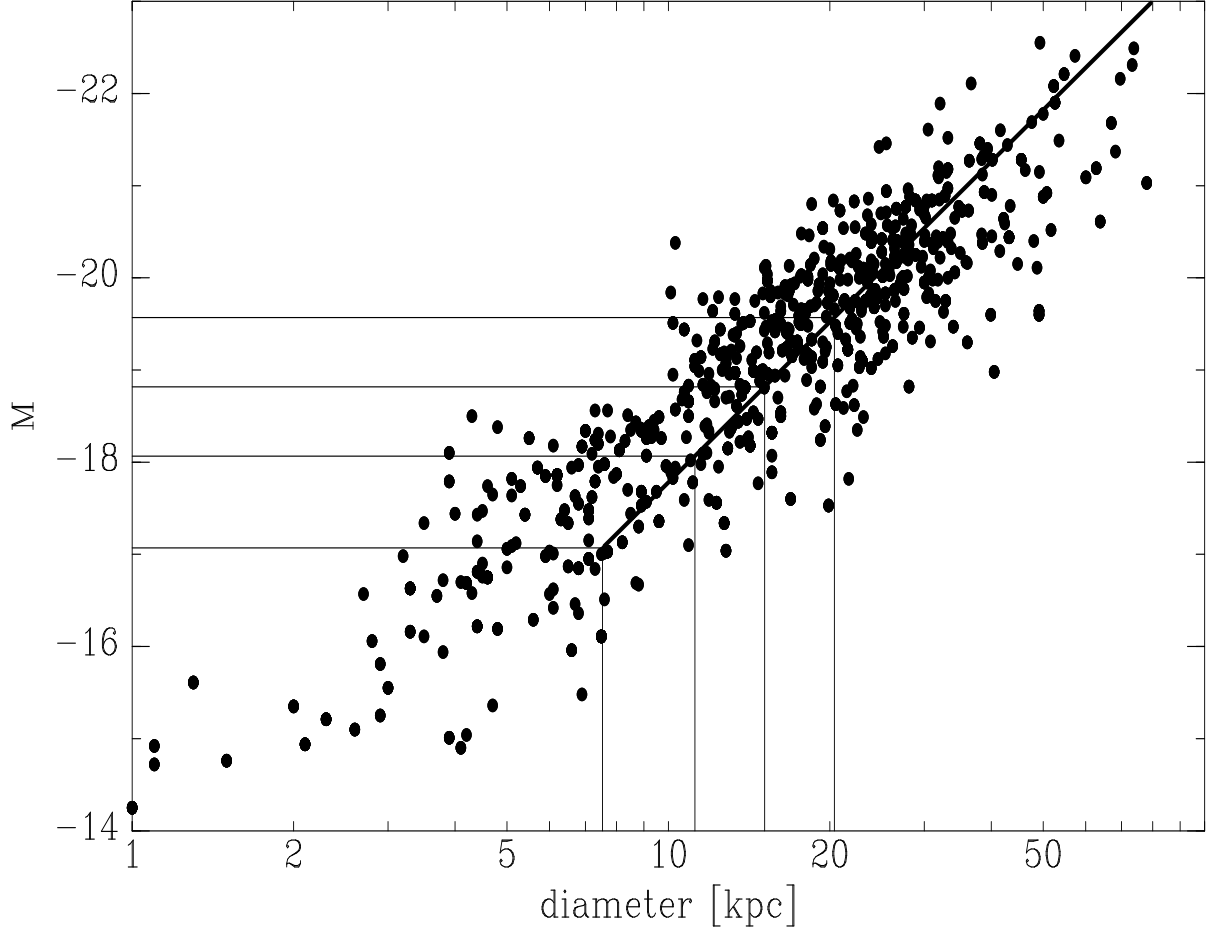


Fig. 3.— Correlation between galaxy luminosity and galaxy diameter, for galaxies in the RC3 for which both are given (excluding irregulars). The horizontal lines correspond to galaxies with luminosity  $L_*$ ,  $0.5 L_*$ ,  $0.25 L_*$  and  $0.1 L_*$ . The vertical lines correspond to the corresponding diameters that we use throughout the paper: 20.4, 14.6, 11.2 and 7.5 kpc. The diagonal line is a least squares fit (correlation coefficient 0.8) for  $M < -16$  and  $D_{gal} > 7.5$  kpc, and has the functional form  $M = -5.78 \log R - 12$ , corresponding to  $\log L = 2.31 \log R - 3.03$ . *Selection criteria:* all galaxies in the RC3 with both magnitude and diameter given.

conversion, we find 1366 galaxies in the RC3 with  $D_{gal} > 7.5$  kpc (equivalent to  $L > 0.1 L_*$ ), and 23 additional ones from *NED*. The RC3 has 1033 galaxies with  $D_{gal} > 14.6$  kpc ( $L > 0.5 L_*$ ), and we add 13 from the *NED* sample. For  $D_{gal} > 20.4$  ( $L > L_*$ ), the RC3 includes 588 galaxies, *NED* adding 4 more.

For a given diameter limit, 80–90% of the galaxies fit the corresponding luminosity criterion. Using the diameter criterion will include about 5% of galaxies that are fainter than the corresponding luminosity, by up to about 1 magnitude. On the other hand, about 10% of the galaxies that are brighter than a given limit are excluded by the diameter criterion. This is a small price to pay for the ability to classify >95% of the galaxies instead of <20%.

We could instead have tried to extract magnitudes from *NED* for individual galaxies, but the magnitudes that *NED* gives are on many different systems, including, but not limited to,  $B_T$  as defined for the RC3, *UBV*, SDSS *ugriz* and photographic. Trying to regularize these would give as much uncertainty as using diameters as a proxy. The only proper way to determine consistent galaxy luminosities would be to measure all galaxies on the same system, such as that used for a portion of the RC3.

As mentioned earlier, we assumed a value of 2000 or 4000  $\text{km s}^{-1}$  for galaxies for which the RC3 does not provide a velocity. In a few cases this resulted in small impact parameters. We then checked whether *NED* gives a velocity for the galaxy. If so, we redid the impact parameter calculation. In the end there are quite a few galaxies whose velocity remains unknown, but which may have impact parameter <1 Mpc to a background target. Most of these galaxies are smaller and less luminous and have similar impact parameter as the galaxy that we associate with the absorber. However, for 13 absorbers there are a total of 16 galaxies with unknown velocity that could have significantly lower impact parameter than the one we list in our results table (see Appendix notes for 1H 0707–495, 3C 249.1, Mrk 509, Mrk 1095, PG 0804+761, PG 1211+143, PG 1302–102, PG 1444+407, RX J0100.4–5113 and VII Zw 118). In three cases the galaxy with the lowest known impact parameter is at  $\rho > 1$  Mpc, but the galaxy with unknown velocity could have  $\rho < 1$  Mpc (see notes for PG 1211+143, RX J0100.4–5113 and VIII Zw 118).

Using the sample of galaxies, we associated absorption lines with some of these, as we discuss in more detail in Sect. 4.3. For the other galaxies, we derived upper limits on the equivalent widths of  $\text{Ly}\alpha$ ,  $\text{Ly}\beta$  and O VI absorption. Table 3 lists all the galaxies with  $v_{gal} < 6000 \text{ km s}^{-1}$  that lie within 1 Mpc of a sightline to a background target (sorted on impact parameter), and for which the ratio of impact parameter to galaxy diameter is <125. We justify the latter criterion in Sect. 4.3. All individual associations in Table 3 are discussed in detail in the Appendix, on a sightline-by-sightline basis. In Table 4 we separately list the detections for lines other than  $\text{Ly}\alpha$ ,  $\text{Ly}\beta$  or O VI.

We have made the full galaxy table available in the on-line version of this paper. This includes *all* galaxies near each sightline. This table is inhomogeneous, however. Near some sightlines deep surveys for dwarf galaxies exist. Near others special searches were done. For some sightlines (especially) in the Virgo cluster region we did not check the diameter in *NED* for some of the additional galaxies with impact parameter  $<1$  Mpc. Although these additional galaxies come from searches for dwarfs, it is possible (but unlikely) that there are cases where a galaxy should have been listed in Table 3 but was not. The on-line table should therefore be treated with care. It is only reliably complete for statistical analyses for large galaxies.

In Tables 5 and 6 we summarize all the detected  $\text{Ly}\alpha$ ,  $\text{Ly}\beta$  and O VI lines, and compare our measurements with previously published values.

Table 3. HI and O VI results<sup>1</sup>

Target	Galaxy	Group	$v_{gal}$ [km s <sup>-1</sup> ]	$D$ [Mpc]	$D_{gal}$ [kpc]	$\rho$ [kpc]	Q	HI	OVI	Ly $\alpha$ [mÅ]	Ly $\beta$ [mÅ]	O VI–1031 [mÅ]	O VI–1037 [mÅ]
(1)	(2)	(3)	(4)	(5)	(6)	(7)	(8)	(9)	(10)	(11)	(12)	(13)	
HS1543+5921	SBS1543+593 <sup>3</sup>	GH158	2889	42.7	7.8	0.3	!	+		>5000@2829			
Mrk205	NGC4319 <sup>3</sup>	GH107	1357	27.7	23.8	6	!	+	–	801±13±4@1289	477±14±8@1283	{C II}	<38
PG0838+770	UGC4527		721	11.8	4.7	10	!	+	–		330±53±13@716	<54	{O I}
3C232	NGC3067 <sup>3</sup>	GH50	1476	23.9	17.0	14	!	+		>5000@1434			
MCG+10–16–111	NGC3613	LGG232	2054	31.2	35.3	41	2	+		301±11±7@2136			
MRK205	NGC4291	LGG284	1757	27.7	15.3	51	!	–	–	<29	{O VI}	<22	{O I}
ESO185–IG13	IC4889		2526	34.5	28.9	62	!	+	+		641±52±14@2635	335±68±15@2627	{Ly $\beta$ }
Mrk110	MCG+09–16–10		457	9.1	1.7	66	!	–		<54			
Mrk335	[vCS96]000254.9 <sup>3,4</sup>		1950	24.3	0.7	78	?	+	–	229±12±3@1954	31±3±9@1966	{H <sub>2</sub> }	<11
PG1259+593	UGC8146 <sup>3</sup>		669	12.5	12.6	80	!	+	+	231±9±3@678	<15	25±5±2@627	13±3±2@622
PG1001+291	UGC5427		495	10.5	3.6	84	!	+	(–)	308±7±12@487	<87	<75	{O I}
PG1216+069	SDSS J121903.72 <sup>4</sup>		3833	59.0	5.1	103	+	+	(–)	148±13±17@3774	{H <sub>2</sub> }	<74	<85
							+	+	(–)	163±12±16@3808	<78	<79	<83
PG1302–102	NGC4939		3111	15.4	24.6	104	!	(–)	(+)	<72	{C II}	19±6±8@3109	<23
PG1216+069		LGG292	[938] <sup>2</sup>	17.7		>104	g	+	(–)	209±27±5@1106	<90	<83	{O I*} <sub>1</sub>
PG1211+143		LGG285	[2266] <sup>2</sup>	36.7		>121	g	+	–	104±8±2@2110	50±9±8@2088	{O I}	<19
ESO185–IG13	IC4888		2490	34.0	10.6	123	!	(–)	(–)		<83	<103	{Ly $\beta$ }
Ton S180	NGC247 <sup>3</sup>	LGG4	159	2.5	15.7	125	!	–	+	{Ly $\alpha$ }	<37	51±10±8@260	34±13±8@285
Mrk477	SDSS J144303.81 <sup>4</sup>		838	14.8	1.5	138	!	–	–		<37	<36	{O I*}
Mrk771	UGC7697 <sup>3</sup>		2536	40.5	24.6	139	!	+	(–)	246±13±3@2557	<95	<94	<89
PH0419–577	NGC1574 <sup>3</sup>	LGG112	925	13.6	13.4	140	?	+	(–)		463±25±15@1112	<54	{O I*}
PG1149–110	NGC3942		3696	56.7	23.3	141	!	+		381±54±3@3728			
Mrk110	NGC2841 <sup>3</sup>	GH44	638	5.9	13.9	144	>	(–)		<68			
MCG+10–16–111		LGG234	1692	27.1		>145	g	+		494±13±4@1654			
HE0340–2703	ESO482–G32		1765	22.3	9.8	152	x			{Ly $\alpha$ }			
PG0804+761	UGC4238 <sup>3</sup>		1544	23.4	16.3	155	!	+	–	114±14±2@1537	{H <sub>2</sub> }	{C II*}	<30
HE0340–2703	NGC1412		1790	22.7	12.3	167	1	+		374±30±6@1785			
Mrk335		PegSpur	713–1108	~12.5	3–18	>170	g	–	–	<43	<14	<15	<13
3C351.0	Mrk892	LGG179A	3617	53.2	10.2	170	2	+		164±10±6@3598	{Ly $\lim$ }	{Ly $\lim$ }	{Ly $\lim$ }
ESO438–G09		LGG230	[1425] <sup>2</sup>	23.4		>173	g	+		579±44±15@1426			
NGC985		LGG71	1406	16.5		>175	g	–	–	<21	<31	<30	<31
PKS2005–489		LGG430	[2955] <sup>2</sup>	40.3		>181	!	–	–	<10	<20	<30	<20
Mrk771	KUG1229+207		1921	31.7	6.5	184	!	+	(–)	243±13±5@1891	{O VI}	<102	<86

Table 3—Continued

Target	Galaxy	Group	$v_{gal}$ [km s <sup>-1</sup> ]	$D$ [Mpc]	$D_{gal}$ [kpc]	$\rho$ [kpc]	Q	HI	OVI	Ly $\alpha$ [mÅ]	Ly $\beta$ [mÅ]	O VI—1031 [mÅ]	O VI—1037 [mÅ]
(1)	(2)	(3)	(4)	(5)	(6)	(7)	(8)	(9)	(10)	(11)	(12)	(13)	
RX J1830.3+7312	NGC6654	LGG420A	1821	23.8	18.2	186	!	+		68±10±3@1968	<66	{Ly $\theta$ }	{H <sub>2</sub> }
MCG+10−16−111	NGC3625	LGG232	1966	31.2	18.1	190	2	+		174±11±9@2022			
3C273.0		LGG292	[938] <sup>2</sup>	17.7		>191	g	+	+	394±7±1@1010	120±4±10@1013	21±3±7@1008	{H <sub>2</sub> }
PG1001+291	UGCA201		1363	22.9	3.3	193	1	−	(−)	<36	<75	{C II}	<63
3C232	Mrk412		4479	67.3	11.7	196	!	+		153±30±4@4526			
U0717+714	UGC3804	LGG141	2887	44.1	22.8	199	!	+	+		41±7±8@2888	66±15±9@2914	<23
Mrk817	SDSS J143903.89 <sup>4</sup>		2134	33.1	4.1	202	1	+	−	131±8±3@2085	25±3±7@2081	{O I}	<9
Mrk876	NGC6140 <sup>3</sup>		910	14.8	27.1	206	+	+	+	476±14±3@936	79±6±33@933	17±4±8@945	<16
							+	+	−	39±7±3@1109	<13	{C II}	<16
MCG+10−16−111	MCG+10−16−118		5357	79.5	16.6	208	!	+		172±8±3@5363			
PG1211+143		LGG289	[182] <sup>2</sup>	22.6		>215	g	−	−	<16	<20	{C II}	<21
Mrk110	UGC5076		571	10.8	3.1	226	!	−		<70			
PG0844+349	[KK98]069		463	9.2	6.4	228	!	−			<31	{Ly $\beta$ }	{O I}
Mrk734		GH78	921	10.0		>230	g	+	(−)		301±35±11@478	<77	{Si II}
							g	+	(−)		149±31±11@757	<76	{H <sub>2</sub> }
HE0340−2703	NGC1398	LGG97	1407	14.5	29.8	244	!	+		292±30±6@1361			
PG0844+349	NGC2683 <sup>3</sup>		410	8.5	23.0	250	!	+	+		25±8±2@351	37±5±2@365	27±5±7@365
PG1259+593	SDSS J125926.78 <sup>4</sup>		2867	43.9	6.5	255	!	−	−	{Ly $\delta$ }	<14	<14	<13
RX J1830.3+7312	MCG+12−17−27	LGG420A	1404	20.9	5.2	262	!	−	(−)	<14	<69	{C II*}	<56
PG1216+069		LGG289	[1282] <sup>2</sup>	22.6		>264	g	+	(−)	119±19±6@1443	<90	<83	<80
PG1216+069		LGG281	[2473] <sup>2</sup>	39.6		>264	g	−	(−)	<37	<87	<104	<89
Mrk106	UGC4879	GH44	600	5.9	2.8	266	>		(−)		{O I*}	{Ly $\beta$ }	<52
PG1351+640	UGC8894		1771	27.9	12.9	274	!	+	−	143±18±3@1771	{O VI}	{H <sub>2</sub> }	<32
Mrk477	UGC9452		2173	33.9	17.1	278	!	−	−		<39	{O I}	<42
3C351.0	2MASX J170712.70 <sup>4</sup>	LGG179A	3099	45.8	7.9	280	!	−		<26	{Ly $\lim$ }	{Ly $\lim$ }	{Ly $\lim$ }
Mrk876	UGC10294		3516	52.1	27.6	282	!	+	+	267±12±3@3481	{O VI}	18±4±7@3508	{H <sub>2</sub> }
PG1216+069		LGG278	[2078] <sup>2</sup>	33.9		>283	g	+	(−)	2400±62±350@1895	1001±73±12@1880	<84	<89
Mrk1383		LGG386	[1701] <sup>2</sup>	27.9		>294	g	−		<31	{O VI}	{O VI}	{flaw}
PG0953+414	NGC3104 <sup>3</sup>		612	11.9	11.5	296	!	+	+	70±9±3@621	<23	39±8±7@637	<22
RX J1830.3+7312	UGC11331	LGG420A	1554	23.8	10.5	296	x		(−)	{Ly $\alpha$ }	{Ly $\kappa$ }	{O VI}	<56
PG1001+291	UGC5340		503	10.5	8.3	296	>	(−)	(−)	{Ly $\alpha$ }	<87	<71	{O I}
PG1351+640	UGCA375		1763	27.7	7.3	299	?	+	−	122±15±3@1447	{Ly $\delta$ }	{H <sub>2</sub> }	<33
3C351.0	NGC6306	LGG179A	3012	49.1	14.3	305	!	−		<26	{Ly $\lim$ }	{Ly $\lim$ }	{Ly $\lim$ }

Table 3—Continued

Target	Galaxy	Group	$v_{gal}$ [km s <sup>-1</sup> ]	$D$ [Mpc]	$D_{gal}$ [kpc]	$\rho$ [kpc]	Q	HI	OVI	Ly $\alpha$ [mÅ]	Ly $\beta$ [mÅ]	O VI—1031 [mÅ]	O VI—1037 [mÅ]
(1)	(2)	(3)	(4)	(5)	(6)	(7)	(8)	(9)	(10)	(11)	(12)	(13)	
PKS2155—304	ESO466—G32		5153	70.2	28.6	306	+	+	—	140±6±3@5101	43±4±8@5099	<10	{Fe II}
							+	+	—	104±7±2@4990	17±2±7@4989	<10	<11
							+	+	—	61±6±3@5164	26±3±8@5157	<10	<11
Mrk478	Mrk475		583	11.7	3.8	306	?	—	—	<14	<57	<45	<60
Mrk290	NGC5963 <sup>3</sup>	LGG396	656	12.7	12.3	307	!	(+)	—		23±10±8@720	<21	<21
Mrk817	UGC9391	GH144	1921	30.1	14.5	308	1	+	—	29±7±2@1922	<9	<19	<9
RX J1830.3+7312	NGC6654A	LGG420A	1558	23.8	18.2	308	!	+	(—)	81±6±3@1549	{Ly $\kappa$ }	{O VI}	<56
3C351.0	NGC6307	LGG179A	3185	49.1	18.8	311	!	—		<26	{LyI}	{LyI}	{LyI}
Mrk290	2MASX J153514.22 <sup>4</sup>	GH158	3092	46.5	8.0	311	x				{C II}	{O VI}	{O VI}
3C273.0		LGG287	[1655] <sup>2</sup>	27.9		>311	g	+	—	380±5±1@1580	236±2±8@1587	{O VI}	<10
3C351.0	NGC6292	LGG179A	3411	49.1	22.1	314	2	+		117±13±5@3465	{LyI}	{LyI}	{LyI}
1H0419—577		LGG114	[1481] <sup>2</sup>	19.1		>317	g	(—)	(—)		<58	{C II*}	<60
Mrk335	ESDO F538—02		2175	27.5	7.2	320	!	—	—	<39	<13	{O I}	<11
MRC2251—178	ESO603—G25		9086	125.9	38.3	322	!	+	—	54±8±2@9032	<29	{Fe II}	<31
MRC2251—178	ESO603—G27		3267	42.7	15.6	322	2	+	—	364±11±5@3212	91±9±18@3203	<27	<31
HE0340—2703	6dF J0342278 <sup>4</sup>		1738	21.9	3.2	325	x			{Ly $\alpha$ }			
3C351.0	SDSS J170327.95 <sup>4</sup>	LGG179A	3313	48.9	7.7	327	!	—		<32	{LyI}	{LyI}	{LyI}
PG0953+414	KUG0956+420		1682	27.2	4.9	332	!	—		<26	{O VI}	{O VI}	{H <sub>2</sub> }
PG1001+291	UGC5464		1011	17.9	7.2	337	1	+	(—)	267±14±5@1069	<77	<71	<66
RX J1830.3+7312	CGCG340—51	LGG420A	1469	21.9	4.3	337	!	—		<14	<65	{C II*}	{unid}
PG1626+554	NGC6182		5138	75.4	38.1	338	!	—	—		<31	<32	<29
HE1228+0131		LGG287	[1655] <sup>2</sup>	27.9		>338	g	+		623±22±4@1700	{O VI}	{O VI}	{flaw}
							g	+	(—)	156±16±10@1482	58±26±11@1476	{C II*}	<77
HE1228+0131	UGC7625		2234	36.1	9.6	339	!	+	(—)	338±21±6@2306	172±31±17@2292	<74	<71
MS0700.7+6338		LGG140	[4404] <sup>2</sup>	64.2		>356	g	+	—		209±16±29@4322	<25	<24
3C232	UGC5272		520	10.7	6.5	359	x			{Ly $\alpha$ }			
Mrk205	UGC7226		2267	34.4	13.8	362	!	—	—	<31	{H <sub>2</sub> }	<23	<20
MCG+10—16—111	CGCG291—61		3188	48.5	14.4	367	!	+		102±12±3@3113			
HE1143—1810	ESO571—G18		1391	23.4	7.5	368	!	—	—		<47	{C II}	<41
RX J1830.3+7312	NGC6690 <sup>3</sup>		488	7.8	8.7	370	x		(—)	{Ly $\alpha$ }	{O I*}	<67	<55
PG0844+349	UGC4621		2306	35.5	10.3	372	+	+	—		64±5±3@2260	<17	<18
							+	+	—		29±6±3@2326	{C III}	<18
Ton S210	NGC253 <sup>3</sup>	LGG4	251	2.6	20.7	374	!	—	+	{Ly $\alpha$ }	<20	25±8±7@288	{H <sub>2</sub> }

Table 3—Continued

Target	Galaxy	Group	$v_{gal}$ [km s <sup>-1</sup> ]	$D$ [Mpc]	$D_{gal}$ [kpc]	$\rho$ [kpc]	Q	HI	OVI	Ly $\alpha$ [mÅ]	Ly $\beta$ [mÅ]	O VI–1031 [mÅ]	O VI–1037 [mÅ]
(1)	(2)	(3)	(4)	(5)	(6)	(7)	(8)	(9)	(10)	(11)	(12)	(13)	
IRAS09149–6206	IRAS09168–6141		3184	46.0		374	!	–			{C II}	<31	{Ar I}
IRAS09149–6206	ESO091–G07	LGG488	2266	37.2	20.1	377	!	–			{C III}	{O I}	<31
PG0838+770		LGG165	1370	21.0		>380	g	(–)	(–)		<55	{H <sub>2</sub> }	<51
HE1228+0131	NGC4517 <sup>3</sup>	LGG292	1121	17.7	53.8	383	>	(–)	(–)	<64	<80	<74	<75
Mrk734	2MASX J112139.77 <sup>4</sup>		5944	89.0	6.2	388	>	(–)	(–)		<77	<79	<87
PG0953+414	Mrk1427		2129	33.5	3.9	390	!	–	–	{Ly $\beta$ }	<17	{O I}	<17
PG0844+349	SDSS J084619.14 <sup>4</sup>		2368	36.3	3.8	391	!	–	–		<18	{C III}	<18
PG1302–102	MCG–2–34–6		1213	21.2	18.2	391	2	+	–	84±24±4@1045	<25	<22	{H <sub>2</sub> }
PG1049–005	UGC5922		1846	30.2	9.2	391	>	(–)		<75			
Mrk335	NGC7817 <sup>3</sup>		2309	29.4	30.4	395	!	+	–	114±17±2@2286	<13	<13	<11
1H0419–577	NGC1533		790	9.2	7.4	396	>	(–)	(–)		<140	{Ly $\epsilon$ }	<57
Mrk478	UGC9540		802	14.8	4.3	400	!	–	–	<16	<60	<46	<53
3C351.0	NGC6310	LGG179A	3386	49.1	28.5	402	!	–		<30	{Ly $\lim$ }	{Ly $\lim$ }	{Ly $\lim$ }
PG1626+554	NGC6143		1595	24.8	6.9	403	!		–		{H <sub>2</sub> }	{O VI}	<32
ESO141–G55	ESO141–G51		3497	48.6	14.2	410	!	–	–	<46	{O VI}	<22	{H <sub>2</sub> }
MRC2251–178	ESO603–IG23		3282	42.9	12.5	412	2	+	–	65±8±6@3046	{C II}	<28	{Ar I}
Mrk1513	UGC11782		1111	13.0	8.4	412	!	–	–	<15	<25	<24	<32
Mrk817	SDSS J143146.90 <sup>4</sup>		1496	24.1	4.8	413	!	–			<8	{C II*}	<10
PG1011–040	IC600		1309	22.2	15.1	417	!	–	–		<24	{C II}	<24
Mrk477	NGC5751		3242	49.1	21.6	419	!	–	–		<41	{flaw}	<46
PG0844+349	KUG0847+350		2354	36.2	4.0	421	!	–	–		<18	{C III}	<18
Mrk9	UGC3943	LGG143	3527	50.2	24.8	422	!		–		{O VI}	<34	{H <sub>2</sub> }
MRC2251–178	ESO603–G31		2271	28.5	9.1	422	!	+	(+)	133±12±3@2265	{Ly $\gamma$ }	{O I*}	40±12±9@2283
Mrk290	NGC5987	GH158	3010	42.7	51.7	424	!		+		{C II}	49±8±7@3073	20±8±7@3073
HE1029–1401	6dF J1033307 <sup>4</sup>		2475	38.7	10.1	427	!	+		168±9±3@2457			
3C273.0	2MASX J122815.85 <sup>4</sup>	LGG281	2286	36.9	5.0	429	2	+	–	31±7±1@2274	<9	<10	<10
Ton S180	NGC45	Scl	468	2.5	6.3	437	!	–	–	<13	<41	<28	{O I}
HE1143–1810	[KKS2000]25		1227	23.4	7.4	437	!	–	–		<52	{C II}	<45
PG0804+761	UGC4527		721	11.8	4.7	438	!	–	–	<10	{O I*}	<11	<11
PG1049–005	IC653	LGG205	5538	83.5	45.2	438	>	(–)		<94			
Mrk817	SBS1430+596	GH144	1855	29.1	6.6	441	1	–	–	<17	{O VI}	<19	<9
PG1149–110	MCG–2–30–33		1273	22.0	5.1	442	!	(–)		<109			
Mrk290	SDSS J153802.76 <sup>4</sup>		3525	52.7	8.6	444	!	–	–		<22	<19	{H <sub>2</sub> }

Table 3—Continued

Target	Galaxy	Group	$v_{gal}$ [km s <sup>-1</sup> ]	$D$ [Mpc]	$D_{gal}$ [kpc]	$\rho$ [kpc]	Q	HI	OVI	Ly $\alpha$ [mÅ]	Ly $\beta$ [mÅ]	O VI–1031 [mÅ]	O VI–1037 [mÅ]
(1)	(2)	(3)	(4)	(5)	(6)	(7)	(8)	(9)	(10)	(11)	(12)	(13)	
PG1444+407	UGC9497		633	12.2	4.0	445	!	–	(–)	<35		<89	
PG0953+414	KUG0952+418		4695	70.2	9.2	449	+	+	–	55±10±1@4670	<22	{Ar I}	<17
							+	+	–	160±12±1@4807	<21	<18	<18
							+	+	–	120±10±1@4961	<17	<17	<17
Mrk106	NGC2841 <sup>3</sup>	GH44	638	5.9	13.9	453	>		(–)		{O I*}	{Ly $\beta$ }	<51
3C249.1	UGC6154		5156	75.5	21.5	457	!	–		<29	<27	{H <sub>2</sub> }	{Fe II}
MCG+10–16–111	NGC3556 <sup>3</sup>	GH94	695	10.2	25.8	462	!	+		173±14±4@942			
PG0838+770	UGC4623		2885	42.7	44.1	467	>	(–)	(–)		<57	<52	<52
PG1302–102	NGC4920	LGG307	1336	22.9	6.8	473	2	+	–	284±30±2@1316	221±8±7@1312	{C II}	<31
PG1049–005	CGCG10–41		1810	29.7	4.5	475	>	(–)		<78			
Mrk771	NGC4826		408	4.6	13.3	479	!	–	(–)	<11	<116	<105	{O I}
1H0707–495	ESO207–G22		1029	14.4	5.0	482	!	+	–		26±7±8@1302	{C II}	<34
IRAS09149–6206	NGC2842	LGG488	2857	37.2	16.7	485	!	–	(–)		<33	<61	{H <sub>2</sub> }
Mrk876	UGC10369		998	16.0	5.9	493	!		–	{Ly $\alpha$ }	{Ly $\beta$ }	<12	{H <sub>2</sub> }
Mrk734	NGC3692		1726	10.0	9.2	497	>	(–)	(–)		<75	<71	<69
RX J0048.3+3941	UGC578		1471	18.4	5.9	499	!		–		{O VI}	{C II*}	<23
Mrk734	SDSS J111938.66 <sup>4</sup>		3054	47.7	5.3	500	>		(–)		{C II}	<72	{Ar I}
Mrk290	CGCG297–17	GH158	3282	49.2	8.7	501	!		–		{C II*}	{flaw}	<18
Mrk771	NGC4561	LGG289	1403	22.6	9.9	502	1	+	(–)	321±13±2@1184	<109	<95	<89
3C249.1	UGC5854		1808	27.6	7.8	505	1	–	–	<29	{O VI}	{H <sub>2</sub> }	<26
PG1216+069		LGG288	505	11.5		>506	>		(–)	{Ly $\alpha$ }	{O I*}	<86	{O I*}
Mrk817	UGC9477		2325	35.8	7.7	508	!	–	–	<15	<9	<20	{flaw}
Mrk110	NGC2681	GH44	692	5.9	6.2	513	>	(–)		<71			
Mrk501	CGCG225–6		4648	68.3	10.7	517	1	(–)	–	<53	<72	<37	<37
Mrk501	NGC6257		4692	68.9	18.4	521	1	+	–	150±26±4@4593	<71	<36	<39
PG1149–110	NGC3892	LGG248	1697	28.3	24.3	529	!	+		437±69±73@1665			
ESO438–G09	NGC3621		727	6.6	23.8	530	>	–		<56			
3C351.0	UGC10770		1108	17.3	5.9	531	!	–		<30	{Ly $\lim$ }	{Ly $\lim$ }	{Ly $\lim$ }
Mrk421	NGC3432 <sup>3</sup>		616	10.8	21.3	538	!	–	–		<15	<11	<11
3C249.1	UGC5841		1766	27.0	12.2	538	!	–	–	<29	{O VI}	{H <sub>2</sub> }	<26
Mrk290	SDSS J153733.02 <sup>4</sup>	GH158	2932	44.2	9.6	540	!		–		{C II}	<20	<18
PG1149–110	MCG–2–30–39		1483	25.0	13.6	541	!	(–)		<126			
HE0226–4110	NGC986A		1406	16.7	8.6	542	!	–	–	<31	<21	{C II–HVC}	<18



Table 3—Continued

Target	Galaxy	Group	$v_{gal}$ [km s <sup>-1</sup> ]	$D$ [Mpc]	$D_{gal}$ [kpc]	$\rho$ [kpc]	Q	HI	OVI	Ly $\alpha$ [mÅ]	Ly $\beta$ [mÅ]	O VI–1031 [mÅ]	O VI–1037 [mÅ]
(1)	(2)	(3)	(4)	(5)	(6)	(7)	(8)	(9)	(10)	(11)	(12)	(13)	
BC249.1	NGC3329 <sup>5</sup>		1812	27.7	14.3	543	1	+	–	40±9±3@1861	{O VI}	{H <sub>2</sub> }	<27
PG1116+215	UGC6258		1454	24.8	14.4	543	!	+		91±10±2@1479	<14	{C II*}	{Ly $\xi$ }
HE0340–2703	ESO482–G46		1525	19.0	18.7	543	>	(–)		<69			
Mrk817	NGC5667	GH144	2001	30.8	15.2	549	1	–	–	<16	<9	{O I}	<9
PKS0558–504	ESO205–G34		1026	13.8	5.2	552	!	–	–	<21	<21	<20	{H <sub>2</sub> }
Mrk478	UGC9519	GH147	1692	23.1	5.3	554	1	–	–	<17	{O VI}	<41	<57
Mrk817	NGC5678 <sup>3</sup>	GH144	1922	30.8	29.7	556	1	–	–	{Ly $\alpha$ }	<9	<19	<9
Fon S180	2MASX J005700.66 <sup>4</sup>		2657	33.8	4.9	560	!	+	–	38±10±1@2792	<27	<26	<28
HE0226–4110	NGC954 <sup>3</sup>	LGG62	5353	69.9	33.0	562	!	+	+	60±7±2@5235	{flaw}	41±6±4@5240	{O IV}
Mrk290	SBS1533+574	GH158	3310	49.6	7.1	563	!		–		{C II*}	{flaw}	<17
Mrk1095	UGC3303		522	6.4	6.8	571	!		–		{O I*}	<31	{O I}
Mrk876	UGC10194		870	14.4	6.9	573	!	–	–	{Ly $\alpha$ }	<13	<12	<16
ESO438–G09	2MASX J111343.40 <sup>4</sup>		2100	33.1	4.8	577	!	+		265±30±13@2215			
Mrk106	NGC2681		692	5.9	6.2	581	!		–		{O I*}	<32	<56
PG1259+593	UGC8046		2572	39.7	11.8	584	1	–	–	<25	<14	{O I*}	<14
IRAS09149–6206	RKK1037	LGG488	2242	32.5		585	!	–	(–)		{C III}	{O I}	<31
BC351.0	SDSS J170349.45 <sup>4</sup>		5183	75.6	6.6	594	!	+		182±10±4@5175	{Ly $\lim$ }	{Ly $\lim$ }	{Ly $\lim$ }
PG1259+593	UGC8040		2522	39.0	16.8	595	1	+	–	291±11±1@2275	67±6±2@2269	{O VI@643}	<13
HE1143–1810	NGC3887		1209	20.9	20.2	596	!	–	–		<51	<47	<46
PG1216+069	NGC4296		4227	64.6	25.4	596	!	–	(–)	<36	<82	<83	<84
PKS2005–489	ESO233–G37		4950	68.8	26.4	599	2	+	–	307±5±6@4973	46±7±7@4959	<20	<20
RX J0048.3+3941	UGC655		829	9.4	6.9	602	!		–		<36	<25	{H <sub>2</sub> }
Mrk509	NGC6985A		5777	80.0	30.7	607	!	–	–	{N V}	<12	<12	<11
PG1216+069		LGG287	[1655] <sup>2</sup>	27.9		>607	g	(–)		{Ly $\alpha$ }	<89	{O VI}	{flaw}
IRAS F22456–5125	ESO238–G05		706	7.0	5.9	616	!	(–)	–		<63	<45	<56
MCG+10–16–111		LGG244	[1230] <sup>2</sup>	20.5		>616	!	–		<30			
Mrk734	IC2763		1574	26.6	10.4	617	>	(–)	(–)		<73	{O VI}	<94
VII Zw118	UGC3648	LGG140	4530	65.9	25.9	620	1	+	–	64±16±2@4613	<37	<19	<19
MCG+10–16–111	UGC6249	GH94	1058	17.9	8.1	620	2	–		<28			
BC351.0	Ark514	LGG179A	3736	55.0	10.1	624	!	–		<29	{Ly $\lim$ }	{Ly $\lim$ }	{Ly $\lim$ }
PKS0558–504	NGC2104 <sup>3</sup>		1181	15.7	9.1	626	!	–	–		<21	{C II}	<25
BC263	NGC3682		1543	24.5	11.8	626	!	–	–		<31	{C II*}	<31
PG1351+640	UGCA374	GH122	2133	33.1	8.6	631	!	–	(–)	<35	<24	{O I}	<52

Table 3—Continued

Target	Galaxy	Group	$v_{gal}$ [km s <sup>-1</sup> ]	$D$ [Mpc]	$D_{gal}$ [kpc]	$\rho$ [kpc]	Q	HI	OVI	Ly $\alpha$ [mÅ]	Ly $\beta$ [mÅ]	O VI—1031 [mÅ]	O VI—1037 [mÅ]
(1)	(2)	(3)	(4)	(5)	(6)	(7)	(8)	(9)	(10)	(11)	(12)	(13)	
3C351.0	SDSS J170112.68 <sup>4</sup>	LGG179A	3788	55.7	6.8	632	!	—		<29	{Ly $\lim$ }	{Ly $\lim$ }	{Ly $\lim$ }
PKS2155—304	ESO466—G29	LGG450	2772	36.2	15.8	633	!	—	—	<20	<9	<11	<10
3C263	UGC6448	GH94	991	16.8	5.1	634	!	—	—		<32	<29	<55
PG1444+407	UGC9502		5672	84.3	27.9	637	!	+	(—)	103±11±4@5638	<80	<86	<85
RX J1830.3+7312	NGC6643	LGG420A	1489	23.8	26.4	638	!	—		<14	<62	{H <sub>2</sub> }	{unid}
PG1149—110	LCRS B115151.0 <sup>4</sup>		3009	46.8	20.4	640	!	(—)		<118			
3C249.1	UGC5814		1881	28.6	13.3	641	!		—	{Ly $\alpha$ }	{O VI}	{H <sub>2</sub> }	<27
PG1149—110	LCSB S1630P		1971	32.0	11.2	642	!	(—)		<125			
PG1216+069	NGC4246		3725	57.5	40.1	644	!		(—)	{Ly $\alpha$ }	{H <sub>2</sub> }	<74	<85
Mrk478	NGC5727 <sup>3</sup>		1491	24.7	16.1	645	1	+	—	254±14±2@1573	<44	<42	<47
PKS2155—304	2dF GRSS407Z162	LGG450	2832	36.2	6.5	648	!	—	—	<20	<9	<11	<10
PG1302—102	MCG—2—33—95		2753	43.2	17.4	657	!	—	—	<77	<23	<30	<23
PG1302—102	MCG—2—33—75		1247	21.7	6.8	658	!	—	—	<78	<24	{C II}	<30
3C232	UGC5340		503	10.5	8.3	660	x			{Ly $\alpha$ }			
ESO141—G55	IC4843		3975	55.5	24.2	662	!	—	—	<38	{O I}	<22	{H <sub>2</sub> }
Mrk279	UGC8737		1873	29.1	19.0	664	!	—	—	<15	{O VI}	<9	<9
ESO185—IG13	2MASX J194221.91 <sup>4</sup>		2998	41.3	8.4	672	>		(—)		{C II}	<84	{Ly $\beta$ }
Mrk335	UGC44		5936	81.2	21.5	675	!	—	—	<24	<12	<10	<9
1H0717+714	UGC3909 <sup>3</sup>		945	14.8	11.3	677	!		—		{H <sub>2</sub> }	<23	<41
PG1011—040	LCRS B101019.9 <sup>4</sup>		3395	51.9	9.8	680	!		—		{H <sub>2</sub> }	<22	{H <sub>2</sub> }
PG1216+069	IC3136		5594	84.2	28.8	684	!	—	(—)	<32	<72	<92	<93
PG1049—005	UGC6011	LGG205	5547	83.5	33.5	685	>	(—)		<93			
PG1001+291	UGC5478		1378	23.1	11.2	686	!	—	(—)	<35	<74	{H <sub>2</sub> }	<65
PG1216+069	NGC4257		2756	43.6	16.0	689	!	—	(—)	<36	<87	<98	<86
PG1049—005	UGC5943		4544	68.7	22.4	689	>	(—)		<87			
Mrk876	NGC6135		3644	53.9	14.1	690	!	—	—	<30	{H <sub>2</sub> }	{H <sub>2</sub> }	<14
PG1259+593	NGC4814 <sup>3</sup>		2513	38.9	35.0	694	1	—	—	<24	<14	<14	<14
Mrk335	UGC12893		1108	12.1	6.0	697	?	+	—	57±9±3@1308	<14	{H <sub>2</sub> }	<12
Mrk501	UGC10625		2048	31.1	11.7	700	!	—	—	<21	<36	{O I}	<36
1H0419—577		LGG119	[1266] <sup>2</sup>	16.4		>700	g	(—)			<53	{C II}	{OI*}
Ton S210	NGC45	Scl	468	2.5	6.3	702	!	—	—	{Ly $\alpha$ }	<42	<21	{O I}
3C351.0	UGC10745	LGG179A	3059	45.2	13.1	710	!	—		<26	{Ly $\lim$ }	{Ly $\lim$ }	{Ly $\lim$ }
PKS2155—304	MCG—5—52—1	LGG450	2540	36.2	6.2	718	!	—	—	<21	<9	<11	<10

Table 3—Continued

Target	Galaxy	Group	$v_{gal}$ [km s <sup>-1</sup> ]	$D$ [Mpc]	$D_{gal}$ [kpc]	$\rho$ [kpc]	Q	HI	OVI	Ly $\alpha$ [mÅ]	Ly $\beta$ [mÅ]	O VI–1031 [mÅ]	O VI–1037 [mÅ]
(1)	(2)	(3)	(4)	(5)	(6)	(7)	(8)	(9)	(10)	(11)	(12)	(13)	
PKS2155–304	ESO466–G43	LGG450	2608	33.9	14.8	719	!	–	–	<20	<9	<11	<10
Mrk290	NGC5981		1764	27.5	22.5	725	!	–	–		{O VI}	{H <sub>2</sub> }	<20
HS0624+6907	UGC3580 <sup>3</sup>		1201	18.2	18.0	729	!	–	(–)	<29	<40	{C II}	<66
PG1001+291	UGC5272		520	10.7	6.5	731	>	(–)	(–)	{Ly $\alpha$ }	<87	<70	{O I}
Mrk290	NGC5907 <sup>3</sup>	LGG396	667	13.4	49.1	734	!	–	–		{H <sub>2</sub> }	<22	<22
PKS0558–504	NGC2101		1192	15.8	9.0	734	!	–	–		<21	{C II}	<25
Fairall9	NGC484	LGG19	5200	69.0	39.1	735	!	–	(–)	<19	{H <sub>2</sub> }	<77	<75
VIIZw118	UGC3642 <sup>3</sup>	LGG140	4498	64.2	28.2	738	1	–	–	<26	{H <sub>2</sub> }	<19	{H <sub>2</sub> }
IRAS09149–6206	ESO091–G02		3045	43.9		740	!	–	–		{C II}	<32	{Ar I}
IRAS09149–6206	IRAS09106–6258	LGG488	2997	43.2		741	!	–	–		{C II}	<32	<33
PKS2155–304	2dF GRSS408Z175	LGG450	2679	36.2	6.7	741	!	–	–	<20	<9	<11	<10
PG1216+069	NGC4247		3838	59.1	18.8	742	2	(–)	(–)	{Ly $\alpha$ }	<78	<79	<83
Mrk477	NGC5687		2119	33.1	23.1	743	!	–	–		<38	{O I}	<41
Mrk477	KUG1437+524		2181	34.1	9.6	743	!	–	–		<39	{O I}	<42
3C263	UGC6390	GH94	1008	17.0	10.3	747	!	–	–		<31	<29	<54
Mrk478	UGC9562	GH147	1253	23.1	6.4	748	!	–	(–)	<17	<45	{C II}	<58
PG1011–040	MCG–1–26–12		662	12.7	10.4	750	!	–	–		{H <sub>2</sub> }	<23	<25
Mrk110	UGC4913		2371	36.4	13.7	751	>	–	–	<68			
VIIZw118	UGC3748		2479	36.6	12.2	753	!	+	–	333±16±2@2438	70±8±7@2444	{H <sub>2</sub> }	<21
PG0953+414	NGC3184		593	23.4	23.4	758	!	–	–	{Ly $\alpha$ }	<22	{O VI}	<22
HE1228+0131	MCG0–32–15		6948	103.5	26.2	756	!	–	(–)	<45	<75	<75	<72
Mrk477	SBS1436+529B		3389	51.3	10.0	761	x				{O VI}	{flaw}	{H <sub>2</sub> }
ESO141–G55	IC4824		953	12.4	9.7	769	!		–		{H <sub>2</sub> }	{H <sub>2</sub> }	<28
3C273.0	UGC7625		2234	36.1	9.6	771	2	+	–	20±5±1@2160	<9	{O I}	<10
Mrk106	CGCG265–14		3334	50.1	13.1	772	x				{O VI}	{flaw}	{H <sub>2</sub> }
Ton S180	ESO541–G05		1958	23.8	8.3	774	1	+	–	54±10±2@1939	<27	{O VI}	<27
Ton S180	ESO474–G45		1863	18.6	7.2	777	1	–	–	<22	{O VI}	<28	<29
PG1302–102	MCG–2–33–97		2705	42.5	14.9	782	!	–	–	<79	<23	<29	<23
PKS2005–489	2MASX J200943.13 <sup>4</sup>		5116	71.2	16.6	787	2	+		330±3±6@5071	170±9±8@5079	{H <sub>2</sub> }	{Fe II}
PHL1811	SDSS J215446.45 <sup>4</sup>		5498	75.1	12.0	787	!	+	–	35±3±2@5402	{Ly $\gamma$ }	{H <sub>2</sub> }	<20
ESO141–G55	ESO141–G42		935	12.1	10.6	790	!		–		{H <sub>2</sub> }	{H <sub>2</sub> }	<28
Mrk876	UGC10376		3246	48.1	19.3	799	!	–	–	<31	{C II}	{C II*}	{H <sub>2</sub> }
Fairall9	ESO113–G35	LGG19	5063	69.0	19.6	799	!	–	(–)	<19	<67	<75	{Fe II}

Table 3—Continued

Target	Galaxy	Group	$v_{gal}$ [km s <sup>-1</sup> ]	$D$ [Mpc]	$D_{gal}$ [kpc]	$\rho$ [kpc]	Q	HI	OVI	$Ly\alpha$ [mÅ]	$Ly\beta$ [mÅ]	O VI–1031 [mÅ]	O VI–1037 [mÅ]
(1)	(2)	(3)	(4)	(5)	(6)	(7)	(8)	(9)	(10)	(11)	(12)	(13)	
Fairall9	ESO115–G21		513	4.8	6.8	799	!		(–)			<57	{OI*}
PG0838+770	UGC4238 <sup>3</sup>		1544	23.4	16.3	803	!	(–)	(–)		<54	<48	<49
Mrk501	NGC6239 <sup>3</sup>		922	15.1	11.3	807	!	–	–		<36	<38	<74
IRAS09149–6206	ESO126–G10		2152	31.3	15.8	808	!	–	(–)		{C III}	{OI}	<32
RX J0048.3+3941	CGCG535–25		4001	54.6	9.5	810	!		–		{OI}	<24	{H <sub>2</sub> }
HE1143–1810	ESO572–G06	LGG263	1737	28.4	9.9	811	!	–	–		<46	{O VI}	<42
NGC985	SDSS J023305.84 <sup>4</sup>		5680	77.5	5.9	811	!	–	–	{N V}	<29	{H <sub>2</sub> }	<28
PG1149–110	PGC37027		2379	37.9	14.5	812	!			<156			
PG0844+349	NGC2649		4244	63.1	29.1	814	!		–		{C III}	<18	<18
PG1444+407	SDSS J145001.59 <sup>4</sup>		4814	72.0	8.0	817	!	–	(–)	<32		<84	<88
PG1302–102	NGC4933		2965	46.2	34.9	820	!	–	–	<77	<24	<30	<24
PG1341+258	CGCG132–10		3188	49.5	6.9	825	!	–		<36			
PG0844+349	UGC4660		2203	34.1	11.6	826	!		–		{O VI}	<16	<18
PKS2155–304	ESO466–G36	LGG450	2380	33.8	12.7	829	!	–	–	<24	<9	<11	<10
PG0804+761	UGC3909 <sup>4,5</sup>		945	14.8	11.3	829	?	+	–	159±7±2@1144	52±10±2@1119	{C II}	<31
PG1302–102	MCG–1–33–60	LGG307	1487	22.4	20.1	830	!	–	–	<79	<24	{H <sub>2</sub> }	<24
Mrk110	UGC4906		2322	35.6	20.7	834	>	(–)		<67			
ESO438–G09	ESO438–G15		3353	50.9	29.6	838	>	(–)		<69			
PG0804+761	UGC4466	LGG165	1416	21.0	8.4	839	!	–	–	<16	<13	{H <sub>2</sub> }	<11
3C351.0	SDSS J171138.94 <sup>4</sup>	LGG179A	3855	56.6	6.3	839	!	–		<29	{LyIim}	{LyIim}	{LyIim}
PG1216+069	IC773		5477	82.5	26.9	841	!	–	(–)	<32	<80	<83	<92
PKS0558–504	ESO205–G07		2000	27.4	7.0	841	!	–	–		<21	{H <sub>2</sub> }	<20
VIIZw118	UGC3660	LGG140	4262	64.2	31.0	845	1	–	–	<26	{H <sub>2</sub> }	<20	<19
3C249.1	UGC5701		1621	24.9	9.5	845	!	–	–	<28	{H <sub>2</sub> }	{O VI}	<31
MRC2251–178	MCG–3–58–13		3271	42.8	10.0	846	!		–	{Lyα}	{C II*}	<35	<32
Mrk290	NGC5879 <sup>3</sup>	LGG396	772	13.4	16.2	848	!	–	–		<35	<21	{H <sub>2</sub> }
HE1143–1810	ESO571–G16		3637	55.6	26.8	851	!		–		{H <sub>2</sub> }	<43	<37
PG1011–040	2MASX J101213.26 <sup>4</sup>		5619	83.7	20.2	852	!	–	–		<24	<22	<24
MRC2251–178	NGC45	Scl	468	2.5	6.3	852	x			{Lyα}	{OI*}	{Lyγ}	{OI}
Mrk501	NGC6255 <sup>3</sup>		918	15.0	15.8	854	!	–	–		<36	<38	<75
3C249.1	CGCG351–57 <sup>5</sup>		6755	98.3	14.3	858	!	+	+	245±15±3@6672	34±12±3@6653	<27	{H <sub>2</sub> }
H1821+643	NGC6690 <sup>3</sup>		488	7.8	8.7	858	!		–	{Lyα}	{OI*}	<15	{OI}
Mrk279	NGC5832 <sup>3</sup>		453	8.4	9.1	861	!	–	–	<11	<19	<10	{OI}

Table 3—Continued

Target	Galaxy	Group	$v_{gal}$ [km s <sup>-1</sup> ]	$D$ [Mpc]	$D_{gal}$ [kpc]	$\rho$ [kpc]	Q	HI	OVI	Ly $\alpha$ [mÅ]	Ly $\beta$ [mÅ]	O VI–1031 [mÅ]	O VI–1037 [mÅ]
(1)	(2)	(3)	(4)	(5)	(6)	(7)	(8)	(9)	(10)	(11)	(12)	(13)	
PG1302–102	MCG–2–33–85	LGG307	1582	22.4	11.6	863	!	–	–	{Ly $\beta$ }	{H <sub>2</sub> }	{O VI}	<26
IRAS09149–6206	ESO091–G12	LGG488	2866	37.2	10.8	863	!	–	(–)		<33	<58	<30
IRAS09149–6206	ESO091–G03	LGG488	1906	37.2	23.6	865	!		(–)		{C III}	{H <sub>2</sub> }	<35
ESO141–G55	IC4826		1925	26.3	10.5	865	!	(–)	–	<83	{H <sub>2</sub> }	{H <sub>2</sub> }	<23
HE1228+0131	NGC4385	LGG283	2140	34.2	21.8	866	!	(–)	(–)	<58	<69	{O I}	<64
ESO141–G55	IC4819		1841	25.1	21.1	868	!	(–)	–	<87	{O VI}	{H <sub>2</sub> }	<22
Ton S210	NGC613 <sup>3</sup>		1475	17.1	27.4	872	!	–	–	<64	<21	{C II*}	<19
PG0804+761	UGC4202		2296	34.2	12.0	875	!	+	–	28±7±2@2282	{Ly $\epsilon$ }	<31	<12
Ton S180	NGC24	LGG4	554	4.5	7.5	876	!	–	–	<16	<39	<28	<26
Mrk9	UGC3897	LGG143	3529	51.8	19.4	877	!		–		{O VI}	<34	{H <sub>2</sub> }
ESO141–G55	ESO141–G46	LGG427	4079	57.0	23.2	878	!	–	–	<37	<24	<22	<22
Mrk106	UGC4984		3386	50.8	15.5	881	x				{O VI}	{flaw}	{H <sub>2</sub> }
PG1302–102	UGCA307		824	15.6	9.1	882	!	–	–	<67	<33	<23	<24
HE1143–1810	ESO572–G09	LGG263	1737	27.3	12.9	884	!	–	–		<46	{O VI}	<42
1H0717+714	UGC3921		2475	36.6	11.7	888	!	–	–		<24	{H <sub>2</sub> }	<23
ESO141–G55	ESO142–IG08		4292	59.9	7.0	889	!	–	–	<35	{H <sub>2</sub> }	<23	<22
PG1116+215	NGC3501		1134	10.0	11.3	889	!	–	–	<25	<14	<14	<14
PG1116+215	UGC6324		1083	19.6	9.9	894	!	–	–	<25	<14	<15	<15
Mrk9	UGC4121 <sup>3</sup>		1092	17.3	11.8	895	!	–	–		<33	<32	<70
Mrk501	NGC6207		850	14.2	12.2	895	!	–	–		<39	<36	<75
PG1444+407	SDSS J145045.59 <sup>3,5</sup>		2582	40.1	4.2	897	!	+	(–)	95±14±4@2630	<85	<145	<80
PG1011–040	NGC3115		658	12.6	26.6	900	!		–		{H <sub>2</sub> }	<23	<25
PG1302–102	UGCA312	LGG307	1307	22.5	8.6	900	!		–	{Ly $\alpha$ }	{Ly $\beta$ }	{C II}	<24
1H0717+714	UGC3580 <sup>3</sup>		1201	18.2	18.0	900	!	–			<25	{C II}	{O I*}
PG1302–102	NGC4802	LGG307	1013	18.3	12.8	901	!	–	–	{Ly $\alpha$ }	<24	<23	{H <sub>2</sub> }
RX J0100.4–5113	ESO151–G19		1386	16.6	6.5	902	!	–	–	<62	<45	<27	<38
1H0717+714	IC2184		3605	52.8	12.8	903	!		–		{H <sub>2</sub> }	<23	{H <sub>2</sub> }
Mrk9	UGC3885	LGG143	3809	51.0	15.3	904	!		–		{H <sub>2</sub> }	<33	{H <sub>2</sub> }
PG0804+761	NGC2591	LGG165	1323	21.0	18.5	907	!	–	–	<16	<13	{C II}	<11
Mrk290	NGC5866B	LGG396	844	13.4	10.5	907	!	–	–		<37	<22	<22
PG1149–110	Mrk1309		1715	28.4	13.2	909	x			{Ly $\alpha$ }			
HE0340–2703	2MASX J034134.24 <sup>4</sup>		4125	56.0	10.9	913	x			{Ly $\alpha$ }			
1H0707–495	ESO207–G09		1159	16.1	8.0	914	!	–	–		<27	{C II}	<36

Table 3—Continued

Target	Galaxy	Group	$v_{gal}$ [km s <sup>-1</sup> ]	$D$ [Mpc]	$D_{gal}$ [kpc]	$\rho$ [kpc]	Q	HI	OVI	Ly $\alpha$ [mÅ]	Ly $\beta$ [mÅ]	O VI–1031 [mÅ]	O VI–1037 [mÅ]
(1)	(2)	(3)	(4)	(5)	(6)	(7)	(8)	(9)	(10)	(11)	(12)	(13)	
Mrk335	NGC7798 <sup>3</sup>		2404	30.8	12.4	915	!	–	–	<39	<13	<12	<11
PG1553+113	UGC10014		1121	18.9	7.1	916	!	–	–		<35	<32	<30
PG1341+258	NGC4826		408	4.6	13.3	924	x			{Ly $\alpha$ }			
1H0717+714	UGC3940		2462	36.6	14.7	927	!	–	–		<23	{H <sub>2</sub> }	<23
PG1302–102	DDO163	LGG314	1123	20.0	11.0	930	!	–	–	<85	<25	<23	<32
ESO438–G09	ESO438–G14		2130	33.4	7.8	932	!	(–)		<100			
HS0624+6907	UGC3403		1264	18.9	12.6	932	!	–	(–)	<28	<39	{C II}	<70
Mrk279	FGC1680		3865	57.5	14.1	937	!	–	–	<11	{OI}	<9	<8
ESO438–G09	2MASX J110443.60 <sup>4</sup>		2391	37.1	8.6	939	!	(–)		<103			
MS0700.7+6338	UGC3685		1797	26.9	25.9	941	!		–		{O VI}	{H <sub>2</sub> }	<24
Ton S210	ESO413–G02		5588	75.8	17.9	942	!	–	–	<57	<18	<19	<19
HE0340–2703	ESO419–G03		4109	55.8	26.9	942	1	+		167±26±5@4100			
PG1049–005	NGC3365		986	17.9	23.2	943	>	(–)		<62			
3C263	NGC3945 <sup>3</sup>	GH94	1220	10.2	15.6	950	!	–	–		<32	{C II}	<28
3C263	UGC6534	GH94	1273	20.9	15.2	955	!	–	–		<30	{C II}	<29
HE0226–4110	NGC986 <sup>3</sup>		2005	25.4	28.6	955	!	–	–	<32	{O VI}	<28	<18
MCG+10–16–111	UGC6335		2927	44.7	20.6	957	!	–		<24			
3C263	UGC7490		467	9.0	8.7	961	!		–			<29	{OI}
PG1049–005	NGC3521 <sup>3</sup>		805	15.4	49.2	962	!	–		<44			
PG0844+349	UGC4704		596	11.1	13.2	967	!	–	–		<30	<19	<18
Mrk586	NGC851		3111	40.8	11.9	967	!		–		{C II}	<30	<31
HE0226–4110	ESO298–G15 <sup>3</sup>		1415	16.7	9.3	969	!	–	–	<31	<20	{C II}	<18
HE0340–2703	NGC1406		1075	12.5	13.8	972	>	(–)		<69			
HE0340–2703	NGC1425		1510	18.7	31.6	974	>	(–)		<68			
HE1143–1810	ESO572–G07	LGG263	1466	24.5	9.3	976	!	–	–		<47	{C II*}	<43
PKS2155–304	NGC7163	LGG450	2875	33.8	19.2	979	!	–	–	<20	<9	<11	<10
HE0226–4110	ESO299–IG01		5366	73.3	10.7	980	!	–	–	<25	<18	<27	<20
RX J1830.3+7312	UGC11193		1513	22.6	8.9	985	!	–		<14	{Ly $\kappa$ }	{H <sub>2</sub> }	{unid}
ESO185–IG13	ESO185–G03		3031	41.8	14.6	985	>		(–)		{C II}	<89	{Ly $\beta$ }
PG1302–102	UGCA308	LGG307	1322	22.8	9.4	986	!		–	{Ly $\alpha$ }	{Ly $\beta$ }	{C II}	<24
PG1302–102	NGC4818 <sup>3</sup>	LGG307	1065	19.2	24.0	987	!	–	–	{Ly $\alpha$ }	<26	<23	<31
PG1302–102	NGC4948A	LGG314	1553	23.7	10.5	991	!	–	–	<82	<23	<22	<23
NGC985	DDO23	LGG59	2110	25.8	15.3	993	?	(+)	–	69±20±2@1924	<31	<29	<30

Table 3—Continued

Target	Galaxy	Group	$v_{gal}$ [km s <sup>-1</sup> ]	$D$ [Mpc]	$D_{gal}$ [kpc]	$\rho$ [kpc]	Q	HI	OVI	Ly $\alpha$ [mÅ]	Ly $\beta$ [mÅ]	O VI–1031 [mÅ]	O VI–1037 [mÅ]
(1)	(2)	(3)	(4)	(5)	(6)	(7)	(8)	(9)	(10)	(11)	(12)	(13)	
PG1302–102	NGC5068 <sup>3</sup>		672	5.2	10.9	995	?	(+)	–	42±13±2@2183	<31	{O I}	<29
Mrk1095	UGC3258		2821	38.9	8.6	999	!	(–)	–	<70	{H <sub>2</sub> }	<24	{Ly $\delta$ }
RX J1830.3+7312	UGC11334		4582	66.3	37.8	1022	!	–	–	<33	<31	<39	<28
							i	+	(–)	45±6±2@4770	{Ly $\lim$ }	<57	<53
							i	+	(–)	47±9±2@4260	{H <sub>2</sub> }	{S VI}	<63
Mrk106	UGC4800		2433	37.1	17.5	1030	i	+	–		77±12±10@2407	<29	<34
HE1029–1401	MCG–2–27–9		4529	68.0	37.7	1035	i	+		56±10±3@4567			
Mrk421	HS1059+3934		3274	50.4	3.8	1041	i	+	–	84±9±2@3007	{C II}	<10	{Ar I}
HE1029–1401	MCG–2–27–1		2028	32.2	13.9	1065	i	+		90±10±3@2004			
Mrk110	UGC5354		1171	13.8	8.6	1171	i	+		115±27±4@1297			
RX J0100.4–5113	ESO195–G17 <sup>5</sup>		4708	63.9	18.6	1189	i	+	(–)	83±27±4@4874	<55	<39	<42
Mrk586	NGC864		1560	18.7	25.4	1239	i	+	–		49±11±9@1464	{C II*}	<31
PG1001+291	UGC5461		4799	72.0	20.5	1249	i	+	(–)	242±11±5@4602	<62	<72	<77
Mrk1095	UGC3262		4285	59.8	17.4	1306	i	+	–	44±10±4@4048	<35	<28	{H <sub>2</sub> }
RX J1830.3+7312	UGC11295		2370	35.1	15.7	1307	i	+	(=)	56±6±2@2383	<64	{H <sub>2</sub> }	<53
VII Zw118	UGC3685 <sup>5</sup>		1797	26.9	25.9	1414	i	+	–	38±9±2@1697	{O VI}	{O VI}	{H <sub>2</sub> }
PKS0405–12	2MASX J040607.61 <sup>4</sup>		3436	46.5	5.7	1489	i	+	–	51±9±5@3574	<19	<18	{H <sub>2</sub> }
Ton S180	ESO474–G25		2850	36.5	11.1	1509	i	+	–	35±9±2@3001	{C II}	<27	<28
Ton S180	2MASX J010208.03 <sup>4</sup>		5611	76.0	16.6	1547	i	+	–	255±10±2@5519	37±9±7@5516	<28	<27
Mrk290	NGC5971		4306	63.9	29.5	1586	i	+	–	34±15±3@4640	<33	<18	<17
PG1116+215	NGC3649		4979	75.2	26.9	1742	i	+		111±12±1@4884	41±4±3@4879	{Ly $\epsilon$ }	{Ly $\eta$ }
PG1259+593	MCG+10–19–23		4522	67.6	13.8	1869	i	+	–	64±7±4@4501	{H <sub>2</sub> }	<15	<16
PG1211+143	CGCG69–129 <sup>5</sup>		4987	75.5	10.0	1919	i	+	–	165±7±4@4932	31±10±7@4940	<19	<18
							i	+		231±7±4@5015	57±14±8@5027	{H <sub>2</sub> }	{Fe II}
Mrk110	UGC4984		3386	50.8	15.5	1975	i	+		484±22±4@3579			
H1821+643	NGC6636		4290	61.3	39.0	2434	i	+	–	38±5±2@4084	<20	<15	<15
MRC2251–178	NGC7381		4152	60.5	11.9	2470	i	+	–	34±7±2@4371	<49	<30	<31
H1821+643	NGC6667		2582	37.8	25.7	2475	i	+	–	17±5±1@2836	<14	<20	<15
H1821+643	FGC2210		5065	73.2	17.0	2832	i	+	–	22±5±1@5253	{flaw}	{H <sub>2</sub> }	<16
MCG+10–16–111	NGC3809 <sup>5</sup>	LGG251	3443	49.0	14.6	2910	i	+		31±10±3@3541			
							i	+		50±9±2@3792			
MCG+10–16–111	SDSSJ104924 <sup>5</sup>		4162	62.3	8.0	4351	i	+		52±11±2@4043			
PG0804+761	UGC3889 <sup>5</sup>		5249	76.2	26.1	4541	i	+	–	338±8±2@5549	72±5±3@5530	{H <sub>2</sub> }	<13

Table 3—Continued

Target	Galaxy	Group	$v_{gal}$ [km s <sup>-1</sup> ]	$D$ [Mpc]	$D_{gal}$ [kpc]	$\rho$ [kpc]	Q	HI	OVI	Ly $\alpha$ [mÅ]	Ly $\beta$ [mÅ]	O VI–1031 [mÅ]	O VI–1037 [mÅ]
(1)	(2)	(3)	(4)	(5)	(6)	(7)	(8)	(9)	(10)	(11)	(12)	(13)	
Mrk509	MCG–1–54–3 <sup>5</sup>		2231	29.1	17.3	4834	i	+	–	224±16±1@2545	41±5±7@2544	<25	<13
PKS0405–12	---					>5000	i	+		35±10±2@5035	{flaw}	<19	{C II}
Mrk817	---					>5000	i	+	–	25±5±2@4670	<22	<11	<9

Note. — 1: Description of columns. Column 1: Name of the extragalactic target, using the conventions of Wakker et al. (2003). Column 2: Name of the galaxy near the sightline. With few exceptions, these names are the preferred names in the RC3 (first NGC, then UGC, ESO or other), or, if not present in the RC3, the preferred name in *NED*. Column 3: Group number, if a galaxy belongs to a GH or LGG galaxy group. Column 4: The galaxy’s heliocentric radial velocity. Column 5: Derived distance (see text for details). Column 6: Galaxy diameter, calculated from the angular diameter given in the RC3 or NED and the galaxy’s distance (see Sect. 2.2). Column 7: Impact parameter between background UV target and foreground galaxy, calculated from the latter’s distance and the angular separation between the galaxy’s center and the background target. Column 8: Reliability of associating the detected absorption lines with the listed galaxy. “!” for unambiguous detections or non-detections; “+” when there is more than one absorber associated with one galaxy; “2” if there are two absorbers associated with two galaxies, but it is possible that the choice could be reversed; “1” when a choice was made between two galaxies for assigning the absorber, giving a non-detection to one of them; “g” for absorbers associated with a group, rather than a particular galaxy; “?” for the ambiguous associations; “>” for non-detections with upper limit worse than 50 mÅ; “x” if none of the lines is measureable; “i” indicates absorbers for which no associated galaxy with  $\rho < 1$  Mpc can be found, though if there is a galaxy with  $\rho < 5$  Mpc, that galaxy is listed (see Sect. 4.3 for more details). Columns 9, 10: “+” implies that the detected HI or OVI line can clearly be associated with the listed galaxy; “(+)” is given for uncertain detections. A “–” implies a non-detection with  $3\sigma$  equivalent width limit better than 50 mÅ, while “(–)” is for non-detections with worse equivalent width limits. Columns 11–14: Measurement results for Ly $\alpha$ , Ly $\beta$ , O VI  $\lambda$ 1031.926 and O VI  $\lambda$ 1037.617. Four numbers for detections: “equivalent width  $\pm$  statistical error  $\pm$  systematic error @ fitted velocity”.  $3\sigma$  upper limit for non-detections, calculated as 3 times the quadrature sum of the statistical and fixed-pattern error. Entries that are an ion’s name in curly brackets indicate cases where blending with absorption due to the listed ion makes it impossible to measure the intergalactic line associated with the listed galaxy; “flaw” indicates that the FUSE detector flaw near 1043 Å interferes with the detection or non-detection. 2: For these sightlines there are several galaxies in a group with similar impact parameter and velocity, so no unambiguous target-galaxy association can be made, and just the group is listed, with the velocity in Col. 4 the average velocity of the group galaxies. 3: We found orientations for these galaxies (used in Sect. 5.4) from the following papers: Blackman (1981, NGC 613), Bosma (1981; NGC 2841), Bosma et al. (1988, NGC 5963), Bowen et al. (2002; NGC 4319), Broeils & van Woerden (1994; NGC 2683, NGC 5879, NGC 6690), Carignan & Puche (1990; NGC 247), Carilli & van Gorkom (1992; NGC 3067), Casertano & van Gorkom (1991; NGC 3521), Chengalur & Kanekar (2002; SBS 1543+593), Côté et al. (2005; UGC 4238, NGC 6140), Fridman et al. (2005; NGC 4814), García-Ruiz et al. (2002; NGC 3432, UGC 3909), Garrido et al. (2005; NGC 3104, NGC 5832), Gopal-Krishna & Irwin (2000; NGC 3556), Jarvis et al. (1988; NGC 1574), Kobulnicky & Gebhardt (2000; NGC 4818), Krum & Salpeter (1979; NGC 4517), Márquez et al. (2002, NGC 5678, NGC 6239, UGC 3580), Mathewson et al. (1992; NGC 954, NGC 2104, ESO 298-G15), Noordermeer et al. (2005, UGC 3642), Oosterloo & Shostak (1993; NGC 7798), Pisano et al. (2004; NGC 986, NGC 5727), Puche et al. (1991; NGC 253), Putman et al. (2006, UGC 7697). Rhee & van Albada (1996, NGC 6255, NGC 7817, UGC 8146),



Sancisi (1976; NGC 5907), Stil & Israel (2002; NGC 3945, UGC 4121), van Gorkom et al. (1996; [vCS96]000254.9+195654.3), and Whiteoak & Gardner (1977; NGC 5068). All but one ([vCS96]000254.9+195654.3) of these are  $L > 0.1 L_*$  galaxies, and all but eight are spirals. 4: Full names of these galaxies are: [vCS96]000254.9+195654.3; SDSS J023305.84−081908.8; SDSS J084619.14+351858.2; SDSS J111938.66+112643.3; SDSS J125926.78+591735.0; SDSS J143146.90+580030.9; SDSS J143903.89+584717.6; SDSS J144303.81+535457.5; SDSS J145001.59+402142.4; SDSS J145045.59+413742.5; SDSS J153733.02+583447.7; SDSS J153802.76+573018.3; SDSS J170112.68+601500.0; SDSS J170327.95+610631.5; SDSS J170349.45+601806.1; SDSS J171138.94+604341.8; SDSS J215446.45−084616.9; 2MASX J010208.03−2245597; 2MASX J005700.66−232044.2; 2MASX J034134.24−274918.7; 2MASX J040607.61−102327.2; 2MASX J101213.26−040226.2; 2MASX J110443.60−290633.2; 2MASX J111605.92+583003.6; 2MASX J112139.77+112924.2; 2MASX J111343.40−274328.8; 2MASX J122815.85+024202.5; 2MASX J153514.22+573052.9; 2MASX J170712.70+605514.4; 2MASX J194221.91−550627.5; 2MASX J200943.13−481105.2; 6dF J0342278−260243; 6dF J1033307−144736; LCRS B101019.9−032413; LCRS B115151.0−113904. 5: The listed galaxies are the nearest galaxy with known redshift and  $\Delta v < 400 \text{ km s}^{-1}$ . However, there are other galaxies in the RC3 with unknown redshift that would have significantly lower impact parameters if their velocity were similar to that of the absorber.

Table 4. Detections of other ionic lines<sup>1</sup>

Target	Galaxy	Group	$v_{gal}$ [km s <sup>-1</sup> ]	$\rho$ [kpc]	ion	Ion EW@ $v$ [mÅ@km s <sup>-1</sup> ]	HI/O VI?
(1)	(2)	(3)	(4)	(5)	(6)	(7)	(8)
Mrk205	NGC4319	GH107	1357	6	C III	293±33±18@1273	+Lyα,+Lyβ,-OVI
					Si III	283±10±5@1293	"
					C IV λ1548	282±19±2@1280	"
					C IV λ1550	165±17±3@1290	"
3C232	NGC3067	GH50	1476	14	Si III	1043±21±20@1493	+Lyα
					C IV λ1548	1081±39±22@1462	"
					C IV λ1550	761±44±5@1462	"
					N V λ1238	233±35±5@1377	"
ESO185-IG13	IC4889		2526	62	Lyγ	635±98±21@2642	+Lyβ,+OVI
					C III	470±113±42@2625	"
Ton S180	NGC247	ScI	159	125	C III	60±28±7@ 279	+OVI
1H0419-577	NGC1574	LGG112	925	140	C III	430±110±15@1135	+Lyβ,-OVI
MCG+10-16-111		LGG234	1692	>145	Si III	203±10±3@1661	+Lyα
Mrk734		GH78	921	>133	Lyγ	90±79±8@ 745	+Lyβ
					C III	127±56±19@ 485	+Lyβ
Mrk876	NGC6140		910	206	Si III	42±9±1@ 912	+Lyα,+Lyβ,+OVI
	UGC10294		3516	282	Lyγ	27±12±7@3480	+Lyα,+OVI
PG1216+069				283	Lyγ	744±157±25@1864	+Lyα,+Lyβ
3C273.0		LGG287	1655	>311	Lyγ	158±5±9@1598	+Lyα,+Lyβ,-OVI
					Si III	68±4±1@1589	"
HE1228+0131		LGG287	1655	>338	Lyγ	405±91±9@1718	+Lyα,Lyβ
					C III	342±100±16@1711	"
					C IV λ1548	71±17±5@1722	"
					C IV λ1550	50±17±5@1725	"
MS0700.7+6338		LGG140	4404	>356	C III	159±65±19@4335	+Lyβ,-OVI
PG1302-102	NGC4920	LGG307	1336	473	C III	58±16±16@1310	+Lyα,+Lyβ,-OVI
HE0226-4110	NGC954	LGG62	5353	562	C III	23±9±3@5259	+Lyα,+OVI
					C IV λ1548	39±11±2@5232	"
PKS2005-489	2MASX J200943.13 <sup>2</sup>		5116	787	C III	117±23±9@5065	+Lyα,+Lyβ,-OVI
					Si III	29±4±2@5073	"

Note. — 1: Description of columns: Column 1: AGN name; Column 2: Associated galaxy; Column 3: Galaxy group if galaxy is in group; Column 4: Heliocentric systemic velocity of galaxy; Column 5: Impact parameter; Column 6: Ion detected; Column 7: Measurement result, giving “equivalent width ± statistical error ± systematic error @ fitted velocity”; Column 8: Entries show whether Lyα, Lyβ and/or O VI were also detected (+) or not (-); if line info is missing there is no data for that ion. 2: Full name is 2MASX J200943.13-481105.2.

Table 5. Ly $\alpha$  and Ly $\beta$  detections and comparison with values in the literature

Object	Literature Values			Ref. <sup>1</sup>	This paper					Flags <sup>4</sup>		Galaxy	$\rho$	Note
	$v(\text{Ly}\alpha)$ [km s <sup>-1</sup> ]	EW(Ly $\alpha$ ) [mÅ]	EW(Ly $\beta$ ) [mÅ]		$v(\text{Ly}\alpha)$ [km s <sup>-1</sup> ]	EW(Ly $\alpha$ ) [mÅ]	EW(Ly $\beta$ ) [mÅ]	$b(\text{Ly}\alpha)^3$ [km s <sup>-1</sup> ]	$b(\text{Ly}\beta)^3$ [km s <sup>-1</sup> ]	Ly $\alpha$	Ly $\beta$			
(1)	(2)	(3)	(4)	(5)	(6)	(7)	(8)	(9)	(10)	(11)	(12)	(13)	(14)	(15)
1H 0419–577					1112		463±25±15		79	+		NGC1574	140	
1H 0707–495					1302		26±7±8		19	+		ESO207–G22	482	
1H 0717+714					2888		41±7±8		32	+		UGC3804	199	6
3C 232	1428	6400±230		Ke+2005	1434	DLA		–				NGC3067	14	
					4526	153±30±4		94		+		Mrk412	196	
3C 249.1					1861	40±9±3		29		+		NGC3329	543	
					6672	245±15±3	39±13±3	58	59	+		CGCG351–57	858	
3C 273.0	1015	369±36		PSS2000 <sup>2</sup>	1010	394±7±1	120±4±10	53	44			LGG292	>191	
	1013	371±17	158±17	Se+2001		”	”					”		
	1001	390±11		Tr+2008		”	”					”		
	1586	373±30	251±11	PSS2000 <sup>2</sup>	1580	380±5±1	236±2±8	49	38			LGG287	>311	
	1589	367±13		Se+2001		”	”					”		
	1589	377±12		Tr+2002		”	”					”		
					2160	20±5±1	<9	32		+		UGC7625	711	7
	2290	35±30		PSS2000	2274	31±7±1	<9	44				2MASX J122815	429	7
3C 351.0					3465	117±13±5		41		+		NGC6292	314	
					3598	164±10±6		46		+		Mrk892	170	
					5175	182±10±4		43		+		SDSS J170349	594	
ESO 141–G55				Sh+2000										5
ESO 185–IG13					2635		641±52±14		110	+		IC4889	62	
ESO 438–G09	1469	510±20		BPB2002	1426	579±44±15		114				LGG230	>173	
	2211	230±40		BPB2002	2215	265±30±13		58				2MASX J111343	577	
Fairall 9				Sh+2000										5
H 1821+643					2836	17±5±1	<15	20		+		NGC6667	2475	
					4084	38±5±2	<21	20		+		NGC6636	2434	
					5253	22±5±1		20		+		FGC2210	2832	
HE 0226–4110	3645	50±3	<18	DS2008		<36				–				
	5234	80±12		Le+2006	5235	60±7±2		17				NGC954	562	
	5237	91±12		Tr+2008		”						”		
HE 0340–2703					1361	292±30±6		55		+		NGC1398	244	
					1785	374±30±6		71		+		NGC1412	167	
					4100	167±26±5		35		+		ESO419–G03	942	

Table 5—Continued

Object	Literature Values			Ref. <sup>1</sup>	This paper					Flags <sup>4</sup>		Galaxy	$\rho$ [kpc]	Note
	$v(\text{Ly}\alpha)$ [km s <sup>-1</sup> ]	EW(Ly $\alpha$ ) [mÅ]	EW(Ly $\beta$ ) [mÅ]		$v(\text{Ly}\alpha)$ [km s <sup>-1</sup> ]	EW(Ly $\alpha$ ) [mÅ]	EW(Ly $\beta$ ) [mÅ]	$b(\text{Ly}\alpha)^3$ [km s <sup>-1</sup> ]	$b(\text{Ly}\beta)^3$ [km s <sup>-1</sup> ]	Ly $\alpha$	Ly $\beta$			
(1)	(2)	(3)	(4)	(5)	(6)	(7)	(8)	(9)	(10)	(11)	(12)	(13)	(14)	(15)
HE 1029–1401	1979	103±45		Mc+2002	2004	90±10±3		53				MCG–2–27–1	1065	
	1971	110±39		PSS2004		”						”		
	2202	45±31		PSS2004		<27				–				
	2324	183±32		PSS2004	2457	168±9±3		47				6dF J1033307	427	
	4523	59±37		PSS2004	4557	56±10±3		59						
HE 1228+0131	889	46±13		R+2003						–				
	1490	138±42		PSS2000	1482	156±16±10	58±26±11	28	26		+	LGG287	>338	
	1482	158±14		R+2003		”						”		
	1666	385±94		PSS2000	1700	623±22±4	468±38±22	86			+	LGG287	>338	8
	1685	497±13		R+2003		”						”		
	1745	241±99		PSS2000		”				–				
	1721	410±11		R+2003		”						”		
	1860	142±81		PSS2000		”				–				
	1834	115±14		R+2003		”						”		
	2301	439±57		PSS2000	2306	338±21±6	172±31±17	50	65		+	UGC7625	339	
	2303	360±18		R+2003		”						”		
	5262	41±10		Ar+2006	5262	<29				–				
HS 0624+6907	2883	DLA		BTJ2001	2830	DLA		–				SBS1543+593	0.3	
HS 1543+5921	936	200±10		BPB2002	942	173±14±4		59				NGC3556	462	9
MCG+10–16–111	1472	620±20		BPB2002	1654	494±13±4		71				LGG234	>145	
	1844	540±20		BPB2002						–				
	2012			BPB2002	2022	174±11±9		65				NGC3625	190	
	2133			BPB2002	2136	301±11±7		58				NGC3613	41	
	3104	100±20		BPB2002	3113	102±12±3		62				CGCG291–61	367	
	3578	110±20		BPB2002	3541	31±10±3		52				NGC3809	2910	
	3783			BPB2002	3792	50±10±2		41				NGC3809	2910	
	4034	90±10		BPB2002	4043	52±11±2		88				SDSS J104924	4351	
					5363	172±8±3		53		+		MCG+10–16–118	208	
								77				ESO603–G31	422	10
MRC 2251–178	2237	39±34		PSS2004	2265	133±12±3						”		
	2281	52±46		PSS2004		”								
	3035	60±32		PSS2004	3046	65±8±6		65				ESO603–IG23	412	
	3205	349±37		PSS2004 <sup>2</sup>	3212	364±11±5	91±9±18	77	55		+	ESO603–G27	322	

Table 5—Continued

Object	Literature Values			Ref. <sup>1</sup>	This paper					Flags <sup>4</sup>		Galaxy	$\rho$ [kpc]	Note
	$v(\text{Ly}\alpha)$ [km s <sup>-1</sup> ]	EW(Ly $\alpha$ ) [mÅ]	EW(Ly $\beta$ ) [mÅ]		$v(\text{Ly}\alpha)$ [km s <sup>-1</sup> ]	EW(Ly $\alpha$ ) [mÅ]	EW(Ly $\beta$ ) [mÅ]	$b(\text{Ly}\alpha)^3$ [km s <sup>-1</sup> ]	$b(\text{Ly}\beta)^3$ [km s <sup>-1</sup> ]	Ly $\alpha$	Ly $\beta$			
(1)	(2)	(3)	(4)	(5)	(6)	(7)	(8)	(9)	(10)	(11)	(12)	(13)	(14)	(15)
Mrk 106 Mrk 110	4368	40±28		PSS2004	4371	34±7±2	<50	56				NGC7381	2470	
	9021	51±28		PSS2004	9032	54±8±2	<29	52				ESO603–G25	322	
					2407		77±12±10		35		+	UGC4800	1030	
					1297	115±27±4		37		+		UGC4984	1975	
Mrk 205					3579	484±22±4		71		+		UGC5354	1702	
Mrk 279					1289	801±13±4	477±14±8	–	76	+	+	NGC4319	6	
Mrk 290				Sh+2000										5
					720		23±10±8		14		+	NGC5963	307	
Mrk 335	4667	60±18		PSS2000	4640	34±15±3	<33	20				NGC5971	1586	
					1308	57±9±3	<14	19		+		UGC12893	697	
	1965	229±30		PSS2000 <sup>2</sup>	1954	229±12±3	31±3±9	35	26		+	[VCS96]000254.9	78	
	1970	170		St+1995		”						”		
	1957	210±19	59±8	DS2008		”		20				”		
	2295	81±26		PSS2000 <sup>2</sup>	2286	114±17±2	<13	66				NGC7817	395	
	2290	73		St+1995		”						”		
	2275	78±3	<13	DS2008		”		33				”		
	4267	33±16		PSS2000 <sup>2</sup>		<29				–				
	4270	26		St+1995		”				–		”		
Mrk 421	3046	92±10		SSP1996	3007	84±9±2		40				HS1059+3934	1041	
	3035	86±15		PSS2000 <sup>2</sup>		”						”		
	3035	87±15		Mc+2002		”						”		
	3022	82±8		SWFS2005		”						”		
Mrk 478	1582	194±31		PSS2004 <sup>2</sup>	1573	254±14±2	<44	68				NGC5727	645	
Mrk 501	4661	161±43		PSS2000	4593	150±26±4	<71	47				NGC6257	521	
	4660	154		St+1995		”						”		
Mrk 509	2560	209±32		PSS2000 <sup>2</sup>	2545	224±16±1	41±5±7	47	40		+	MCG–1–54–3	4834	
	2548	211±32		Mc+2002		”	”					”		
Mrk 586					1464		49±11±9		23		+	NGC864	1239	
Mrk 734					478		301±31±11		50		+	GH78	>230	
					757		149±31±11		31		+	GH78	>230	
Mrk 771	1186	294±56		PSS2004	1184	321±13±2	<109	59				NGC4561	502	
	1895	216±56		PSS2004	1891	243±13±5		50				KUG1229+207	184	

Table 5—Continued

Object	Literature Values			Ref. <sup>1</sup>	This paper					Flags <sup>4</sup>		Galaxy	$\rho$ [kpc]	Note
	$v(\text{Ly}\alpha)$ [km s <sup>-1</sup> ]	EW(Ly $\alpha$ ) [mÅ]	EW(Ly $\beta$ ) [mÅ]		$v(\text{Ly}\alpha)$ [km s <sup>-1</sup> ]	EW(Ly $\alpha$ ) [mÅ]	EW(Ly $\beta$ ) [mÅ]	$b(\text{Ly}\alpha)^3$ [km s <sup>-1</sup> ]	$b(\text{Ly}\beta)^3$ [km s <sup>-1</sup> ]	Ly $\alpha$	Ly $\beta$			
(1)	(2)	(3)	(4)	(5)	(6)	(7)	(8)	(9)	(10)	(11)	(12)	(13)	(14)	(15)
Mrk 817	2563	248±42		PSS2004	2557	246±13±3	<96	59				UGC7697	139	
	2557	290±70		Co+2005		”						”		
	1933	29±13		PSS2000	1922	29±7±2	<9	50				UGC9391	308	
	1933	29±13		PWW2004		”						”		
	2097	135±15	40±4	PSS2000 <sup>2</sup>	2085	131±8±3	25±3±7	43	59			SDSS J143903	202	
Mrk 876	2097	135±15	25±7	PWW2004		”						”		
	4682	23±11		PSS2000	4670	25±5±2	<22	44				...	>5000	
	935	390±70		Co+2005	936	476±14±3	79±6±33	77	76			NGC6140	206	
	959	324±52	170±40	Sh+2000		”						”		11
					1109	39±7±3	<13	13		+		NGC6140	206	
Mrk 926	3486	236±50		DSRS2006	3481	267±12±3		37				UGC10294	282	
Mrk 1095	4040	48±18		PSS2004										5
Mrk 1513				PSS2000	4048	44±10±4	<35	35				UGC3262	1306	
MS 0700.7+6338				PSS2004										5
NGC 985					4322		209±16±29		38		+	LGG140	>356	
PG 0804+761	1913	120±10		BPB2002	1924	69±20±2	<31	132				DDO23	993	
	2156	51±42		PSS2004	2183	42±13±2	<31	65				DDO23	993	
	2183	80±10		BPB2002		”						”		
	1147	165±29		PSS2004 <sup>2</sup>	1144	159±7±2	52±10±2	47	68		+	UGC3909	829	12
	1530	78±28		PSS2004	1537	114±14±2		107				UGC4238	155	
PG 0838+770	1621	41±27		PSS2004		”						”		
	1570	260±30		Co+2005		”						”		
					2282	28±7±2		32		+		UGC4202	875	
	5552	324±44		PSS2004	5549	338±8±2	72±5±3	59	35		+	UGC3889	4541	
					716		330±53±13		53		+	UGC4527	10	
PG 0844+349					351		25±8±2		8		+	NGC2683	250	
PG 0953+414					2260		64±5±3		25		+	UGC4621	372	
					2326		29±6±3		23		+	UGC4621	372	
					621	70±9±2	<22	41		+		NGC3104	296	
	4671	58±12		SSTR2002	4670	55±10±1	<22	35				KUG0952+418	449	
	4803	162±13		SSTR2002 <sup>2</sup>	4807	160±12±1	<21	50				KUG0952+418	449	
	4961	123±12		SSTR2002 <sup>2</sup>	4961	120±10±1	<17	31				KUG0952+418	449	

Table 5—Continued

Object	Literature Values			Ref. <sup>1</sup>	This paper					Flags <sup>4</sup>		Galaxy	$\rho$ [kpc]	Note
	$v(\text{Ly}\alpha)$ [km s <sup>-1</sup> ]	EW(Ly $\alpha$ ) [mÅ]	EW(Ly $\beta$ ) [mÅ]		$v(\text{Ly}\alpha)$ [km s <sup>-1</sup> ]	EW(Ly $\alpha$ ) [mÅ]	EW(Ly $\beta$ ) [mÅ]	$b(\text{Ly}\alpha)^3$ [km s <sup>-1</sup> ]	$b(\text{Ly}\beta)^3$ [km s <sup>-1</sup> ]	Ly $\alpha$	Ly $\beta$			
(1)	(2)	(3)	(4)	(5)	(6)	(7)	(8)	(9)	(10)	(11)	(12)	(13)	(14)	(15)
PG 1001+291					487	308±7±12	<87	41		+		UGC5427	84	
	1078	300±60		BBP1996	1069	267±14±5	<77	47				UGC5464	337	
					4602	242±11±5	<62	55		+		UGC5461	1249	
PG 1049−005	5583	80		Co+2005		<93				−				
PG 1116+215	1478	95±11		STSR2004	1479	91±10±2	<14	35				UGC6258	543	
	1499	82±33		PSS2004 <sup>2</sup>		”						”		
	4902	113±10		STSR2004	4884	111±12±1	41±4±3	50	17	+		NGC3649	1742	
PG 1149−110	4913	90±32		PSS2004 <sup>2</sup>		”						”		
	1660	1100±30		BPB2002	1665	437±69±7		101				NGC3892	529	
	3716	390±10		BPB2002	3728	381±54±3		82				NGC3942	141	
PG 1211+143	2130	186±19		PSS2004 <sup>2</sup>	2110	104±8±2	50±9±8	53	47	+		LGG285	>121	
	4944	189±46		PSS2004 <sup>2</sup>	4932	165±7±4	31±10±7	52	68	+		CGCG69−129	1919	
	5036	154±40		PSS2004 <sup>2</sup>	5015	231±7±4	57±14±8	62	58	+		CGCG69−129	1919	
PG 1216+069	1124			TJBP2005	1106	209±27±5	<90	115				LGG292	>104	
					1443	119±19±6	<90	55		+		LGG289	>264	
	1650	1630±160		BBP1996						−				
	1895	DLA		TJBP2005	1895	2400±62±350	1001±73±12	−	−		+	LGG278	>283	
					3774	148±13±17		31		+		SDSS J121903	103	
					3808	163±12±16	<78	32		+		SDSS J121903	103	
PG 1259+593	687	190±24	21±6	RSTS2004 <sup>2</sup>	678	25±9±3	<15	62				UGC8146	80	
	679	330±80		Co+2005		”						”		
	630	292±23		Tr+2008		”						”		
	2278	301±15	75±6	RSTS2004 <sup>2</sup>	2275	291±11±1	67±6±2	44	35			UGC8046	584	
	4502	73±6			4501	64±7±4		28				MCG+10−19−23	1869	
PG 1302−102	1311	293±0		DSRS2006 <sup>2</sup>	1316	284±30±2	221±8±7	37	35		+	NGC4920	473	
					1045	84±24±4	<25	41		+		MCG−2−34−6	391	
PG 1341+258	1425	120±20		BPB2002		<31				−				
PG 1351+640				PSS2004	1447	122±15±23		64		+		SDSS J134711	482	13
					1771	143±18±3		92		+		UGC8894	274	
PG 1444+407					2630	95±14±4	<85	62		+		SDSS J145045	897	
					5638	103±11±4	<80	38		+		UGC9502	637	
PHL 1811	3558	240±50		Je+2003 <sup>2</sup>		O VI@0.0809				−				14

Table 5—Continued

Object	Literature Values			Ref. <sup>1</sup>	This paper			$b(\text{Ly}\alpha)^3$	$b(\text{Ly}\beta)^3$	Flags <sup>4</sup>		Galaxy	$\rho$	Note
	$v(\text{Ly}\alpha)$ [km s <sup>-1</sup> ]	EW(Ly $\alpha$ ) [mÅ]	EW(Ly $\beta$ ) [mÅ]		$v(\text{Ly}\alpha)$ [km s <sup>-1</sup> ]	EW(Ly $\alpha$ ) [mÅ]	EW(Ly $\beta$ ) [mÅ]			Ly $\alpha$	Ly $\beta$			
(1)	(2)	(3)	(4)	(5)	(6)	(7)	(8)	(9)	(10)	(11)	(12)	(13)	(14)	(15)
PKS 0405–12	5309	210±60		Je+2003 <sup>2</sup>		O VI@0.0809				–				14
					5402	35±3±2		8		+		SDSS J215446	787	
	3567	53±11		Le+2007	3574	51±9±5	<19	17				2MASX J040607	1489	
	4472	35±11		Le+2007		<34				–				
PKS 2005–489	5039	45±14		Le+2007	5035	35±10±2		25				...	>5000	
	2752	24±15		PSS2004		(26±3±2)	<20			–				15
	4947	299±26		PSS2004 <sup>2</sup>	4973	307±5±6	46±7±7	77	35		+	ESO233–G37	599	
PKS 2155–304	5061	281±21		PSS2004 <sup>2</sup>	5071	330±3±6	170±9±9	61	38		+	2MASX J200943	787	
	2632	42±40		PSS2000		<20	<9			–				
	2785	36±22		PSS2000		<20	<9			–				
	4031	21±11		PSS2000		<20	<9			–				
RX J0100.4–5113	4951	64±23		PSS2000 <sup>2</sup>						–				16
	5013	82±22		PSS2000 <sup>2</sup>	4990	104±7±2	17±2±7	29	22	(+)	+	ESO466–G32	306	
	5119	218±20		PSS2000 <sup>2</sup>	5101	140±6±3	43±4±8	32		(+)	+	ESO466–G32	306	
				PSS2000	5164	61±6±3	26±3±8	35		(+)	+	ESO466–G32	306	
RX J1830.3+7312					4874	83±27±4	<55	64		+		ESO195–G17	1189	
Ton S180	1536	110±20		BPB2002	1549	81±6±3		41				NGC6654A	308	
	1938	110±20		BPB2002	1968	68±10±3	<66	111				NGC6654	174	
	2368	100±20		BPB2002	2383	56±6±2	<64	32				UGC11295	1307	
	4246	50±10		BPB2002	4260	47±9±2		38				UGC11334	1022	
	4752	90±50		BPB2002	4770	45±6±2		41				UGC11334	1022	
VII Zw 118	1919	66±28		PSS2004	1939	54±10±2	<27	44				ESO451–G05	774	
	2774	49±26		PSS2004	2792	38±10±1	<27	32				2MASX J005700	560	
	2985	41±23		PSS2004	3001	35±9±2		34				ESO474–G25	1509	
	5502	268±54		PSS2004	5519	255±10±2	37±9±7	58	29		+	2MASX J010208	1547	
VII Zw 118	1721	54±29		PSS2004	1697	38±9±2		41				UGC3685	1414	
	2463	355±35	110±50	Sh+2000	2438	333±16±2	70±8±7	65	38			UGC3748	753	17
	2426	189±15		Mc+2002		"						"		
	2469	144±11		Mc+2002		"						"		
	2382	68±38		PSS2004		"						"		
	2460	267±35		PSS2004 <sup>2</sup>		"						"		
	4595	35±20		PSS2004	4613	64±16±2	<37	89				UGC3648	620	



Table 5—Continued

Object	Literature Values				This paper					Flags <sup>4</sup>		Galaxy	$\rho$	Note
	$v(\text{Ly}\alpha)$ [km s <sup>-1</sup> ]	EW(Ly $\alpha$ ) [mÅ]	EW(Ly $\beta$ ) [mÅ]	Ref. <sup>1</sup>	$v(\text{Ly}\alpha)$ [km s <sup>-1</sup> ]	EW(Ly $\alpha$ ) [mÅ]	EW(Ly $\beta$ ) [mÅ]	$b(\text{Ly}\alpha)^3$ [km s <sup>-1</sup> ]	$b(\text{Ly}\beta)^3$ [km s <sup>-1</sup> ]	Ly $\alpha$	Ly $\beta$			
(1)	(2)	(3)	(4)	(5)	(6)	(7)	(8)	(9)	(10)	(11)	(12)	(13)	(14)	(15)
	4693	45±31		PSS2004			”					”		

Note. — 1: References: St+1995 - Stocke et al. 1995 (Mrk 335, Mrk 501); SSP1996 - Shull, Stocke, Penton 1996 (Mrk 421); BBP1996 - Bowen, Blades, Pettini, 1996; (PG1001+291, PG1216+069); PSS2000 - Penton, Stocke, Shull, 2000a (3C273.0, HE 1228+0131, Mrk 290, Mrk 335, Mrk 421, Mrk 501, Mrk 509, Mrk 817, Mrk 1095, PKS 2155–304); Sh+2000 - Shull et al. 2000 (ESO 141-G55, Fairall 9, Mrk 279, Mrk 876, VII Zw 118); BTJ2001 - Bowen, Tripp, Jenkins, 2001 (HS 1543+5921); Se+2001 - Sembach et al. 2001 (3C 273.0); BPB2002 - Bowen, Pettini, Blades, 2002 (ESO 438-G09; MCG+10-16-111; PG1149-110; PG 1341+258); Mc+2002 - McLin et al. 2002 (HE 1029–1401, Mrk 421, Mrk 509, VII Zw 118); SSTR2002 - Savage et al. 2002 (PG 0953+414); Tr+2002 - Tripp et al. 2002 (3C 273.0); Je+2003 - Jenkins et al. 2003 (PHL 1811); R+2003 - Rosenberg et al. 2003 (HE 1228+0131); PSS2004 - Penton, Stocke, Shull, 2004; PWW2004 - Pisano et al. 2004 (Mrk 817); RSTS2004 - Richter et al. 2004 (PG 1259+593); STSR2004 - Sembach et al. 2004 (PG 1116+215); Co+2005 - Coté et al. 2005 (Mrk 771, Mrk 876, PG 0804+761, PG 1049–005, PG 1259+215); Ke+2005 - Keeney et al. 2005 (3C 232); SWFS2005 - Savage et al. 2005a (Mrk 421); TJPB2005 - Tripp et al. 2005 (PG 1216+069); DSR2006 - Danforth et al. 2006 (Mrk 876, PG 1302–102); Ar+2006 - Aracil et al. 2006; (HS 0624+6907); Le+2006 - Lehner et al. 2006 (HE 0226-4110); Le+2007 - Lehner et al. 2007 (PKS 0405-12); DS2008 - Danforth & Shull 2008 (Mrk 335, HE 0226-4110); Tr+2008 - Tripp et al. 2008 (3C273.0, HE 0226–4110, PG 1259+593). 2: Line also listed in Danforth et al. (2006). 3: These columns give the width of a gaussian fitted to the absorption line, corrected for instrumental broadening. 4: A “+” in these columns indicates Ly $\alpha$  or Ly $\beta$  lines that have not been published previously, while a “–” is given for features that we do not think are significant, but which were claimed to be Ly $\alpha$  by other authors. 5: The entry refers to the fact that no absorption line was reported in the listed reference, and we agree. 6: (1H 0717+714): This absorption feature is possibly CII in complex A, but the apparent corresponding OVI feature and the lack of absorption in the higher Lyman lines at this velocity suggests that it is Ly $\beta$ . 7: (3C 273.0): Tripp et al. (2002) showed the Ly $\alpha$  absorber at 2233 km s<sup>-1</sup>, but did not present equivalent widths. 8: (HE 1228+0131): Penton et al. (2000) listed three Ly $\alpha$  components, but the low S/N ratio justifies only one. 9: (MCG+10-16-111): Bowen et al. (2002) listed a strong Ly $\alpha$  line at 1472 km s<sup>-1</sup>, plus one without equivalent width measurement at 1645 km s<sup>-1</sup>; however, the strong line is clearly the one centered at 1654 km s<sup>-1</sup>, while there is no real evidence for absorption centered at 1472 km s<sup>-1</sup>; similarly, a large equivalent width was listed at 1844 km s<sup>-1</sup>, with secondary components at 2012 and 2133 km s<sup>-1</sup>, but we only find two absorbers centered at 2022 and 2136 km s<sup>-1</sup>. 10: (MRC 2251-178): Penton et al. (2004) listed two components, but the S/N ratio justifies only one. 11: (Mrk 876): Shull et al. (2000) did not correct the Ly $\beta$  measurement for the very strong contamination by H<sub>2</sub>. 12: (PG 0804+761): The feature at 2282 km s<sup>-1</sup> is clearly visible, but not listed by Penton et al. (2004). The feature at 1537 km s<sup>-1</sup> was listed as two features at 1530 and 1621 km s<sup>-1</sup> by Penton et al. (2004), which may be correct; however, we list it as a single feature. The fitted widths of the Ly $\alpha$  and Ly $\beta$  at 1144 km s<sup>-1</sup> differ considerably, probably because one of the four FUSE exposures has an extra noise bump on the lower-velocity side; this also causes the apparent misalignment of the absorption seen in Fig. 2. 13: (PG 1351+640): Penton et al. (2004) did not list these two features, although they are stronger than 3  $\sigma$ . 14: (PHL 1811): Jenkins et al. (2003) listed

two lines as possible  $\text{Ly}\alpha$  at  $3558$  and  $5309 \text{ km s}^{-1}$ , but these are actually intrinsic  $\text{O VI } \lambda\lambda 1031.926, 1037.617$  absorption -  $\text{Ly}\alpha$ ,  $\text{NV}$ ,  $\text{III}$  and  $\text{SVI}$  are also detected. 15: (PKS 2005-489): There is a feature at  $1226.89 \text{ \AA}$ , listed as  $\text{Ly}\alpha$  by Penton et al. (2004), but it is more likely to be  $\text{Si III}$  absorption at  $5070 \text{ km s}^{-1}$  (see the extended note in the Appendix for this target). 16: (PKS 2155-304): The component structure listed by Penton et al. (2000) is very different than the structure seen in the spectrum (see Appendix for details); no fitted widths are given for two of the  $\text{Ly}\beta$  absorptions because they are confused by the FUSE detector flaw. 17: (VII Zw 118): McLin et al. (2002) and Penton et al. (2004) broke this absorber into two components, but the S/N ratio does not really justify this.

Table 6. O VI detections and comparison with values in the literature

Object	Literature Values			Ref. <sup>1</sup>	This paper			Qual <sup>3</sup>	Flag <sup>4</sup>	Galaxy	$\rho$ [kpc]	Note
	$v(\text{O VI})$ [km s <sup>-1</sup> ]	EW(1031) [mÅ]	EW(1037) [mÅ]		$v(\text{O VI})$ [km s <sup>-1</sup> ]	EW(1031) [mÅ]	EW(1037) [mÅ]					
(1)	(2)	(3)	(4)	(5)	(6)	(7)	(8)	(9)	(10)	(11)	(12)	(13)
1H 0717+714					2914	66±15±9	<23	?	+	UGC3804	199	
3C 273.0	1013	26±10	<30	Se+2001	1008	21±3±7		!		LGG292	>191	
	1015	35±6		DSRS2006		"				"		
	1001	31±7		Tr+2008		"				"		
	1589		17±10	Se+2001	1580		<10		−	LGG287	>311	
	1586		<9 <sup>2</sup>	DSRS2006			"			"		
ESO 185−IG13					2627	335±68±15		!	+	IC4889	62	
HE 0226−4110	5234	40±10		Le+2006	5240	41±6±4		+		NGC954	562	5
	5237	54±10		Tr+2008		"				"		
MRC 2251−178	3205	29±16	<24 <sup>2</sup>	DSRS2006	3212	<27	<31		−	ESO603−G27	322	6
					2283		40±12±9	?	+	ESO603−G31	422	
Mrk 290	2850	<100		PWW2004	3073	49±8±7	20±8±7	+	+	NGC5987	424	7
Mrk 335	1965		<10 <sup>2</sup>	DSRS2006	1954		<11			[vCS86]000254.9	78	
	2295		<10 <sup>2</sup>	DSRS2006	2286	<13	<11			NGC7817	395	
Mrk 421	3022	<19		SWFS2006	3007	<10				HS1059+3934	1041	
	3035	<9 <sup>2</sup>		DSRS2006		"	"			"		
Mrk 478	1582		<67 <sup>2</sup>	DSRS2006	1573	<42	<47			NGC5727	645	
Mrk 509	2560	<19 <sup>2</sup>	<13 <sup>2</sup>	DSRS2006	2545	<25	<13			...	...	
Mrk 817	2097		<21	PWW2004	2085		<9			SDSS J143903.89+584717.6	202	
	2097		<6 <sup>2</sup>	DSRS2006			"			"		
Mrk 876	958	26±7		DSRS2006	945	17±4±8	<15	+		NGC6140	206	9
	3486	<16 <sup>2</sup>		DSRS2006	3508	18±4±7		!	+	UGC10294	282	
PG 0804+761	1147	36±10		DSRS2006		=C II			−			10
	5552		<9 <sup>2</sup>	DSRS2006	5549		<13			...	...	
PG 0844+349					365	37±5±2	27±5±7	+	+	NGC2683	250	
PG 0953+414					637	39±8±7	<22	+	+	NGC3104	296	11
	4806	<23	<19	SSTR2002	4807	<18	<18			KUG0952+418	449	
	4965	<19	<14	SSTR2002	4961	<17	<17			KUG0952+418	"	
PG 1116+215	1499		45±11	DSRS2006			=Lyξ		−			12
	4913	<14 <sup>2</sup>	<184	DSRS2006		=Lyε	=Lyη					
PG 1211+143	2130		45±14	DSRS2006	2110		<19		−	LGG285	>121	13
	4944	<23 <sup>2</sup>	<13 <sup>2</sup>	DSRS2006	4932	<19	<18			CGCG69−129	1919	

Table 6—Continued

Object	Literature Values			Ref. <sup>1</sup>	This paper			Qual <sup>3</sup>	Flag <sup>4</sup>	Galaxy	$\rho$ [kpc]	Note
	$v(\text{O VI})$ [km s <sup>-1</sup> ]	EW(1031) [mÅ]	EW(1037) [mÅ]		$v(\text{O VI})$ [km s <sup>-1</sup> ]	EW(1031) [mÅ]	EW(1037) [mÅ]					
(1)	(2)	(3)	(4)	(5)	(6)	(7)	(8)	(9)	(10)	(11)	(12)	(13)
PG 1259+593	687	63±22	<51	RSTS2004	627	25±5±2	13±3±2	!		UGC8146	80	14
	687	14±9		DSRS2006		"	"			"		
	630	40±5	26±6	Tr+2008		"	"			"		
	2278	15±4		RSTS2004	2275		<13		—	UGC8046	584	
	2280		<15 <sup>2</sup>	DSRS2006			"			"		
PG 1302−102	3109				3109	19±6±8		?	+	NGC4939	104	15
PHL 1811	3537	<63 <sup>2</sup>		DSRS2006		=Ly $\gamma$			—			16
PKS 2005−489	4947	<15 <sup>2</sup>	<14 <sup>2</sup>	DSRS2006	4973	<20	<20			ESO233−G37	599	
	5061	<59 <sup>2</sup>	<125 <sup>2</sup>	DSRS2006	5071	=H <sub>2</sub>				2MASXJ200943	787	17
PKS 2155−304	5013	<15 <sup>2</sup>	<6 <sup>2</sup>	DSRS2006	4990	<10				ESO466−G32	306	
	5119	<8 <sup>2</sup>	<34 <sup>2</sup>	DSRS2006	5101	<10	<11			ESO466−G32	306	
Ton S180	251	47±10		W+2003	260	51±10±8	34±13±8	!	+	NGC247	125	
	5502	<20 <sup>2</sup>	<20 <sup>2</sup>	DSRS2006	5519	<28	<27			2MASX J010208.0302245597	1547	
Ton S210					288	25±8±7		+	+	NGC253	374	
VIII Zw 118	2460		<18 <sup>2</sup>	DSRS2006	2438		<21			UGC3748	753	

Note. — 1: References: Se+2001 - Sembach et al. 2001 (3C 273.0); SSTR2002 - Savage et al. 2002 (PG 0953+414); W+2003 - Wakker et al. 2003 (Ton S180); PWW2004 - Pisano et al. 2004 (Mrk 290, Mrk 817); RSTS2004 - Richter et al. 2004 (PG 1259+593); SWFS2005 - Savage et al. 2005a (Mrk 421); DSRS2006 - Danforth et al. 2006; Le+2006 - Lehner et al. 2006 (HE 0226-4110). Tr+2008 - Tripp et al. 2008 (3C 273.0, HE 0226-4110, PG 1259+593). 2: Note that Danforth et al. (2006) give  $4\sigma$  upper limits to equivalent widths for absorption lines with a width of 1 resolution element ( $\sim 7$  or  $\sim 20$  km s<sup>-1</sup>), whereas our  $3\sigma$  upper limits are based on assuming a typical linewidth of 60 km s<sup>-1</sup>. 3: Quality flag for detections; “!” implies a secure identification, “+” means that the identification is probably correct, “?” is given when the line(s) identified as O VI need confirmation. 4: This column indicates a new detection (“+”) or a change in interpretation (“−”), i.e. a claimed detection or limit that we do not agree with. 5 (HE 0226−4110): The O VI  $\lambda 1031.926$  line is contaminated by interstellar H<sub>2</sub> L(4-0) R(1)  $\lambda 1057.380$ , while O VI  $\lambda 1037.617$  is contaminated by O VI  $\lambda 787.711$  at  $z=0.3406$ ; Tripp et al. (2008) did not correct the equivalent width for the contribution of H<sub>2</sub>. 6 (MRC 2251−178): The O VI claimed by Danforth et al. (2006) is probably not real, as it is located in the detector flaw near 1043 Å that is seen in almost all FUSE spectra; on the other hand, they did not list the possible O VI  $\lambda 1037.617$  line near 2283 km s<sup>-1</sup>, although this line has no confirming Ly $\beta$  or O VI  $\lambda 1031.926$ . 7 (Mrk 290): The negative-velocity side of the 1037 line at 3073 km s<sup>-1</sup> is contaminated by Galactic Ar I  $\lambda 1048.220$ ; only the positive-velocity side is measured, and the result is doubled. 9 (Mrk 876): The value listed by Danforth et al. (2006) does not take into account the contamination by H<sub>2</sub> L(6-0) P(4)  $\lambda 1035.783$ ; the O VI  $\lambda 1031.926$  line at 3508 km s<sup>-1</sup> was missed by Danforth et al. (2006). 10 (PG 0804+761): The intergalactic O VI  $\lambda 1031.926$  line claimed by Danforth et al. (2006) is actually C II absorption at  $-140$  km s<sup>-1</sup> associated with the high-velocity cloud complex A (see also the extended sightline note on PG 0804+761 in the Appendix). 11 (PG 0953+414): This O VI

line was missed by Danforth et al. (2006). 12 (PG 1116+215): The feature at  $1042.6 \text{ \AA}$  is not O VI  $\lambda 1031.926$  at  $1499 \text{ km s}^{-1}$ , as claimed by Danforth et al. (2006), but Ly $\xi$  at  $z=0.13847$ ; Sembach et al. (2002) showed the first 10 HI lines in this system, but another 8 are detected, some of which make deriving a lower limit for O VI near  $4913 \text{ km s}^{-1}$  impossible. 13 (PG 1211+143): The feature claimed by Danforth et al. (2006) as O VI  $\lambda 1037.617$  at  $2130 \text{ km s}^{-1}$  clearly is not present. 14 (PG 1259+593): Richter et al. (2004) integrated several wiggles over a wide velocity range, to end up with a  $63 \text{ m\AA}$  equivalent width; we integrate just the feature that is matched by an apparent O VI  $\lambda 1037.617$  line, which Richter et al. (2004) listed as O VI  $\lambda 1031.926$  at  $v=2278 \text{ km s}^{-1}$ . 15 (PG 1302–102): This is not a secure detection; O VI  $\lambda 1037.617$  is in the wing of Ar I  $\lambda 1048.220$ , and would be a  $1.5\sigma$  detection; Ly $\beta$  is hidden by Galactic C II  $\lambda 1036.337$ . Ly $\alpha$  may be present, but the *STIS*-E140M spectrum is very noisy, and the detection limit is  $72 \text{ m\AA}$ ; we list this detection only because the feature is clearly visible by eye, and we find associated O VI for all other bright ( $L > 0.1 L_*$ ) field galaxies with impact parameter  $< 300 \text{ kpc}$  (see Sect. 5.3.3). 16 (PHL 1811): Since the absorptions at  $1230.04$  and  $1236.8 \text{ \AA}$  are intrinsic O VI, rather than intergalactic Ly $\alpha$  as originally listed by Jenkins et al. (2003), the lower-limit to EW(O VI) given by Danforth et al. (2006) is inappropriate. 17 (PKS 2005–489): Danforth et al. (2006) gave upper limits, but there are a H $_2$  and Fe II lines that completely cover any possible redshifted O VI absorption.

### 3. Absorption Line Results

In this section we first compare our line identifications listed in Tables 3, 4, 5 and 6 with those claimed in previous work (Sect. 3.1). We then discuss a number of analyses that can be done from the perspective of the  $\text{Ly}\alpha/\text{Ly}\beta/\text{OVI}$  lines, without reference to the galaxies near the sightlines, specifically the distribution of linewidths (Sect. 3.2), the frequency of absorbers ( $dN/dz$ , Sect. 3.3), and the evolution of linewidths over time (Sect. 3.4). Since the width and  $dN/dz$  distributions and their implications have been presented and discussed previously (Penton et al. 2004; Lehner et al. 2007 for  $\text{Ly}\alpha$  and Tripp et al. 2008 for O VI), and since our distributions are similar, we defer to those papers for a more detailed discussion of the implications.

#### 3.1. Comparison with Previous Work

A number of previous authors have published measurements for very low redshift  $\text{Ly}\alpha$  and O VI absorbers at  $z < 0.017$ . Among these are Bowen et al. (1996, 2002), Penton et al. (2000a, 2000b, 2002, 2004), Côté et al. (2005), Danforth et al. (2006) and Danforth & Shull (2008). Where Bowen et al. and Côté et al. concentrated on looking for absorption associated with nearby galaxies (with sample sizes of 7 and 5 sightlines, respectively), Penton et al. looked at the statistics of all  $\text{Ly}\alpha$  absorbers found in their 30 sightlines and Danforth & Shull (2008) studied the O VI absorption in the Penton et al. sample.

Our sample includes the sightlines from these papers, but we also include 30 new sightlines for which low-redshift data have not yet been published. Of the 129 HI systems that we list (see Tables 3 and 5) Bowen et al. (1996, 2002) previously published values for 23, Côté et al. (2005) for 5, and Penton et al. (2000a, b, 2002, 2004) for 48. A few other papers also presented systems in some sightlines, but 45 systems (33% of the sample, 29  $\text{Ly}\alpha$  lines and 36  $\text{Ly}\beta$  lines) are presented here for the first time.

We do not confirm 20 of the previously published HI systems. These are indicated by a “–” in Column 8 or 9 in Table 5 and they are discussed individually in the Appendix. Nine of these disagreements are for systems that are listed as  $<3\sigma$  detections in the various Penton et al. papers (toward HE 1029–1401, HE 1228+0131, Mrk 335, PKS 2005–489 and PKS 2155–304), while three are due to different interpretations of some of the spectra in Bowen et al. (2002) (toward MCG+10-16-111, PG 1216+069 and PG 1341+258). Of the remaining six, four were listed as  $<4\sigma$  detections by the respective authors (toward HE 0226–4110, HE 1228+0131, HS 0624+607 and PKS 0405–12), while two toward PHL 1811 were misidentified as redshifted O VI lines. So, on balance, the only systems with

whose reality we do not agree were at the limit of detection.

For O VI the literature comparison shows a much worse situation. Sembach et al. (2001), Richter et al. (2004), and Lehner et al. (2006) previously published O VI absorptions toward 3C 273.0, PG 1259+593 and HE 0226–4110, respectively. We agree with all of their low- $z$  detections. Danforth et al. (2006) previously systematically analyzed the low-redshift O VI absorbers. We agree with only three of the six relevant detections that they listed (toward 3C 273.0, PG 1259+593 and Mrk 876). We also find three new O VI lines in sightlines that they studied (toward MRC 2251–178, Mrk 876 and PG 0953+414). In addition, we find seven new O VI absorbers in other sightlines (1H 0717+714, ESO 185-IG13, Mrk 290, PG 0844+349, PG 1302–102, Ton S180 and Ton S210), making for a total of fourteen positively identified O VI absorbers at  $v < 6000 \text{ km s}^{-1}$ . All these systems are commented on in Sect. 3.2 and in the Appendix.

Danforth et al. (2006) and Danforth & Shull (2008) listed O VI detections and non-detections for all Ly $\alpha$  systems in their sightline sample, but we only compared to our results for the 33 systems at  $v < 6000 \text{ km s}^{-1}$ . As mentioned above, we agree with three of their detections, and do not confirm three other detections. We further agree with 20 of their non-detections, but we consider seven non-detections to have been given in error (see below). I.e., we agree with 23 of 33 (70%) of their results. Since we find three new detections in their sightlines, the detection statistics are not affected much, even though the samples overlap for only three of the fourteen positive identifications.

The three absorption lines for which do not agree with the Danforth et al. (2006) claim that they are redshifted O VI are the following. a) A  $29 \pm 16 \text{ mÅ}$  line at  $3205 \text{ km s}^{-1}$  toward MRC 2251–178, complementing strong Ly $\alpha$  and Ly $\beta$ ; as can be seen in Fig. 2, there is no convincing evidence for O VI absorption at this velocity, so we set an upper limit of  $27 \text{ mÅ}$ . b) O VI at  $1147 \text{ km s}^{-1}$  toward PG 0804+761; this feature is more likely to be C II  $\lambda 1037.337$  in the Galactic high-velocity cloud complex A (see Appendix). c) A  $45 \pm 14 \text{ mÅ}$  O VI  $\lambda 1037.617$  absorber at  $2130 \text{ km s}^{-1}$  toward PG 1211+143; Fig. 2 clearly shows no evidence for a feature here and we set an upper limit of  $19 \text{ mÅ}$ .

For seven non-detections listed by Danforth et al. (2006), we instead argue for a detection in three cases (see above). For four others (toward PG 1116+215, PHL 1811 and PKS 2005–489) there are other absorption lines (Ly $\gamma$ , Ly $\eta$ , Ly $\xi$ , H $_2$ ) at the velocity of O VI corresponding to a Ly $\alpha$  detection. So, in practice it is not possible to set a useful upper limit.

### 3.2. Discussion of O VI Absorbers

In this subsection we summarize the O VI absorbers in our sample. The spectra can be seen in Fig. 2. We derive column densities using the apparent optical depth method (Sembach & Savage 1992). We also refer to line widths, which were measured by fitting a gaussian to the apparent optical depth profile and correcting the result for instrumental broadening (see also Sect. 3.2). The data for the O VI absorbers are collected in Table 7, listing the equivalent widths, linewidths and column densities for the O VI lines, as well as other lines detected in each system.

#### *1H0717+714 at 2915 km s<sup>-1</sup>*

In the direction toward 1H0717+714 there is absorption at 1041.960 Å that is best interpreted as O VI λ1031.926 at a velocity of 2915 km s<sup>-1</sup> (reported here for the first time). The feature is located just longward of geocoronal O I\* λ1041.688 emission, and we measure it using the orbital-night only data, although it is visible in the combined data. The line is 66±15 mÅ, where the 3σ detection limit for a 60 km s<sup>-1</sup> wide line is 12 mÅ. In the combined day+night data the detection limit is 7 mÅ, so the feature is clearly significant. The corresponding O VI λ1037.617 line is not seen, with a detection limit of 24 mÅ. The expected value is 33±8±8 mÅ, using the statistical error near the O VI λ1037.617 line, and a systematic error based on the O VI λ1031.926 line, but any O VI λ1037.617 absorption would also be contaminated by H<sub>2</sub> L(5-0) P(4) λ1047.550.

The feature at 1035.603 Å is very likely to be the corresponding Lyβ absorption, although its apparent velocity differs by 27 km s<sup>-1</sup> from that of the O VI line. This feature is unlikely to be interstellar C II λ1036.337 at -207 km s<sup>-1</sup> originating in an ionized envelope of the high-velocity cloud complex A, observed about one degree away. Assuming that this HVC has a metallicity of 0.1 solar, the logarithmic carbon abundance would be -4.61, and if the feature is C II, the implied total hydrogen column density would be ~2×10<sup>18</sup> cm<sup>-2</sup>. However, there is no evidence for H I absorption at -207 km s<sup>-1</sup> in the higher Lyman lines. Thus, intergalactic Lyβ at 2888 km s<sup>-1</sup> is the best interpretation for the feature at 1035.603 Å. The spectrum near C II also shows a feature centered at -150 km s<sup>-1</sup>, and this does have corresponding H I absorption in the Lyman lines, with a column density compatible with the possible 1–2×10<sup>18</sup> cm<sup>-2</sup> seen in the 21-cm spectrum. It is likely that this component originates in the outskirts of complex A.



Table 7. Intergalactic O VI systems at  $z < 0.017^1$

Object	Line	$v$ [km s <sup>-1</sup> ]	$W$ [mÅ]	$b$ [km s <sup>-1</sup> ]	$\log N$ [cm <sup>-2</sup> ]
(1)	(2)	(3)	(4)	(5)	(6)
1H 0717+714	Ly $\beta$	2888	41 $\pm$ 7 $\pm$ 8	29 $\pm$ 4	13.86 $\pm$ 0.08 $\pm$ 0.06
1H 0717+714	O VI $\lambda$ 1031	2915	66 $\pm$ 15 $\pm$ 9	32 $\pm$ 2	13.81 $\pm$ 0.17 $\pm$ 0.04
1H 0717+714	O VI $\lambda$ 1037		<23		<13.87
3C 273.0	Ly $\alpha$	1010	394 $\pm$ 7 $\pm$ 1	53 $\pm$ 3	14.27 $\pm$ 0.08 $\pm$ 0.01
3C 273.0	Ly $\beta$	1013	120 $\pm$ 4 $\pm$ 10	44 $\pm$ 2	14.32 $\pm$ 0.02 $\pm$ 0.02
3C 273.0	O VI $\lambda$ 1031	1008	21 $\pm$ 3 $\pm$ 7	34 $\pm$ 6	13.24 $\pm$ 0.15 $\pm$ 0.15
ESO 185–IG13	Ly $\beta$	2635	641 $\pm$ 52 $\pm$ 14	88 $\pm$ 3	>15.35
ESO 185–IG13	O VI $\lambda$ 1031	2627	335 $\pm$ 67 $\pm$ 15	87 $\pm$ 7	14.63 $\pm$ 0.15 $\pm$ 0.01
ESO 185–IG13	C III $\lambda$ 977	2625	470 $\pm$ 113 $\pm$ 42	108 $\pm$ 16	14.18 $\pm$ 0.35 $\pm$ 0.19
HE 0226–4110	Ly $\alpha$	5235	60 $\pm$ 7 $\pm$ 2	17 $\pm$ 3	13.17 $\pm$ 0.06 $\pm$ 0.01
HE 0226–4110	O VI $\lambda$ 1031	5240	41 $\pm$ 6 $\pm$ 4	17 $\pm$ 3	13.57 $\pm$ 0.08 $\pm$ 0.02
HE 0226–4110	C III $\lambda$ 977	5259	23 $\pm$ 9 $\pm$ 3	19 $\pm$ 4	12.64 $\pm$ 0.23 $\pm$ 0.15
HE 0226–4110	C IV $\lambda$ 1548	5232	39 $\pm$ 11 $\pm$ 2	7 $\pm$ 4	13.03 $\pm$ 0.20 $\pm$ 0.14
MRC 2251–178	Ly $\alpha$	2265	133 $\pm$ 12 $\pm$ 3	64 $\pm$ 4	13.43 $\pm$ 0.05 $\pm$ 0.01
MRC 2251–178	O VI $\lambda$ 1037	2283	40 $\pm$ 12 $\pm$ 9	35 $\pm$ 5	13.87 $\pm$ 0.25 $\pm$ 0.08
Mrk 290	O VI $\lambda$ 1031	3073	49 $\pm$ 8 $\pm$ 7	34 $\pm$ 4	13.63 $\pm$ 0.08 $\pm$ 0.06
Mrk 290	O VI $\lambda$ 1037	3073	20 $\pm$ 8 $\pm$ 7	31 $\pm$ 3	13.46 $\pm$ 0.14 $\pm$ 0.17
Mrk 876	Ly $\alpha$	936	476 $\pm$ 14 $\pm$ 3	77 $\pm$ 2	14.27 $\pm$ 0.08 $\pm$ 0.01
Mrk 876	Ly $\beta$	933	79 $\pm$ 6 $\pm$ 33	75 $\pm$ 2	14.14 $\pm$ 0.04 $\pm$ 0.03
Mrk 876	O VI $\lambda$ 1031	945	17 $\pm$ 4 $\pm$ 8	29 $\pm$ 3	13.18 $\pm$ 0.13 $\pm$ 0.16
Mrk 876	O VI $\lambda$ 1037		<16		<13.13
Mrk 876	Si III $\lambda$ 1206	912	42 $\pm$ 9 $\pm$ 1	10 $\pm$ 4	12.34 $\pm$ 0.15 $\pm$ 0.11
Mrk 876	Ly $\alpha$	3481	267 $\pm$ 12 $\pm$ 3	37 $\pm$ 3	>14.06
Mrk 876	O VI $\lambda$ 1031	3508	18 $\pm$ 4 $\pm$ 7	29 $\pm$ 4	13.18 $\pm$ 0.15 $\pm$ 0.16
PG 0844+349	Ly $\beta$	351	25 $\pm$ 8 $\pm$ 2	6 $\pm$ 2	13.66 $\pm$ 0.09 $\pm$ 0.03
PG 0844+349	O VI $\lambda$ 1031	365	37 $\pm$ 5 $\pm$ 2	28 $\pm$ 2	13.57 $\pm$ 0.08 $\pm$ 0.02
PG 0844+349	O VI $\lambda$ 1037	365	27 $\pm$ 5 $\pm$ 7	..	13.74 $\pm$ 0.09 $\pm$ 0.04
PG 0953+414	Ly $\alpha$	621	70 $\pm$ 9 $\pm$ 3	41 $\pm$ 3	13.19 $\pm$ 0.06 $\pm$ 0.01
PG 0953+414	Ly $\beta$		<23		<13.52
PG 0953+414	O VI $\lambda$ 1031	637	39 $\pm$ 8 $\pm$ 7	53 $\pm$ 2	13.57 $\pm$ 0.11 $\pm$ 0.07
PG 1259+593	Ly $\alpha$	678	231 $\pm$ 9 $\pm$ 3	62 $\pm$ 3	13.81 $\pm$ 0.02 $\pm$ 0.01
PG 1259+593	Ly $\beta$		<15		<13.26
PG 1259+593	O VI $\lambda$ 1031	627	25 $\pm$ 5 $\pm$ 2	24 $\pm$ 4	13.33 $\pm$ 0.11 $\pm$ 0.03
PG 1259+593	O VI $\lambda$ 1037	622	13 $\pm$ 3 $\pm$ 2	15 $\pm$ 3	13.41 $\pm$ 0.12 $\pm$ 0.06
PG 1302–102	Ly $\alpha$		<72		<13.21
PG 1302–102	O VI $\lambda$ 1031	3109	19 $\pm$ 6 $\pm$ 8	13 $\pm$ 5	13.23 $\pm$ 0.15 $\pm$ 0.15
PG 1302–102	O VI $\lambda$ 1037		<23		<13.34
Ton S180	Ly $\beta$		<37		<13.76
Ton S180	O VI $\lambda$ 1031	260	51 $\pm$ 10 $\pm$ 8	24 $\pm$ 4	13.68 $\pm$ 0.09 $\pm$ 0.05
Ton S180	O VI $\lambda$ 1037	285	34 $\pm$ 13 $\pm$ 8	33 $\pm$ 5	13.75 $\pm$ 0.24 $\pm$ 0.09
Ton S180	C III $\lambda$ 977	279	60 $\pm$ 28 $\pm$ 7	41 $\pm$ 8	13.10 $\pm$ 0.26 $\pm$ 0.16
Ton S210	Ly $\beta$		<20		<13.45
Ton S210	O VI $\lambda$ 1031	288	25 $\pm$ 8 $\pm$ 7	41 $\pm$ 6	13.38 $\pm$ 0.13 $\pm$ 0.10

Note. — 1: Column (1) gives the target name. Column (2) gives the O VI lines and other lines in the system that are detected or, in the cases of Ly $\alpha$ , Ly $\beta$ , O VI, where it is possible to set an upper limit. Columns (3), (5) and (6) give the central (heliocentric) velocity, linewidth and logarithmic column density derived from a gaussian fit to the apparent optical depth profile (see Sembach & Savage 1992). Column (4) gives the equivalent width, with upper limits determined by integrating over a 60 km s<sup>-1</sup> wide window centered on the central velocity of the detected ion.

The galaxy nearest the sightline is UGC 3804, at  $v_{gal}=2887 \text{ km s}^{-1}$ ,  $\rho=199 \text{ kpc}$ , with diameter  $22.8 \text{ kpc}$ . It is a member of the LGG 141 group, but most of the group galaxies have impact parameters  $>650 \text{ kpc}$ .

Nominally, the velocity of  $\text{Ly}\beta$  and  $\text{O VI } \lambda 1031.926$  differ by  $27 \text{ km s}^{-1}$ , but the S/N in the O VI spectrum is too low to know for sure. The linewidths of the  $\text{Ly}\beta$  and  $\text{O VI } \lambda 1031.926$  absorption are very similar ( $29$  vs  $32 \text{ km s}^{-1}$ ). Thus, the velocity offset between H I and O VI suggests collisional ionization, while the similarity in the linewidths suggests photoionization (although the O VI line would be relatively wide). However, we conclude that the measurements are too noisy to properly distinguish between the different ionization origins.

### *3C 273.0 at $1010 \text{ km s}^{-1}$*

This  $\text{O VI } \lambda 1031.926$  absorption is relatively clear, and it was previously reported by Sembach et al. (2001), Danforth & Shull (2005) and Tripp et al. (2008). The strong  $\text{Ly}\alpha$  and  $\text{Ly}\beta$  lines originate in LGG 292, one of the groups near the Virgo cluster. The nearest group galaxy is MCG0-32-16 ( $v_{gal}=1105 \text{ km s}^{-1}$ ,  $D_{gal}=6.3 \text{ kpc}$ ), with impact parameter  $191 \text{ kpc}$ . A number of smaller galaxies have  $\rho=200\text{--}500 \text{ kpc}$ . As can be seen in Fig. 2, the  $\text{O VI } \lambda 1037.617$  line is strongly contaminated by  $\text{H}_2 \text{ L}(5\text{--}0) \text{ R}(3) \lambda 1041.158$  absorption. Although the  $\text{Ly}\alpha$  line is very strong, the H I column densities derived from the  $\text{Ly}\alpha$  and  $\text{Ly}\beta$  lines match. The O VI line is only slightly narrower than the H I lines ( $b=34 \text{ km s}^{-1}$  vs  $b\sim 50 \text{ km s}^{-1}$ ). Nominally this implies a temperature of  $8.5\times 10^4 \text{ K}$  and  $b(\text{turbulent})\sim 30 \text{ km s}^{-1}$ . As the H I and O VI velocities are close ( $1010$  vs  $1008 \text{ km s}^{-1}$ ), the system is likely to be mostly photoionized gas. although the temperature would be very high for gas in photoionization equilibrium.

### *ESO 185-IG13 at $2627 \text{ km s}^{-1}$*

The  $\text{Ly}\beta$  line in this spectrum is so strong that it is saturated. Similarly, the  $\text{O VI } \lambda 1031.926$  at  $2627 \text{ km s}^{-1}$  is very strong, so even though we can only use orbital-night-only data, and even though the spectrum is rather noisy, the detection is clear. The  $\text{O VI } \lambda 1037.617$  line, unfortunately, is hidden by the intrinsic  $\text{Ly}\beta$  absorption, but it would probably be visible in a spectrum with higher S/N ratio. The sightline to ESO 185-IG13 is the seventh closest to another galaxy in our sample. IC 4889 ( $v_{gal}=2526 \text{ km s}^{-1}$ ,  $D_{gal}=28.9 \text{ kpc}$ ) has impact parameter  $62 \text{ kpc}$ . The  $\text{Ly}\beta$  and O VI lines are very broad ( $88$  vs  $87 \text{ km s}^{-1}$ ) and close in velocity. However, the saturation of the  $\text{Ly}\beta$  line limits the value of the line width comparison. The O VI could be either photoionized or collisionally ionized.

### *HE 0226–4110 at $5240 \text{ km s}^{-1}$*

Near a velocity of  $5240 \text{ km s}^{-1}$  there is a set of narrow lines that is likely to contain

intergalactic Ly $\alpha$ , Ly $\beta$  and O VI  $\lambda$ 1031.926. These were previously reported by Lehner et al. (2006) and Tripp et al. (2008), but were not listed by Danforth & Shull (2005, 2008). The Ly $\alpha$  line is clear, though rather narrow ( $b=17 \text{ km s}^{-1}$ ), which sets an upper limit on the gas temperature of 6500 K. The Ly $\beta$  line is confused by the FUSE detector flaw near 1043 Å. So although there appears to be a feature where Ly $\beta$  is expected, it can't be reliably measured. At the velocity of the O VI  $\lambda$ 1037.617 line is a H<sub>2</sub> line (L(4-0) R(1)  $\lambda$ 1049.960), but the H<sub>2</sub> model that is based on all H<sub>2</sub> lines combined shows that the feature is too strong. The best explanation is additional intergalactic O VI at 5240 km s<sup>-1</sup>. After correcting for the H<sub>2</sub> line, the linewidth and velocity of this feature matches that of Ly $\alpha$ , strongly suggesting that the gas is photoionized. Unfortunately, the corresponding O VI  $\lambda$ 1037.617 is contaminated by intergalactic O IV  $\lambda$ 787.711 at  $z=0.34035$  (see Lehner et al. 2006).

This sightline passes 562 kpc from NGC 954 ( $v_{gal}=5353 \text{ km s}^{-1}$ ,  $D_{gal}=33.0 \text{ kpc}$ ), a member of a group of galaxies with  $v\sim 5000 \text{ km s}^{-1}$  that is not included in Garcia et al. (1993). The impact parameter is the largest for any of the O VI absorbers in our sample, but the galaxy surveys in this part of the sky are not very deep, so there is a good chance that an  $L>0.1 L_*$  galaxy with lower impact parameter can be found.

#### *MRC 2251–178 at 2283 km s<sup>-1</sup>*

In this sightline a clear Ly $\alpha$  feature at 2265 km s<sup>-1</sup> appears to be matched by an O VI  $\lambda$ 1037.617 line at 2283 km s<sup>-1</sup>, although this feature has a significance of only about  $3.5\sigma$ . Both the Ly $\alpha$  and the O VI line may have two (matching) components. The O VI  $\lambda$ 1031.926 line is contaminated by strong geocoronal emission, even in the orbital-night-only data. This is therefore one of the most uncertain O VI detections. There is a suggestion that both the Ly $\alpha$  and the O VI absorptions have two components, but the S/N ratio of the data is not good enough to definitively decide this. If the O VI line is real, it can be associated with ESO 603-G31 ( $v_{gal}=2271 \text{ km s}^{-1}$ ,  $D_{gal}=9.1 \text{ kpc}$ ) at impact parameter 422 kpc. Danforth & Shull (2005) did not report this feature, nor did they give a lower limit. If we assume that the structure inside the line is real, photoionization is the most likely explanation for this, since the lines would be narrow. If instead the structure is noise (quite likely), then we conclude that the width of the H I line ( $b=64\pm 4 \text{ km s}^{-1}$ ) is about twice that of the O VI line ( $b=35\pm 5 \text{ km s}^{-1}$ ), which would imply  $T\sim 1.8\times 10^5 \text{ K}$  and  $b(\text{turbulent})\sim 30 \text{ km s}^{-1}$ . Thus the gas in this system is probably collisionally ionized.

#### *Mrk 290 at 3073 km s<sup>-1</sup>*

In this sightline, a clearly significant ( $49\pm 8 \text{ mÅ}$ ) feature at 1042.504 Å is best explained as intergalactic O VI absorption at 3073 km s<sup>-1</sup>. There are no interstellar lines at this wavelength. The feature cannot be Ly $\beta$  at 5163 km s<sup>-1</sup>, as there is no matching, stronger, Ly $\alpha$

line in the *GHR*S spectrum. The  $\text{Ly}\alpha$  line corresponding to the O VI has not been observed, but a *COS* spectrum is planned; detecting  $\text{Ly}\alpha$  would confirm the O VI interpretation. The corresponding  $\text{Ly}\beta$  line is obscured by saturated Galactic C II absorption. There does appear to be a matching O VI  $\lambda 1037.617$  absorption. Although this is blended on one side with Galactic Ar I  $\lambda 1048.220$ , no other Galactic interstellar absorption line has a wing on the positive-velocity side. Moreover, if we measure just the positive-velocity side of this feature, its strength and width match the values expected from the O VI  $\lambda 1031.926$  absorption. On balance, this O VI absorber appears secure. However, there is not enough information to determine the origin of the ionization of O VI.

Several galaxies with  $v_{gal} \sim 3100 \text{ km s}^{-1}$  have impact parameters of 300–600 kpc. In Table 3 we associate the absorber with NGC 5987 ( $\rho=424 \text{ kpc}$ ), as it is by far the largest ( $v_{gal}=3010 \text{ km s}^{-1}$ ,  $D_{gal}=51.7 \text{ kpc}$ ).

#### *Mrk 876 at 945 km s<sup>-1</sup>*

Toward Mrk 876 there is a feature at  $1035.179 \text{ \AA}$  that we interpret as a blend of  $\text{H}_2$  L(6-0) P(4) at  $1035.783 \text{ \AA}$  and O VI  $\lambda 1031.926$  redshifted to a velocity of  $945 \text{ km s}^{-1}$ . As can be seen in Fig. 2, the  $\text{H}_2$  model does not exactly match this feature, unlike what is the case for the other  $\text{H}_2$   $J=4$  lines (see e.g. the Mrk 876–UGC 10294 panel in Fig. 2). After removal of the  $\text{H}_2$  absorption, a  $4\sigma$  absorption remains, which we interpret as intergalactic O VI  $\lambda 1031.926$ , because there also is  $\text{Ly}\alpha$  and  $\text{Ly}\beta$  absorption at its velocity; these lines were previously reported by Shull et al. (2000) and Côté et al. (2005). Finally, there is a  $42 \pm 9 \text{ m\AA}$  feature at  $1210.170 \text{ \AA}$  that is most likely Si III at  $912 \text{ km s}^{-1}$ .

The  $\text{Ly}\alpha$  line is broad ( $b=75 \text{ km s}^{-1}$ ) and at a velocity of  $936 \text{ km s}^{-1}$ . The S/N ratio of the *STIS*-E140M spectrum is insufficient to determine whether this line is a single or multi-component absorber, although the apparent optical depth profile looks compatible with a single component. The corresponding  $\text{Ly}\beta$  absorption is strongly contaminated by two-component  $\text{H}_2$  L(6-0) R(3)  $\lambda 1028.985$  absorption, but after correcting for this contamination, the implied HI column density matches that of the  $\text{Ly}\alpha$  line to within the errors.

Although the width of the O VI line is difficult to measure, it is less than half that of the  $\text{Ly}\alpha$  line ( $b=29 \text{ km s}^{-1}$ ). The difference in the HI and O VI linewidths implies  $T=3 \times 10^5 \text{ K}$  and  $b(\text{turbulent})=23 \text{ km s}^{-1}$ , implying the origin of the ionization is almost certainly collisional ionization.

A large ( $D_{gal}=27.1 \text{ kpc}$ ) isolated galaxy (NGC 6140,  $v_{gal}=910 \text{ km s}^{-1}$ ) lies only 206 kpc from the sightline, and it is the only candidate galaxy to associate with the absorber.

#### *Mrk 876 at 3508 km s<sup>-1</sup>*

The strong Ly $\alpha$  line at 3481 km s<sup>-1</sup> (previously reported by Danforth & Shull 2005) is matched by Ly $\beta$  absorption, although the latter is blended with Galactic O VI  $\lambda$ 1037.617, and no equivalent width can be measured. The presence of Ly $\beta$  is shown by the fact that the apparent optical depth profiles of Galactic O VI  $\lambda$ 1031.926 and O VI  $\lambda$ 1037.617 do not match, the only sightline in the FUSE sample for which this is the case (see Wakker et al. 2003). A  $4.5\sigma$  ( $17\pm4$  mÅ) feature at 1044.001 Å is best explained as a corresponding O VI  $\lambda$ 1031.926 line at 3501 km s<sup>-1</sup>, even though it is offset in velocity from Ly $\alpha$  by 27 km s<sup>-1</sup>. Danforth & Shull (2005) reported an upper limit of 16 mÅ at this velocity. There is only one galaxy that can clearly be associated with the absorption: UGC 10294 ( $v_{gal}=3516$  kpc,  $D_{gal}=27.6$  kpc,  $\rho=282$  kpc). The widths of the Ly $\alpha$  and O VI  $\lambda$ 1031.926 lines are similar (37 vs 29 km s<sup>-1</sup>), which would support the idea that this system consists of photoionized gas. However, such an origin does not explain the 27 km s<sup>-1</sup> velocity offset, so collisional ionization is more likely.

#### *PG 0844+349 at 365 km s<sup>-1</sup>*

The FUSE spectrum of this target has several features that are difficult to interpret, but which we decided are Ly $\beta$ , O VI  $\lambda$ 1031.926 and O VI  $\lambda$ 1037.617 at  $\sim 360$  km s<sup>-1</sup>. Unfortunately, this velocity is such that any Ly $\alpha$  line would be hidden in the Galactic Ly $\alpha$  line. In the O VI  $\lambda$ 1031.926 part of the spectrum there are three clear features. We interpret the two at the most positive velocities as Ly $\beta$  at 2260 and 2326 km s<sup>-1</sup>, especially since there is a strong feature in the low-resolution *FOS* spectrum near these velocities. Normally, we would be inclined to identify the third feature also as Ly $\beta$ , although this line is only a  $3\sigma$  detection, and appears to be extremely narrow. Furthermore, the spectrum lies below the continuum at the wavelengths where O VI  $\lambda$ 1037.617 is expected, even though this falls between a H<sub>2</sub> line (L(5-0) R(2)  $\lambda$ 1038.689) and Galactic O I  $\lambda$ 1039.230. The low quality of the Ly $\beta$  measurement makes it difficult to determine the origin of the ionization of O VI even though the O VI line appears to be broader than the Ly $\beta$  line and there is a velocity offset.

#### *PG 0953+414 at 637 km s<sup>-1</sup>*

Toward this target there are two clear features that can be interpreted as Ly $\alpha$  at 621 km s<sup>-1</sup> and O VI  $\lambda$ 1031.926 at 637 km s<sup>-1</sup>, which have not been reported before. Both of these features are very significant ( $70\pm9$  and  $39\pm8$  mÅ), and intergalactic O VI is the most likely interpretation for the feature at 1034.129 Å. This system can be associated with NGC 3104 ( $v_{gal}=612$  km s<sup>-1</sup>,  $D_{gal}=11.5$  kpc,  $\rho=296$  kpc), which is the only galaxy with  $v\sim 600$  km s<sup>-1</sup> and  $\rho<600$  kpc. The widths of the Ly $\alpha$  and O VI  $\lambda$ 1031.926 lines are difficult to measure because the H I line is noisy and in the wing of Galactic Ly $\alpha$ . They are similar, though large ( $b=41\pm3$  and  $53\pm2$  km s<sup>-1</sup>). Since the velocities differ by 16 km s<sup>-1</sup>, this O VI system may originate in a collisionally ionized gas.

*PG 1259+593 at 627 km s<sup>-1</sup>*

In the spectrum of this target there is a set of aligned features. The Ly $\alpha$  line at 678 km s<sup>-1</sup> is clear, and fairly broad. Tripp et al. (2008) interpreted this as a two-component system, probably basing this on the possibly double O VI line. However, the noise in the Ly $\alpha$  spectrum is too high to be certain. Therefore, we list this as a single system. The expected corresponding Ly $\beta$  line is weak, and, if present, would be hidden by H<sub>2</sub> L(6-0) P(2)  $\lambda$ 1028.104. At velocities of 627 and 622 km s<sup>-1</sup> there is a matching set of O VI features, whose equivalent widths are in the ratio 2:1. We interpret this set of absorbers as an intergalactic system associated with UGC 8146 ( $v_{gal}=669$  km s<sup>-1</sup>,  $D_{gal}=12.6$  kpc,  $\rho=80$  kpc), even though there is a dwarf galaxy (SDSS J130206.46+584142.8,  $D_{gal}=1.8$  kpc) with slightly lower impact parameter (72 kpc). These features were previously reported by Richter et al. (2004), Côté et al. (2005), Danforth et al. (2006) and Tripp et al. (2008).

The widths of the two O VI lines appear to differ ( $b=24\pm4$  and  $15\pm3$  km s<sup>-1</sup>), but this can be attributed to the noisiness of the data. The average of these is about a factor three smaller than the width of the Ly $\alpha$  line ( $b=62\pm3$  km s<sup>-1</sup>). However, mostly because the H I and O VI velocities differ by 51 km s<sup>-1</sup>, collisional ionization is the more likely explanation for the origin of this system.

*PG 1302–102 at 3109 km s<sup>-1</sup>*

The possible O VI  $\lambda$ 1031.926 absorber at 3109 km s<sup>-1</sup> that we list toward PG 1302–102 is the least certain detection in our sample. Ly $\beta$  is hidden by Galactic C II absorption, O VI  $\lambda$ 1037.617 would be too weak and blends with Ar I  $\lambda$ 1048.220. For Ly $\alpha$  only an upper limit of 72 mÅ can be set. However, since two of the seven Ly $\alpha$  lines in systems with O VI have  $W\sim70$  mÅ, the Ly $\alpha$  non-detection is not problematic. The O VI  $\lambda$ 1031.926 line itself is not strong, but appears clear (see Fig. 2). The line is narrow ( $b=13$  km s<sup>-1</sup>), so if this system is real, it probably consists of photoionized material, as turbulent broadening usually is at least this large.

The galaxy NGC 4939 ( $v_{gal}=3111$  km s<sup>-1</sup>,  $D_{gal}=24.6$  kpc) lies only 104 kpc from the sightline. It is the only galaxy with velocity near 3109 km s<sup>-1</sup> with  $\rho<900$  kpc, and thus the only candidate for associating with the absorber. The small impact parameter to this galaxy is one of the arguments we use to interpret the feature as a real line, as we find all other  $L>0.1 L_*$  field galaxies with impact parameter  $<350$  kpc have associated Ly $\alpha$  absorption.

*Ton S180 at 260 km s<sup>-1</sup>*

In this sightline there is a clear pair of O VI lines, centered at 260 km s<sup>-1</sup> (first reported by Wakker et al. 2003). The separately derived column densities are compatible with each

other. However, no HI is detected, as Ly $\beta$  is blended with geocoronal O I\*  $\lambda$ 1027.431, and any Ly $\alpha$  would be hidden by the Galactic Ly $\alpha$  absorption. On the other hand, there is a possible C III line centered at 279 km s $^{-1}$  that goes with the O VI detection. On balance, the identification of the O VI lines appears secure. In spite of their relatively low velocity (below 400 km s $^{-1}$ ), we identify the lines as intergalactic, rather than as originating in the Milky Way halo, since no other Galactic high-velocity gas with high positive velocities is known in the part of the sky where Ton S180 is located, and because NGC 247 ( $v_{gal}$ =159 km s $^{-1}$ ,  $D_{gal}$ =15.7 kpc) has an impact parameter of only 125 kpc. There is not enough information to determine the origin of the ionization of O VI.

#### *Ton S210 at 288 km s $^{-1}$*

The feature at 1032.933 Å is interpreted as probable O VI  $\lambda$ 1031.926 at 288 km s $^{-1}$ , even though there is no corroborating Ly $\alpha$  (hidden in Galactic Ly $\alpha$ ), Ly $\beta$  (confused by geocoronal O I\*  $\lambda$ 1027.431) or O VI  $\lambda$ 1037.617 (blended with H $_2$  L(5-0) R(2)  $\lambda$ 1038.689). However, there are no other intergalactic absorption systems that produce e.g. Ly $\beta$  or metal lines at this wavelength, so O VI  $\lambda$ 1031.926 is the most likely interpretation. If so, this line is associated with NGC 253 ( $v_{gal}$ =251 km s $^{-1}$ ,  $D_{gal}$ =20.7 kpc,  $\rho$ =374 kpc). However, the velocity of this absorber is low enough that another possibility is that the gas is located in the Local Group. There is not enough information to constrain the origin of the O VI absorption.

In their analysis of 78 O VI absorbers, Tripp et al. (2008) plotted the O VI/H I column density ratio vs  $N(\text{H I})$  and found a strong correlation between the two. If we do this for the 11 systems in Table 7 with both H I and O VI results, we find that our systems follow the same relation, with  $N(\text{H I})$  ranging from 13.17 to 14.27, which falls in the middle of the range found by Tripp et al. (2008). Further, for the most part, the linewidths of our O VI/H I absorbers follow the distribution found by Tripp et al. (2008) (see Sect. 3.2). This suggests that the conclusions of Tripp et al. (2008) concerning the nature of the low-redshift O VI absorbers are also valid for these 11 systems.

As discussed above, we have a reasonably good handle on the origin of the ionization in 8 of the 14 systems. Based on the linewidth and velocity offset comparison, we conclude that collisional ionization is likely for five absorbers (toward MRC 2251–178, Mrk 876 (both systems), PG 0953+414 and PG 1259+593), while for three photoionization is more likely (toward 3C 273.0, HE 0226–4110 and PG 1302–102). The origin of the O VI ionization remains undetermined in 6 of the 14 systems.

As can be seen from the cases above, 10 of the 14 O VI absorbers originate within 550 kpc from an  $L_*$  galaxy, and the other four originate within 450 kpc of an 0.1  $L_*$  galaxy. We therefore agree with Stocke et al. (2006) that *in general, low-redshift intergalactic O VI*



*only originates within 500 kpc from bright galaxies.*

### 3.3. Distribution of $\text{Ly}\alpha$ , $\text{Ly}\beta$ and O VI Linewidths

Figure 4 shows the distributions of fitted linewidths, separately for each of four lines –  $\text{Ly}\alpha$ ,  $\text{Ly}\beta$ , O VI  $\lambda 1031.926$  and O VI  $\lambda 1037.617$ . The widths have been corrected for instrumental broadening, although this makes only a slight difference, as the resolution is  $6.5 \text{ km s}^{-1}$  for *STIS*-E140M data and  $\sim 30$  and  $20 \text{ km s}^{-1}$  for *STIS*-G140M and FUSE data, respectively, while the full width at half maximum (FWHM) of the lines typically is much larger. We removed saturated  $\text{Ly}\alpha$  lines, some weak lines with low significance and lines in noisy spectra, as well as lines observed with the *GHERS*, as its line-spread function has broad wings. We also removed lines that are blended with  $\text{H}_2$  or with the FUSE detector flaw or which are otherwise problematic (such as multi-component lines).

For  $\text{Ly}\alpha$  we find  $\langle b \rangle = 50 \text{ km s}^{-1}$ , median  $49 \text{ km s}^{-1}$  and dispersion  $19 \text{ km s}^{-1}$ , where Penton et al. (2000b) measured  $\langle b \rangle = 38 \text{ km s}^{-1}$ , median  $35 \text{ km s}^{-1}$  and dispersion  $16 \text{ km s}^{-1}$ , while Danforth & Shull (2008) give a median of  $28 \text{ km s}^{-1}$  and dispersion  $16 \text{ km s}^{-1}$ . Although 47 of our 115  $\text{Ly}\alpha$  lines overlap with the Penton et al. (2000b) sample, the discussion in the next subsection suggests that the difference in the medians may be significant and that the typical linewidth at  $z=0-0.017$  may be larger than at  $z=0.017-0.2$ .

A new result is our derivation of these values for  $\text{Ly}\beta$ :  $\langle b \rangle = 42 \text{ km s}^{-1}$ , median  $38 \text{ km s}^{-1}$  and dispersion  $20 \text{ km s}^{-1}$ , i.e. on average the  $\text{Ly}\beta$  lines seem to be slightly narrower than the  $\text{Ly}\alpha$  lines. This may indicate that some of the  $\text{Ly}\alpha$  lines that we thought were well-measured are still affected by saturation and other effects.

For O VI,  $\langle b \rangle = 29 \text{ km s}^{-1}$ , median  $29 \text{ km s}^{-1}$  and dispersion  $11 \text{ km s}^{-1}$  (excluding the noisy, apparently broad detection associated with IC 4889). Thus, the average/median is smaller for O VI than for H I. As discussed in Sect. 3.2, we find individual cases where  $b(\text{O VI}) < b(\text{H I})$ , but also cases where the linewidths are similar. Tripp et al. (2008) showed the linewidth distribution of 74 O VI absorbers that were found in a sample of 16 AGNs with redshifts up to 0.5. We show their distribution by the dotted line in Fig. 4 (scaling to our sample size of 14). When compared to the 14 absorbers at  $z < 0.017$  that form our sample, it is clear that the two distributions are similar.

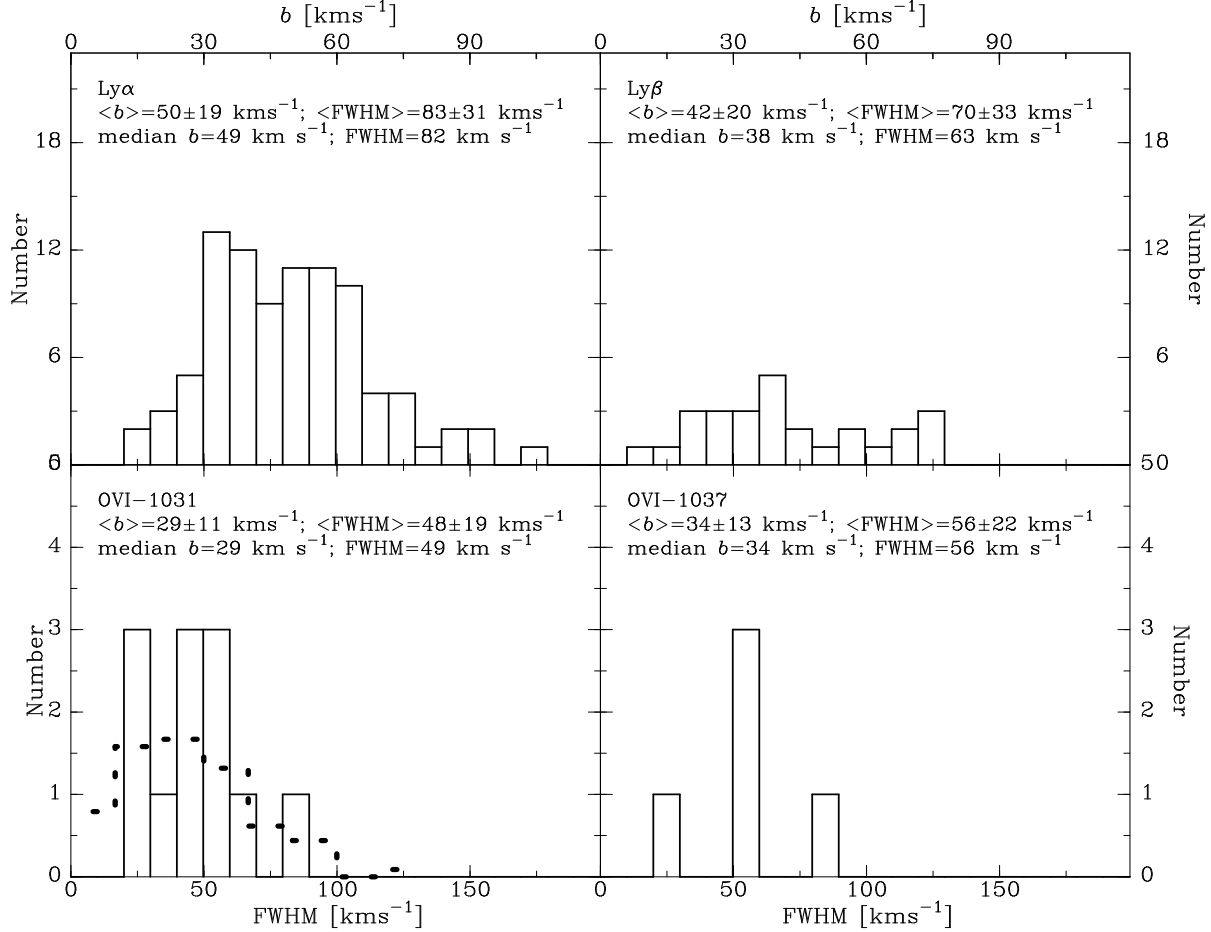


Fig. 4.— Distributions of fitted linewidths for four different lines (Ly $\alpha$ , Ly $\beta$ , OVI  $\lambda$ 1031.926 and OVI  $\lambda$ 1037.617), as indicated in the top left corner of each panel.  $b$  values for Ly $\alpha$  and Ly $\beta$  are listed in Table 5, those for OVI in Table 7. The top x-scale gives  $b$ -values, the bottom x-scale the full-width-at-half-maximum (FWHM). *Selection criteria:* all lines that are not contaminated by H $_2$  absorption, the FUSE detector flaw near 1043 Å, or blended with other absorption lines. The dotted line in the OVI  $\lambda$ 1031.926 panel shows the distribution found by Tripp et al. (2008), scaled to our sample size.

Table 8.  $dN(\text{OVI})/dz$  values<sup>1</sup>

item (1)	This paper (2)	Danforth & Shull (2005) <sup>2</sup> (3)	Tripp et al. (2008) (4)	Thom & Chen (2008) (5)
path@ $W_{\text{lim}}=50 \text{ m}\text{\AA}$	0.4	2.0	2.8	2.4
# sightlines	76	31	16	16
$W_{\text{lim}}$ scale <sup>3</sup>	1.0	1.3	1.0	1.5
$W_{\text{lim}}=15 \text{ m}\text{\AA}$		19±3 (38)		
$W_{\text{lim}}=20 \text{ m}\text{\AA}$	50±22 (10)			
$W_{\text{lim}}=30 \text{ m}\text{\AA}$	16±9 (7)	17±3 (35)	15.6±2.9±2.4 (41)	10.4±2.2 (22)
$W_{\text{lim}}=50 \text{ m}\text{\AA}$	8±5 (3)	9±2 (19)		6.7±1.7 (16)
$W_{\text{lim}}=70 \text{ m}\text{\AA}$	2±3 (1)		8.8±2.1±1.7 (27)	
$W_{\text{lim}}=100 \text{ m}\text{\AA}$		3±2 (6)	4.5±1.5±1.2 (14)	
$W_{\text{lim}}=200 \text{ m}\text{\AA}$			2.2±1.2±0.8 (6)	
$W_{\text{lim}}=300 \text{ m}\text{\AA}$			0.9±1.0±0.5 (3)	

Note. — 1: Entries gives the published values for low-redshift  $dN(\text{OVI})/dz$ , followed by the number of detections (in parentheses) at the given equivalent width limit. 2: Danforth & Shull (2008) show a plot of  $dN/dz$  based on more data, but they do not give a table. However, the distribution in their plot follows the numbers in Danforth & Shull (2005). 3: The different studies used different ways to define the equivalent width limit at a given wavelength. The listed values are those reported in the original publications. However, to properly compare the  $dN/dz$  values the equivalent width limits need to be scaled with the values in row three. E.g.,  $dN/dz$  (Danforth & Shull at 30 mÅ) should be compared to  $dN/dz$  (this paper at 40 mÅ).

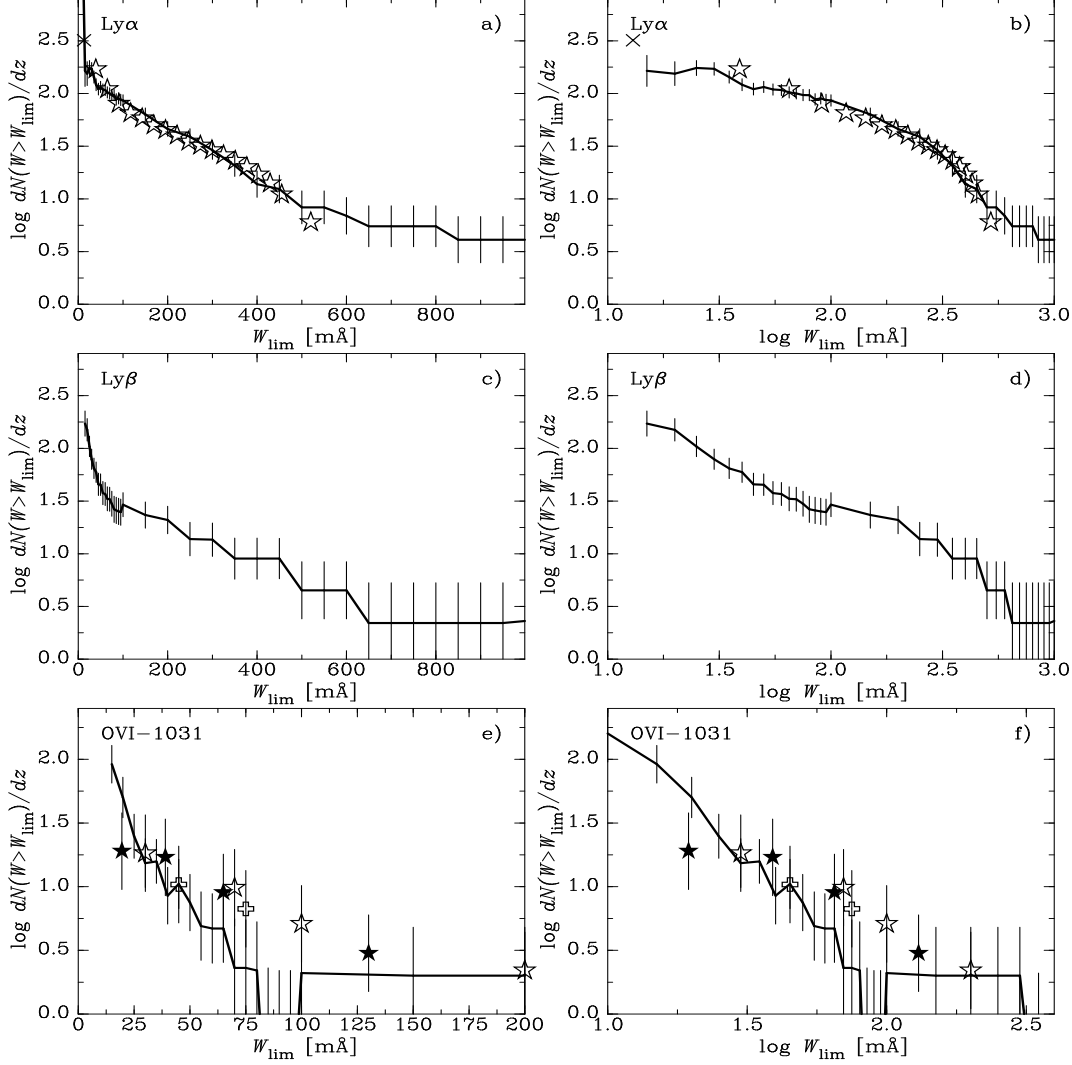


Fig. 5.— Plots of the frequency of occurrence of Ly $\alpha$ , Ly $\beta$  and OVI. Linear equivalent width limit scale on the left, logarithmic scale on the right. Our results, based on 102 Ly $\alpha$ , 34 Ly $\beta$  and 11 OVI detections at  $v=400\text{--}5000\text{ km s}^{-1}$ , are shown as the solid line with error bars. The stars in panels a and b show the distribution of Penton et al. (2004), corrected for the difference in the way that equivalent width limits are measured (see Sect. 2.3). In panels e and f the closed stars show the  $dN/dz$  distribution of Danforth & Shull (2005), the open stars that of Tripp et al. (2008) and the open pluses that of Thom & Chen (2008), with corrections for the difference in equivalent width limit calculation when necessary. *Selection criteria:* all 133 Ly $\alpha$ , Ly $\beta$ , OVI lines at  $v=400\text{--}5000\text{ km s}^{-1}$  with  $W > W_{\text{lim}}$ .

### 3.4. $dN/dz$ – Frequency of Intergalactic Ly $\alpha$ , Ly $\beta$ and O VI $\lambda$ 1031.926

In Fig. 5 we present plots for the frequency with which Ly $\alpha$ , Ly $\beta$  and O VI  $\lambda$ 1031.926 occur ( $dN/dz$ ), as function of the limiting equivalent width. This is a fundamental quantity that can be predicted by theoretical models (e.g., Cen et al. 2001; Fang & Bryan 2001; Furlanetto et al. 2005; Cen & Fang 2006), as well as one that can be converted to an estimate of the baryon density associated with the ion. Penton et al. (2004) and Tripp et al. (2008) presented their results for  $dN/dz$  for Ly $\alpha$  and O VI  $\lambda$ 1031.926 absorbers in the low redshift universe, which in their case meant  $z < 0.5$  in 15 and 16 sightlines, respectively.

Estimating  $dN/dz$  as function of limiting equivalent width  $W_{\text{lim}}$  requires counting the number of absorbers with equivalent width  $W$  larger than  $W_{\text{lim}}$  and dividing by the total path  $\Delta z$  over which these absorbers could have been detected. In practice, this calculation is not trivial, because the limiting equivalent width varies widely between the different sightlines in our sample, and even within a single spectrum (e.g., if there are strong emission lines intrinsic to the background AGN). We thus calculate the  $3\sigma$  equivalent width upper limit for a  $60 \text{ km s}^{-1}$  wide absorber as function of wavelength for each of Ly $\alpha$ , Ly $\beta$  and O VI  $\lambda$ 1031.926. For a given  $W_{\text{lim}}$  we then find the total velocity range between 400 and  $5000 \text{ km s}^{-1}$  over which lines with  $W > W_{\text{lim}}$  could have been detected. We subtract the ranges where Galactic or higher-redshift intergalactic lines block the possible detection of intergalactic lines. This includes both ionic and molecular low- and high-velocity Galactic absorption. We also estimate an error for the pathlength, taking into account the fuzzy edges of the Galactic absorption lines ( $50 \text{ km s}^{-1}$  per sightline for Ly $\alpha$ ,  $200 \text{ km s}^{-1}$  per sightline for Ly $\beta$  and O VI  $\lambda$ 1031.926). In our 76 sightlines, in the velocity range  $v=400\text{--}5000 \text{ km s}^{-1}$  ( $z=0.0013\text{--}0.0167$ ), and for  $W_{\text{lim}} > 100 \text{ mÅ}$ , we build up  $\Delta z=0.68$  for Ly $\alpha$ ,  $\Delta z=0.41$  for Ly $\beta$  and  $\Delta z=0.48$  for O VI  $\lambda$ 1031.926. This can be compared to the values  $\Delta z=1.1$  for Ly $\alpha$  in Penton et al. (2004) and  $\Delta z=3.2$  for O VI  $\lambda$ 1031.926 in Tripp et al. (2008). For lower  $W_{\text{lim}}$ , the redshift path decreases ( $\Delta z=0.51, 0.33, 0.40$  for Ly $\alpha$ , Ly $\beta$ , O VI  $\lambda$ 1031.926, respectively at  $W_{\text{lim}}=50 \text{ mÅ}$ ), until it hits zero at  $W_{\text{lim}} \sim 20 \text{ mÅ}$ .

The resulting  $dN/dz$  distributions are shown in Fig. 5, with a log-log scale in the right column and a linear scale in the left column. The error estimate for each  $dN/dz$  combines  $\sqrt{\# \text{ detections}}$  with the estimated error in the path; the latter is only important at the lowest values of  $W_{\text{lim}}$ .

In Figs. 5a, b, the connected points with error bars show our data, i.e.  $\log dN(\text{Ly}\alpha)/dz$  for velocities  $< 5000 \text{ km s}^{-1}$  ( $z < 0.0167$ ). The stars show the results from Penton et al. (2004), which were taken from the plot in their paper, although we multiplied  $W_{\text{lim}}$  by a factor 1.3 to account for the difference in the way the equivalent width limits are calculated (see Sect. 2.3). It is clear that the two distributions are basically identical, implying that

the somewhat higher redshifts Ly $\alpha$  absorbers at  $v=5000\text{--}20000\text{ km s}^{-1}$  in the Penton et al. (2004) sample should have the same relationship to galaxies as we find below in Sects. 4 and 5.

We make three additional remarks. First, Penton et al. (2004) showed a Ly $\alpha$  point at  $W_{\text{lim}}=10\text{ m}\text{\AA}$ , even though only two of their detections are weaker than  $20\text{ m}\text{\AA}$ , and there is almost no redshift path at  $W_{\text{lim}}<20\text{ m}\text{\AA}$  ( $\Delta z<0.02$ ); this point is shown by the crosses in Figs. 5a, b. Second, in the  $\log dN/dz$  vs  $\log W_{\text{lim}}$  plot (Fig. 5b), our Ly $\alpha$  distribution appears to show a slight turnover for the weakest absorbers ( $W_{\text{lim}}<25\text{ m}\text{\AA}$ ). This is most likely an indication that we may have missed some weak lines. Only with more sensitive data (such as will be provided by COS) will it be possible to extend the measurements to  $W<20\text{ m}\text{\AA}$ . Third, we find relatively more strong ( $W>500\text{ m}\text{\AA}$ ) Ly $\alpha$  absorbers per unit redshift than did Penton et al. (2004). They find two (both toward PG 1211+143, at  $v>5000\text{ km s}^{-1}$ ) for  $\Delta z=1.1$ , while we find six (toward 3C 232, HS 1543+5921, PG 1216+069, Mrk 205, HE 1228+0131 and ESO 438-G09) for  $\Delta z=0.7$ . None of these six sightlines was in the Penton et al. (2004) sample. The net result of this is that the dropoff in  $dN/dz$  at high equivalent width limits is not as steep as found by Penton et al. (2004) found. We can also compare to the results of Weymann et al. (1998), who showed  $dN/dW$  for strong lines found in the *FOS* QSO Absorption Line Key Project ( $\Delta z\sim 30$ ), though not  $dN/dz$  as function of  $W_{\text{lim}}$ . However, above some (high) value of the equivalent widths, the redshift path will stay the same, so that the shape of  $dN/dW$  will be the same as that of  $dN/dz$ . Their  $dN/dW$  is a power-law between  $W=300$  and  $900\text{ m}\text{\AA}$ . Our sample shows an apparent rise in the number of absorbers at  $W_{\text{lim}}>500\text{ m}\text{\AA}$ . This difference suggests that the results at high equivalent widths are affected by object selection bias, especially since some sightlines were a-priori selected to pass close to or even through nearby galaxies. In particular, these are 3C 232, ESO 438-G09, HS 1543+5921, Mrk 205 and MCG+10-16-111, which yield four of the six strongest lines.

Figures 5c,d shows  $dN(\text{Ly}\beta)/dz$ , which has not been shown in previous papers. For a given equivalent width limit, there are 2–3 times fewer Ly $\beta$  lines per unit redshift than Ly $\alpha$  lines. Since the ratio of the optical depths of Ly $\alpha$  and Ly $\beta$  is 5.3, this means that more Ly $\beta$  lines are detected than would naively be expected. We used the measured linewidths (corrected for instrumental broadening) to convert the equivalent widths to optical depths, and checked the ratio of Ly $\alpha$  and Ly $\beta$  in the 26 systems in which both lines are detected. Both lines are unsaturated, not contaminated and well-measured in just eight systems (at  $3212\text{ km s}^{-1}$  toward MRC 2251–178,  $1954\text{ km s}^{-1}$  toward Mrk 335,  $2545\text{ km s}^{-1}$  toward Mrk 509,  $2085\text{ km s}^{-1}$  toward Mrk 817,  $1144\text{ km s}^{-1}$  toward PG 0804+761,  $4932\text{ km s}^{-1}$  toward PG 1211+143,  $2275\text{ km s}^{-1}$  toward PG 1259+593 and  $5519\text{ km s}^{-1}$  toward Ton S180). In each of these systems the optical depth ratio is found to be near the expected value of 5.3 (within the errors). In the other 18 systems the derived optical depth ratio ranges from 0.70

to 7.0, with an average of 3.2. For the cases with unsaturated Ly $\alpha$  lines, the Ly $\beta$  lines tend to be in multi-component systems or in noisy spectra, making the measurements uncertain. When Ly $\alpha$  is saturated, the equivalent width does not increase as fast with increasing column density as is the case for Ly $\beta$ , resulting in a ratio of Ly $\alpha$  and Ly $\beta$  equivalent widths that is smaller than the ratio of optical depths.

Table 8 and Figs. 5e, f present our  $dN(\text{O VI})/dz$  results and compare them to the three previous studies of low-redshift  $dN(\text{O VI})/dz$ : Danforth & Shull (2005; 40 systems at  $z < 0.15$ ), Tripp et al. (2008; 91 systems at  $z = 0.15\text{--}0.5$ ) and Thom & Chen (2008; 27 systems at  $z = 0.15\text{--}0.5$ ). We note that Tripp et al. (2008) discussed a difference between O VI components and O VI systems, since some of their O VI detections come in groups; we compare to their results for systems.

Before discussing the similarities and differences between the four studies, we note that different conventions are used to calculate the detection limits (see Sect. 2.3). To repeat: Danforth & Shull (2005) defined  $W_{\text{lim}}$  as a  $4\sigma$  non-detection of a line one resolution element ( $20 \text{ km s}^{-1}$ ) wide; Tripp et al. (2008) defined  $W_{\text{lim}}$  as three times the error for a 15-pixel ( $55 \text{ km s}^{-1}$ ) wide line; Thom & Chen (2008) defined  $W_{\text{lim}}$  as a  $3\sigma$  non-detection for a line with  $b = 10 \text{ km s}^{-1}$ . We define  $W_{\text{lim}}$  as the  $3\sigma$  error over a  $60 \text{ km s}^{-1}$  interval. As Fig. 4 shows, all detected O VI lines have  $\text{FWHM} > 30 \text{ km s}^{-1}$ , i.e., the integration range will typically be  $60 \text{ km s}^{-1}$  or more. Thus, using a narrower integration interval to define the detection limit underestimates that limit. A proper comparison between the different studies thus requires increasing the equivalent width limits of Danforth & Shull (2005) by a factor  $\sqrt{60/20} * 3/4 \sim 1.3$  and those of Thom & Chen (2008) by a factor  $\sqrt{60/(1.66 * 10)} = 1.5$ .

With these corrections, we can see in Figs. 5e,f that the different studies agree that  $dN(\text{O VI})/dz$  at a  $30 \text{ m}\text{\AA}$  equivalent width limit is about 17. However, we find fewer strong systems ( $W > 70 \text{ m}\text{\AA}$ ) than expected from the number of O VI systems seen at  $z = 0.1\text{--}0.5$ . The Tripp et al. (2008) study has 27 systems over a path  $\Delta z = 3.1$  for  $W_{\text{lim}} = 70 \text{ m}\text{\AA}$ . For our path  $\Delta z = 0.43$  we would thus expect to find four systems. We find just one, although we would have counted the detection toward ESO 185-IG13 if we had had better data. Similarly, for  $W_{\text{lim}} = 100 \text{ m}\text{\AA}$  we expect two detections, but find one (toward ESO 185-IG13). Since we are working with a relatively small total pathlength and small number statistics, the discrepancy is not problematic.

Figures 5e,f also show that our high value for  $dN(\text{O VI})/dz$  at  $W_{\text{lim}} = 20 \text{ m}\text{\AA}$  ( $50 \pm 22$ ) is compatible with extrapolating the other studies. We derive this from a redshift path  $\Delta z = 0.1195$  built up in the 17 FUSE sightlines that have  $S/N > 20$ , and which yield six detections with  $W(\text{O VI}) > 20 \text{ m}\text{\AA}$ . The *Cosmic Origins Spectrograph* (COS) will provide an increase in the typical  $S/N$  at  $\lambda > 1200 \text{ \AA}$  from about 10 to about 30–50, giving a typical

detection limit of about 10–15 mÅ. Compared to the Tripp et al. (2008) survey, we thus expect to see an increase in the number of detected O VI absorbers per unit redshift interval in the COS data of a factor about two.

The discussion above leads us to the conclusion that: *To compare the different published analyses of the distribution of the number of absorption lines between  $z=0$  and  $z=0.5$  as function of limiting equivalent width, it is necessary to take into account the different definitions of the detection limits that were used. After correcting, we find that the distributions for Ly $\alpha$  and O VI found in different studies do agree for equivalent width limits between 20 and 40 mÅ.*

### 3.5. Time Evolution of Ly $\alpha$ Linewidths

Lehner et al. (2007) did a detailed study of the distribution of 316 Ly $\alpha$  lines toward seven QSOs at  $z < 0.5$  with high-quality *STIS*-E140M spectra. They compared their sample to those of Kim et al. (2001, 2002; 2315 Ly $\alpha$  lines at  $z=1.5$ –3.6) and Janknecht et al. (2006; 1325 Ly $\alpha$  lines at  $z=0.6$ –1.9), and plotted the relative number of broad ( $b > 40$  km s $^{-1}$ ) absorption lines in different redshift intervals (0.5 units wide). If the broadening is thermal,  $b=40$  km s $^{-1}$  corresponds to a temperature of  $10^5$  K. Lehner et al. (2007) found that the fraction of broad Ly $\alpha$  lines increases with decreasing redshift, suggesting that the intergalactic medium may be heating up over time. We revisit this analysis and add our measurements at  $z=0$ –0.017.

We note that Kim et al. (2001) gave the S/N ratio of the optical (VLT/UVES) data as “typically 40–50”. The mid-UV spectra used by Janknecht et al. (2006) have S/N ratios of 10–15 per resolution element. The seven high-quality low-redshift spectra of Lehner et al. (2007) also have S/N about 10–15 per resolution element. Thus, the quality of the several UV datasets is comparable, while that of the higher-redshift optical data is better.

For each of the detected Ly $\alpha$  lines in the three samples referenced above, values were given for the fitted column density and linewidth. We convert these to equivalent widths ( $W$ ) and optical depths ( $\tau$ ) and then look at the distribution of linewidths, using redshift intervals 0.1 wide for  $z < 1$ , and 0.2 wide for  $z > 1$ , excluding lines with  $W(\text{rest}) > 500$  mÅ and  $\tau > 2$ . These criteria remove saturated lines, for which the fitted  $b$ -value is not a good measure of the intrinsic width. We also checked the Lehner et al. (2007) sample in more detail and further remove lines that are clear blends, as well as ones that are hard to discern. For our sample we only include the 225 well-measured lines in their sample of 316.

Figure 6 shows some of the resulting parameters of the linewidth distribution, as function of both redshift and lookback time. In Figs. 6a,b we give the fraction of lines with



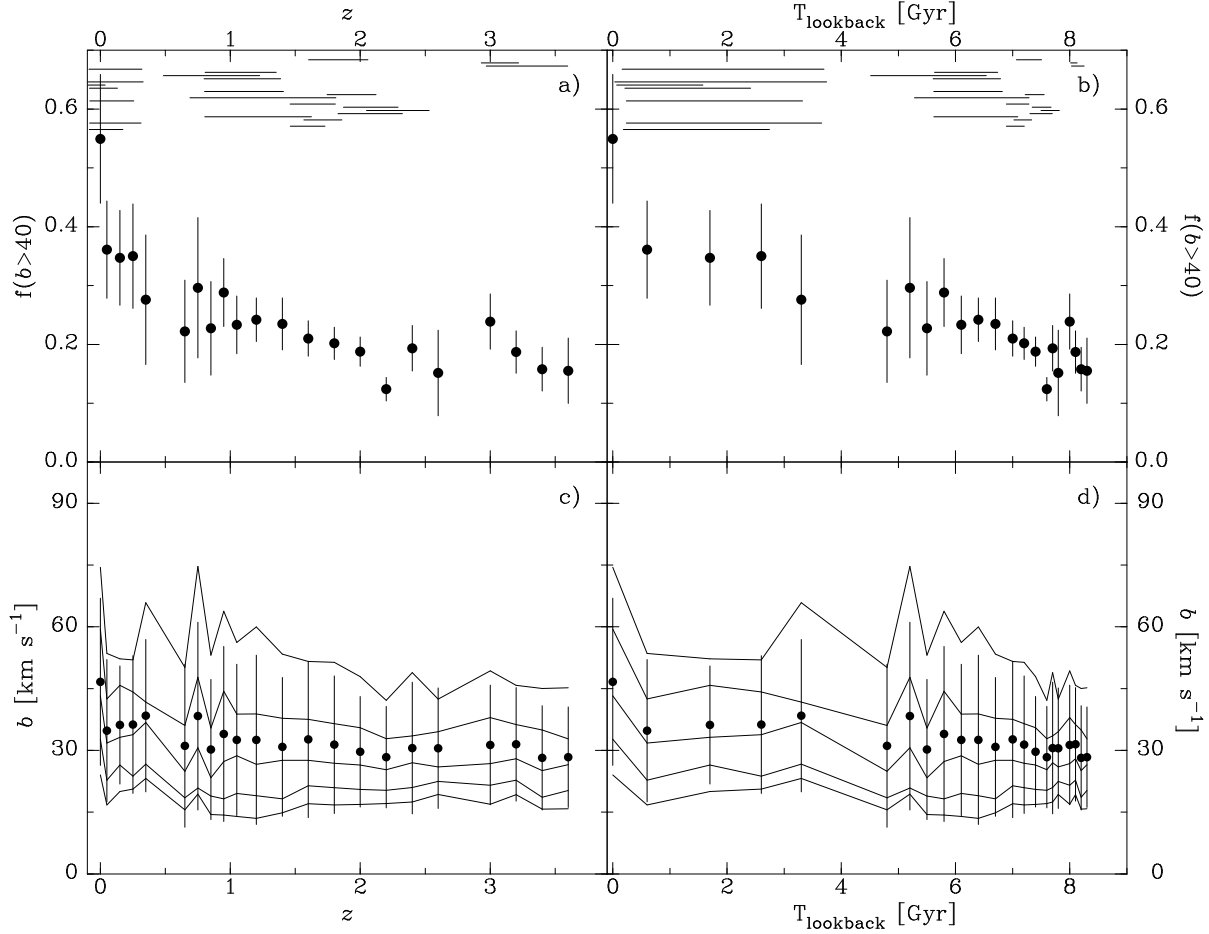


Fig. 6.— Parameters of the distribution of  $\text{Ly}\alpha$  linewidths as function of redshift ( $z$ ) or lookback time. Top panels: fraction of lines with  $b > 40 \text{ km s}^{-1}$ . At  $z < 1.0$  the redshift interval is 0.1, at  $z > 1.0$  it is 0.2. The short horizontal lines near the top of panel a show the redshift ranges of individual QSOs used to derive the linewidth distribution. Bottom panels: horizontal lines show the 10th, 25th, 50th, 90th and 95th percentile of the distribution of  $b$ -values. The points and vertical lines show the average and dispersion in each redshift interval. *Selection criteria:*  $\text{Ly}\alpha$  lines with  $W(\text{rest}) < 500 \text{ m}\text{\AA}$  and implied optical depth  $< 2$ .

$b > 40 \text{ km s}^{-1}$  (the parameter shown by Lehner et al. 2006), with errors based on Poisson statistics. Figures 6c,d shows curves that represent the 10th, 25th, 50th, 75th and 90th percentile of the distribution, as well as points and bars giving the average and dispersion. We also include the redshift ranges of the individual QSO spectra (line segments at the top of panels a and b). This shows that most of the irregularities in the distributions are associated with the edges of the spectra. For instance, for the  $z=2.3\text{--}2.7$  interval almost all  $\text{Ly}\alpha$  lines come from the spectrum of HE 1347–2457, but at  $z < 2.36$  other QSOs contribute. Similarly, the depression at  $z=1.4$  happens at the break between the optical sample of Kim et al. (2001, 2002) and the *STIS*-E230M sample of Janknecht et al. (2006). Further, the wild fluctuations at  $z=0.6\text{--}0.9$  occur because these bins are based on a relatively noisy spectrum ( $S/N \sim 10$ ) of a single QSO, PG 1634+706. Finally, the  $z=0.45$  bin uses data from the long-wavelength edges of the *STIS* spectra, where the noise increases and variations in the detector sensitivity may result in fluctuations. So, lines that are narrower or broader than average may become more difficult to discern. Obviously, a more thorough analysis of each of these spectra is required before one can conclude that the fluctuations in the distribution of  $b$  are real or artifacts.

With these caveats, clear trendlines can be seen. The 10th percentile of the distribution stays more or less constant at  $16 \text{ km s}^{-1}$ , while from  $z=3.5$  to  $z \sim 0$  the 50th percentile (i.e. the median) increases from 25 to  $\sim 35 \text{ km s}^{-1}$ , and the 90th percentile increases from 40 to  $\sim 60 \text{ km s}^{-1}$ . Similarly, the fraction of lines wider than  $b=40 \text{ km s}^{-1}$  increases from 10% at  $z=3.5$  to 55% at  $z=0$ . Fig. 6b suggests a mostly continuous increase in the fraction of wide lines as the universe evolves. Because of the apparent problems with instrumental breaks, it is not possible to derive the precise manner in which the linewidths have increased over time. The data support a linear increase over time. Note, however, that our sample (at  $z=0$ ) has a substantially larger fraction of wide lines than the lowest redshift point in the Lehner et al. (2007) sample (at  $z=0.05$ ). This may be caused by the differing particular set of sightlines in the two samples.

The largest fraction of wide lines and the largest average linewidth occur at  $z=0$ . In spite of the large fluctuations and large errors in  $f(b > 40)$ , the difference between the points at  $z=0$  and  $z=0.1\text{--}0.4$  is likely significant. To confirm this, it will be necessary to reassess all linewidth measurements, using the same method at all redshifts. We note that compared to Lehner et al. (2007), we only used the reliable lines in their sample, i.e., we excluded lines with large optical depth or blends. This did not fundamentally change the conclusion derived in that paper.

To summarize, we conclude from Fig. 6 that *the widths of the  $\text{Ly}\alpha$  lines have increased over cosmic time, that the  $z=0$  sample has the largest fraction of wide lines, and that the*

*distribution function of the linewidths is the widest at the present time.*

#### 4. Galaxies Associated with Absorbers

In making the associations between absorbers and galaxies near the sightline, some previous authors (such as Bowen et al. 1996, 2002) implicitly used the assumption that  $\text{Ly}\alpha$  absorbers are associated with the halos of the galaxies near them (a reasonable assumption when concentrating on sightlines with low impact parameters to galaxies). However, other authors argued that most absorbers are intergalactic. For instance, Impey et al. (1999) compared their absorber sample with galaxy surveys in the Virgo region, and concluded that galaxy halos are not responsible for the absorbers. Penton et al. (2002) concurred, except that they allowed that strong absorbers with small impact parameters may originate in halos. A number of other authors analyzed imaging surveys of galaxies up to  $z \sim 0.2$  near several sightlines (e.g. Tripp et al. 1998; Sembach et al. 2004; Tumlinson et al. 2005; Prochaska et al. 2006). However, the field of view is usually small, the luminosity limit is not constant and most faint galaxies are not found, so the results have not been unambiguous. The advantage of our approach of looking at the very nearest galaxies is that the galaxy content of the survey volume is relatively uniformly well known, at least down to a given luminosity limit ( $0.5 L_*$  at  $5000 \text{ km s}^{-1}$ ,  $0.1 L_*$  at  $2500 \text{ km s}^{-1}$ ).

In this section we present several analyses of the  $\text{Ly}\alpha/\text{Ly}\beta/\text{OVI}$  detections that look at the galaxies near each of the absorbers. For the first two analyses we do not make a-priori assumptions about which galaxy a particular absorption line might be associated with, by just looking at the probability of finding galaxies of a given luminosity near the absorber as function of impact parameter and absorber-galaxy velocity difference (Sect. 4.1). We then compare the distribution of galaxy-absorber impact parameters to that of galaxy-galaxy separations (Sect. 4.2). In these two subsections we establish that absorbers do associate with galaxies. Therefore, we continue with a description of the particular associations that we make, which are listed in Table 3 (Sect. 4.3). This leads to a discussion of the issue of “void absorbers” (Sect. 4.4). Having established the individual galaxy-absorber associations, we look at the distribution of velocity differences  $v(\text{abs}) - v(\text{gal})$  (Sect. 4.5), at the distribution of absorber linewidths as function of impact parameter (Sect. 4.6), and at the relation between absorber equivalent width and impact parameter (Sect. 4.7).

Table 9. Fraction of Ly $\alpha$  absorbers having a galaxy within  $\rho$  and  $\Delta v$ <sup>1</sup>

$\rho$ [kpc] (1)	$\Delta v$ [km s <sup>-1</sup> ] (2)	all (3)	$L > 0.1 L_*$ (4)	$L > 0.25 L_*$ (5)	$L > 0.5 L_*$ (6)	$L > L_*$ (7)
<200	<200	28; 21%	20; 15%	18; 13%	14; 10%	8; 6%
<200	<400	30; 22%	23; 17%	20; 15%	15; 11%	9; 6%
<200	<1000	31; 23%	24; 18%	21; 15%	15; 11%	9; 6%
<400	<200	60; 45%	49; 36%	44; 33%	34; 25%	23; 17%
<400	<400	63; 47%	52; 39%	47; 35%	37; 27%	27; 20%
<400	<1000	63; 47%	52; 39%	47; 35%	37; 27%	27; 20%
<1000	<200	93; 69%	78; 58%	67; 50%	52; 39%	36; 27%
<1000	<400	100; 75%	83; 62%	70; 52%	54; 40%	39; 29%
<1000	<1000	100; 75%	83; 62%	70; 52%	54; 40%	39; 29%
<2000	<200	111; 83%	95; 71%	80; 60%	63; 47%	44; 33%
<2000	<400	122; 91%	103; 77%	86; 64%	68; 51%	47; 35%
<2000	<1000	122; 91%	103; 77%	86; 64%	68; 51%	47; 35%
<3000	<200	113; 84%	97; 72%	82; 61%	64; 48%	44; 33%
<3000	<400	128; 96%	109; 81%	92; 69%	71; 53%	49; 36%
<3000	<1000	128; 96%	109; 81%	92; 69%	71; 53%	49; 36%

Note. — 1: This table gives number and percentage of Ly $\alpha$  absorbers associated with galaxies. E.g. on the fourth line in Col. (7), there are 23 (or 17%) absorbers for which it is possible to find a galaxy with luminosity  $>L_*$  that lies within 400 kpc and whose systemic velocity differs by less than 200 km s<sup>-1</sup> from that of the absorber. For this count no difference is made between group and field galaxies. The total number of absorbers is 133.

#### 4.1. The Fraction of Absorbers Having a Galaxy of Given $L$ Within $\rho$ , $\Delta v$

In Table 9 we summarize the fraction of Ly $\alpha$  absorbers for which we can find a galaxy of a given luminosity within some impact parameter and differing in velocity by less than a given value. Note that we do the opposite analysis (i.e. we ask whether an absorber can be found near a particular galaxy) in Sect. 5.2. To construct Table 9, we find the nearest galaxy that fits the impact parameter, velocity difference and luminosity criterion. The table shows that for the great majority (128 of 133, or 96%) of intergalactic absorbers a galaxy can be found with impact parameter  $\rho < 3$  Mpc and velocity difference  $\Delta v < 400$  km s $^{-1}$ . As the criteria are made more strict, the fraction decreases. If there is a galaxy within a given impact parameter limit, most absorbers have velocities that are within 200 km s $^{-1}$  from that galaxy, with generally just a few having  $\Delta v = 200$ –400 km s $^{-1}$ . The fraction of absorbers decreases by a factor of about 2.2 as the luminosity limit of the nearest galaxy is increased from  $0.1 L_*$  to  $L_*$ . Further, for any given impact parameter and velocity difference limit, about 15–20% of the absorbers do not have a galaxy brighter than  $0.1 L_*$  as the nearest galaxy. Only 23 systems (17%) occur within what would generally be called the halo of a luminous galaxy, i.e. within 400 kpc and 200 km s $^{-1}$  of a galaxy with  $L > L_*$ , and only 8 of these originate in the inner part of these halos ( $\rho < 200$  kpc).

We can also determine the median impact parameter for finding a galaxy brighter than a given luminosity and with  $\Delta v < 400$  km s $^{-1}$  to an absorber. We find that 50% of the absorbers with  $v < 2500$  km s $^{-1}$  has a galaxy with  $L > 0.1 L_*$  within 370 kpc. The median impact parameter for an absorber with  $v < 3700$  km s $^{-1}$  to an  $L > 0.25 L_*$  galaxy is 390 kpc, while for absorbers with  $v < 5000$  km s $^{-1}$  it is 730 kpc to an  $L > 0.5 L_*$  galaxy and 870 kpc to an  $L > L_*$  galaxy.

Based on Table 9 we conclude that *for almost all Ly $\alpha$  absorbers there is a galaxy with  $\rho < 3$  Mpc having  $\Delta v < 400$  km s $^{-1}$ , and most (81%) of these are brighter than  $0.1 L_*$ . On the other hand, only a small fraction ( $\sim 20\%$ ) occurs within the halos of  $L > L_*$  galaxies.*

#### 4.2. Distribution of Nearest-Neighbor Separations

A different way of exploring the relation between absorbers and galaxies is to compare the 3-D separation between galaxies to the 3-D separation between absorbers and galaxies. This was previously done by Penton et al. (2002) and Stocke et al. (2006). Penton et al. (2002) used relatively complete galaxy surveys down to at least  $L_*$  near fifteen of their sightlines, while Stocke et al. (2006) used a combination of galaxy surveys, containing  $10^6$  galaxies with known redshifts. In their Fig. 3 (Penton et al. 2002) and Fig. 1 (Stocke et al.

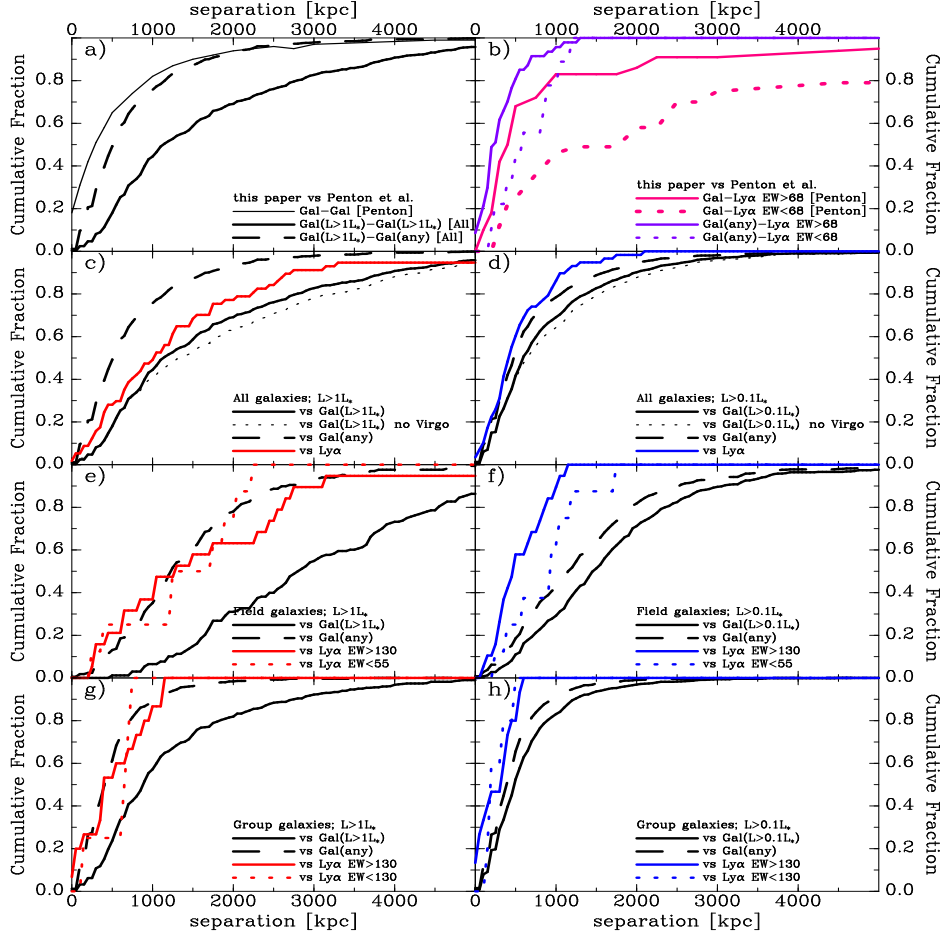


Fig. 7.— Galaxy-galaxy and absorber-galaxy nearest-neighbor distributions. For a given separation the curves give the fraction of galaxies closer to each other galaxy or absorber. Galaxy-galaxy separations are calculated using directions and estimated distances. Galaxy-absorber separations are 1.25 times the impact parameter (see text). Black curves give galaxy-galaxy nearest-neighbor distributions; solid black curves are given when comparing galaxies with the same luminosity limit, dashed black curves when looking at the separation for any galaxy from the reference galaxies. Colored curves give the nearest galaxies to absorbers, red when the galaxy has  $L > L_*$ , blue when the galaxy has  $L > 0.1 L_*$ , purple for all galaxies, magenta for the distributions given by Penton et al. (2002). Solid colored curves include Ly $\alpha$  absorbers stronger than some equivalent width limit, while dotted colored curves include only Ly $\alpha$  absorbers below some equivalent width. In panels a/b we compare our results to those of Penton et al. (2002), in panels c/d all galaxies were included, in panels e/f only field galaxies, and in panels g/h only group galaxies. *Selection criteria:*  $L > 0.1 L_*$  (i.e.  $D_{gal} > 7.5$  kpc) and  $v < 2500$  km s $^{-1}$ , or  $L > L_*$  (i.e.  $D_{gal} > 20.4$  kpc) and  $v < 5000$  km s $^{-1}$ , classified as in the field or member of a group, and all Ly $\alpha$  lines with equivalent width above or below the given value.

2006), these authors presented the cumulative nearest-neighbor galaxy distribution, i.e., the fraction of galaxies whose nearest neighbor is separated by less than a given value. We first analyze our data in the manner presented by these authors and then add some new twists.

To calculate our version of the nearest-neighbor distributions, we start with the direction and distance of every galaxy with  $L > L_*$  and  $v_{gal} < 4500 \text{ km s}^{-1}$  and find the nearest  $L > L_*$  galaxy with  $v_{gal} < 5000 \text{ km s}^{-1}$ . We use a  $4500 \text{ km s}^{-1}$  limit for the base galaxy to avoid edge effects, since otherwise we might miss the nearest galaxy if it has  $v_{gal} > 5000 \text{ km s}^{-1}$ . A  $500 \text{ km s}^{-1}$  velocity difference corresponds to about 10 Mpc, which is larger than all but a few of the largest separations that are found. For a given impact parameter we then find the fraction of  $L_*$  galaxies whose nearest neighbor  $L_*$  galaxy is closer. We also do this calculation using only  $L > 0.1 L_*$  galaxies with  $v < 2000 \text{ km s}^{-1}$ . Comparing these distributions to the nearest  $L_*$  or  $0.1 L_*$  neighbor of an absorber, we can determine whether or not absorbers associate more with galaxies of a given luminosity than the galaxies associate with each other.

We further look at the nearest neighbor galaxy of any luminosity to each  $L > L_*$  or  $> 0.1 L_*$  galaxy. This comparison allows a comparison of the typical impact parameter of an absorber to the typical separation between dwarf galaxies and bright galaxies, even though the dwarf galaxy sample is incomplete.

Since the galaxy-galaxy nearest-neighbor separations were calculated in 3-dimensional space, while the absorber-galaxy impact parameters are 2-dimensional projections, we assume that the gas cloud with impact parameter  $\rho$  can lie up to  $\rho$  kpc in front or behind the projection plane. Assuming a random placing along this line, the 3-D separation between an absorber and a galaxy will on average be a factor 1.25 times the impact parameter. All absorber-galaxy separations in Fig. 7 are thus increased by this factor over the raw impact parameters.

In Fig. 7a, b we compare the Penton et al. (2002) curves to our data, using the same luminosity and equivalent width criteria. The thin solid line in panel a shows their galaxy-galaxy distribution. The Stocke et al. (2006) curves are the same as those of Penton et al. (2002). The thick solid black line gives our version of the distribution of the nearest  $L_*$  neighbor for  $L_*$  galaxies. The dashed black line gives the distribution for the nearest neighbor of any luminosity to  $L_*$  galaxies, using only galaxies with  $v_{gal} < 2500 \text{ km s}^{-1}$ . The faint galaxies include many Virgo dwarfs, and many dwarf galaxies that lie near well-studied bright galaxies or near some of the AGN sightlines. The comparison between the dashed black and thin black curve in Fig. 7a shows that the nearest neighbor function for this inhomogeneous sample is quite similar to that found by Penton et al. (2002). We conclude that Penton et al. (2002) showed the nearest-neighbor of any luminosity to each  $L_*$  galaxy,

although their text and figure caption would suggest that they showed the distribution of the separation between  $L_*$  galaxies. Stocke et al. (2006) explicitly addressed this issue and mention that they used both approaches.

The Penton et al. (2002) galaxy-absorber distributions are shown in Fig. 7b by the magenta lines, separately for strong ( $W > 68 \text{ mÅ}$ ) and weak ( $W < 68 \text{ mÅ}$ ) lines. Comparing the galaxy-galaxy and galaxy-absorber distributions, Penton et al. (2002) as well as Stocke et al. (2006) concluded that the typical nearest neighbor galaxy to a strong absorber is about as close as that galaxy’s nearest neighbor, while weak lines occur much further from galaxies. This would imply that absorbers are *not* generally associated with galaxy halos, but instead occur in intergalactic filaments. As presented, their analysis is correct, but we find that there is more to the story, and that the conclusion needs to be modified.

The purple lines in Fig. 7b give our version of the galaxy-absorber nearest neighbor distribution for  $\text{Ly}\alpha$  absorbers with equivalent width  $>68 \text{ mÅ}$  and  $<68 \text{ mÅ}$ . It is clear that the Penton et al. (2002) curves have a kink at around 1.5 Mpc impact parameter, whereas ours are more smooth across this impact parameter range. That is, we find a continuous distribution of the number of absorbers as function of impact parameter, whereas Penton et al. (2002) found a deficit of absorbers with  $\rho \sim 1.5 \text{ Mpc}$ . The purple curve is also significantly higher than the Penton et al. (2002) galaxy- $\text{Ly}\alpha$  curve for impact parameters above 500 kpc, which means that we can find galaxies with  $\rho = 500\text{--}1500 \text{ kpc}$  near some absorbers, where Penton et al. (2002) found relatively fewer.

In Fig. 7c, d, we present our nearest-neighbor distributions, using the  $L > L_*$  sample in Fig. 7c, the  $L > 0.1 L_*$  sample in Fig. 7d. We also show the galaxy-galaxy distributions that are obtained when excluding galaxies within  $30^\circ$  from the Virgo cluster (thin black lines). These distributions are compared to the galaxy-absorber distributions – red for the distance between absorbers and  $L > L_*$  galaxies, blue for  $L > 0.1 L_*$  galaxies. We conclude that:

- (1) For 50% of  $L > L_*$  galaxies, the nearest  $L_*$  galaxy is at a separation  $< 1.2 \text{ Mpc}$ , while the nearest  $L_*$  galaxy to an absorber has a median impact parameter 1.1 Mpc. The nearest  $L > 0.1 L_*$  galaxy on average lies 600 kpc from another  $L > 0.1 L_*$  galaxy, while for  $\text{Ly}\alpha$  lines such a galaxy is on average found within 450 kpc. We note that Stocke et al. (2006) quoted values of 1.8 Mpc and 250 kpc for the median separations between  $L_*$  and  $0.1 L_*$  galaxies. We have not identified the origin of this discrepancy, but it may partly be due to the inhomogeneity in the magnitude systems used to define the different galaxy catalogues that were used
- (2) The Virgo cluster has a significant effect on the median separation between galaxies. Excluding it leads to a median nearest  $L_*$  neighbor for an  $L_*$  galaxy of 1.4 Mpc.



(3) The nearest  $L_*$  galaxy to an absorber has a median separation of 1.1 Mpc, while the nearest  $0.1 L_*$  galaxy lies at 450 kpc. The strongest lines ( $W > 68 \text{ mÅ}$ ) have a median distance to  $L_*/0.1 L_*$  galaxies of 900/400 kpc, while the median for weak lines ( $W < 68 \text{ mÅ}$ ) is 1750/950 kpc. Stocke et al. (2006) quoted 1130/445 kpc for strong lines and 2150/1455 kpc for weak lines. The large difference in median separations for strong and weak lines led Stocke et al. (2006) to conclude that strong lines correlate more strongly with galaxies than weak lines. Our data support this, though we also conclude that the difference may not be as pronounced as Stocke et al. (2006) found.

There is a big problem with the galaxy-galaxy distributions in Fig. 7c, d, however. This is that in galaxy groups the nearest neighbor will typically be closer than the nearest neighbor to a field galaxy. Gaseous halos of galaxies in groups may touch and possibly merge, or alternatively, the group environment may destroy them. Halos around field galaxies are much more likely to form a single structure.

To deal with this problem, we separate the absorber and galaxy samples into absorbers/galaxies in the field and in groups. We count a galaxy as a group galaxy if it was identified as such in the GH+LGG group sample that we discussed previously (Sect. 2.4), or if it falls within a group’s outline on the sky and within the velocity range of the group galaxies used to define the group. For absorbers, we overlaid the sightlines on maps of the distribution of group galaxies, and we counted absorbers as associated with a group if the sightline passes through or close to the edge of a group. This is the case for 19 of the systems. The other 96 absorbers occur in the field.

Some have argued that all galaxies really are members of groups. One could also argue that the GH/LGG definitions of groups is arbitrary. Nevertheless, using these defined groups will separate the galaxies into a set of galaxies located in regions of high or low galaxy density, and thus the general conclusion remains valid.

Following Penton et al. (2002) and Stocke et al. (2006), we divide the absorber sample into strong and weak lines. However, rather than using  $68 \text{ mÅ}$ , we set the dividing line at  $130 \text{ mÅ}$ , as this is the median for our sample.

The curves in Fig. 7c, d would seem to indicate that the typical impact parameter of a  $\text{Ly}\alpha$  absorber to a galaxy is not much smaller than the typical distance between galaxies. However, we use Fig. 7e–h to show that this is because field and group galaxies were averaged. In Figs. 7e–h we can see the following:

(1) The median distance between  $L_*$  field galaxies is 2.9 Mpc (see solid black line in Fig. 7e) while the median separation between a field  $\text{Ly}\alpha$  absorber and the nearest  $L_*$  galaxy is 1.5 Mpc (thick red line). Conversely, for only 14% of  $L_*$  galaxies in the field is the nearest

$L_*$  galaxy closer than 1.5 Mpc.

(2) The dashed black line in Fig. 7e shows that half of the  $L_*$  field galaxies have a smaller galaxy within about 1.2 Mpc. This is comparable to the typical distance between an absorber and an  $L_*$  galaxy. That is, in the field the typical separation between an  $L_*$  galaxy and another, smaller, galaxy is similar to the typical separation between it and an absorber. A KS-test can test whether the differences are statistically significant. Comparing the distributions of the 396 galaxies and that of the 39 strong ( $EW > 130 \text{ m}\text{\AA}$ ) or 21 weak ( $EW < 55 \text{ m}\text{\AA}$ ) absorbers, the hypothesis that they differ is rejected only at the 50% (for strong lines) or 75% (for weak line) confidence level.

(3) On average, field  $\text{Ly}\alpha$  absorbers occur significantly closer to the nearest  $0.1 L_*$  field galaxy (median impact parameter 600 kpc) than these galaxies are to each other (median impact parameter 1.5 Mpc) – compare the solid black line with the blue lines in Fig. 7f. The KS-test rejects the hypothesis that the distributions are the same at the  $>99.9\%$  confidence level.

(4) The typical separation between an absorber and the nearest field  $L > 0.1 L_*$  galaxy (median 600 kpc) is smaller than the typical separation between the nearest galaxy of any luminosity to an  $L > 0.1 L_*$  galaxy (1.1 Mpc) – compare blue and dashed black lines in Fig. 7f.

(5) When looking at the separation between  $L > 0.1 L_*$  field galaxies and absorbers, the strong absorbers occur on average closer to those galaxies than the weak absorbers – compare solid and dotted blue lines in Fig. 7f. The KS-test rejects the hypothesis that the distributions for the strong ( $EW > 130 \text{ m}\text{\AA}$ ) and weak ( $EW < 55 \text{ m}\text{\AA}$ ) lines are the same at the 99.3% level.

(6) In galaxy groups the median distance between  $L_*$  galaxies is 900 kpc (solid black line in Fig. 7g), between  $0.1 L_*$  galaxies it is 500 kpc (solid black line in Fig. 7h).

(7) For half of the  $\text{Ly}\alpha$  absorbers that originate in groups it is possible to find an  $L_*$  or  $0.1 L_*$  galaxy within 550 or 350 kpc, respectively (solid colored lines in Figs. 7g, h). The KS-test rejects the hypothesis that the distribution of the 1761  $L > 0.1 L_*$  group galaxies is the same as that of the 13 strong or 19 weak absorbers with  $>98.5\%$  confidence. On the other hand, there is no difference between strong and weak absorbers in this case: the KS-test rejects the hypothesis that they are the same only at the 64% confidence level, i.e., the difference is a  $0.5\sigma$  effect. Thus, as is the case for field absorbers, these  $\text{Ly}\alpha$  absorbers typically occur closer to galaxies than the galaxies do to each other, though the contrast is not as pronounced.

(8) Comparing Fig. 7c–h shows that when combining the field and group sample, the averaging of the galaxy-galaxy nearest-neighbor distributions and the galaxy-absorber nearest-neighbor distributions works out such that the two curves are close together in the combined

sample, because group galaxies are closer together than absorbers are to field galaxies.

From these comparisons we conclude that *Ly $\alpha$  absorbers are associated with  $L > 0.1 L_*$  galaxies, both in the field and in groups. Reaching this conclusion requires looking at group and field galaxies and absorbers separately.*

As a final note, we mention that an alternative way of comparing the galaxy-galaxy and galaxy-absorber distributions is to use the two-point correlation function. This was done by Wilman et al. (2007), who used the 381 absorbers from the HST QSO Absorption Line Key Project and a sample of 685 galaxies at  $z < 1$  to calculate the two-point correlation function for a number of absorber column density intervals as function of impact parameter and line-of-sight separation. They find that the absorber-galaxy two-point correlation function is more concentrated toward small separations than the galaxy-galaxy function, and also that the absorber-galaxy function extends out to beyond 1 Mpc. This analysis thus supports our contention that absorbers associate more with galaxies than that the galaxies associate with each other.

### 4.3. Associating Ly $\alpha$ /Ly $\beta$ /O VI with Individual Galaxies

Now that we have established that absorbers associate with galaxies, we discuss the general properties of the associations that we make to construct Table 3. But first we summarize the different a-priori criteria that were used in previous work. These papers used either  $H_0 = 100 \text{ km s}^{-1}$  or  $H_0 = 71 \text{ km s}^{-1}$ . We rescale all distances and impact parameters to the latter, but when discussing results from other papers we include a factor  $h_{71}^{-1} = 71/H_0$  as a reminder.

Lanzetta et al. (1995) identified 46 galaxies at  $z = 0.07\text{--}0.55$  having impact parameter  $\rho = 25\text{--}500 h_{71}^{-1} \text{ kpc}$  in fields toward six QSOs observed with the *Faint Object Spectrograph* (FOS) on HST. These data allowed a search for absorbers with equivalent width  $> 150 \text{ m\AA}$ . They found associated absorbers ( $|\Delta v| < 500 \text{ km s}^{-1}$ ) near 20 galaxies.

Bowen et al. (1996) analyzed absorptions near 38 galaxies at  $z = 0\text{--}0.08$  with  $\rho = 60\text{--}700 h_{71}^{-1} \text{ kpc}$  using FOS spectra of 10 QSOs. Nine were found to have associated Ly $\alpha$ .

Tripp et al. (1998) studied the relation between galaxies and Ly $\alpha$  absorbers in two QSO sightlines (H 1821+643 and PG 1116+215). They found 17 galaxy-absorber pairs with  $\rho < 1 \text{ Mpc}$  and  $\Delta v < 350 \text{ km s}^{-1}$ . Within  $\rho < 600 \text{ kpc}$  and  $\Delta v < 1000 \text{ km s}^{-1}$  they found a galaxy for 100% of the absorbers. They further found that the weakest Ly $\alpha$  absorbers ( $W < 100 \text{ m\AA}$ ) associate with galaxies slightly less than the strong absorbers.

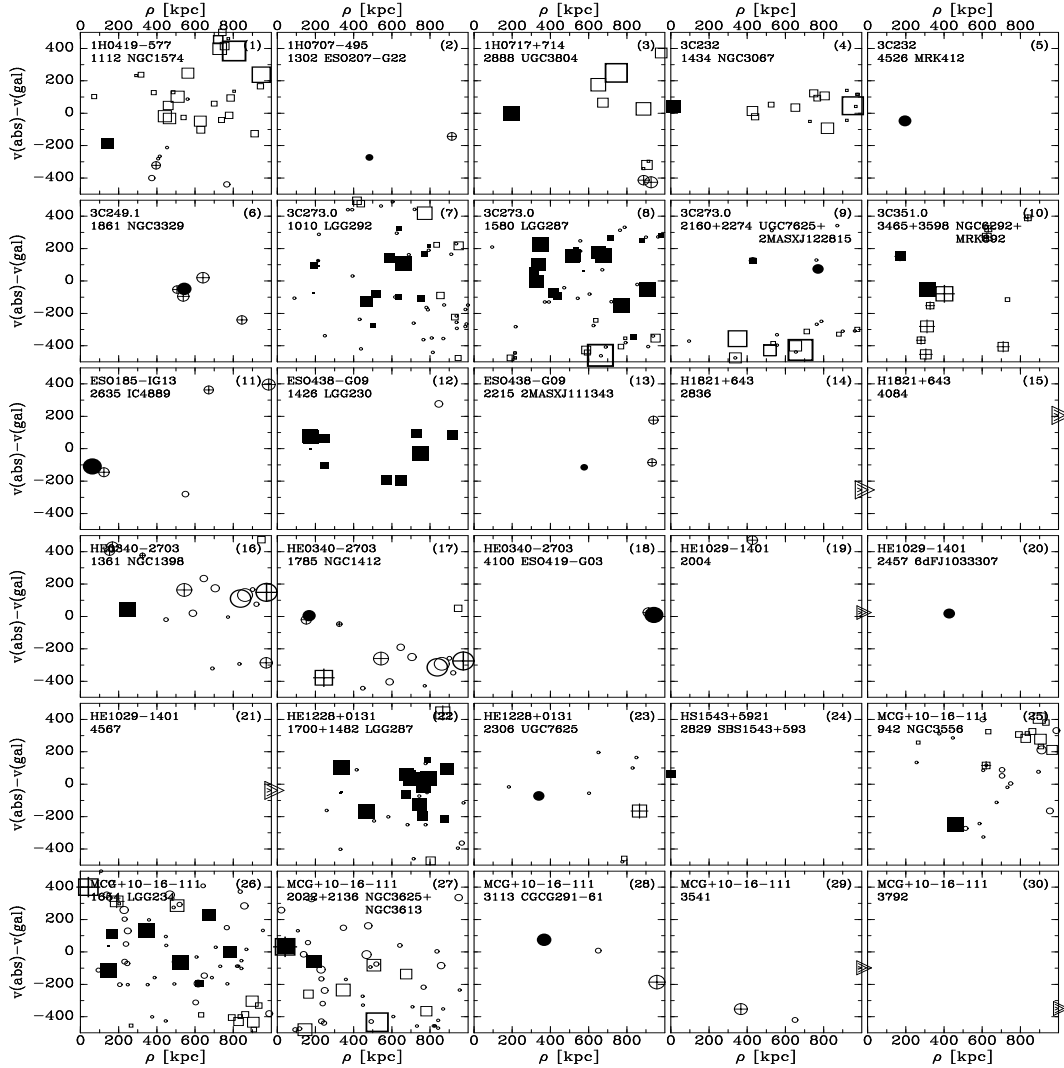


Fig. 8.— For each absorber, this figure shows the impact parameter (horizontal axis) vs the difference between the velocity of the absorption line and the systemic velocity of the galaxies near it (vertical axis). The velocity is usually that of  $\text{Ly}\alpha$  but can be for  $\text{Ly}\beta$  or O VI if no  $\text{Ly}\alpha$  data is available. The absorber’s velocity and the galaxy associated with it in Table 3 are given on the second line of the label in the top left of each panel. The top right label shows a panel number. Circles are for field galaxies, squares for galaxies listed as part of a GH or LGG group. Filled symbols represent the galaxies that are associated with the absorber. If the association is with a group, all group galaxies are given a closed symbol. Open symbols with a plus in them are for galaxies for which a non-detection is listed in Table 3. If there is no associated galaxy within 1 Mpc, a rightward pointing triangle is shown, whose size and velocity placement are set by the nearest galaxy at  $\rho > 1$  Mpc. The size of each symbol scales with the galaxy’s diameter to the power  $2/3$ .

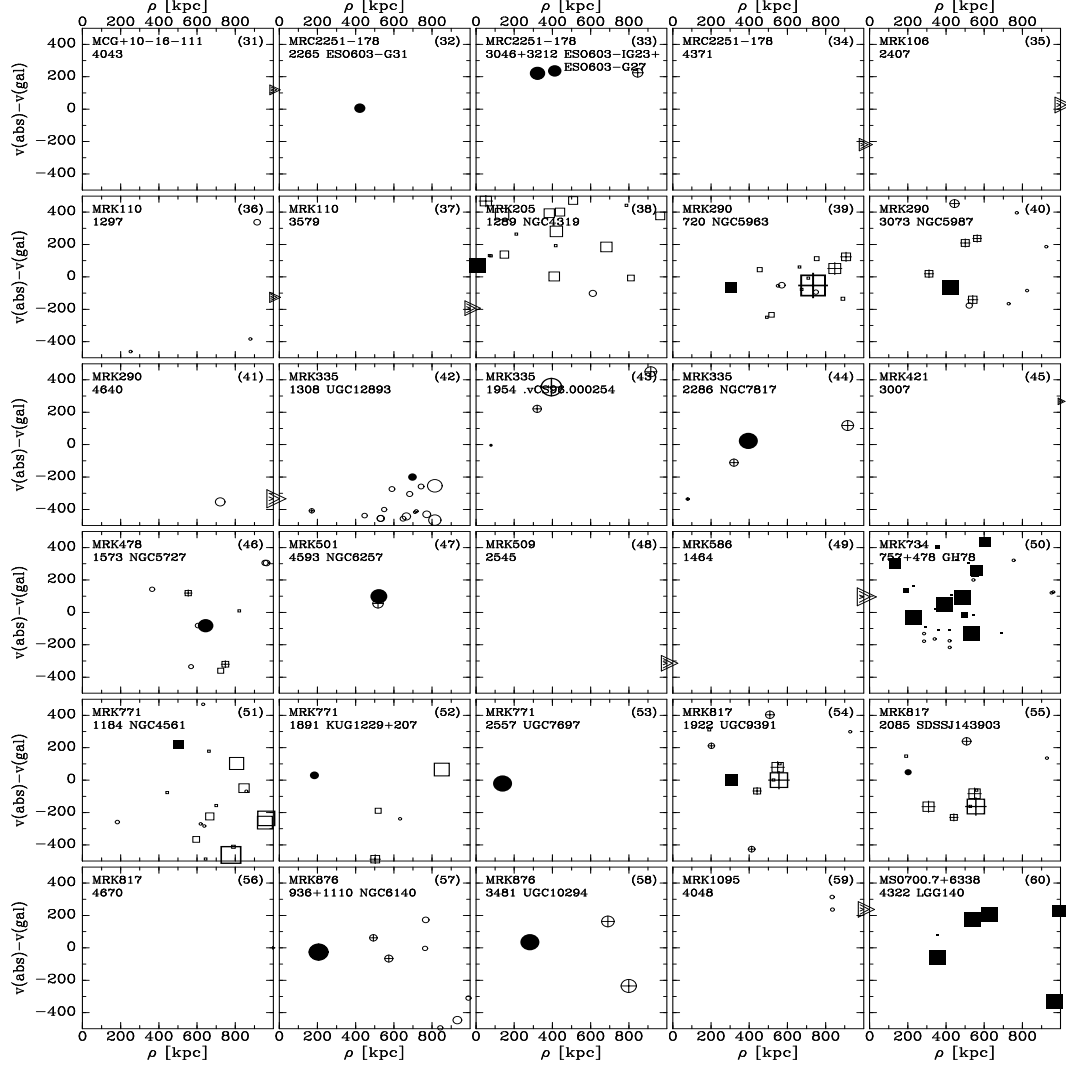


Fig. 8.— Continued.

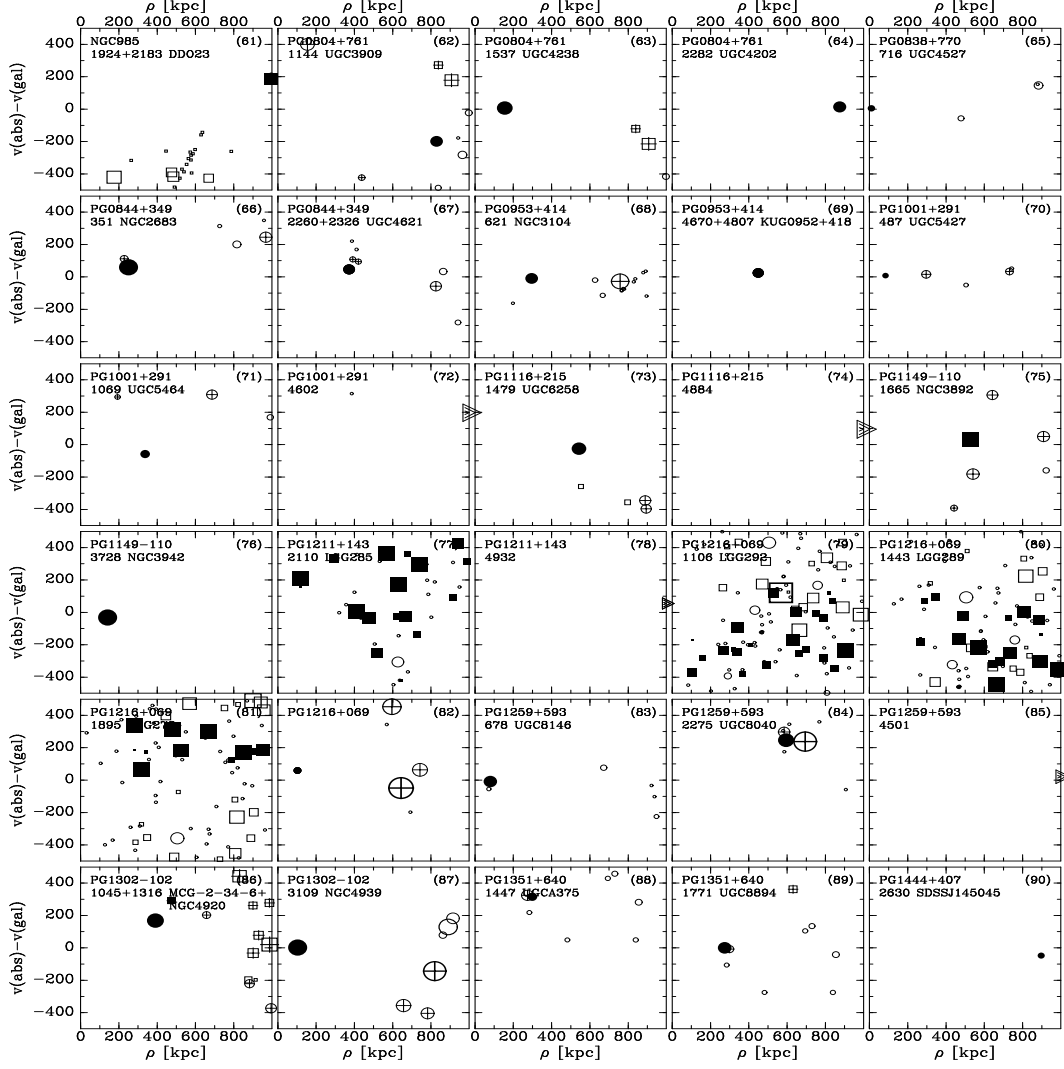


Fig. 8.— Continued.

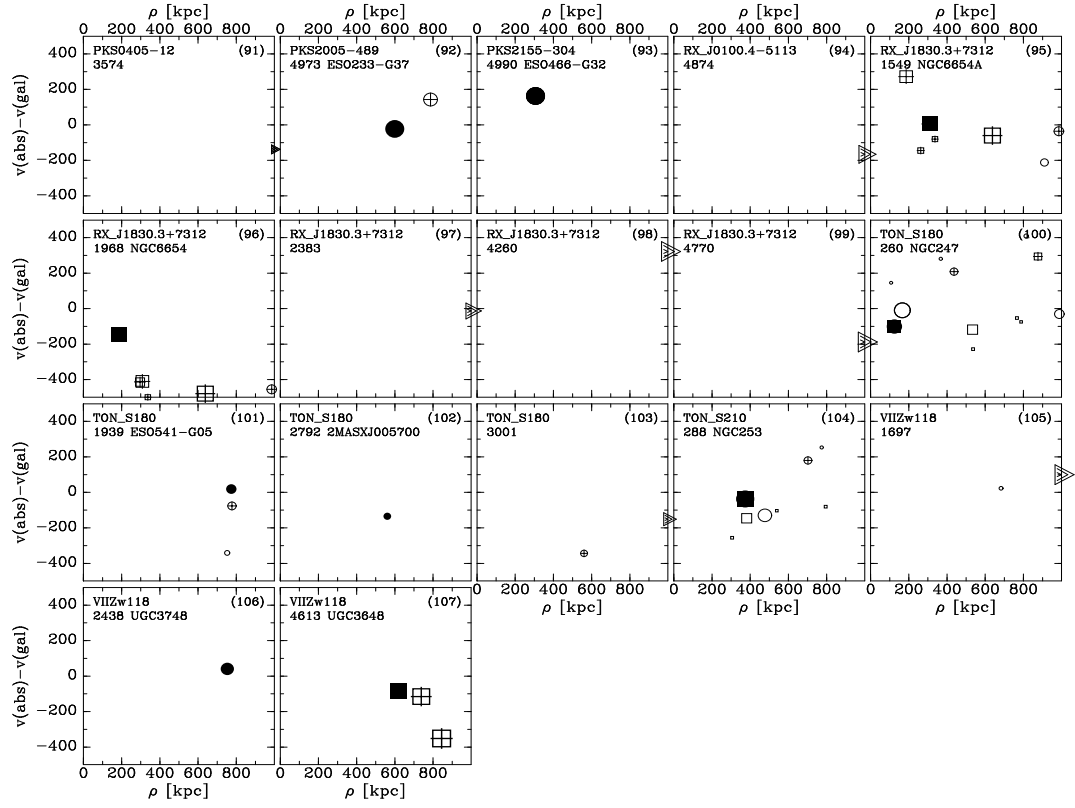


Fig. 8.— Continued.

Impey et al. (1999) discussed ten low-resolution QSO spectra observed with the *GHRs*. All sightlines were in the general direction of the Virgo cluster. Eleven of the intergalactic Ly $\alpha$  lines in their sample were correlated against a sample of galaxies complete to  $M_B = -16$  ( $0.04 L_*$ ). From this comparison, they concluded that absorbers are not preferentially associated with galaxy halos, looking at impact parameters  $< 2$  Mpc and velocity differences  $< 300 \text{ km s}^{-1}$ .

Bowen et al. (2002) obtained STIS-G140M spectra of seven AGN sightlines passing close to ( $\rho < 700 h_{71}^{-1} \text{ kpc}$ ) eight nearby galaxies, deciding in favor of an association between Ly $\alpha$  absorption and galaxy if the velocity difference was less than about  $500 \text{ km s}^{-1}$ . They considered the complications that occur when associating an absorber with the galaxy nearest in velocity. For systems with multiple absorbers this can mean that a weak absorber is associated with the galaxy with low impact parameter, while a strong absorber is associated with a smaller galaxy with higher impact parameter. In their sample this happens for the sightlines to ESO 438-G09, MCG+10-16-111 and RX J1830.3+7312. As can be seen from the discussions in the Appendix, these three are among the more problematic sightlines, and in this respect Bowen et al. (2002) got unlucky with their sample.

Penton et al. (2002) studied 15 sightlines and listed the nearest three galaxies to each Ly $\alpha$  absorber, where they used a “retarded Hubble flow” model to convert velocity differences into spatial distances. That is, they assumed that  $D(\text{gal-abs}) = \rho$  when  $|\Delta v| < 300 \text{ km s}^{-1}$  and add (in quadrature) a line-of-sight radial distance as  $(|\Delta v| - 300)/H_0$ . Stocke et al. (2006) used the same method, but extended the velocity range to  $\pm 500 \text{ km s}^{-1}$ . The problem with this method is that it weighs the impact parameter on the sky much more than the velocity difference. Further, any galaxy with  $\Delta v > 370 \text{ km s}^{-1}$  is a-priori assumed to be more than 1 Mpc away from the absorber, while  $\Delta v = 440 \text{ km s}^{-1}$  already implies 2 Mpc. We therefore decided not to introduce this complication in our analyses.

Prochaska et al. (2006) looked for galaxies with  $R$  magnitude  $< 20$  near metal-line absorbers toward PKS 0405–12. They claimed to be complete down to  $L = 0.1 L_*$  for  $\rho < 1$  Mpc at  $z = 0.1$  and concluded that the OVI absorbers toward this sightline arise in individual halos, galaxy groups, filamentary structure as well as voids, i.e. in a variety of environments.

Clearly, a variety of criteria have been used in the literature. To determine the “best” criteria more data are needed, as well as an approach that is not a-priori biased to assuming a maximum impact parameter or maximum velocity difference. Combined with the relative completeness of the galaxy sample at velocities  $< 5000 \text{ km s}^{-1}$ , our sample of sightlines and absorbers is just large enough that we do not have to choose the association criteria a-priori.

In Fig. 8 we graphically show the justification for each association that we make between



an absorption line and a galaxy. We generally associate the absorption line with the galaxy with the smallest combination of  $\rho$  and  $\Delta v = v(\text{gal}) - v(\text{abs})$ , where a velocity difference of a few hundred  $\text{km s}^{-1}$  is considered equivalent to an impact parameter of about a Mpc. However, sometimes we prefer a larger galaxy over a dwarf galaxy with slightly lower  $\rho$  but higher  $\rho/D_{\text{gal}}$ .

For 33% (44 of 133) of the systems listed in Table 3 an unambiguous association can be made with a galaxy, and in 42 of these the velocity difference is  $< 200 \text{ km s}^{-1}$ . For instance toward 1H0717+714, we detect  $\text{Ly}\beta$  at  $2892 \text{ km s}^{-1}$ . There is one large group galaxy (UGC 3804 in LGG 141,  $D_{\text{gal}} = 22.8 \text{ kpc}$ ) with impact parameter 199 kpc, shown by the filled square in Fig. 8. A few other group galaxies lie further away ( $\rho > 650 \text{ kpc}$ ) and are shown by the open squares.

For a few sightlines (Mrk 876, PG 0844+349, PG 0953+414, PG 1216+069, PKS 2155–304), there are two or three  $\text{Ly}\alpha$  detections listed in Table 3 as associated with one galaxy. This happens when there are no other galaxies with which the absorption line could reasonably be associated.

For another few sightlines (3C 273.0, 3C 351.0, MCG+10-11-116, MRC 2251–178, PG 1302–102, PKS 2005–489) two HI absorption features are seen with similar velocity, and they can be associated with two galaxies that have fairly similar impact parameter. Then both galaxies are listed in Table 3 as having associated absorption, with the associations made to minimize the total velocity difference. In these cases, it is possible to argue that one galaxy should be associated with both detections, or that the association should be reversed. However, this will generally make no difference for doing statistical analyses. In Fig. 8 just one panel is shown in these cases, rather than a separate panel for each absorption line.

Toward 3C 249.1, HE 0340–2703 (twice), Mrk 478, Mrk 501, Mrk 771, Mrk 817 (twice), PG 1001+291, PG 1259+593, Ton S180 and VII Zw 118 there are multiple galaxies with similar impact parameter and similar velocity difference, but only one intergalactic absorption feature. We then list the largest galaxy in Table 3, and list non-detections for the rest. In such cases the listed galaxy may or may not be the proper one to chose.

Toward 3C 273, ESO 438-G09, HE 1228+0131, MCG+10–16–111, Mrk 734, MS 0700.7+6338, PG 1211+143 and PG 1216+069 the sightline passes through a dense group of galaxies. In their spectra we find a total of 13 systems, for which we don’t list a particular galaxy in Table 3 as the associated galaxy, but instead we list the group itself, using the smallest impact parameter to a member of the group.

The cases summarized above add up to 93 of the 133 absorbing systems. For almost all of these a well-justified association can be made between the absorption and a galaxy with

low ( $<1$  Mpc) impact parameter. And if the association is not clear-cut, there are galaxies with similar impact parameter to choose from. This leaves 40 absorbers without clear-cut association with a galaxy. Seven of these (toward 1H 0149–577, Mrk 335 (2 lines), NGC 985 (2 lines), PG 0804+761 and PG 1351+643) are ambiguous. For instance, toward NGC 985 the only known galaxy with small velocity difference has large impact parameter, while galaxies with lower impact parameter would have unusually high velocity difference. Or, toward 1H 0419–577 the candidates are a medium-sized galaxy at  $\rho=140$  kpc and another galaxy half its size at  $\rho=70$  kpc. All of these cases are discussed in detail in the Appendix.

Finally, in the directions to H 1821+643, HE1029–1401, MCG+10–11–116, MRC 2251–178, Mrk 106, Mrk 110, Mrk 290, Mrk 421, Mrk 509, Mrk 586, Mrk 817, Mrk 1095, PG 0804+761, PG 1001+291, PG 1116+215, PG 1211+143, PG 1259+593, PKS 0405–12, RX J0100.4–5113, RX J1830.3+7312, Ton S180 and VII Zw 118 there are a total of 33 intergalactic HI lines at a velocity for which we cannot find a galaxy with impact parameter less than 1 Mpc. These cases are collected at the end of Table 3. In these sightlines, the search for associated galaxies was extended to impact parameters of 5 Mpc. We can find a galaxy within 2 Mpc for 22 absorbers, and within 3 Mpc for 28. In all but two cases it is possible to find a galaxy within 5 Mpc, and this is the galaxy listed in Table 3. However, since we do not list all the non-detections for galaxies with impact parameter between 1 and 5 Mpc, these detections are treated slightly differently in the remainder of the paper.

Among all the associations there are 14 cases where O VI is seen. Twelve of these fall into the clear-association category, one is in a multi-component system (toward Mrk 876), and one is associated with a group (toward 3C 273).

Of the 128 associations between an intergalactic HI absorber and a galaxy listed in Table 3, just 15 have  $|\Delta v| > 200 \text{ km s}^{-1}$ . Seven of these occur for galaxies with  $\rho=400$ –1000 kpc and seven have the nearest galaxy at  $\rho > 1$  Mpc. The remaining one is the line at  $1447 \text{ km s}^{-1}$  ( $\Delta v=316 \text{ km s}^{-1}$ ) toward PG 1351+640, which is ambiguously associated with UGCA 375, at  $v_{gal}=1763 \text{ km s}^{-1}$  (see Sect. 4.3). There are only two other cases for which the nearest galaxy with  $\rho < 3$  Mpc also has  $|\Delta v| > 300 \text{ km s}^{-1}$ . These are the line at  $4638 \text{ km s}^{-1}$  toward Mrk 290, for which the nearest galaxy with similar velocity is NGC 5971 ( $\rho=1586$  kpc,  $\Delta v=332 \text{ km s}^{-1}$ ), and the line at  $3792 \text{ km s}^{-1}$  toward MCG+10-16-111, with  $\Delta v=349 \text{ km s}^{-1}$  and the nearest galaxy NGC 3809 at  $\rho=2910$  kpc.

In Table 3 we do not list galaxies with  $\rho < 1$  Mpc for which  $\rho/D_{gal} > 125$ , where  $D_{gal}$  is the galaxy’s diameter. This criterion allows us to avoid listing non-detections for many dwarf galaxies that are close to a larger galaxy with similar impact parameter. We also avoid listing many dwarf galaxies whose impact parameter is much larger than that of a large galaxy with which the absorption can be associated. However, by looking at the ratio

of impact parameter to diameter (rather than just the diameter) we do allow small galaxies with small impact parameter to appear in the table of results. The criterion is based on the fact that we found that  $\rho/D_{gal} < 125$  for all but one likely associations that have  $\rho < 1$  Mpc. Even when the nearest galaxy to an absorber is at  $\rho > 1$  Mpc,  $\rho/D_{gal}$  is  $< 125$  for half the cases. In fact, for half the associations  $\rho/D_{gal}$  is  $< 23$  and for 90% it is  $< 80$ . Note, however, that for many of the analyses presented in Sects. 4 and 5 we include *all* galaxies with impact parameter  $< 1$  Mpc, even if they are not listed in Table 3.

Summarizing the results of our attempts at associating absorbers with galaxies we conclude that: *For the majority (100 of 133, 75%) of absorption lines, it is possible to find a galaxy within 1 Mpc and  $400 \text{ km s}^{-1}$ . For about half of these (54) there is just one galaxy that is a likely candidate. For most of the other half, there either are two galaxies equally likely to be associated with the absorber (12 cases) or there are two absorption lines and two likely galaxies (12 cases). In a small number of cases (13) the absorption occurs in a group of galaxies and no unambiguous choice can be made. Ambiguities also exist for a small fraction (7 cases) of absorbers outside groups.*

#### 4.4. Ly $\alpha$ Absorbers in Voids

A question that is complementary to asking whether Ly $\alpha$  absorbers associate with galaxies is whether there are any Ly $\alpha$  absorbers that lie in voids. This question was studied most clearly by Penton et al. (2002), who defined a “void absorber” as a Ly $\alpha$  line for which there is no galaxy within 3 Mpc. They based their 3 Mpc void size on the contention that it is the median distance from a random point in the universe to the nearest  $L_*$  galaxy. As Fig. 7c shows, this is true if one only looks at galaxies with  $L > L_*$ . A 3 Mpc definition for the separation from the nearest  $L_*$  galaxy would imply that half of the  $L_*$  galaxies lie in voids.

Taking a nearest-neighbor distance of 3 Mpc as the limit for a void absorber, we can find a galaxy within that distance and with  $|\Delta v| < 400 \text{ km s}^{-1}$  for 99 of the 102 Ly $\alpha$  lines at  $v < 5000 \text{ km s}^{-1}$ . This would imply a  $3 \pm 2\%$  fraction of void absorbers. In particular, these would be the lines at  $2545 \text{ km s}^{-1}$  toward Mrk 509 (nearest galaxy at  $\rho = 4834 \text{ kpc}$ ), at  $4043 \text{ km s}^{-1}$  toward MCG+10-16-111 (nearest galaxy at  $\rho = 4351 \text{ kpc}$ ), and at  $4670 \text{ km s}^{-1}$  toward Mrk 817 (nearest known galaxy at  $\rho = 8739 \text{ kpc}$ ). The fact that all three lines are at  $v > 4000 \text{ km s}^{-1}$  suggests that maybe the galaxy surveys near these sightlines were not deep enough to find all galaxies. We note that near Mrk 509 there are five galaxies with unknown velocity (and  $L \sim 0.25 L_*$ ) whose impact parameter would be between 1.5 and 2.5 Mpc, if their velocity were about  $2500 \text{ km s}^{-1}$ . In that case the detection would no longer be considered a “void detection” (see Appendix for more details). Similarly, MCG+10-17-2A could have

$\rho=1.4$  Mpc from MCG+10-16-111 if that galaxy’s velocity is about  $4043 \text{ km s}^{-1}$ . Thus, it is quite possible that there are galaxies within 2 Mpc of the two best current candidates for “void absorbers”

If we impose that the nearest galaxy has to be brighter than  $0.1 L_*$ , there are two more candidate void absorbers: the line at  $3574 \text{ km s}^{-1}$  toward PKS 0405–12 (nearest  $L>0.1 L_*$  galaxy at  $\rho=4492$  kpc; Table 3 lists 2MASX J04060761–1023272 with  $D_{gal}=5.7$  kpc,  $\rho=1489$  kpc) and the line at  $3007 \text{ km s}^{-1}$  toward Mrk 421 (nearest  $>0.1 L_*$  galaxy at  $\rho=4840$  kpc; nearest galaxy HS 1059+3934 with  $D_{gal}=3.8$  kpc,  $\rho=1041$  kpc).

In principle, some of the candidate void absorbers could instead represent gas expanding at very-high-velocity from the AGN. For Mrk 421 this expansion velocity would be  $5993 \text{ km s}^{-1}$ , for Mrk 509 it would be  $7767 \text{ km s}^{-1}$ , and for Mrk 817 it is  $4760 \text{ km s}^{-1}$ . These would be comparatively large expansion velocities, however. Tripp et al. (2008) concluded that absorbers with velocity differing more than  $2500 \text{ km s}^{-1}$  from that of the AGN are almost certain to be intergalactic, rather than associated with the AGN. Thus, the absorbers toward Mrk 421. Mrk 509 and Mrk 817 are unlikely to be associated with the AGNs.

The foregoing discussion does not use a complete sample of galaxies, however. If we do restrict ourselves to complete samples, we find that there may be no absorbers that can be classified as a “void absorber”. At velocities below  $2500 \text{ km s}^{-1}$ , where our galaxy sample is complete down to  $L>0.1 L_*$ , we can find an  $L>0.1 L_*$  galaxy within  $\rho<1.4$  Mpc for *all* of the 58 absorption lines with  $v<2500 \text{ km s}^{-1}$ . We can find an  $L>0.25 L_*$  galaxy for 71 of the 75 absorbers with  $v<3700 \text{ km s}^{-1}$ , and an  $L>0.5 L_*$  galaxy for 92 of the 102 absorbers with  $v<5000 \text{ km s}^{-1}$ . Finally, there are 17 absorbers among the 102 with  $v<5000 \text{ km s}^{-1}$  for which we cannot find an  $L>L_*$  galaxy within 3 Mpc. This fraction of  $17/102$  or  $17\pm4\%$  is the equivalent of the value of  $22\pm8$  that Penton et al. (2002) quoted for the fraction of absorbers in voids – they looked at four sightlines to compare the locations of  $L>L_*$  galaxies relative to absorbers at  $v<20000 \text{ km s}^{-1}$ . We note that 12 of our 17 void absorbers have  $v>3000 \text{ km s}^{-1}$ . So, it is conceivable that galaxies were still missed near the sightlines with candidate void absorbers.

Looking only at the 58 absorbers with  $v<2500 \text{ km s}^{-1}$ , we find an  $L>0.1 L_*$  galaxy within 1.4 Mpc for each of these, as well as a  $>0.25 L_*$  galaxy within 2.2 Mpc, and a  $>0.5 L_*$  galaxy within 2.5 Mpc. Finally, for 54 of the 58 absorbers there is an  $L>L_*$  galaxy within 2.6 Mpc. Thus, using a 3 Mpc limit, there are *no* void absorbers when looking for galaxies brighter than  $0.5 L_*$ , and there is a  $7\pm3\%$  fraction when looking for  $L_*$  galaxies. This would suggest that there are *no* void absorbers if the galaxy sample is sufficiently complete at a luminosity limit better than  $0.5 L_*$ .

McLin et al. (2002) looked in more detail near seven of the void absorbers claimed by Penton et al. (2002) (four at  $v < 5000 \text{ km s}^{-1}$ ), determining redshifts of galaxies down to  $\sim 0.1 L_*$  lying within  $20' - 40'$  of the sightlines. They did not find any galaxies with  $\rho < 250 \text{ kpc}$ . However, for three of the four at  $v < 5000 \text{ km s}^{-1}$  we find an  $L > 0.3 L_*$  galaxy within  $1.1 \text{ Mpc}$  ( $\text{Ly}\alpha$  at  $2426 \text{ km s}^{-1}$  toward VII Zw 118, UGC 3748 at  $753 \text{ kpc}$ ;  $\text{Ly}\alpha$  at  $1979 \text{ km s}^{-1}$  toward HE 1029–1401, MCG–2-27-1 at  $1065 \text{ kpc}$ ;  $\text{Ly}\alpha$  at  $2548 \text{ km s}^{-1}$  toward Mrk 509, MCG–54-3 at  $2231 \text{ kpc}$ ). Only for the  $3007 \text{ km s}^{-1}$  line toward Mrk 509 is the nearest  $L > 0.1 L_*$  galaxy (UGC 6383) at large impact parameter ( $4840 \text{ kpc}$ ). All these galaxies have angular separation larger than  $1$  degree, so the  $20' - 40'$  field used by McLin et al. (2002) may have been too small to find all the relevant galaxies.

Based on these results, we conclude that *it depends on the luminosity limit and completeness of the galaxy sample whether an absorber is called a “void absorber” or not*. Further, *we find that there may not be any void absorbers (i.e. absorbers occurring more than  $3 \text{ Mpc}$  from the nearest galaxy) if a luminosity limit of  $0.1 L_*$  is used*. In fact, we find a  $> 0.1 L_*$  galaxy within  $1.5 \text{ Mpc}$  of each of  $58$  absorbers with  $v < 2500 \text{ km s}^{-1}$ , and a  $> 0.5 L_*$  galaxy within  $2.5 \text{ Mpc}$  of each absorber with  $v < 2500 \text{ km s}^{-1}$ . Finally, *we find that just  $10\%$  of the absorbers with  $v < 5000 \text{ km s}^{-1}$  lies more than  $3 \text{ Mpc}$  from the nearest  $0.5 L_*$  galaxy*. Finally, where Penton et al. (2002) found a fraction of  $22 \pm 8\%$  for absorbers more than  $3 \text{ Mpc}$  from the nearest  $L_*$  galaxy, we find a fraction of  $17 \pm 4\%$  for absorbers with  $v < 5000 \text{ km s}^{-1}$ , but just  $7 \pm 3\%$  when only looking at absorbers with  $v < 2500 \text{ km s}^{-1}$ .

#### 4.5. Velocity Difference Between $\text{Ly}\alpha/\text{O VI}$ Absorbers and Associated Galaxies

To determine (a-posteriori) the best velocity difference criterion for associating an absorber with a galaxy, we show in Fig. 9 the distribution of the difference between the velocity of the absorber (either  $\text{Ly}\alpha$  or  $\text{Ly}\beta$  in the top panels,  $\text{O VI}$  in the bottom panels) and the associated galaxy (as listed in Table 3, and as discussed in the Appendix and Sect. 4.3). In the left panels we show the distribution when selecting only the unambiguous cases with  $\rho < 1 \text{ Mpc}$ , while on the right all associations are included. Clearly, the distribution of unambiguous cases is basically symmetrical around  $\Delta v = 0$ ; excluding the two outliers, the dispersion is  $60 \text{ km s}^{-1}$ , with a range from  $-118$  to  $+147 \text{ km s}^{-1}$ . The full distribution (right panels) includes the cases with multiple absorbers associated with one galaxy, cases with one or two lines and two galaxies with similar impact parameter and velocity, detections associated with a group and detections with the nearest galaxy at  $\rho > 1 \text{ Mpc}$ .

As we limited ourselves to the part of the universe where most galaxies have previously

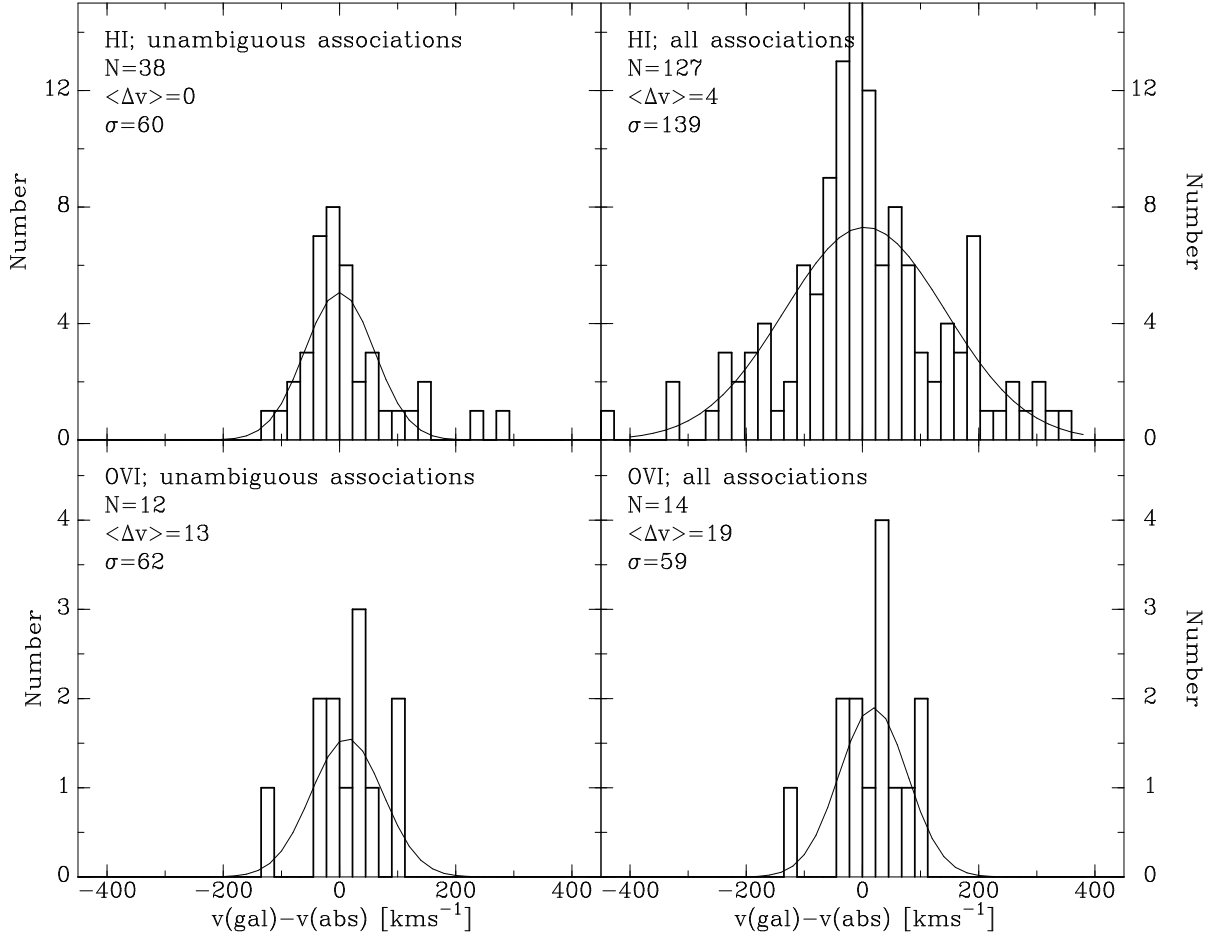


Fig. 9.— Histograms of the difference in velocity between an absorber and the galaxy that we associate with it. Top panels: HI lines ( $\text{Ly}\alpha$  or  $\text{Ly}\beta$ ), bottom panels: O VI lines. Left panels: only unambiguous associations are included (see Sect. 4.3). Right panels: all associations listed in Table 3 are included. The smooth curves represent gaussians with the average velocity and dispersion given in the labels.

been found, our sample of galaxies is more complete than that used in previous studies. Therefore, we draw the conclusion that *for unambiguous associations (i.e. just a few galaxies are known within 1 Mpc and  $400 \text{ km s}^{-1}$ , just one or two of which are bright), the difference in velocity between the intergalactic absorption and the galaxy’s systemic velocity ranges from  $-118$  to  $147 \text{ km s}^{-1}$ , with a dispersion of  $60 \text{ km s}^{-1}$ . This suggests that in general it is OK to use a limit of  $\Delta v < 400 \text{ km s}^{-1}$  for associating an absorber with a galaxy, although if there are no galaxies with low impact parameter and low velocity difference in individual cases larger velocity differences might exist.*

#### 4.6. $\text{Ly}\alpha$ Linewidths versus Impact Parameter

In Fig. 10 we look at the distribution of fitted line widths of  $\text{Ly}\alpha$  versus impact parameter. In the top panel we show the scatter plot for all lines. Absorbers that we associate with groups are shown by stars, field absorbers by circles. Closed symbols correspond to reliable absorbers, open circles to unreliable ones. Unreliable lines are those that are saturated as well as lines for which the width measurement is questionable, either because the spectrum is too noisy, or the line is too shallow. Finally, small symbols are for lines where the association with a galaxy is ambiguous, i.e. the assigned impact parameter is unreliable. In the bottom panel we include only reliable field absorbers with a clear association with a galaxy (see discussion in Sect. 4.3).

The outlier at (206 kpc,  $21 \text{ km s}^{-1}$ ) in both panels is the secondary  $\text{Ly}\alpha$  line at  $1109 \text{ km s}^{-1}$  seen toward Mrk 876. The outlier at (993 kpc,  $219 \text{ km s}^{-1}$ ) in the top panel corresponds to the line at  $1924 \text{ km s}^{-1}$  seen toward NGC 985. This is a weak line, which may have multiple components. Also, the association we list with DDO 23 is one of the most ambiguous in the sample. In fact, Bowen et al. (2002) associated it with NGC 988, which has impact parameter 175 kpc, but in that case  $v(\text{Ly}\alpha) - v(\text{gal})$  would be  $419 \text{ km s}^{-1}$ , larger than for any other absorber-galaxy association. Associating the line with the LGG 71 group is also problematic, since the highest velocity for any group galaxy is  $1665 \text{ km s}^{-1}$  ( $\rho=446 \text{ kpc}$ ). If the line is indeed a single broad line, its location in Fig. 10 would suggest that there should be galaxy with low impact parameter, which could be NGC 988. A *COS* spectrum of this target could resolve these issues.

Both panels of Fig. 10 shows a clear pattern: at all impact parameters there is a large spread in measured linewidths, but there is a trend for the maximum linewidth to increase with decreasing impact parameter. The histograms in the bottom panel show the 10th, 50th and 90th percentile of the distribution of linewidths. At impact parameters above 200 kpc, the 50th percentile (i.e. the median) is  $75\text{--}80 \text{ km s}^{-1}$ , but for the 0–200 kpc bin it

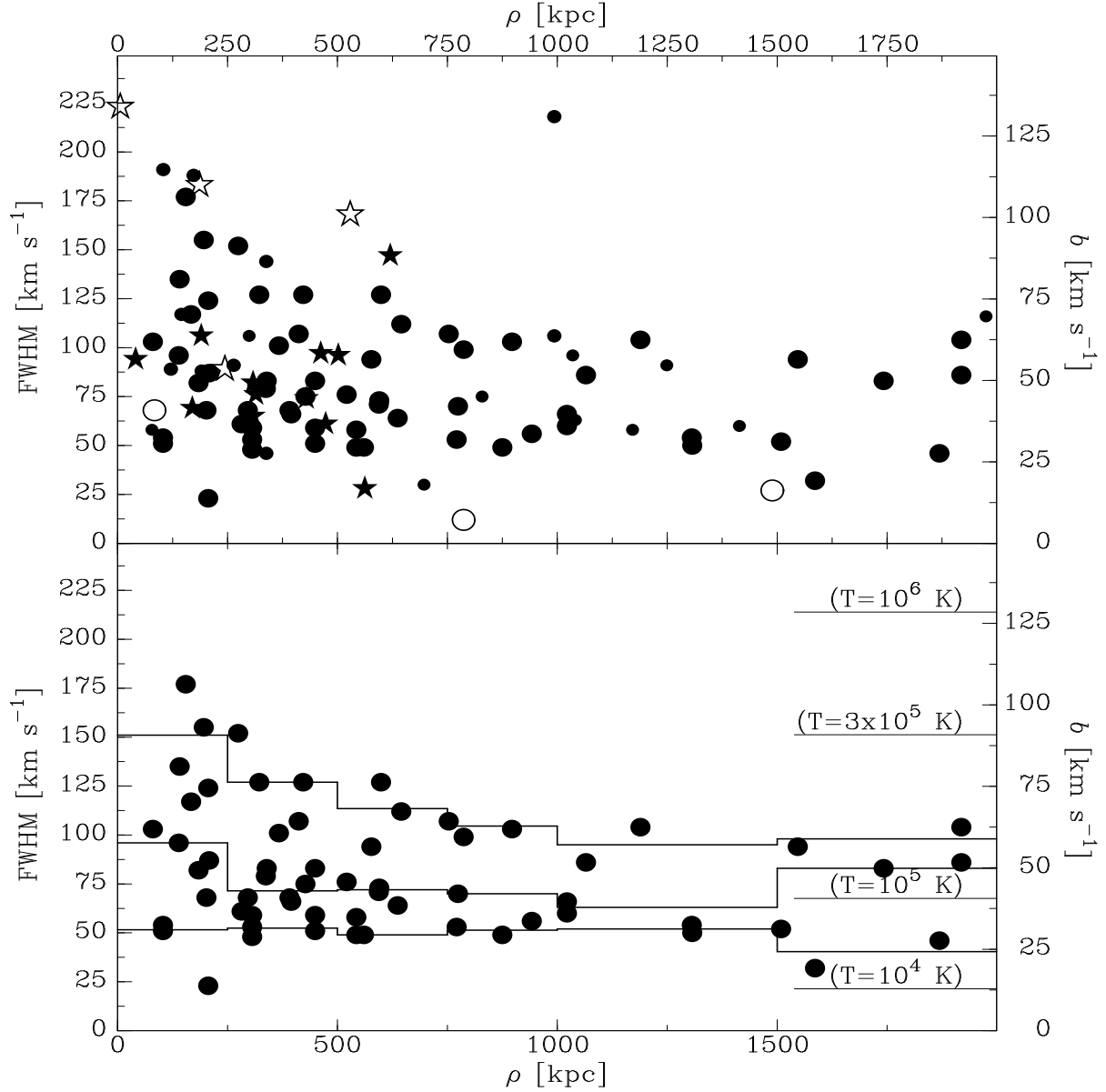


Fig. 10.— Plot of the linewidth of Ly $\alpha$  lines versus the impact parameter. Top panel: all Ly $\alpha$  absorbers. Bottom panel: including only well-measured absorbers clearly associated with field galaxies. Filled symbols are for reliably measured lines, open symbols for problematic lines (e.g. saturated, noisy). Circles are given for field galaxies, stars for group galaxies. Labels on the right side in the bottom panel show the temperature corresponding to some FWHM/ $b$ -values for gas at the given temperature. The histograms give the 10th, 50th and 90th percentile of the distribution in 250 kpc ( $\rho < 1$  Mpc) or 500 kpc ( $\rho > 2$  Mpc) wide bins.



is  $105 \text{ km s}^{-1}$ . Also, the upper envelope of the distribution shows a clear trend of increasing maximum linewidth with decreasing impact parameter.

On the right side of the bottom panel of Fig. 10 we also show horizontal lines at FWHMs of 21, 68, 151 and  $214 \text{ km s}^{-1}$ , corresponding to the thermal width of H I at temperatures of  $10^4$ ,  $10^5$ ,  $3 \times 10^5$ , and  $10^6 \text{ K}$ . However, the width of the H I absorption line is not necessarily thermal. It is often assumed that  $\text{Ly}\alpha$  absorbers consist of photoionized gas and such modeling gives consistent results (e.g. Penton et al. 2004). Also, some lines may have multiple components. Alternatively, the gas may be highly turbulent. However, a turbulent width of  $100 \text{ km s}^{-1}$  is an order of magnitude higher than typical values seen inside galaxy disks. If the gas is orbiting a galaxy, but stretched over many kpc, the projection of its orbital velocity may change from the front to the back side, broadening the observed profile. For cloud densities in the gas typical of that of clouds in the Milky Way corona ( $\sim 10^{-3} \text{ cm}^{-2}$ , Fox et al. 2005), a cloud with total hydrogen column density  $\sim 10^{20} \text{ cm}^{-2}$  would be about 30 kpc deep. Orbiting with  $200 \text{ km s}^{-1}$  at 100 kpc, the changing velocity projection then introduces a velocity gradient of about  $8 \text{ km s}^{-1}$ , much smaller than the observed  $50 \text{ km s}^{-1}$  increase in the maximum velocity width.

A final possibility is that large velocity gradients were introduced for the gas in the extended halos by tidal effects. Near the Milky Way, the Magellanic Stream provides evidence for such processes, and in the Galactic Standard of Rest reference system it has an apparent velocity gradient of  $400 \text{ km s}^{-1}$  over  $180^\circ$ . Sightlines through the stream result in profiles that when fit by a single-gaussian can have FWHM up to  $\sim 80 \text{ km s}^{-1}$ . This is much smaller than the absorber linewidths at low impact parameter. However, we cannot exclude that the apparent linewidths will be larger if the sightline passes through a tidal feature along its long axis. On the other hand, it is unlikely that the axis of the feature and the sightline line up exactly in many cases. On balance, tidal stretching may be one of the causes of the line broadening, but it is unlikely to be the explanation for *all* of the lines that are broader than  $150 \text{ km s}^{-1}$ .

At present, the S/N ratios of spectra with candidate broad lines are too low to analyze the detailed shapes of the profiles and decide whether they can be described by a single component gaussian. The installation of *COS* on HST will allow observations with sufficiently high S/N ratio to check this. With this caveat in mind, however, Fig. 10 suggests that *there is an increase in the temperature of the gas within a few hundred kpc of galaxies. Such behavior inside gravitational wells is predicted in hydrodynamical simulations of structure formation in the universe (Cen & Ostriker 1999; Davé et al. 2001; Cen & Fang 2006).*

#### 4.7. Ly $\alpha$ Equivalent Width versus Impact Parameter

The question of an anti-correlation between the equivalent width of Ly $\alpha$  absorbers and the impact parameter to the nearest galaxy has been the subject of much discussion and disagreement in the literature. Lanzetta et al. (1995) reported an anti-correlation between equivalent width ( $W$ ) and  $\rho$ , but they only had 7 detections with  $\rho < 100 h_{71}^{-1}$  kpc. Tripp et al. (1998) plotted nine absorbers at  $\rho < 600 h_{71}^{-1}$  kpc, and these do show an anti-correlation between  $W$  and  $\rho$ . Chen et al. (2001) claimed a tight anti-correlation between  $W$  and  $\rho$  for their 34 associations with  $\rho < 200 h_{71}^{-1}$  kpc. In particular, they claimed that  $\log W = -(0.96 \pm 0.11) \log \rho + \text{constant}$ . However, also they showed plots of the difference between  $\log W$  predicted by this equation and the actual  $\log W$ , and these reveal that the residuals have a large spread of  $\pm 0.5$  dex. Chen et al. (2001) further claimed that the anti-correlation improves if the luminosity of the associated galaxy is taken into account. Impey et al. (1999) combined earlier studies with their sample of 139 Ly $\alpha$  lines, and saw a more mixed picture, concluding that at high impact parameters there is no anti-correlation between  $W$  and  $\rho$ , but at  $\rho < 200 h_{71}^{-1}$  kpc there is a trend of finding higher  $W$  at lower  $\rho$ . The well-defined sample of 6 clear associations with  $\rho < 200 h_{71}^{-1}$  kpc of Bowen et al. (2002) also lead them to conclude that  $\log W$  and  $\log \rho$  do anti-correlate. Penton et al. (2002) studied this once more, using their sample of 81 low-redshift absorbers and concluded that at  $\rho > 50 h_{71}^{-1}$  kpc the  $W$  vs.  $\rho$  plot is a scatter plot. At lower  $\rho$  they did not find a strong anti-correlation, but the lowest measured  $W$  is 500 mÅ, so that viewed over a wide range of  $\rho$  there seems to be some relation.

We show our results in Fig. 11, using linear scales in the top two panels, logarithmic scales in the bottom two. In the studies listed above only logarithmic scales were used for  $W$  and  $\rho$ , but as we discuss below, this obscures the real conclusion that can be drawn from the scatter plot. In the left panels of Fig. 11 we use the impact parameters and equivalent widths given in Table 3. In the plot on the right we check to see what happens if we were only able to find the nearest  $L > L_*$  galaxy to an absorber.

For comparing with the literature results (bottom panels), we include the relations given by Chen et al. (2001) (dotted line) and Penton et al. (2002) (solid line). This shows that our impact parameters are typically much larger than those of Chen et al. (2001). The distribution of points at  $\rho > 100$  kpc looks like a scatter plot, except when looking at the nearest  $L > L_*$  galaxy, in which case there seems to be an impact parameter dependent lower envelope, i.e.  $W < 100$  mÅ only occurs at  $\rho > 0.5$  Mpc,  $W < 50$  mÅ at  $\rho > 1$  Mpc and  $W < 25$  mÅ at  $\rho > 2.5$  Mpc from the nearest  $L_*$  galaxy. A similar pattern holds when looking at the impact parameter relative to  $L > 0.1 L_*$  galaxies, for which  $W < 100$  mÅ occurs at  $\rho > 150$  kpc,  $W < 50$  mÅ at  $\rho > 300$  kpc and  $W < 25$  mÅ at  $\rho > 750$  kpc.

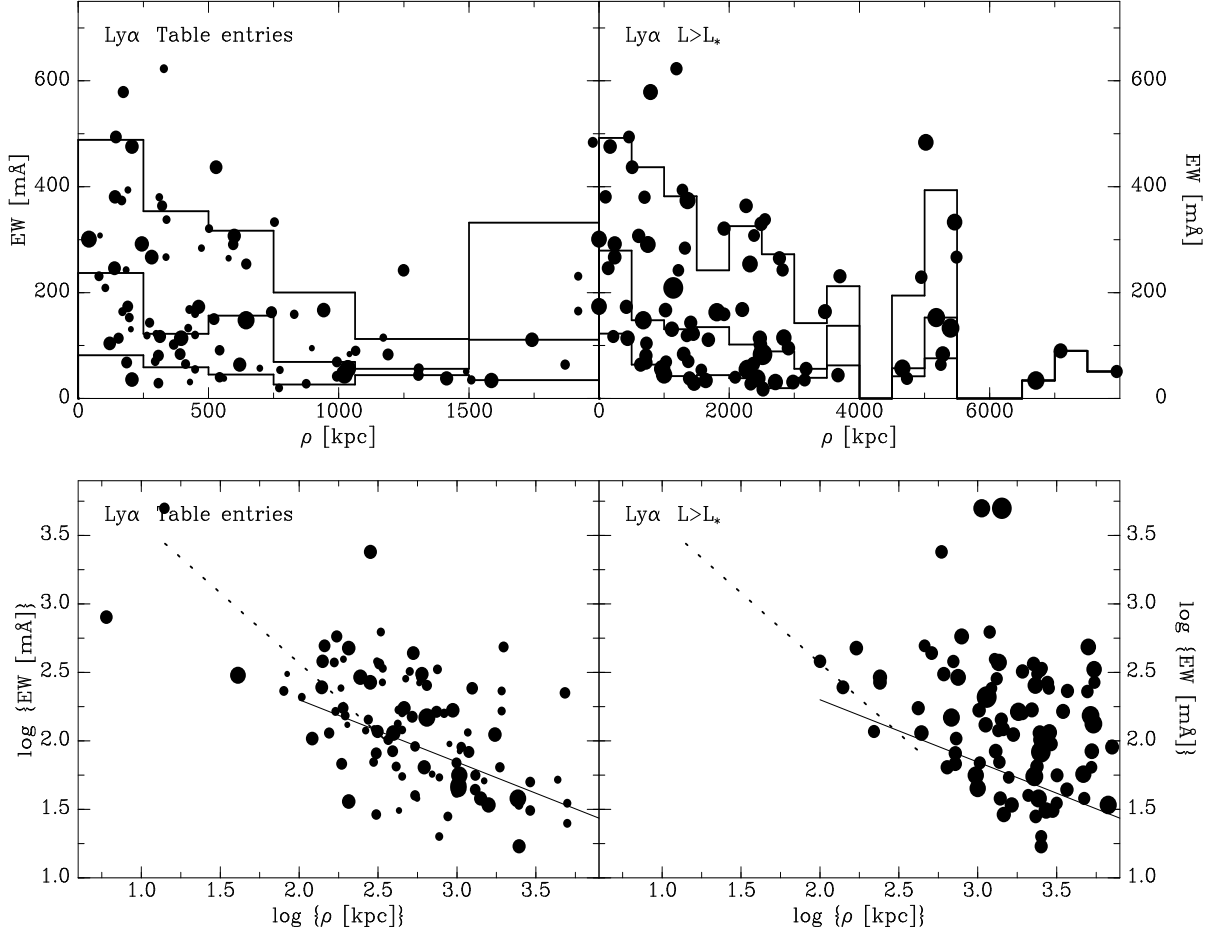


Fig. 11.— Scatter plot of the Ly $\alpha$  equivalent width against impact parameter. Left panels: results for the absorbers listed in Table 3 (two absorbers with equivalent width  $>1000$  mÅ are not shown in the top left panel). The symbol size scales as the 2/3rd power of the galaxy diameter. Right panels: impact parameters to the nearest  $L > L_*$  galaxy. Top panels: linear scales, bottom panels: logarithmic scales. The histograms in the top panels show the 10th, 50th and 90th percentiles of the distribution of equivalent width in 250 or 500 kpc wide impact parameter bins. In the bottom panels the dotted line gives the relation between equivalent width and impact parameter claimed by Chen et al. (2001), while the solid line is the relation given by Penton et al. (2002).

On the other hand, strong lines occur mostly in the neighborhood of galaxies, with just two of the ten  $>400$  mÅ lines occurring at impact parameters  $\rho > 350$  kpc (at  $1665 \text{ km s}^{-1}$  toward PG 1149–110,  $\rho = 529$  kpc, and at  $3579 \text{ km s}^{-1}$  toward Mrk 110,  $\rho = 1975 \text{ km s}^{-1}$ ). At the  $>300$  mÅ level 19 of 23 lines (82%) occur within 600 kpc of a galaxy, and 16 of 23 (70%) have  $\rho < 350$  kpc. This includes 6 of the 10 detections that we associate with a group rather than a single galaxy. We can look at this in reverse, and note that for about 10% of the strong lines the nearest galaxy has impact parameter  $>1$  Mpc (5 of 38 with  $W > 200$  mÅ, 2 of 23 with  $W > 300$  mÅ, and 1 of 10 with  $W > 400$  mÅ).

The top panels of Fig. 11 show that using a logarithmic scale for the equivalent width hides an important facet of the relation between  $W$  and  $\rho$ . The bins in the top panels give the 10th, 50th and 90th percentile of the distribution of  $W$  in a 250 kpc (at  $\rho < 1$  Mpc) or 500 kpc (at  $\rho > 1000$  kpc) wide interval. The 10th percentile remains more or less constant with impact parameter (except for the lowest impact parameters to the nearest  $L_*$  galaxy), while the 90th percentile strongly anti-correlates with  $\rho$ , especially at  $\rho < 1500$  kpc. Note that the top panels do not show the four strongest lines, three of which occur inside a galaxy ( $\rho = 0.3$  kpc toward HS 1543+5921,  $\rho = 6$  kpc toward Mrk 205,  $\rho = 14$  kpc toward 3C 232 and the sub-DLA at  $1895 \text{ km s}^{-1}$  toward PG 1216+069). It is clear that at any impact parameter, the distribution of equivalent widths of Ly $\alpha$  absorbers is wide, but the maximum equivalent width is larger at smaller impact parameters.

We checked whether there was any difference in the distribution when selecting only field or group galaxies, or when selecting only galaxies with diameters in a given range, or when comparing galaxies with  $v_{gal} < 2500$  vs. galaxies with  $v_{gal} < 5000 \text{ km s}^{-1}$ . In all but one cases the 10th, 50th and 90th percentile bins are basically identical. The lone exception is that all the lines stronger than 100 mÅ at  $\rho > 1500$  kpc occur at velocities above  $2500 \text{ km s}^{-1}$ . Since the galaxy sample is less complete for the fainter galaxies, it is possible that a better search for galaxies could turn up an  $L < 0.1 L_*$  galaxy with lower impact parameter.

From Fig. 11 we derive the following conclusions: *At any impact parameter there is a wide range in Ly $\alpha$  equivalent widths, but the strongest lines are stronger at lower impact parameter. Also: 80% of strong ( $W > 300$  mÅ) lines occur within 600 kpc of a galaxy, while 70% originate within 350 kpc. On the other hand, weak lines only occur far from  $L_*$  galaxies, and the weaker the line, the larger the minimum impact parameter; specifically all Ly $\alpha$  lines with  $W < 25$  mÅ have  $\rho > 750/2500$  kpc to the nearest  $0.1/1.0 L_*$  galaxy, while all Ly $\alpha$  lines with  $W < 50$  mÅ have  $\rho > 300/1000$  kpc to the nearest  $L > 0.1/1.0 L_*$  galaxy.*

## 5. Absorbers Near Galaxies

This section presents a number of analyses from the perspective of the galaxies. By restricting ourselves to very low redshift, we can use general surveys and catalogs to produce a fairly complete galaxy sample. Looking at many sightlines, we can thus study the detection fraction as function of impact parameter using different selection criteria. First we look at the amount of intergalactic gas as function of the density of galaxies near the absorbers (Sect. 5.1). In Sect. 5.2 we tabulate the fraction of galaxies having an absorber within a given impact parameter and velocity, while in Sect. 5.3 we show histograms of the detection fraction as function of impact parameter, using several criteria to select galaxies. We also combine all the sightlines to create a synthetic map of a galaxy’s gaseous envelope (Sect. 5.4).

### 5.1. Ly $\alpha$ Equivalent Width versus Galaxy Density

A way of looking at the relation between galaxies and absorbers is to look at the density of galaxies in the neighborhood of an absorber. Bowen et al. (2002) did this for the six sightlines in their sample. They calculated the number of galaxies in a cylindrical volume with impact parameter  $<2$  Mpc and velocity within  $\pm 500$  km s $^{-1}$  from the absorber. Since the Hubble constant is 71 km s $^{-1}$  Mpc $^{-1}$ , the depth of such a cylinder may be larger than its width. However, galaxies usually have large peculiar velocities and thus  $\Delta v/H_o$  is not a good measure of the differential distance of the galaxy along the line of sight. Bowen et al. (2002) adopted 500 km s $^{-1}$ , arguing that this is near the maximum observed for groups. They also made the point that one should compare the galaxy density to the total equivalent width (or column density) of the absorbers in a velocity interval – if there are multiple absorbers, taking each absorber separately would underestimate the density of intergalactic gas. With this method and criteria, Bowen et al. (2002) found that there was a very tight correlation between the galaxy density and the total Ly $\alpha$  equivalent width for the six main absorbing systems in their sample. Côté et al. (2005) added four more systems, and although their plot of  $\log W$  vs  $\log n$  showed larger scatter, they thought that they confirmed the conclusion of Bowen et al. (2002).

In Fig. 12 we show our results, for several choices for the maximum impact parameter and velocity difference between absorber and galaxies. For each absorber, we first add the equivalent width of it and all other absorbers within  $\Delta v < 500$  or  $< 1000$  km s $^{-1}$ . We then count the number of galaxies with  $L > 0.1 L_*$  in each cylinder and divide by its volume. In each of the four panels we show the systems in Bowen et al.’s (2002) study as filled stars and the systems of Côté et al. (2005) as filled squares. We looked at this scatter plot for cylinders with radius 0.2, 0.5, 1, 2 and 3 Mpc and velocity range 200, 400, 500, 1000 and

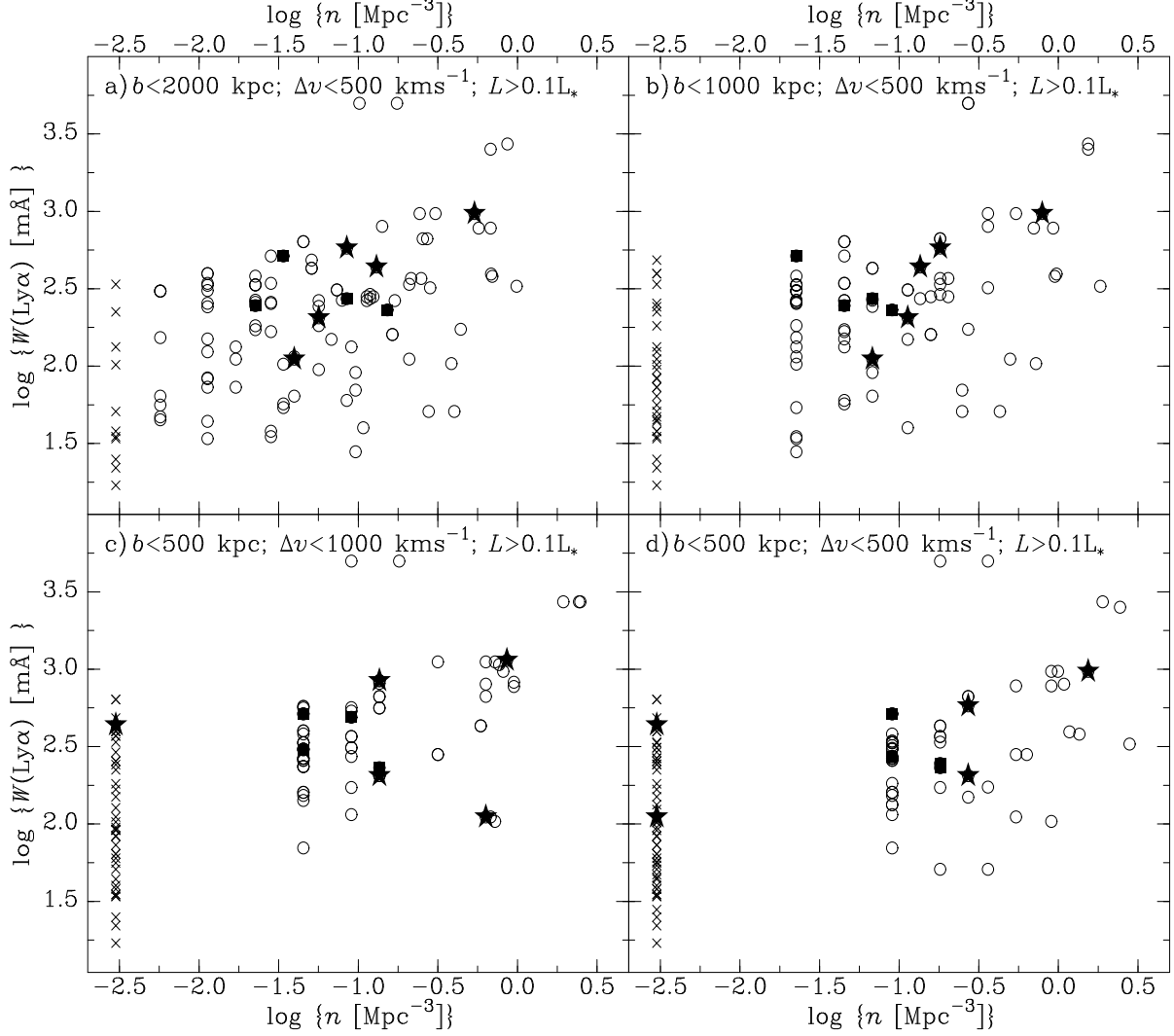


Fig. 12.— Scatter plot of the total Ly $\alpha$  equivalent width within 500 or 1000 km s $^{-1}$  from an absorber versus the number density of galaxies with  $L > 0.1 L_*$  in a cylinder with radius 500, 1000 or 2000 kpc (see labels). Open circles show the data for all detections in our sample, while filled stars are for the absorbers in the sample of Bowen et al. (2002) and filled squares correspond to the absorbers discussed by Côté et al. (2005). In each panel, the column of crosses corresponds to having no galaxy in the box, while the second column gives the density with just one galaxy in each box. *Selection criteria:* all Ly $\alpha$  lines; all galaxies fitting the criteria, where for  $L > 0.1 L_*$  also  $v < 2500$  km s $^{-1}$  and for  $L > L_*$   $v < 5000$  km s $^{-1}$ .

3000 km s<sup>-1</sup>, as well as separately for absorbers with  $v < 2500$  km s<sup>-1</sup> and  $v > 2500$  km s<sup>-1</sup> and using different luminosity limits for the galaxies. All of these choices lead to the same conclusions.

Figure 12a presents the plot using the criteria used by Bowen et al. (2002) ( $\rho < 2$  Mpc,  $\Delta v < 500$  km s<sup>-1</sup>). The filled stars then fall on a line (correlation coefficient 0.88), and the filled squares scatter near this line. However, it is clear that this must be an artifact of the particular set of systems that Bowen et al. (2002) and Côté et al. (2005) observed. The scatter plot does suggest that there is a tendency for an increase of the maximum total equivalent width with increasing galaxy density (correlation coefficient 0.95), but there clearly is no strong general correlation (the correlation coefficient for all data is 0.40). If we look at a somewhat smaller box (1 Mpc by 500 km s<sup>-1</sup>, panel b), we come to the same conclusion. If we look closer to the absorbers, using a 500 kpc by 1000 km s<sup>-1</sup> box, we find that there may a rough correlation between the amount of absorbing intergalactic gas and the galaxy density (panel c). But looking even closer (panel d), the properties of the scatter plot revert to those of the larger boxes.

In Fig. 12c a number of outliers are located at  $\log n = -0.2$ ,  $\log W = 2.05$ . Two of these correspond to the detections at 1924 and 2183 km s<sup>-1</sup> toward NGC 985. As discussed in Sect. 4.3 and in the notes to NGC 985, and as can be seen in Fig. 8, this is an absorber that is very difficult to associate with a galaxy. The galaxies in the nearby group LGG 71 range in velocity from 1145 to 1781 km s<sup>-1</sup>, and the sightline passes 175 kpc from the edge of the group. The derived galaxy density is thus sensitive to the parameters of the cylinder. For  $\Delta v = 1000$  km s<sup>-1</sup> many group galaxies are included, but for  $\Delta v = 500$  km s<sup>-1</sup> they are not, so that the point falls on what appeared to be a linear relation between  $\log W$  and  $\log n$ . The third outlier corresponds to the line at 2110 km s<sup>-1</sup> seen toward PG 1211+143, which is normal in every other aspect.

From Fig. 12 we conclude that *there is no correlation between the total Ly $\alpha$  equivalent and the galaxy density near the absorber, although the maximum Ly $\alpha$  equivalent width may depend on the galaxy density. At all galaxy densities there is a wide range in the observed Ly $\alpha$  equivalent widths.*

## 5.2. The Fraction of Galaxies of Given $L$ Having a Ly $\alpha$ Absorber Within $\rho$ , $\Delta v$

In Table 10 we look at the fraction of galaxies that have an associated Ly $\alpha$  absorber stronger than either 50 or 300 mÅ within a given impact parameter and velocity difference. This table is the complement to Table 9. To construct Table 10 we first find for each galaxy

with  $v_{gal} < 2500 \text{ km s}^{-1}$  the impact parameter to an AGN sightline, and we check the  $3\sigma$  Ly $\alpha$  equivalent width error at the velocity of the galaxy. Then we note whether or not there is an intergalactic line within a given impact parameter and velocity difference. We use a velocity limit of  $2500 \text{ km s}^{-1}$ , rather than  $5000 \text{ km s}^{-1}$  because then our galaxy sample is basically complete down to  $0.1 L_*$ , and then we can compare the fractions across different luminosities.

Each entry in the table consists of three parts. The middle part is the number of galaxies with equivalent width limit  $< 50 \text{ m}\text{\AA}$  (first group of 15 rows) or  $< 300 \text{ m}\text{\AA}$  (second group of 15 rows), impact parameter less than the number in Col. 1, and luminosity larger than the limits given in Cols. 3–6. The first part of the entry is the number of these galaxies for which there is a Ly $\alpha$  or Ly $\beta$  absorption line with  $W > 50$  or  $> 300 \text{ m}\text{\AA}$  whose velocity differs from the galaxy’s systemic velocity by less than the number in Col. 2. The third part of each entry is the ratio of these two numbers, converted to a percentage. So, for example, there are 135 galaxies with  $v_{gal} < 2500 \text{ km s}^{-1}$  and  $L > 0.1 L_*$  within 1 Mpc of an AGN sightline, in whose spectrum the  $3\sigma$  equivalent width limit is  $< 50 \text{ m}\text{\AA}$  at the velocity of the galaxy. For 68 (50%) of these, the AGN spectrum shows a  $> 50 \text{ m}\text{\AA}$  Ly $\alpha$  or Ly $\beta$  line with velocity within  $400 \text{ km s}^{-1}$  of the systemic velocity of the galaxies.

We summarize the conclusions that can be drawn from this table below. We also looked at the fractions separately for field and group galaxies and even for the four sightlines going through or near the Virgo cluster (3C 273.0, HE 1228+0131, PG 1211+143 and PG 1216+069). The fractions are basically the same, however, typically differing by less than 10%.

From Table 10 we can draw the following conclusions: (1) *At low impact parameter ( $< 400 \text{ kpc}$ ), it is possible to find a  $> 50 \text{ m}\text{\AA}$  Ly $\alpha$  pabsorber within  $1000 \text{ km s}^{-1}$  for all galaxies, and within  $400 \text{ km s}^{-1}$  for the majority ( $\sim 80\%$ ) of them.* (2) *Detecting a  $> 300 \text{ m}\text{\AA}$  Ly $\alpha$  absorber within  $400 \text{ km s}^{-1}$  is possible for  $\sim 40\text{--}50\%$  of galaxies with  $\rho < 400 \text{ kpc}$  and for  $\sim 45\%$  of galaxies with  $\rho < 200 \text{ kpc}$ .* (3) *The fraction of galaxies with a Ly $\alpha$  line within a given velocity difference does not depend on their luminosity.* (4) *At higher impact parameters the fraction of galaxies with an associated Ly $\alpha$  line decreases.*



Table 10. Fraction of galaxies with  $v < 2500 \text{ km s}^{-1}$  and a  $\text{Ly}\alpha$  absorber within  $\rho$  and  $\Delta v$ <sup>1</sup>

$\rho$ [kpc] (1)	$\Delta v$ [km s <sup>-1</sup> ] (2)	$L > 0.1 L_*$ (3)	$L > 0.25 L_*$ (4)	$L > 0.5 L_*$ (5)	$L > L_*$ (6)
<i>W</i> > 50 mÅ					
<200	<200	4 of 9; 44%	4 of 8; 50%	4 of 8; 50%	1 of 3; 33%
<200	<400	7 of 9; 77%	6 of 8; 75%	6 of 8; 75%	2 of 3; 66%
<200	<1000	9 of 9; 100%	8 of 8; 100%	8 of 8; 100%	3 of 3; 100%
<400	<200	9 of 22; 40%	9 of 16; 56%	6 of 11; 54%	2 of 5; 40%
<400	<400	17 of 22; 77%	13 of 16; 81%	9 of 11; 81%	4 of 5; 80%
<400	<1000	22 of 22; 100%	16 of 16; 100%	11 of 11; 100%	5 of 5; 100%
<1000	<200	34 of 135; 25%	27 of 95; 28%	20 of 62; 32%	6 of 30; 20%
<1000	<400	68 of 135; 50%	47 of 95; 49%	33 of 62; 53%	14 of 30; 46%
<1000	<1000	101 of 135; 74%	72 of 95; 75%	48 of 62; 77%	24 of 30; 80%
<2000	<200	86 of 451; 19%	70 of 312; 22%	47 of 211; 22%	22 of 105; 20%
<2000	<400	200 of 451; 44%	150 of 312; 48%	99 of 211; 46%	46 of 105; 43%
<2000	<1000	305 of 451; 67%	222 of 312; 71%	147 of 211; 69%	73 of 105; 69%
<3000	<200	152 of 966; 15%	112 of 669; 16%	79 of 457; 17%	35 of 230; 15%
<3000	<400	360 of 966; 37%	262 of 669; 39%	177 of 457; 38%	80 of 230; 34%
<3000	<1000	550 of 966; 56%	395 of 669; 59%	276 of 457; 60%	134 of 230; 58%
<i>W</i> > 300 mÅ					
<200	<200	5 of 14; 35%	5 of 13; 38%	4 of 10; 40%	2 of 4; 50%
<200	<400	6 of 14; 42%	6 of 13; 46%	5 of 10; 50%	2 of 4; 50%
<200	<1000	7 of 14; 50%	7 of 13; 53%	6 of 10; 60%	2 of 4; 50%
<400	<200	8 of 33; 24%	7 of 25; 28%	6 of 17; 35%	3 of 9; 33%
<400	<400	12 of 33; 36%	11 of 25; 44%	9 of 17; 52%	5 of 9; 55%
<400	<1000	15 of 33; 45%	14 of 25; 56%	11 of 17; 64%	6 of 9; 66%
<1000	<200	21 of 174; 12%	18 of 121; 14%	15 of 80; 18%	7 of 43; 16%
<1000	<400	39 of 174; 22%	30 of 121; 24%	26 of 80; 32%	12 of 43; 27%
<1000	<1000	77 of 174; 44%	56 of 121; 46%	42 of 80; 52%	22 of 43; 51%
<2000	<200	48 of 569; 8%	41 of 397; 10%	31 of 269; 11%	13 of 138; 9%
<2000	<400	115 of 569; 20%	88 of 397; 22%	65 of 269; 24%	29 of 138; 21%
<2000	<1000	218 of 569; 38%	165 of 397; 41%	114 of 269; 42%	60 of 138; 43%
<3000	<200	97 of 1216; 7%	74 of 855; 8%	55 of 585; 9%	24 of 309; 7%
<3000	<400	228 of 1216; 18%	173 of 855; 20%	125 of 585; 21%	61 of 309; 19%
<3000	<1000	403 of 1216; 33%	295 of 855; 34%	207 of 585; 35%	108 of 309; 34%

### 5.3. $\text{Ly}\alpha$ , $\text{Ly}\beta$ and O VI Detection Fraction as Function of Impact Parameter

In this section we study the fraction of  $\text{Ly}\alpha$  absorbers as function of impact parameter to the associated galaxy. We can do this because our galaxy sample is more or less complete, so we can properly count non-detections. Some previous studies also discussed detection fractions, but only for relatively bright galaxies and relatively small impact parameters. We first compare the numbers in these studies to our results, scaling the impact parameters listed in the other studies to a Hubble constant of  $H_0=71 \text{ km s}^{-1}$  (Sect. 5.3.1). We then describe how we construct the detection fraction histograms as function of impact parameter (Sect. 5.3.2), including a correction for incompleteness in the *NED* data, and justifying our selection criteria. The results are shown in Tables 11 and 12, as well as Figs. 13 to 17. We discuss them systematically in Sects. 5.3.3 ( $\text{Ly}\alpha$  for field galaxies), 5.3.4 ( $\text{Ly}\alpha$  for group galaxies), 5.3.5 ( $\text{Ly}\beta$ ) and 5.3.6 (O VI).

#### 5.3.1. Comparison with Previous Studies

Lanzetta et al. (1995) reported a 100% detection fraction for impact parameters  $\rho < 100 \text{ h}_{71}^{-1} \text{ kpc}$  and equivalent width limit  $W_{\text{lim}} > 150 \text{ m}\text{\AA}$ , decreasing to 66% for  $\rho < 230 \text{ h}_{71}^{-1} \text{ kpc}$  and 11% at  $\rho > 230 \text{ h}_{71}^{-1} \text{ kpc}$ . However, because of the nature of their survey (a single limiting apparent magnitude over a large redshift range), it is not completely clear how to compare this to our sample. If we use a limit of  $D_{\text{gal}} > 11 \text{ kpc}$  ( $L > 0.25 L_*$ ), we find percentages of 80%, 50% and 8% for the three fractions of lines with  $W_{\text{lim}} > 150 \text{ m}\text{\AA}$ , i.e. the same pattern, but about three quarters as many detections.

Bowen et al. (1996) found a 44% fraction for  $\rho < 430 \text{ h}_{71}^{-1} \text{ kpc}$ ,  $L > 0.5 L_*$  and  $W > 300 \text{ m}\text{\AA}$ . Using the same criteria we find 7 detections for 31 galaxies, or 23%, which is about half as many. In their subsequent paper, Bowen et al. (2002) claimed a 100% detection fraction for  $\rho < 285 \text{ h}_{71}^{-1} \text{ kpc}$ ,  $L > 0.5 L_*$  and  $W > 45 \text{ m}\text{\AA}$ . With just their sightlines, we find 4 of 5 (80%) galaxies are detected, while the complete sample gives 67% (12 of 18). Clearly, with a relatively low equivalent width limit, most luminous galaxies with low impact parameter are found to have associated  $\text{Ly}\alpha$  absorption.

For the two sightlines toward H 1821+643 and PG 1116+215, Tripp et al. (1998) found that there was an  $\text{Ly}\alpha$  line within  $1000 \text{ km s}^{-1}$  of all 42 galaxies with  $\rho < 600 \text{ h}_{71}^{-1} \text{ kpc}$  in their sample (note that often more than one galaxy is associated with a particular absorber). The luminosity cutoff of the galaxy sample of Tripp et al. (1998) varied with redshift – at  $z < 0.10$  (where a substantial fraction of their absorbers occurs), their limit  $B < 19$  corresponds to about an  $L_*$  galaxy. We find an absorber for 90% (10 of 11) of  $L > L_*$  galaxies with  $\rho < 600 \text{ kpc}$

and  $\Delta v < 1000 \text{ km s}^{-1}$ .

In the Impey et al. (1999) study, eleven absorbers found in *GHR*S G140L spectra ( $0.8 \text{ \AA}$ , or  $\sim 150\text{--}190 \text{ km s}^{-1}$  resolution) were compared against galaxies in the Virgo cluster region, with the sample complete down to  $M_B = -16$  ( $0.04 L_*$ ). The  $3\sigma$  detection limit varies between about 30 and  $120 \text{ m\AA}$ . They claimed a detection fraction of 60% for galaxies with impact parameter  $< 385 h_{71}^{-1} \text{ kpc}$  and  $L > 0.25 L_*$ , and 20% for  $\rho < 700 h_{71}^{-1} \text{ kpc}$  and  $L > L_*$ . Using the same impact parameter and luminosity criteria and choosing  $W_{\text{lim}} > 60 \text{ m\AA}$ , we find fractions of 56% (22 detections for 39 galaxies) and 41% (14 detections for 34 galaxies), respectively.

Finally, Chen et al. (2001) looked at 47 galaxies with  $z = 0.07\text{--}0.89$  with  $\rho < 180 h_{71}^{-1} \text{ kpc}$ , and find associated detections for 34 of these (61%). For their detection limit ( $\sim 300 \text{ m\AA}$ ) we find 5 detections for 14 galaxies with  $\rho < 180 h_{71}^{-1} \text{ kpc}$ , or 36%, i.e. a detection fraction that is about half as high.

### 5.3.2. Constructing Detection Fraction Histograms

Figures 13 through 17 show the number of galaxies, number of detections and detection fraction as function of impact parameter, using different sets of criteria, separately for each of  $\text{Ly}\alpha$ ,  $\text{Ly}\beta$  and OVI. In Table 11 we list the number of galaxies, number of detections and the detection fraction for the same criteria. We now first discuss the criteria used to construct these figures, then we discuss the results. Unless noted otherwise, we only use sightlines for which the limiting equivalent width is  $100 \text{ m\AA}$  or better.

In each of these figures, the top three panels show the number of galaxies in 100 kpc impact parameter bins, with the taller bins corrected for incompleteness in the *NED* sample (see below). Hatched regions in the top panels give the number of detections. The dotted lines show the expected distributions, calculated as the ratio of the area in the impact parameter bin to the area in a 2 Mpc radius circle, scaled by the total number of galaxies with  $\rho < 2 \text{ Mpc}$ . The bottom panels give the fraction of galaxies with an associated detection.

The correction for *NED* completeness is necessary because the standard *NED* search only allows one to find galaxies within  $5^\circ$  from a given direction. This is not a problem for the RC3 part of the galaxy sample. Therefore, at an impact parameter of  $\rho_0 \text{ Mpc}$ , the *NED* part of the sample is complete only for galaxies with  $v_{\text{gal}} > 813 \rho_0 \text{ km s}^{-1}$ . Since we only look at galaxies with  $v_{\text{gal}} > 400 \text{ km s}^{-1}$ , the *NED* sample is complete for impact parameters  $< 500 \text{ kpc}$ . Therefore, we corrected for the incompleteness at a given impact parameter  $\rho_0$  by scaling the number of additional galaxies from *NED* by the ratio of the total number with  $\rho < 500 \text{ kpc}$  to the number with  $\rho < 500 \text{ kpc}$  and  $v_{\text{gal}} > 813 \rho_0$ . Thus, there are two overlapping

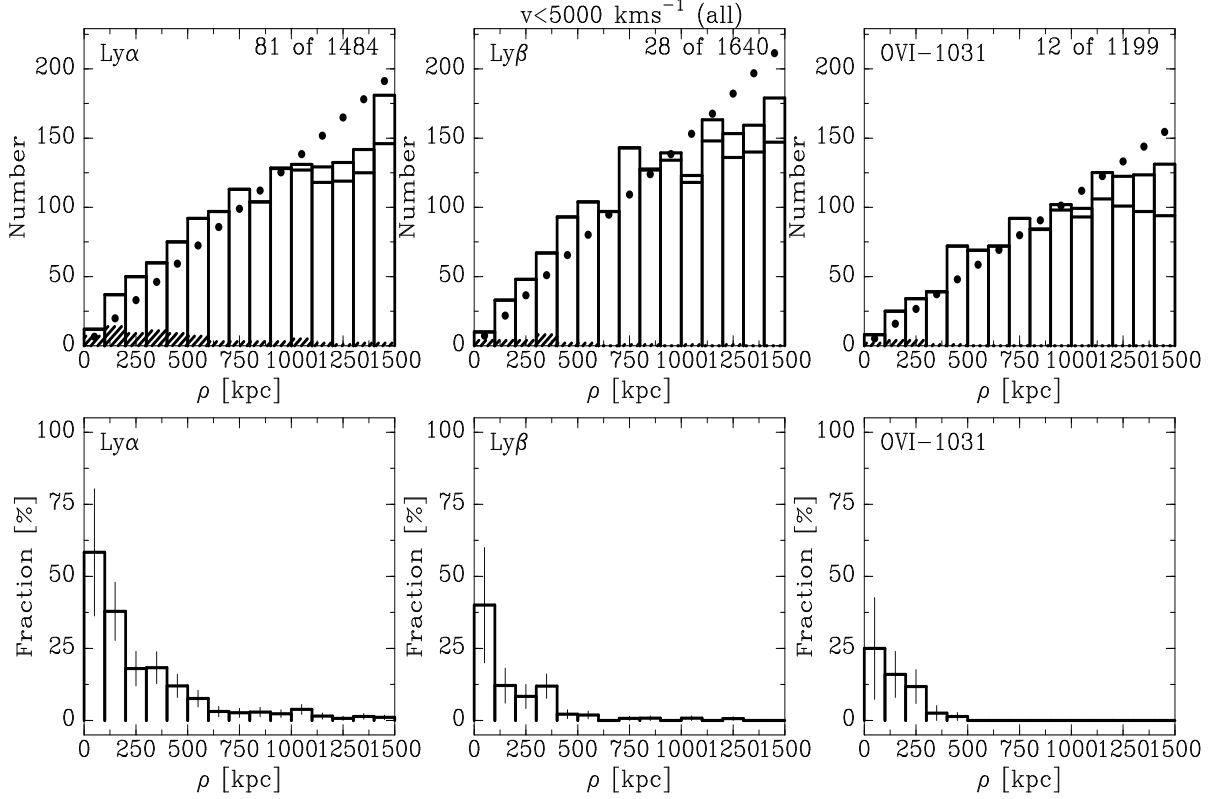


Fig. 13.— Distribution of number of galaxies, number of detections and fraction of detected galaxies as function of impact parameter. This includes every galaxy with systemic velocity 400–5000 km s<sup>−1</sup> and  $\rho < 2$  Mpc near any of the 76 sightlines in our sample, independent of brightness, size, completeness of the galaxy survey near the sightline, or group membership. The histograms in the top panels show the number of galaxies in impact parameter bins of 100 kpc. At  $\rho > 1$  Mpc there are two histograms, with the lower one giving the actual number and the higher values taking into account a correction for the incompleteness of the *NED* sample (see Sect. 5.3.2). The dotted lines show the expected numbers for a sample of galaxies with random impact parameters. The hatched areas in the top panels show the distribution of detections. The bottom panels give the fraction of galaxies with which we associate a detection; the thin vertical bars provide an estimate of the error in the fraction, found from  $\sqrt{\# \text{detections}}$ . Finally, the numbers in the top right corner give the total number of detections and galaxies in the plot. *Selection criteria:* galaxies of any luminosity with  $v = 400\text{--}5000$  km s<sup>−1</sup>, all Ly $\alpha$ , Ly $\beta$ , O VI lines found where the equivalent width error is  $< 100$  mÅ.

Table 10—Continued

$\rho$ [kpc]	$\Delta v$ [kms <sup>-1</sup> ]	$L > 0.1 L_*$	$L > 0.25 L_*$	$L > 0.5 L_*$	$L > L_*$
(1)	(2)	(3)	(4)	(5)	(6)

Note. — 1: This table gives the number and percentage of galaxies with  $v < 2500$  kms<sup>-1</sup> brighter than a given luminosity limit for which it is possible to find a Ly $\alpha$  absorber within a given impact parameter and velocity difference and detected line strength larger than 50 mÅ (upper half of table) or 300 mÅ (lower half of table).

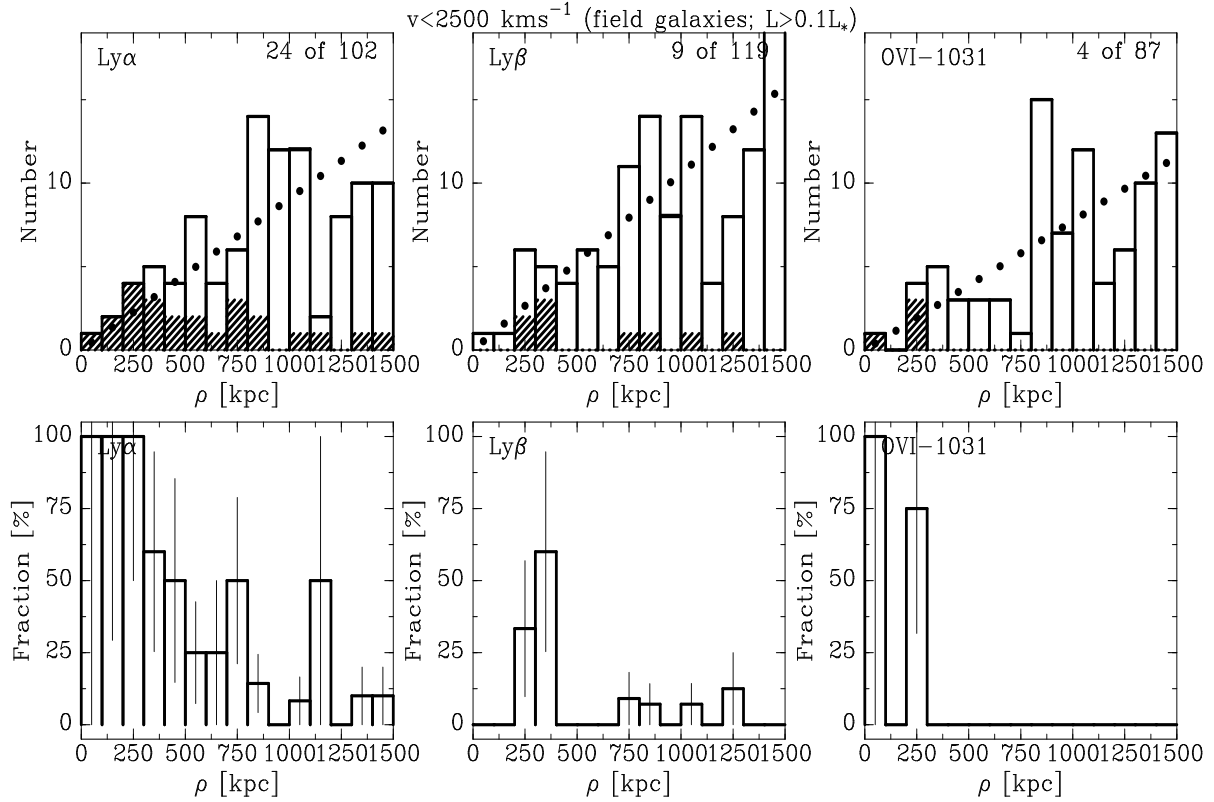


Fig. 14.— Same as Fig. 13. *Selection criteria:* galaxies with  $D_{gal} > 7.5$  kpc (equivalent to  $L > 0.1 L_*$ ) and  $v = 400$ – $2500$  kms<sup>-1</sup>, and not listed as a member of a galaxy group by Geller & Huchra (1982, 1983) and/or Garcia (1993). All Ly $\alpha$ , Ly $\beta$ , O VI lines with  $v < 2500$  kms<sup>-1</sup> found where the equivalent width error is  $< 100$  mÅ.

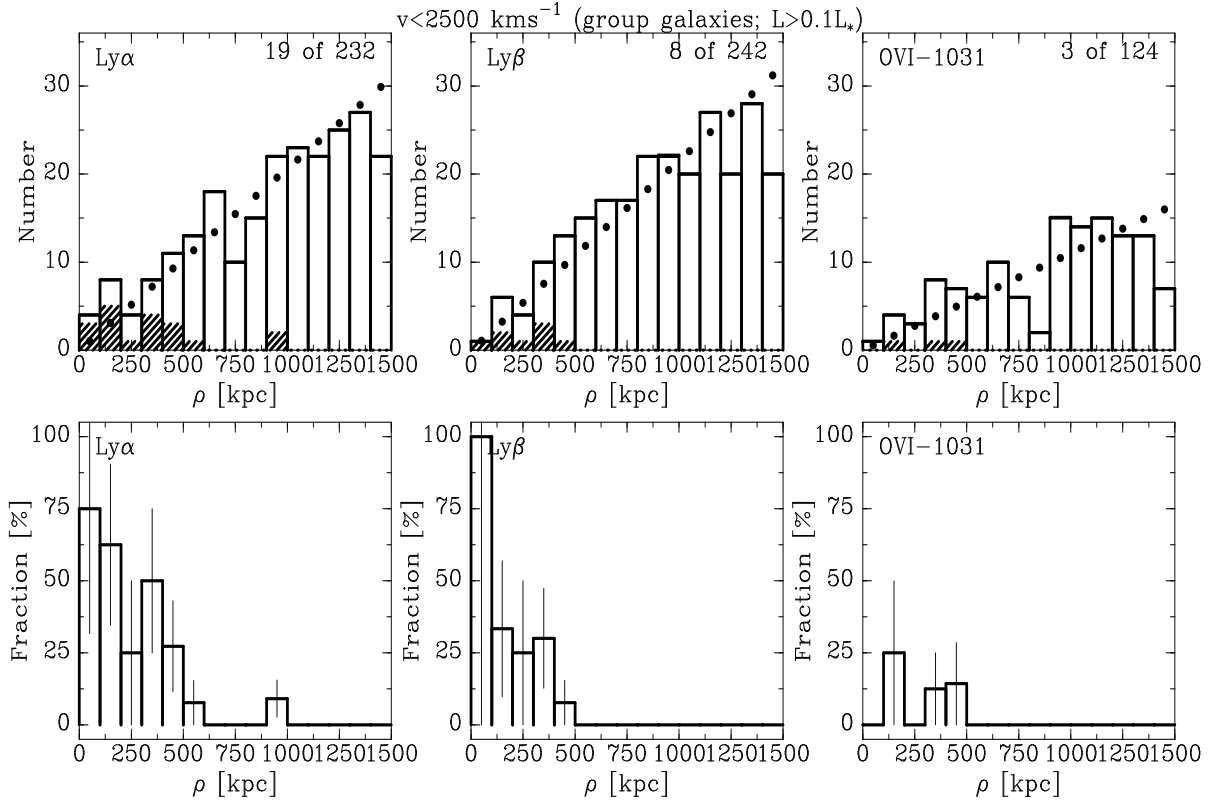


Fig. 15.— Same as Fig. 13. *Selection criteria:* galaxies with  $D_{gal} > 7.5 \text{ kpc}$  (equivalent to  $L > 0.1 L_*$ ) and  $v = 400\text{--}2500 \text{ km s}^{-1}$ , that are listed as a member of a galaxy group by Geller & Huchra (1982, 1983) and/or Garcia (1993). All Ly $\alpha$ , Ly $\beta$ , OVI lines with  $v < 2500 \text{ km s}^{-1}$  found where the equivalent width error is  $< 100 \text{ m\AA}$ .

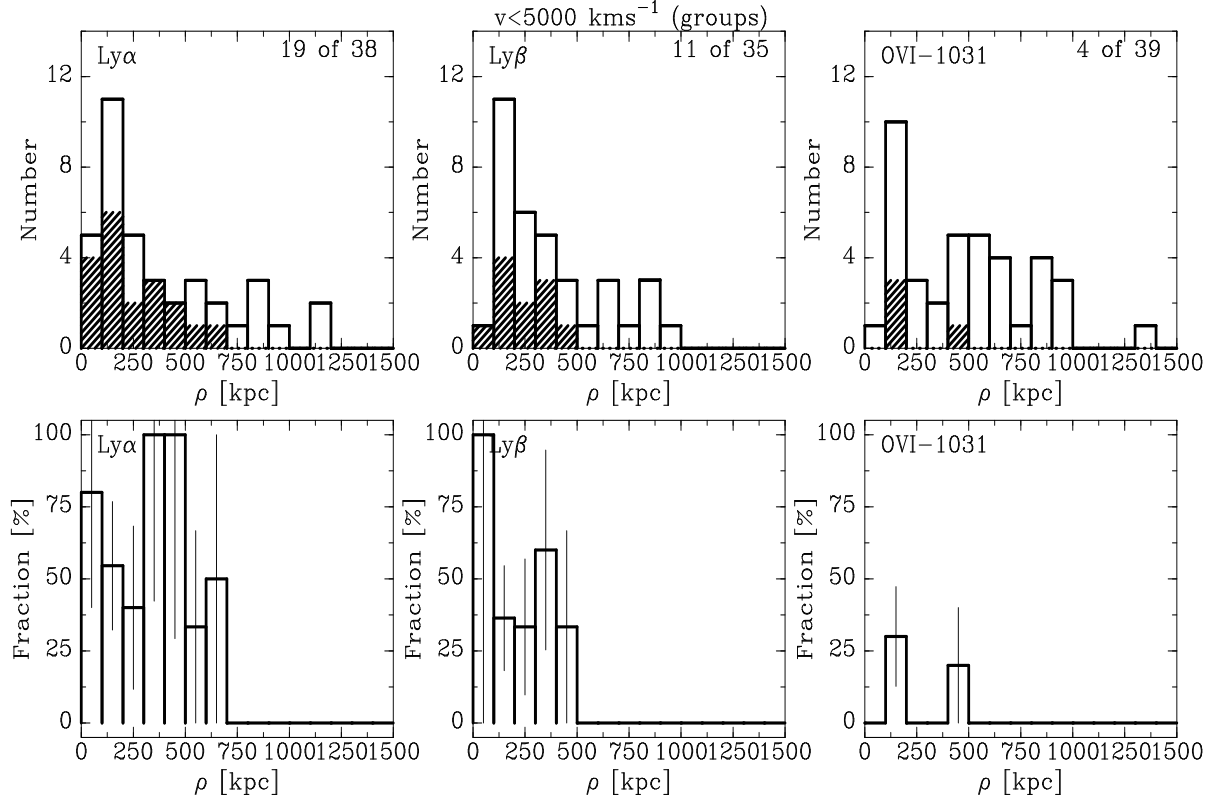


Fig. 16.— Same as Fig. 13, except that we only count one detection or non-detection for each galaxy group. The impact parameter,  $\rho$ , is that to the group galaxy nearest the sightline. Only cases where  $\rho$  is less than half the diameter of the group are included.

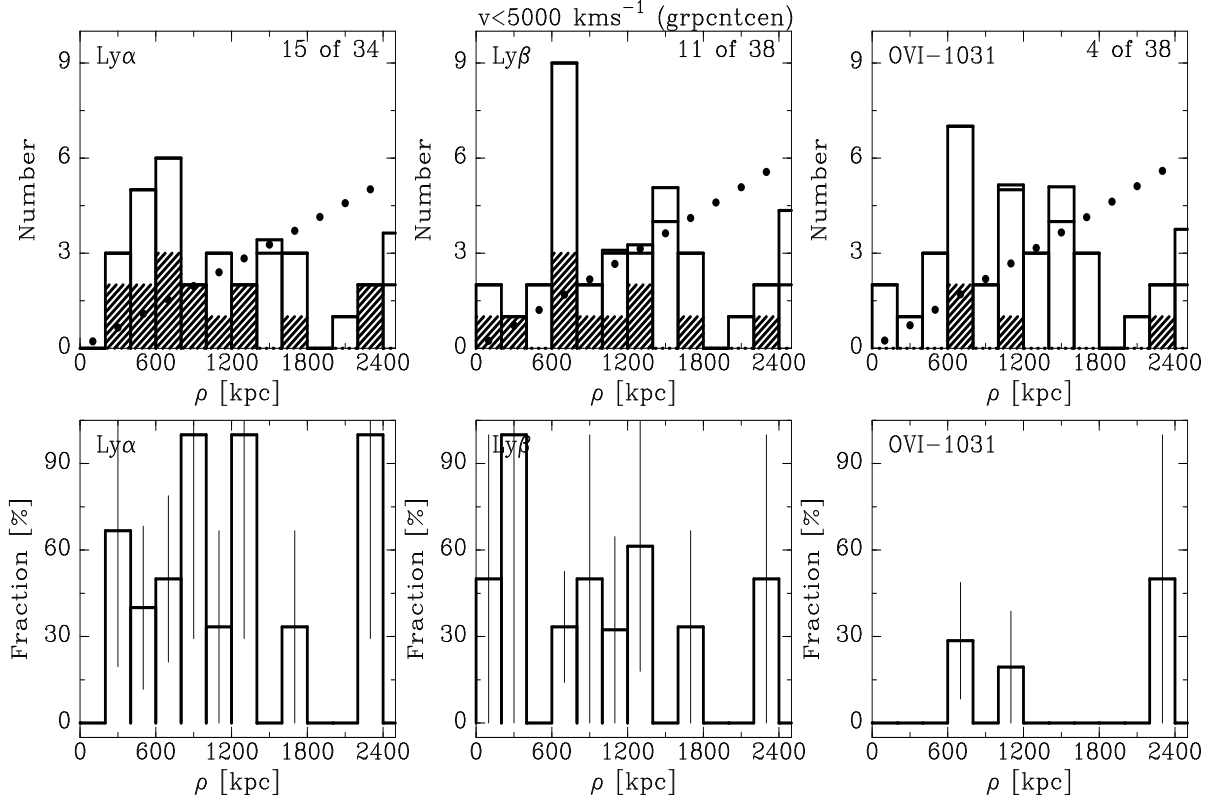


Fig. 17.— Same as Fig. 13, except that we only count one detection or non-detection for each galaxy group, and unlike what is the case for Fig. 16, the impact parameter is that to the center of the group.



Table 11. Detection fraction vs. impact parameter<sup>1</sup>

$\rho$	all(Ly $\alpha$ )			field, $v < 2500 \text{ km s}^{-1}$ (Ly $\alpha$ ) $L > 0.1 L_*$			groups (Ly $\alpha$ )			all (O VI)		
[kpc]	#gal	#det	frac.	#gal	#det	frac.	#gal	#det	frac.	#gal	#det	frac.
(1)	(2)	(3)	(4)	(5)	(6)	(7)	(8)	(9)	(10)	(11)	(12)	(13)
0–100	12	7	58%	1	1	100%	5	4	80%	8	2	25%
100–200	37	14	38%	2	2	100%	11	6	55%	25	4	16%
200–300	50	9	18%	4	4	100%	5	2	40%	34	4	12%
300–400	60	11	18%	5	3	60%	3	3	100%	39	1	3%
400–500	75	9	12%	4	2	50%	2	2	100%	72	1	1%
500–600	92	7	8%	8	2	25%	3	1	33%	69	0	0%
600–700	97	3	3%	4	1	25%	2	1	50%	72	0	0%
700–800	113	3	3%	6	3	50%	1	0	0%	92	0	0%
800–900	104	3	3%	14	2	14%	3	0	0%	84	0	0%
900–1000	128	3	2%	12	0	0%	1	0	0%	98	0	0%
1000–1100	131	5	4%	12	1	8%	0	0	0%	93	0	0%
1100–1200	129	2	2%	2	1	50%	2	0	0%	106	0	0%
1200–1300	132	1	1%	8	0	0%	0	0	0%	101	0	0%
1300–1400	141	2	1%	10	1	10%	0	0	0%	97	0	0%
1400–1500	180	2	1%	10	1	10%	0	0	0%	94	0	0%
1500–1600	166	2	1%	9	0	0%	0	0	0%	92	0	0%
1600–1700	200	0	0%	12	0	0%	0	0	0%	99	0	0%
1700–1800	180	1	1%	26	0	0%	0	0	0%	95	0	0%
1800–1900	185	1	1%	17	0	0%	0	0	0%	93	0	0%
1900–2000	202	2	1%	12	0	0%	0	0	0%	126	0	0%

Note. — 1: For each impact parameter interval given in Col. (1), the table gives the number of galaxies, the number of galaxies associated with an absorber and the fraction of absorbers, using four different selection criteria. For the first group (all(Ly $\alpha$ )) all galaxies and Ly $\alpha$  lines with  $v < 5000 \text{ km s}^{-1}$  are used. For the second group (field,  $v < 2500 \text{ km s}^{-1}$ ), only field galaxies and absorbers with  $v < 2500 \text{ km s}^{-1}$  are counted; in this context a “field” galaxy is one that was not listed as a group member by Geller & Huchra (1983) or Garcia (1993). The third group (groups(Ly $\alpha$ )) counts Ly $\alpha$  lines and galaxy groups, using the group galaxy with the smallest impact parameter. For the fourth group (all(O VI)), we count all galaxies and O VI absorbers with  $v < 5000 \text{ km s}^{-1}$ . So, for instance, there are 5 field galaxies with  $v < 2500 \text{ km s}^{-1}$  and impact parameter 300–400 kpc, and 3 Ly $\alpha$  lines were associated with these galaxies. The numbers in this table are represented graphically in Figs. 13 to 16.

Table 12. Detection fraction summary

Lum. limit	$\rho$	field, Ly $\alpha$			group, Ly $\alpha$			field, O VI			group, O VI		
	[kpc]	#gal	#det	frac.	#gal	#det	frac.	#gal	#det	frac.	#gal	#det	frac.
(1)	(2)	(3)	(4)	(5)	(6)	(7)	(8)	(9)	(10)	(11)	(12)	(13)	(14)
L>0.1 L $_{*}$ <sup>1</sup>	0-350	7	7	100 $^{+0}_{-37}$ %	21	13	61 $^{+17}_{-17}$ %	6	4	66 $^{+33}_{-33}$ %	13	1	7 $^{+7}_{-7}$ %
	350-700	21	7	33 $^{+12}_{-12}$ %	45	4	8 $^{+4}_{-4}$ %	14	1	7 $^{+7}_{-7}$ %	26	2	7 $^{+5}_{-5}$ %
	700-1500	74	9	12 $^{+4}_{-4}$ %	165	1	0 $^{+0}_{-0}$ %	68	0	0 $^{+0}_{-0}$ %	85	0	0 $^{+0}_{-0}$ %
	1500-3000	297	0	0 $^{+0}_{-0}$ %	566	0	0 $^{+0}_{-0}$ %	221	0	0 $^{+0}_{-0}$ %	339	0	0 $^{+0}_{-0}$ %
L>0.25 L $_{*}$ <sup>2</sup>	0-350	10	9	90 $^{+10}_{-30}$ %	25	14	56 $^{+14}_{-14}$ %	9	7	77 $^{+22}_{-29}$ %	13	2	15 $^{+10}_{-10}$ %
	350-700	22	8	36 $^{+12}_{-12}$ %	40	3	7 $^{+4}_{-4}$ %	14	0	0 $^{+0}_{-0}$ %	33	3	9 $^{+5}_{-5}$ %
	700-1500	58	6	10 $^{+4}_{-4}$ %	141	1	0 $^{+0}_{-0}$ %	64	0	0 $^{+0}_{-0}$ %	77	0	0 $^{+0}_{-0}$ %
	1500-3000	259	2	0 $^{+0}_{-0}$ %	463	2	0 $^{+0}_{-0}$ %	205	0	0 $^{+0}_{-0}$ %	280	0	0 $^{+0}_{-0}$ %
L>0.5 L $_{*}$ <sup>3</sup>	0-350	6	5	83 $^{+16}_{-37}$ %	18	11	61 $^{+18}_{-18}$ %	7	5	71 $^{+28}_{-31}$ %	6	2	33 $^{+23}_{-23}$ %
	350-700	15	6	40 $^{+16}_{-16}$ %	29	5	17 $^{+7}_{-7}$ %	15	0	0 $^{+0}_{-0}$ %	26	3	11 $^{+6}_{-6}$ %
	700-1500	56	9	16 $^{+5}_{-5}$ %	100	1	1 $^{+1}_{-1}$ %	53	0	0 $^{+0}_{-0}$ %	62	0	0 $^{+0}_{-0}$ %
	1500-3000	228	5	2 $^{+0}_{-0}$ %	367	0	0 $^{+0}_{-0}$ %	183	0	0 $^{+0}_{-0}$ %	232	0	0 $^{+0}_{-0}$ %
L>L $_{*}$ <sup>3</sup>	0-350	4	3	75 $^{+25}_{-43}$ %	9	6	66 $^{+27}_{-27}$ %	6	5	83 $^{+16}_{-37}$ %	4	1	25 $^{+25}_{-25}$ %
	350-700	7	2	28 $^{+20}_{-20}$ %	13	3	23 $^{+13}_{-13}$ %	8	0	0 $^{+0}_{-0}$ %	19	3	15 $^{+9}_{-9}$ %
	700-1500	35	6	17 $^{+6}_{-6}$ %	55	0	0 $^{+0}_{-0}$ %	31	0	0 $^{+0}_{-0}$ %	36	0	0 $^{+0}_{-0}$ %
	1500-3000	111	4	3 $^{+1}_{-1}$ %	232	0	0 $^{+0}_{-0}$ %	92	0	0 $^{+0}_{-0}$ %	156	0	0 $^{+0}_{-0}$ %

Note. — 1: also  $v_{gal}<2500$  km s $^{-1}$ ; 2: also  $v_{gal}<3700$  km s $^{-1}$ ; 3: also  $v_{gal}<5000$  km s $^{-1}$ .

histograms in the top panels of Fig. 13, with the bottom one giving the actual number of galaxies in the sample, and the top histogram showing the corrected number. The detection fraction is calculated using the corrected data.

There still is a small deficit at  $\rho > 1500 \text{ km s}^{-1}$ . This deficit is caused by a deficit in *NED*-only galaxies with  $v_{gal} = 1000\text{--}1100 \text{ km s}^{-1}$ , which leads to a slightly lower scaling factor for impact parameters  $> 1.3 \text{ Mpc}$ . This deficit in turn is caused by a combination of two factors. First, in the sightlines toward the Virgo cluster (3C 273.0, HE 1228+0131, PG 1211+143 and PG 1216+069) there is a relative deficit of galaxies near  $1100 \text{ km s}^{-1}$ . Second, there are three sightlines toward galaxy groups with  $v \sim 1700 \text{ km s}^{-1}$  (MCG+10-16-111, Mrk 1383, NGC 985) leading to a relative increase in the counts near that velocity.

For Fig. 13, we counted every galaxy with systemic velocity  $400\text{--}5000 \text{ km s}^{-1}$  and impact parameter  $< 2 \text{ Mpc}$  to any of our 76 sightlines, independent of brightness, size, completeness of the galaxy survey near the sightline, or group membership. The first group of columns in Table 11 gives the corresponding numbers. Clearly, there is a smooth decrease of the detection fraction with impact parameter.

This galaxy sample is inhomogeneous, however. Galaxies in groups strongly influence the result, since there usually are many galaxies that can be associated with a single detected line, *and* it is likely that the physical environment in groups differs from that around field galaxies.

### 5.3.3. *Ly $\alpha$ Detection Fraction for Field Galaxies*

We now discuss the distribution of the detection fraction of Ly $\alpha$ , Ly $\beta$  and O VI as function of impact parameter, separately for field and group galaxies. When combining both kinds, the detection fraction for Ly $\alpha$  at impact parameters  $< 400 \text{ kpc}$  is 20% (see Table 11), but this value is much higher for luminous field galaxies. We find 26 field galaxies with  $\rho < 400 \text{ kpc}$ ,  $v_{gal} < 5000 \text{ km s}^{-1}$  and  $L > 0.1 L_*$ . For 15 of these we detect an associated Ly $\alpha$  line, while for three we have no Ly $\alpha$  data, but we find Ly $\beta$ . For two of the galaxies we would be unable to find either the Ly $\alpha$  or Ly $\beta$  line even if it were present, as it is hidden in the Ly $\alpha$  line associated with another galaxy or the Milky Way. Five of the six remaining non-detections of Ly $\alpha$  or Ly $\beta$  are in noisy spectra, so that the upper limits are not very significant. The 18 luminous galaxies that are found to have an associated Ly $\alpha$  or Ly $\beta$  line are: IC 4889 (62 kpc from ESO 185-IG13, Ly $\beta$  only), UGC 8146 (80 kpc from PG 1259+593), UGC 7697 (139 kpc from Mrk 771), NGC 3942 (141 kpc from PG 1149–110), UGC 4238 (155 kpc from PG 0804+761), NGC 1412 (167 kpc from HE 0340–2703), Mrk 412 (196 kpc from

3C 232), NGC 6140 (206 kpc from Mrk 876, 2 lines), NGC 2683 (250 kpc from PG 0844+349, Ly $\beta$  only), UGC 8849 (274 kpc from PG 1351+640) UGC 10294 (282 kpc from Mrk 876), NGC 3104 (296 kpc from PG 0953+414), ESO 603-G27 (322 kpc from MRC 2251–178), UGC 7625 (339 kpc from HE 1228+0131), CGCG 291-61 (367 kpc from MCG+10-16-111), UGC 4621 (372 kpc from PG 0844+349, Ly $\beta$  only; 2 lines), MCG–2-34-6 (391 kpc from PG 1302–102), and NGC 7817 (395 kpc from Mrk 335). All but three of the Ly $\alpha$  lines (the second component toward Mrk 876, and the lines toward PG 0953+414 and PG 1302–102) have equivalent width  $>100$  mÅ.

The only non-detections of Ly $\alpha$  for  $L>0.1 L_*$  galaxies with impact parameter  $<400$  kpc are associated with NGC 4939 (104 kpc from PG 1302–102), UGC 7226 (362 kpc from Mrk 205) and UGC 5922 (391 kpc from PG 1049–005). However, two of these spectra are relatively noisy (detection limits 72 mÅ for NGC 4939, 31 mÅ for UGC 7226, and 75 mÅ for UGC 5922). In two cases the only limits are for Ly $\beta$ : UGC 9452 (278 kpc from Mrk 477,  $W<39$  mÅ) and UGC 5340 (296 kpc from PG 1001+291,  $W<87$  mÅ). Thus, in each case it is entirely possible that a better spectrum would reveal a line.

For the majority of the associations above, the next nearest field or group galaxy with velocity within  $\pm 500$  km s $^{-1}$  of the Ly $\alpha$  line is at significantly larger impact parameter ( $>493$  kpc), although three of the associated galaxies above do have a dwarf near it with impact parameter similar to that of the main galaxy. For three of the associations there are two Ly $\alpha$  lines, with two associated galaxies at similar impact parameter, but the second galaxy is either at  $\rho>400$  kpc, is a group galaxy, or is (slightly) smaller than 7.5 kpc.

Fig. 14 shows the Ly $\alpha$  detection fraction for field galaxies with  $v_{gal}<2500$  km s $^{-1}$  and  $L>0.1 L_*$  ( $D_{gal}>7.5$  kpc). The second group of three columns in Table 11 gives the corresponding numerical values. This does not include all of the galaxies mentioned above, because some have  $v_{gal}>2500$  km s $^{-1}$ , where the sample is incomplete. There are 24 Ly $\alpha$  detections for 178 field galaxies with  $\rho<2$  Mpc. The distribution for field galaxies with  $v_{gal}<5000$  km s $^{-1}$  and  $L>0.5 L_*$  ( $D_{gal}>14.6$  kpc) is basically identical, with 24 Ly $\alpha$  detections for 137 field galaxies with  $\rho<2$  Mpc.

For both the complete sample and the field sample, the detection fraction for Ly $\alpha$  decreases regularly with impact parameter. Table 11 clearly shows that in spite of the small number statistics, at all impact parameters the detection fraction for Ly $\alpha$  is higher for the field galaxies than for the full sample, by a factor two at  $\rho<100$  kpc, a factor four at  $\rho\sim 500$  kpc and a factor five at  $\rho\sim 900$  kpc. The effect of the small number of galaxies in each impact parameter bin is clearly seen for the 1100–1200 kpc bin. There are in fact nine galaxies with  $D_{gal}>7.5$  kpc in this impact parameter bin, but by accident many are toward sightlines without Ly $\alpha$  data, or at velocities where there are line blends.

Table 12 presents a summary of the detection fractions for Ly $\alpha$  and O VI, separately for field and group galaxies, for three complete samples: galaxies with  $L > 0.1 L_*$  ( $v_{gal} < 2500 \text{ km s}^{-1}$ ),  $L > 0.25 L_*$  ( $v_{gal} < 3700 \text{ km s}^{-1}$ ) and  $L > 0.5 L_*$  ( $v_{gal} < 5000 \text{ km s}^{-1}$ ). In this table we include an estimate of the uncertainty in the detection fraction, based on the square root of the number of detections. This shows that for Ly $\alpha$  detections associated with a complete sample of bright field galaxies the detection fraction is 85–100% for impact parameters  $< 350 \text{ kpc}$ . At larger impact parameters, the detection fraction decreases to almost 0% only for  $\rho > 1500 \text{ kpc}$ .

From the histograms in Fig. 14 and the discussion above, we conclude that *the fraction of  $L > 0.1 L_*$  field galaxies that have an associated Ly $\alpha$  line is 100% for impact parameters  $\rho < 350 \text{ kpc}$  and decreases monotonically to about 0 at  $\rho \sim 1500 \text{ kpc}$ .*

#### 5.3.4. Ly $\alpha$ Detection Fraction for Group Galaxies

There are three ways in which we can compare the detection rate of field galaxies to that of groups and group galaxies: a) we can count group galaxies with  $L > 0.1 L_*$ , b) we can count groups, using the impact parameter to the group galaxy nearest the sightlines, c) or we can count groups, using the impact parameter to the center of the group.

Counting galaxies, Fig. 15 shows that the number of group galaxies with  $v_{gal} < 2500 \text{ km s}^{-1}$  and  $L > 0.1 L_*$  ( $D_{gal} > 7.5 \text{ kpc}$ ) is about twice that of the number of field galaxies (382 vs 178) while the number of detections is similar (19 vs 24). For  $v_{gal} < 5000 \text{ km s}^{-1}$  and  $L > 0.5 L_*$  ( $D_{gal} > 14.6 \text{ kpc}$ ) there are 18 detections for 246 galaxies, with the same distribution. Fig. 15 shows that the detection fraction decreases regularly with impact parameter, just like for field galaxies. However, compared to the field galaxies (for which the detection rate was 100% for  $\rho < 350 \text{ kpc}$ ), the detection rate at  $\rho < 350 \text{ kpc}$  is 61% (13 of 21) for  $L > 0.1 L_*$  and 61% (11 of 18) for  $L > 0.5 L_*$ . These detections include the ones toward 3C 232 (NGC 3067) and Mrk 205 (NGC 4319) where the sightline passes through the disk of the galaxy.

Counting groups in the first way, we determine impact parameters from the group galaxy with  $L > 0.1 L_*$  that has the smallest impact parameter to the sightline. Fig. 16 shows the result for the 38 groups with  $v < 5000 \text{ km s}^{-1}$  for which the sightline passes between the group galaxies or close to the edge of the group (i.e. within half a group’s radius). There are another 19 cases where Table 3 lists a galaxy that is a group member, but the sightline passes far off ( $> \text{one group radius}$ ) to the side of the group. For each of the groups we then checked whether there is a detection associated with a group galaxy or with the group as a whole, which is the case for 19 groups. Because of the small number statistics we can’t really say that there is a regular decrease of detection fraction with impact parameter to

the nearest group galaxy. For impact parameters  $< 350$  kpc, 15 of 24 (63%) of groups are detected, a fraction that is comparable to the number of bright group galaxies associated with an absorption line.

Calculating impact parameters relative to the group center, we find that it is  $> 3$  Mpc for 4 of the groups. For the rest, the detection fraction is consistently about 50% as all impact parameters (Fig. 17), although the number of groups in each 200 kpc wide impact parameter interval is small. Thus, on scales of hundreds of kpc, the gas in groups does not seem to be more concentrated to the group centers.

From the histograms in Fig. 15 to 17 we conclude that *the covering factor of  $\text{Ly}\alpha$  around bright group galaxies ( $L > 0.1 L_*$ ) is about 60% for impact parameters  $< 350$  kpc and that about 50% of galaxy groups have associated  $\text{Ly}\alpha$  absorption.*

### 5.3.5. $\text{Ly}\beta$ Galaxy Detection Fraction

The histograms in Figs. 13, 14, 15 and 16 show that in spite of the small number of detections the galaxy detection fraction for  $\text{Ly}\beta$  has the same distribution as that of  $\text{Ly}\alpha$ , as it should, but with about one third of the number of detections. For the 25  $\text{Ly}\alpha$  lines seen toward  $L > 0.1 L_*$  galaxies with  $\rho < 350$  kpc,  $\text{Ly}\beta$  is detected in five cases, all with  $W(\text{Ly}\alpha) > 100$  mÅ, while a non-detection is found in another five. Three more  $\text{Ly}\alpha$  lines are sufficiently strong that a corresponding  $\text{Ly}\beta$  absorption is expected to be present, but either there is no  $\text{Ly}\beta$  data, or the  $\text{Ly}\beta$  line is blended. Counting these, we find that there should be 8  $\text{Ly}\beta$  lines accompanying the 25  $\text{Ly}\alpha$  lines. Thus, the detection fraction of  $\text{Ly}\beta$  is about one third that of  $\text{Ly}\alpha$ .

### 5.3.6. O VI Galaxy Detection Fraction

As can be seen in Fig. 13 to 16, the analysis of the O VI detection fraction is hampered by the small number of positive detections, so we can only estimate detection fractions with large statistical uncertainties.

We find eight field galaxies for which we can associate an O VI detection with the galaxy (see Sect. 3.2 for a detailed discussion of each case). IC 4889 (62 kpc from ESO 185-IG13,  $D_{gal} = 28.9$  kpc), UGC 8146 (80 kpc from PG 1259+593,  $D_{gal} = 12.6$  kpc), NGC 4939 (104 kpc from PG 1302–102,  $D_{gal} = 24.6$  kpc), NGC 6140 (206 kpc from Mrk 876,  $D_{gal} = 27.1$  kpc), NGC 2683 (250 kpc from PG 0844+349,  $D_{gal} = 23.0$  kpc), UGC 10294 (282 kpc from Mrk 876,  $D_{gal} = 27.6$  kpc), NGC 3104 (296 kpc from PG 0953+414,  $D_{gal} = 11.5$  kpc), and ESO 603-G31

(422 kpc from MRC 2251–178,  $D_{gal}=9.1$  kpc). In addition there are five group galaxies with associated O VI: NGC 247 (125 kpc from Ton S180,  $D_{gal}=15.7$  kpc), UGC 3804 (199 kpc from 1H 0717+714,  $D_{gal}=22.8$  kpc), NGC 253 (374 kpc from Ton S210,  $D_{gal}=20.7$  kpc), NGC 5987 (424 kpc from Mrk 290,  $D_{gal}=51.7$  kpc), and NGC 954 (562 kpc from HE 0226–4110,  $D_{gal}=33.0$  kpc).

Of these 13 cases, the detection toward HE 0226–4110 is not included in the statistics discussed below, as it is at  $v > 5000$  km s $^{-1}$ . Finally, the O VI detection at 1008 km s $^{-1}$  toward 3C 273.0 is a special case in this regard. The nearest galaxy (as listed in Table 3) is MCG 0-32-16 at 191 kpc, the nearest  $L > 0.1 L_*$  galaxy is NGC 4457 ( $D_{gal}=13.8$  kpc) at 469 kpc, while the nearest  $L > 0.5 L_*$  galaxy is NGC 4517 ( $D_{gal}=53.8$  kpc) at 662 kpc.

Of this set of O VI lines, the ones toward ESO 185-IG13, PG 1259+593, Mrk 876 and 3C 273.0 are unambiguously detected. The O VI detections toward PG 0844+349, PG 0953+414, Ton S180, Ton S210, 1H 0717+714, Mrk 290, HE 0226–4110 and MRC 2251–178 are not unambiguous, in the sense that we only see one of the two O VI lines, with the other line either blended or too weak, or the very existence of the feature might be questioned. However, in our judgement, these features are real, they measure as  $>3\sigma$  and intergalactic O VI is in all cases the most likely identification. The least certain identification is that of the O VI line seen toward PG 1302–102. There is no corroborating Ly $\alpha$ , Ly $\beta$  or O VI  $\lambda 1037.617$  and the strength of the feature is just a little over  $3\sigma$ . However, visually the absorption is clear, and it can be seen in each of the two channels of each of the two FUSE observations of the target.

Looking at the O VI detection rate for  $L > 0.1 L_*$  field galaxies with  $v_{gal} < 2500$  km s $^{-1}$  in Table 12, we find a 66% detection rate for  $\rho < 350$  km s $^{-1}$ , with detections for UGC 8146, NGC 6140, NGC 2683 and NGC 3104, as well as non-detections for UGC 5340 (296 kpc from PG 1001+291) and UGC 7625 (339 kpc from HE 1228+0131). Note, however, that both non-detections are for sightlines with relatively low S/N, and all four detected lines are weaker than the detection limits toward these two sightlines. In any case, for this sample, the detection rate is 100% for  $\rho < 296$  kpc, with just one (possible) O VI line at  $\rho > 296$  kpc.

When looking at somewhat brighter field galaxies ( $L > 0.25 L_*$ ,  $v_{gal} < 3700$  km s $^{-1}$ ) with low impact parameter ( $< 350$  kpc), we count detections toward IC 4889, UGC 8146, NGC 4939, NGC 6140, NGC 2683, UGC 10294 and NGC 3104, and non-detections for UGC 7697 (139 kpc from Mrk 771, and ESO 603-G27 (322 kpc from MRC 2251–178), for a 77% detection fraction. However, the detection limit toward Mrk 771 is 94 mÅ, while all but one of the five detections have equivalent width  $< 40$  mÅ; therefore the fact that we do not see O VI is probably not very significant. Thus, we see O VI in all but one sightline with impact parameter  $< 300$  kpc.

Finally, for the brightest galaxy sample ( $L > L_*$ ), we find a 71% detection fraction, counting detections associated with IC 4889, NGC 4939, NGC 6140, NGC 2683 and UGC 10294, and non-detections for UGC 7697 and ESO 603-G27. Thus, where for bright field galaxies the detection fraction of  $\text{Ly}\alpha$  is 85–100%, for O VI it is about 70%, although the small number of sightlines means that there is an uncertainty of about 30% in this number.

The situation is different for group galaxies, as can be seen in Table 11 and Fig. 16. If we count the number of intersected groups, we find that the 76 sightlines pass between the galaxies of 39 groups for which it is possible to find detections and non-detections of O VI. Only four groups (10%) yield a detection: GH 158 toward Mrk 290, LGG 4 toward Ton S180 and Ton S210, LGG 141 toward 1H 0717+714 and LGG 292 toward 3C 273.0. Using different complete samples with different luminosity limits, we also find that the detection fraction for group galaxies is low, typically somewhere between 7% and 15%. We need to mention here, however, that for the 53 group galaxies near our sightlines that have  $D_{gal} > 7.5$  kpc ( $L > 0.1 L_*$ ) and  $\rho < 350$  kpc, we find only two detections, but there is no O VI data available in 15 cases, and in 20 cases the possible O VI line is blended with interstellar absorption. For the 16 galaxies where O VI could have been (but was not) detected, only one  $\text{Ly}\alpha$  absorber is found, but for the 15 cases with no O VI data, there are seven  $\text{Ly}\alpha$  lines. Thus, the O VI detection rate for group galaxies may be artificially depressed. Nevertheless, it does appear to be the case that the O VI detection fraction associated with group galaxies is much lower than that associated with field galaxies, by a factor on the order of five. It might be as much as a factor ten lower, but the statistics are too uncertain to support this strongly. Another difference between the field and group galaxy samples is that we find only one field galaxy that may have associated O VI at impact parameter  $> 300$  kpc, but two of the four group galaxy associations are at  $\rho > 300$  kpc. Again, the small number of detections means that this is not a firm conclusion.

Stocke et al. (2006) used a larger sample of O VI lines (40) and thus were able to look at the distribution of nearest-neighbor galaxies, similar to the analysis done for  $\text{Ly}\alpha$  in Sect. 4.2. They found that the median distance between O VI absorbers and  $L > 0.1 L_*$  galaxies is 335 kpc, and almost all O VI absorbers are found within 400 kpc of such galaxies. This conclusion is confirmed by our results for O VI. In fact, for all of our O VI detections with  $v < 5000 \text{ km s}^{-1}$  we can find an  $L > 0.1 L_*$  galaxy within 450 kpc and  $\Delta v < 120 \text{ km s}^{-1}$ .

A final way of looking at the relation between O VI absorbers and galaxies is to find the nearest galaxy above a given luminosity for each absorber. We find that there is an  $L > 0.25 L_*$  galaxy within 450 kpc and with  $|\Delta v| < 300 \text{ km s}^{-1}$  for each O VI absorber at  $v < 5000 \text{ km s}^{-1}$ , with 9 of 13 having a galaxy within 300 kpc. An  $L > L_*$  galaxy can be found within 200 kpc and  $300 \text{ km s}^{-1}$  for 4 of the 13 absorbers, within 300 kpc for 7 of the 13, and within 450 kpc



for 9 of the 13, with just one case where the nearest such galaxy is at  $\rho > 1$  Mpc. Clearly, the O VI absorbers concentrate near luminous galaxies.

Two recent papers address the question of a correlation between O VI absorbers and galaxies from the theoretical side. Ganguly et al. (2008) used hydrodynamical simulations from Cen & Fang (2006) to generate 10,000 synthetic spectra through these datasets. Identifying O VI absorbers in the spectra and correlating with the simulated galaxies, they found that 80% of the O VI absorbers with  $W > 30$  mÅ lie within 3 Mpc and  $1000 \text{ km s}^{-1}$  of an  $L > 0.1 L_*$  galaxy, 20% have impact parameter  $< 1$  Mpc to such a galaxy, while just 5% lie within 500 kpc. This is clearly incompatible with our findings (and with those of Stocke et al. 2006), since we find that 100% of the O VI absorbers lie within  $120 \text{ km s}^{-1}$  and 450 kpc of a  $0.1 L_*$  galaxy. That is, the observational data show a tight correlation between O VI absorbers and galaxies, while the interpretation of the simulations would suggest that the majority originates in the intergalactic medium far from galaxies.

Oppenheimer & Davé (2008) also looked at the relationship between O VI absorption and galaxies. They derived that most O VI is photoionized, and not directly associated with galaxies, but, they note, “OVI typically is nearest to  $\sim 0.1 L_*$  galaxies”. They also stated that “the majority of O VI absorbers are between 100–300 kpc from their nearest galactic neighbor”, although they do not show a plot of an absorber parameter vs. impact parameter. Their results support our conclusion that a luminosity limit of  $0.1 L_*$  is the appropriate parameter to study the relationship between O VI absorbers and galaxies.

Finally, we note the evidence for O VI near the Milky Way. Sembach et al. (2003) discovered that high-velocity Galactic O VI absorption ( $|v_{\text{LSR}}| < 400 \text{ km s}^{-1}$ ) is seen in 80% of high-latitude sightlines observed with FUSE. Some of this is associated with high-velocity clouds that are about 5–10 kpc above the Galactic disk (see Wakker et al. 2007, 2008), but about half of the detections appears to originate much farther away, at distances of 50–100 kpc (see e.g. Fox et al. 2005). Thus, in a random sightline passing within 100 kpc of the Milky Way, there would be a probability of about 25–50% to detect an O VI absorber. In our sample of extragalactic targets, we find 11 cases with impact parameter  $< 100$  kpc, for 6 of which we can search for O VI  $\lambda 1031.926$  and/or O VI  $\lambda 1037.617$  with detection limit better than 50 mÅ (NGC 4319, 6 kpc from Mrk 205; NGC 4291, 51 kpc from Mrk 205; IC 4489, 62 kpc from ESO 185-IG13; [vCS96] 000254.9+195654.3, 78 kpc from Mrk 335; UGC 8146, 80 kpc from PG 1259+5930). We find O VI in two cases (ESO 185-IG13 and PG 1259+593), just about the expected number.

Summarizing the numbers above: we conclude: (1) *For impact parameters  $< 350$  kpc, the detection rate for O VI is 60–80% for field galaxies, 10–30% for group galaxies, and  $\sim 10\%$  for galaxy groups.* (2) *Only one field galaxy with  $\rho > 300$  kpc may show associated O VI, but*

*three of the five O VI lines associated with a bright group galaxy have  $\rho=300\text{--}450$  kpc. (3) 100% of the O VI detections at  $v<5000$  km s $^{-1}$  can be associated with a galaxy with  $L>0.1 L_*$  at  $\rho<450$  kpc, which appears to be incompatible with a simple interpretation of the results of hydrodynamical simulations.*

#### 5.4. A Synthetic Map of the Gaseous Envelope of Galaxies

Here we ask whether the intergalactic gas near galaxies knows about the direction of rotation of the underlying galaxy. To answer this, it is necessary to know which side of a galaxy is approaching (relative to the systemic velocity). Then we can create a map with the plane of the galaxy rotated to be horizontal and the approaching side on (e.g.) the left. To rotate the galaxies, we use the position angle given in the RC3, if given. If the RC3 gives no position angle, we visually align the galaxies, using the Digital Sky Survey image that can be extracted from *NED*. For 68 galaxies it is not possible to determine a position angle because they are too small or too unstructured. The literature contains data that allows us to determine the orientation (i.e. which is the approaching side) for 44 of the 329 galaxies with  $\rho<1$  Mpc listed in Table 3, with the references given in Note 3. Detections are associated with 17 of these galaxies.

Figure 18 presents the results. The left panels (a, c) include just the galaxies with known position angle, known orientation, and (in case of detections) a clear association between an intergalactic absorber and a galaxy. In the right panel (b) we include all luminous ( $L>0.1 L_*$ ) galaxies with known position angle and inclination with which we either associate a detection or find a non-detection with equivalent limit better than 50 mÅ. For all of these the impact parameter is correct, and the galaxies are rotated to have the major axis horizontal, but if the galaxy’s orientation is unknown, the direction to the AGN sightline might have to be rotated by 180°.

Figure 18a includes 23 edge-on galaxies (inclination  $>60^\circ$ ; 9 with associated detections, 13 with non-detections, one having non-detections against two different AGNs). Figure 18c includes 17 face-on galaxies (inclination  $<60^\circ$ ; 7 with associated detection, 9 with non-detections, and one with two non-detections). The colored symbols show the detections. The symbol shapes encode whether the detection/non-detection is found for just HI, just O VI or both (see figure caption for details). The circles have radii of 350 kpc and 1 Mpc.

From Fig. 18a, c we can see that at impact parameters  $<400$  kpc most galaxies have an associated intergalactic line, while non-detections are generally found at larger impact parameters.

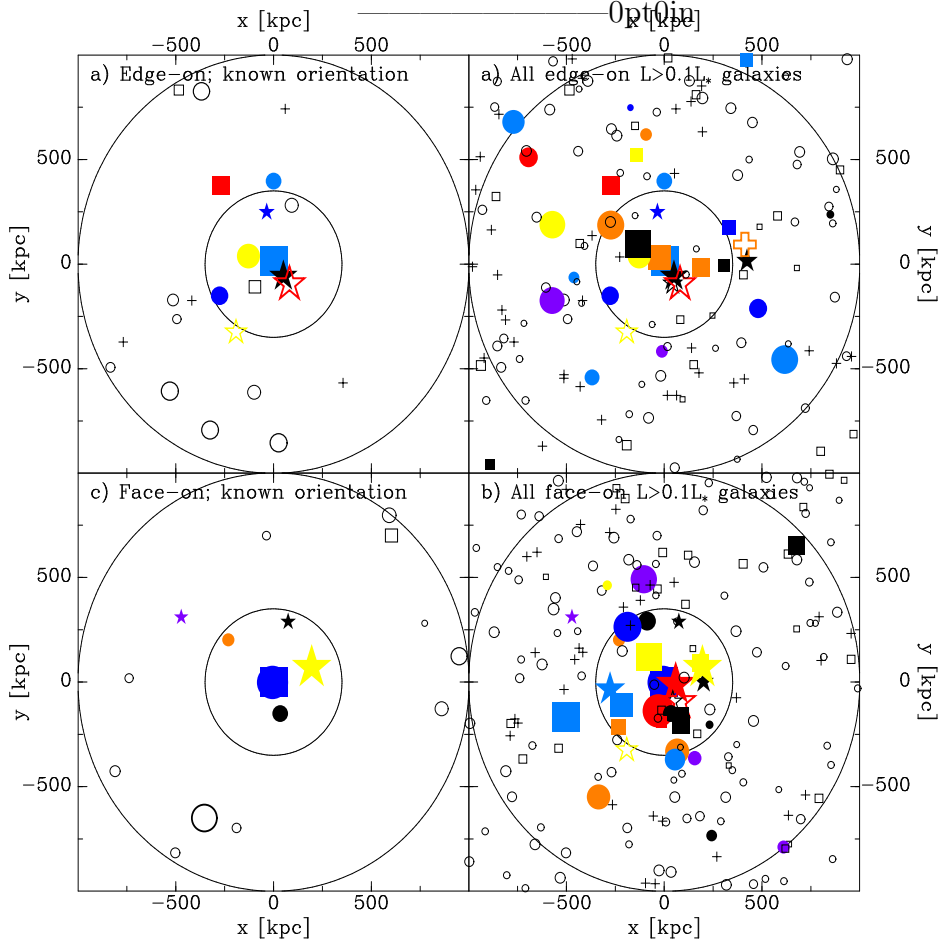


Fig. 18.— Plot combining all sightline-galaxy associations. Each galaxy is rotated to have the galaxy’s major axis horizontal (possible for 261 of the 329 galaxies) (right panels). For a small number this rotation is such that the approaching side is on the left (the galaxies in the left panels). The sightline to the AGN is then placed, using the following symbol code: colored symbols for detections of either  $\text{Ly}\alpha$ ,  $\text{Ly}\beta$  or OVI, open symbols for non-detections. Stars indicate an OVI detection, circles are for HI data with an OVI upper limit, squares when no OVI data are available. An open plus is shown if there is just an OVI detection, a plus for just an OVI upper limit, and a cross if we could not check either of HI and OVI. Colors encode the difference in velocity between the galaxy and the detection, being black if  $\Delta v < 20 \text{ km s}^{-1}$ , yellow if  $\Delta v = 20$  to  $50 \text{ km s}^{-1}$ , orange if  $\Delta v = 50$  to  $100 \text{ km s}^{-1}$ , red when  $\Delta v > 100 \text{ km s}^{-1}$ , light blue if  $\Delta v = -50$  to  $-20 \text{ km s}^{-1}$ , dark blue if  $\Delta v = -100$  to  $-50 \text{ km s}^{-1}$ , and purple when  $\Delta v < -100 \text{ km s}^{-1}$ . The symbol size scales with the square root of the equivalent width of the absorber. If just  $\text{Ly}\beta$  is detected, its equivalent width is scaled by a factor 3. Detections in panel a are for 3C 232–NGC 3067 (lightblue square), PG 1259+593–UGC 8146 (black star), Ton S180–NGC 247 (red star), Mrk 771–UGC 7697 (yellow circle), PG 0844+349–NGC 2683 (dark blue star), PKS 2155–304–ESO 466–G32 (blue circle), Ton S210–NGC 253 (yellow star), Mrk 335–NGC 7817 (lightblue circle), and MCG+10-16-111–NGC 3556 (red square). Note, that toward PKS 2155–304 there are three lines, at 5105, 4990 and  $5164 \text{ km s}^{-1}$ ; we only show the strongest of these. The two non-detection with  $\rho < 350 \text{ kpc}$  are toward Mrk 110–NGC 2841

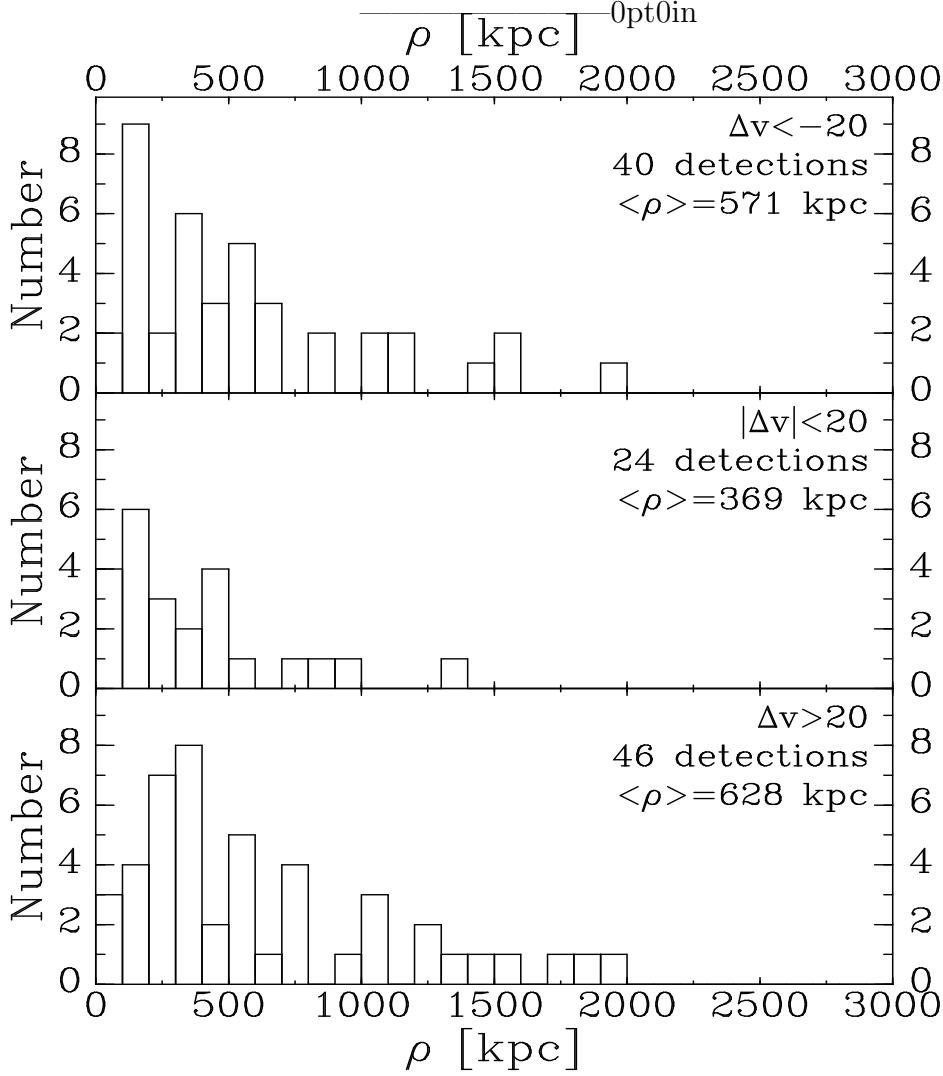


Fig. 19.— Histograms of the number of Ly $\alpha$  absorbers in 100 kpc wide bins of impact parameter, separated by the difference in velocity between the absorbers and the associated galaxy. Top panel: absorber velocity more than 20 km s<sup>-1</sup> more negative than that of the galaxy; bottom panel: absorber velocity more than 20 km s<sup>-1</sup> more positive than that of the galaxy; middle panel: absorber velocity within 20 km s<sup>-1</sup> of that of the galaxy. The labels also give the average impact parameter for all absorbers in the histogram.

Relative to underlying edge-on galaxies, four of the absorbers are relatively close to the galaxy’s plane, and of these one has  $\Delta v < 0$  while lying on the approaching side (toward PKS 2155–304), one has  $\Delta v > 0$  while lying on the receding side (toward Ton S180), one has the “wrong” sign of the velocity difference (toward Mrk 771), while the detection toward PG 1259+593 has small  $\Delta v$ . Four other detections occur away from the underlying galaxies’ plane and have both  $\Delta v < 0$  and  $\Delta v > 0$ . Thus it appears that in general the absorbers do not have velocities that would fit the rotation curves of the underlying galaxies, a conclusion already reached by Côté et al. (2005), who included PG 1259+593 and Ton S180 in their sample. However, with such a small sample more cases are needed to confirm whether this is generally true. Although the orientations of most of the galaxies in Fig. 18b are uncertain by  $180^\circ$ , this figure includes about 15 galaxies with associated detections that could lie in an extended flat disk, for about 10 of which we do not yet know the orientation.

For the detections associated with more face-on galaxies there also is no clear pattern to the velocity differences, which range from  $-68$  to  $+64$   $\text{km s}^{-1}$ . Similarly, when looking at all face-on galaxies (Fig. 18d), there is no clear pattern to the velocity differences (even though the orientation of most symbols is uncertain by  $180^\circ$ ). Both red and blue symbols are seen at almost any position angle.

One systematic pattern is suggested by Fig. 18b and d. We illustrate it in Fig. 19, showing that detections with velocity differences less than  $20$   $\text{km s}^{-1}$  (the black symbols) on average occur almost twice as close to the associated galaxy (average impact parameter  $369$  kpc) as detections having  $|\Delta v| > 20$   $\text{km s}^{-1}$  (average impact parameter  $\sim 600$  kpc). All but one of the 20 associations with  $\Delta v < 20$   $\text{km s}^{-1}$  have  $\rho < 1$  Mpc, whereas all but one of the 33 associations at  $\rho > 1$  Mpc have  $\Delta v > 20$   $\text{km s}^{-1}$ . However, this effect has to remain only a suggestion until we can obtain more data. A KS-test shows that we can only accept the hypothesis that the distributions differ with  $\sim 70\%$  confidence, i.e., it is about a one sigma effect.

From Figs. 18 and 19 we conclude that *intergalactic gas knows about the presence of a nearby galaxy, better matching the galaxies’ velocities the closer in it is, though the gas apparently does not generally know the direction in which the galaxy rotates.*

## 6. Discussion

### 6.1. The Relation Between IGM Absorbers and Galaxies

By combining sightlines analyzed in a number of previous papers aimed at studying low-redshift intergalactic absorption and its relation to galaxies, adding data obtained for

other studies, including FUSE data for O VI and concentrating on just the lowest redshift absorbers and galaxies, we have been able to make progress in understanding the connection between intergalactic gas and galaxies. The advantage of our approach is that we are not limited to finding galaxies with small angular separation to an extragalactic sightline, and in addition our galaxy sample is expected to be complete down to  $0.1 L_*$  for  $v < 2500 \text{ km s}^{-1}$ . Further, we are able to separately look at field and group galaxies, as there is a consistently defined catalogue of galaxy groups for all nearby galaxies.

In previous work arguments have been presented that strong Ly $\alpha$  absorbers are physically associated with galaxies (Lanzetta et al. 1995; Chen et al. 1998; Bowen et al. 2002; Côté et al. 2005), probing their 200–300 kpc radius gaseous halos, while absorbers with larger impact parameters originate in intergalactic filaments. The main arguments in favor of this interpretation are (1) the fact that absorbers with  $\Delta v < 500 \text{ km s}^{-1}$  are almost always found for sightlines with galaxy impact parameters below a few hundred kpc and (2) a claimed anti-correlation between impact parameter and Ly $\alpha$  equivalent width. However, the occurrence of Ly $\alpha$  absorbers with low  $\Delta v$  at large impact parameters, the fact that not all authors find a correlation between equivalent width and impact parameter and the presence of “void absorbers” (Penton et al. 2002) suggests a more complicated picture, in which (almost) all absorbers trace the large-scale structure of intergalactic gas. Some authors even suggest that absorbers close to galaxies may not be associated with them. Cosmological simulations suggest that the galaxies reside in the denser regions of filaments or sheetlike gaseous structures (Davé et al. 1999). In these simulations the density of gas is highest near galaxies and falls off with radius (i.e., the simulations predict that on average stronger lines occur closer to galaxies), but even far from galaxies there is enough gas to produce Ly $\alpha$  absorption.

Our results support the second model, but also explain the results of the studies that concluded that galaxies have large halos. Supporting the conclusion that Ly $\alpha$  absorbers are related to galaxies we find that the properties of the Ly $\alpha$  absorbers change with impact parameter. (1) The 90th percentile of the linewidth distribution increases from FWHM  $\sim 100 \text{ km s}^{-1}$  at  $\rho > 700 \text{ kpc}$  to  $\sim 150 \text{ km s}^{-1}$  at  $\rho = 100 \text{ kpc}$  (Sect. 3.2), although there is a large spread at any impact parameter, while the 10th percentile (widths of  $\sim 50 \text{ km s}^{-1}$ ) is independent of impact parameter. (2) The 90th percentile of the equivalent width distribution increases from  $\sim 100 \text{ mÅ}$  at 1 Mpc to about  $500 \text{ mÅ}$  at  $\rho = 100 \text{ kpc}$ , while no weak lines ( $< 100 \text{ mÅ}$ ) occur at  $\rho < 150 \text{ kpc}$  (Sect. 4.7). (3) For impact parameters  $< 350 \text{ kpc}$  to galaxies brighter than  $0.1 L_*$ , 100% of field and 61% of group galaxies have associated ( $\Delta v < 400 \text{ km s}^{-1}$ ) Ly $\alpha$  absorption (Sects. 5.3.3, 5.3.4). (4) O VI absorption is only found within 500 kpc of luminous ( $L > 0.25 L_*$ ) galaxies (Sect. 5.3.6). Thus, on average, stronger and wider Ly $\alpha$  lines occur near galaxies, while almost all luminous galaxies have an associated Ly $\alpha$  absorber.

On the other hand, there is evidence supporting the conclusion that Ly $\alpha$  absorbers originate in intergalactic filaments. (1) About half of the Ly $\alpha$  lines originate more than 400 kpc away from the nearest galaxy (Sects. 4.1, 4.2, 4.3). (2) A substantial fraction ( $\sim 20\%$ ) of absorbers occurs far from ( $>3$  Mpc) the nearest  $L_*$  galaxy, although few occur far from the nearest  $0.1 L_*$  galaxy – in fact for  $v < 2500 \text{ km s}^{-1}$  we find an  $L > 0.1 L_*$  galaxy within 1.5 Mpc of every absorber (Sect. 4.4). (3) About 10% of strong ( $>200 \text{ m}\text{\AA}$ ) Ly $\alpha$  lines occur far ( $>1$  Mpc) from the nearest galaxy (Sect. 4.7). (4) The fraction of galaxies that have an associated Ly $\alpha$  line decreases regularly with impact parameter, i.e., there is no break in the distribution of detection fraction (Sects. 5.3, 5.4).

The picture that is most consistent with the absorber properties summarized above is one in which the intergalactic gas filaments are densest near galaxies, with area covering factor near 100% within about 300 kpc, but these concentrations merge smoothly into a more tenuous intergalactic medium that connects the galaxies. This picture works when all galaxies brighter than about  $0.1 L_*$  are considered and 50% of the Ly $\alpha$  lines originate within 400 kpc of such a galaxy, 75% within 1 Mpc. If only galaxies with  $L > L_*$  were to be taken into account, a different picture would emerge, one in which a little more than half the galaxies have associated gas within 300 kpc, but most (80%) of the Ly $\alpha$  absorptions originate far ( $\rho > 400$  kpc) from  $L_*$  galaxies.

## 6.2. O VI Absorbers and Thermal Properties of the Gas Near Galaxies

Although we have far fewer O VI detections than were discussed by Tripp et al. (2008) and Danforth & Shull (2008) we find similar values for  $dN(\text{O VI})/dz$  and a basically identical linewidth distribution (Sects. 3.2, 3.3). This leads us to the conclusion that the intergalactic O VI lines seen by Tripp et al. (2008) at redshifts 0.2–0.5 are likely to have the same relation to galaxies as the ones we find in the nearby universe. All 14 O VI absorbers in our sample originate within 560 kpc from an  $L > 0.1 L_*$  galaxy, 13 of which originate near an  $L > 0.25 L_*$  galaxy, 9 ( $65 \pm 20\%$ ) occur within 560 kpc of an  $L > L_*$  galaxy, while 6 ( $40 \pm 20\%$ ) lie within 300 kpc of an  $L > L_*$  galaxy (Sects. 3.2, 5.3.6). Thus, we predict that searches for galaxies near higher redshift O VI absorbers will turn up an  $L_*$  galaxy within 500 kpc about half the time. At  $z=0.08$  this requires a limiting magnitude of about 18.2, while at  $z=0.25$   $L_*$  corresponds to  $m \sim 20.8$ . We conclude that a proper analysis of the relation between O VI absorbers and galaxies requires galaxy surveys that are about 3 times (2.5 magnitudes) deeper than that of Tripp et al. (1998), in order to locate all galaxies brighter than  $0.1 L_*$ .

Three lines of evidence combine to suggest that the denser intergalactic gas near galaxies also is hotter, a property that is predicted by cosmological evolution models (Davé et al.

2001) and is due to the heating of the gas by infall. (1) O VI absorption is only found at impact parameters  $< 500$  kpc from luminous ( $L > 0.25 L_*$ ) galaxies. Even though for many absorbers the O VI appears to be generated by photoionization, a contribution from collisional ionization is suggested in about half of the cases (Sects. 3.2, 5.3.6). (2) At impact parameters below 700 kpc the maximum linewidth of  $\text{Ly}\alpha$  lines increases with decreasing impact parameter (Sect. 4.6). (3) The fraction of wide  $\text{Ly}\alpha$  lines is the largest at  $z=0$  (Sect. 3.4). By itself, item (1) could be explained by the fact that all detected O VI lines have smaller equivalent widths than the H I lines in the same system, so for the weaker H I lines at large impact parameters it would be easier to miss any accompanying O VI. Item (2) might be explained by increasing turbulence in the gas near galaxies or by velocity gradients introduced by tidal stretching, but the linewidths are much larger than would be expected from turbulence or tidal effects; an explanation that we still need to fully exclude is that the broad lines are multi-component absorbers. Item (3) could be explained if the gas has higher turbulence near galaxies and over time the average impact parameter has decreased. However, in combination with the modeling, these three items are most consistent with thermal evolution of infalling intergalactic gas.

### 6.3. The Baryon Content of the IGM

Penton et al. (2002) and Danforth & Shull (2008) combined the count of the number of  $\text{Ly}\alpha$  absorbers per unit redshift, the measured column density distribution of  $\text{Ly}\alpha$  lines with photoionization modeling to derive an estimate of the fraction of baryons in the photoionized  $\text{Ly}\alpha$  forest. They found a fraction of  $29 \pm 4\%$ . Using a different sample of sightlines, Lehner et al. (2007) derived a similar value. Since the fraction of baryons inside galaxies is estimated to be  $\sim 8\%$  (Fukugita & Peebles 2004), the photoionized  $\text{Ly}\alpha$  forest appears to contain about 3–4 times more baryons than the galaxies. We note that this estimate depends on the assumption that it is the general extragalactic radiation field that does the ionizing. The radiation field will be stronger near galaxies, but for an  $L_*$  galaxy like the Milky Way, the extragalactic field dominates outside radii of 50–150 kpc (see Fig. 9 in Fox et al. 2005), which is where almost all  $\text{Ly}\alpha$  forest lines originate. Thus, using the extragalactic radiation field to derive the ionization correction is justified, except possibly for the 10% of the absorbers with  $\rho < 150$  kpc.

With 8% of the baryons inside galaxies, and 30% in the  $\text{Ly}\alpha$  forest, the remaining  $\sim 60\%$  of the baryons is suspected to be in the form of hotter ( $T > 10^5$  K) gas, although the observational data supporting this is sparse. For instance, Nicastro et al. (2005) claimed to have detected the  $10^6$  K IGM, but their conclusion is disputed by Kaastra et al. (2006) and



Rasmussen et al. (2007). Tripp & Savage (2000) estimated that about 10% of the IGM may be traced by O VI absorbers, similar to the number found by Danforth & Shull (2008) in their much larger survey. Lehner et al. (2007) concluded that 10–20% of the baryons show themselves as broad Ly $\alpha$  lines.

We find that for 50% of the Ly $\alpha$  absorbers at  $v < 2500 \text{ km s}^{-1}$  there is an  $L > 0.1 L_*$  galaxy within  $\rho = 370 \text{ kpc}$  and  $\Delta v < 400 \text{ km s}^{-1}$  (see Sect. 4.1). Conversely, 77% of  $L > 0.1 L_*$  galaxies at  $v < 2500 \text{ km s}^{-1}$  have a Ly $\alpha$  absorber with  $\rho < 400 \text{ kpc}$  and  $\Delta v < 400 \text{ km s}^{-1}$  (see Table 10). Thus, it appears that most galaxies have extended envelopes (halos) of associated photoionized and warm collisionally ionized gas that has been detected via narrow and broad Ly $\alpha$  absorption.

To summarize, 8% of the baryons is found inside galaxies, 30% is in the photoionized Ly $\alpha$  forest, 10–20% may be collisionally ionized and seen as broad Ly $\alpha$  lines, and finally, 50% of the Ly $\alpha$  lines originate within 400 kpc of a luminous galaxy. Therefore, we conclude that the gas out to 400 kpc from  $L > 0.1 L_*$  galaxies seen in Ly $\alpha$  absorption represents 20–25% of the baryons, i.e., there are at least 3 times as many baryons in the gaseous envelopes (“halos”) of the galaxies than there are inside the galaxies. The true baryonic content of these extended halos may be larger by another factor  $\sim 2\text{--}3$ , since the Ly $\alpha$  and O VI observations are not sensitive to the hot ( $T > 10^6 \text{ K}$ ) phase of the intergalactic gas predicted by the hydrodynamical structure formation simulations. However, the baryonic content of the gas now detected in these extended structures already greatly exceeds the baryonic content of galaxies and these baryons likely play an important role in galaxy evolution.

Since the critical density to have a closed universe ( $\Omega=1$ ) is  $9.2 \times 10^{-30} \text{ h}_{71}^2 \text{ g cm}^{-3}$ , and since baryons represent 4.6% of this (Fukugita & Peebles 2004), the average baryon density is  $4.2 \times 10^{-31} \text{ g cm}^{-3}$ . We previously found (Sect. 4.2) that on average the nearest neighbor of an  $L_*$  galaxy is at 2.1 Mpc, that of a  $0.5 L_*$  galaxy at 1.65 Mpc and that of a  $0.1 L_*$  galaxy at 940 kpc (these values differ from the medians (1.5, 1.2 and 0.6 Mpc, respectively) because the distribution of nearest-neighbour distances is skewed). Thus, the average  $0.1 L_*$  galaxy has  $4.8 \times 10^{10} M_\odot$  of intergalactic baryons associated with it, every  $0.5 L_*$  has  $2.7 \times 10^{11} M_\odot$  and every  $L_*$  galaxy  $5.4 \times 10^{11} M_\odot$ . Within 400 kpc the mass of intergalactic baryons associated with each kind of galaxy is about half this amount.

Several lines of evidence support the contention that galaxies have been and are still accreting new material. Sancisi et al. (2008) reviewed this and infer that the observations show a visible (i.e. seen in the form of neutral hydrogen) accretion rate for  $L > 0.5 L_*$  on the order of  $0.2 M_\odot \text{ yr}^{-1}$ . Theoretically, a rate on the order of  $1 M_\odot \text{ yr}^{-1}$  is expected (e.g. Chiappini et al. 2001), so Sancisi et al. (2008) concluded that a large fraction of the accreting gas is not neutral. With a rate of  $1 M_\odot \text{ yr}^{-1}$ , in 10 Gyr a  $0.5 L_*$  galaxy would accrete about

$10^{10} M_{\odot}$ . This is a small fraction of the total amount of intergalactic material associated with it, but a substantial fraction of the material that currently lies within 400 kpc.

Whether or not one should call the intergalactic gas near the galaxies a “halo” or “corona” turns out to be a vague question. Certainly, the gas near galaxies knows about their presence. The gas is affected by them, and probably falling in and heating up. However, the increase in maximum linewidth with decreasing impact parameter may have alternative explanations, such as an increase in the amount of tidal material. Also, there may be alternative sources of heating, such as from the mechanical energy deposited by galaxy outflows. In any case, these “halos” have no firm boundary. They merge smoothly into the more tenuous intergalactic filaments connecting galaxies. The term “corona” might be appropriate for the hotter gas, if further studies could show that the hot gas is more concentrated near galaxies. It is possible that the notion that galaxies have “halos” can be kept if the intergalactic gas generally is kinematically related to the underlying galaxies. However, our first attempt at addressing this possibility suggests that the intergalactic lines do *not* know about the rotation of the underlying galaxies, which supports the notion that the intergalactic absorption lines originate in filaments connecting galaxies. Yet, absorption is seen much more frequently near galaxies than away from them, at rates approaching 100% for luminous galaxies. This implies that the galaxies are surrounded by gaseous envelopes.

## 7. Conclusions

We have analyzed intergalactic absorption lines in HST and FUSE spectra of 76 AGNs, searching for detections and non-detections of absorption near the velocity of nearby ( $v_{gal} < 5000 \text{ km s}^{-1}$ ) galaxies near those sightlines. Compared to previous studies of this subject, ours has several advantages – (1) the galaxy sample is much larger, (2) at  $v_{gal} < 2500 \text{ km s}^{-1}$  the galaxy sample is basically complete down to  $0.1 L_*$ , (3) we can separate the sample into group and field galaxies, (4) for each galaxy we can record non-detections as well as associated detections, (5) we can compare O VI with H I. Previous studies (Morris et al. 1993; Lanzetta et al. 1995; Tripp et al. 1998; Impey et al. 1999; Chen et al. 2001; Bowen et al. 2002; Penton et al. 2002; Côté et al. 2005; Aracil et al. 2006; Prochaska et al. 2006) used smaller and/or less complete samples. Although none of these papers combined all our analyses, they pointed to many of the same conclusions. With our study we are also able to reconcile some apparent contradictions between the conclusions reached in these papers. We now summarize the conclusions, which are also highlighted at the end of each subsection in Sects. 3, 4 and 5.

(1 – see Sect. 2.3). We have analyzed 52 HST and 63 FUSE spectra of 76 AGN (both QSOs and Seyfert galaxies), and identify a total of 133 intergalactic absorber systems at

recession velocities  $<6000 \text{ km s}^{-1}$ . We measure 115  $\text{Ly}\alpha$ , 40  $\text{Ly}\beta$ , 13  $\text{O VI } \lambda 1031.926$ , and 5  $\text{O VI } \lambda 1037.617$  lines. Of these systems, 45 are presented for the first time (including 29  $\text{Ly}\alpha$ , 36  $\text{Ly}\beta$ , 8  $\text{O VI } \lambda 1031.926$  and all 5  $\text{O VI } \lambda 1037.617$  lines). On the other hand, we do not confirm 20 previously published  $\text{Ly}\alpha$  lines or 6 previously claimed  $\text{O VI } \lambda 1031.926$  lines.

(2 – see Sect. 3.2). The properties of the  $\text{O VI}$  absorbers in our sample generally match those of the larger well-studied sample of Tripp et al. (2008). Since we find that all our absorbers originate within 550 kpc of an  $L > 0.1 L_*$  galaxy, we suggest that this is generally true for intergalactic  $\text{O VI}$  at low redshift. For eight of the fourteen  $\text{O VI}$  systems we can make some attempt at explaining their origin. In three cases photoionization appears to be the more likely description, while for the other five collisional ionization appears needed to explain the absorber properties.

(3 – see Sects. 3.2 and 3.3). The distributions of  $\text{Ly}\alpha/\text{O VI}$  linewidths,  $dN(\text{Ly}\alpha)/dz$  and  $dN(\text{O VI})/dz$  at  $z=0.01$  are all similar to the distributions found from studies at redshifts 0–0.5, suggesting that the relationship between  $\text{O VI}$  absorbers and galaxies is the same at  $z \sim 0$  as at  $z \sim 0$  to 0.5.

(4 – see Sect. 3.4). The fraction of broad  $\text{Ly}\alpha$  lines is higher in the nearby universe ( $z < 0.017$ ) than at higher redshifts, with 55% of the lines having  $b > 40 \text{ km s}^{-1}$ , compared to 30% at  $\langle z \rangle = 0.25$  (lookback time 2.5 Gyr) and 20% at  $z \sim 2$  (7.5 Gyr ago).

(5 – see Sect. 4.1). For the great majority (96%) of intergalactic absorbers a galaxy (of any luminosity) can be found with impact parameter  $\rho < 3 \text{ Mpc}$  and velocity difference  $\Delta v < 400 \text{ km s}^{-1}$ . For a large fraction (75%) there is a galaxy within  $400 \text{ km s}^{-1}$  and within 1 Mpc, and most of these are brighter than  $0.1 L_*$ . A bright ( $L > L_*$ ) galaxy is found within 400 kpc and  $200 \text{ km s}^{-1}$  for just 17% of the  $\text{Ly}\alpha/\text{Ly}\beta$  lines. Table 9 summarizes the fraction of absorbers for which it is possible to find a galaxy of a given brightness within some impact parameter and velocity difference. This is the complement of Table 10, which gives the fraction of galaxies having an associated  $\text{Ly}\alpha$  absorber.

(6 – see Sect. 4.2). We analyze the distribution of the nearest neighbor galaxy to an absorber and that of the nearest neighbor galaxy to another galaxy. We find that the median distance between group galaxies brighter than  $L > 0.1 L_*$  is 500 kpc, while the median distance between field galaxies brighter than  $L > 0.1 L_*$  is 1.5 Mpc. For absorbers, the nearest-neighbor group galaxy is at a distance of 350 kpc, while in the field the median nearest-neighbor galaxy is at 600 kpc. Therefore, we conclude that most  $\text{Ly}\alpha$  absorbers are associated with galaxies, both in the field and in groups. Previous similar analyses reached the opposite conclusion because they mixed field and group galaxies and only included  $L_*$  galaxies – the median separation between  $L_*$  galaxies is 1.1 Mpc, while the median absorber- $L_*$  galaxy separation

is 1.0 Mpc.

(7 – see Sect. 4.3). For a little more than half of the intergalactic absorbers there is just one galaxy that is likely to be associated with it. For a quarter there either are two equally likely galaxies or there are two absorption lines and two likely galaxies. For about one eighth of the lines the absorption occurs in a group of galaxies and no unambiguous choice can be made. In the remaining 7 cases the association between an absorber and a galaxy is ambiguous, with two or more galaxies equally likely candidates.

(8 – see Sect. 4.4). We conclude that it depends on the luminosity limit and completeness of the galaxy sample whether an absorber occurs far from the nearest galaxy and can be called a “void absorber”. Penton et al. (2002) found a fraction of  $22 \pm 8\%$  of absorbers occurring more than 3 Mpc from an  $L_*$  galaxy, while we find  $17 \pm 4\%$  using these criteria for our full  $v_{gal} < 5000 \text{ km s}^{-1}$  sample. However, an  $L > 0.1 L_*$  galaxy is found within 1.5 Mpc of each absorber with  $v < 2500 \text{ km s}^{-1}$ , where our galaxy sample is complete down to that luminosity limit. Further, just 7% of the absorbers with  $v < 2500 \text{ km s}^{-1}$  occur more than 3 Mpc from an  $L_*$  galaxy.

(9 – see Sect. 4.5). For unambiguous associations, the difference in velocity between the intergalactic absorption and the galaxy’s systemic velocity ranges from  $-118$  to  $147 \text{ km s}^{-1}$ , with a dispersion of  $60 \text{ km s}^{-1}$ . For all associations the range is  $-443$  to  $+349 \text{ km s}^{-1}$ , although  $|\Delta v| > 300 \text{ km s}^{-1}$  for just four of the associations that we make (see Sect. 4.3).

(10 – see Sect. 4.6). At impact parameters less than about 500 kpc the width of the  $\text{Ly}\alpha$  lines increases with decreasing impact parameter. This is unlikely to be caused by kinematical broadening due to projection effects. We cannot completely exclude that turbulent motions are responsible, but the most likely explanation is that there is an increase in the temperature of the gas within a few hundred kpc of galaxies. Such heating inside gravitational wells is predicted in hydrodynamical simulations of structure formation in the universe (Cen & Ostriker 1999; Davé et al. 2001; Cen & Fang 2006).

(11 – see Sect. 4.7). Previous studies of the relation between  $\text{Ly}\alpha$  equivalent width and impact parameter have led to conflicting conclusions. Some authors concluded that there is a strong anti-correlation, others concluded that there is none. We find that some of the confusion is due to the usage of log-log plots as well as to the fact that different ranges in impact parameter are included in different studies. We find that at any impact parameter there is a wide range in equivalent widths. However, the strength of the strongest line does anti-correlate with impact parameter, becoming progressively higher at lower impact parameter. We find that 80% of strong ( $W > 300 \text{ m}\text{\AA}$ ) lines occur within 600 kpc of a galaxy, while 70% originate within 350 kpc. On the other hand, weak lines only occur far from

galaxies, and the weaker the line, the larger the minimum impact parameter; specifically all Ly $\alpha$  lines with  $W < 25$  mÅ have  $\rho > 0.75/2.5$  Mpc to the nearest  $0.1/1.0$   $L_*$  galaxy, while all Ly $\alpha$  lines with  $W < 50$  mÅ have  $\rho > 0.3/1.0$  Mpc. Thus, we conclude that there are patterns in the relation between Ly $\alpha$  equivalent width and impact parameter, but there is no simple one-to-one correspondence.

(12 – see Sect. 5.1). We conclude that total Ly $\alpha$  equivalent width in windows 500–1000 km s $^{-1}$  wide around detections does not directly correlate with the density of galaxies in cylinders of radii of 500–2000 kpc and velocity depths of 500–1000 km s $^{-1}$ . However, we do find that for a given density of galaxies the largest equivalent width found does change with density, such that at a density of 1 galaxy per Mpc $^3$  the equivalent width in a 500 km s $^{-1}$  range can reach 3 Å, whereas at a density of 0.01 galaxy per Mpc $^3$  the maximum equivalent width in a 500 km s $^{-1}$  range is 300 mÅ.

(13 – see Sect. 5.2). For 100% of  $L > 0.1$   $L_*$  galaxies it is possible to find a  $> 50$  mÅ Ly $\alpha$  line with impact parameter  $< 400$  kpc and velocity difference  $\Delta v < 1000$  km s $^{-1}$ , while the percentage is 80% for  $\Delta v < 400$  km s $^{-1}$ . Strong lines ( $> 300$  mÅ) are found within 400 kpc and 400 km s $^{-1}$  for about 50% of the galaxies. At impact parameters  $< 1$  Mpc strong lines with  $\Delta v < 400$  km s $^{-1}$  are found for about 25% of the  $L > 0.1$   $L_*$  galaxies, while a line with  $W > 50$  mÅ is seen for 50% of such galaxies. Table 10 summarizes the fraction of galaxies for which it is possible to find an absorber of a given equivalent width within some impact parameter and velocity difference. This is the complement of Table 9.

(14 – see Sects. 5.3.3 and 5.3.4). Using the individually determined associations listed in Table 3, we find that 100% (7 of 7) of field and 60% (13 of 21) of group galaxies brighter than  $0.1 L_*$  and with velocity  $< 2500$  km s $^{-1}$  have an associated Ly $\alpha$  absorber at impact parameter  $< 350$  kpc. The fraction of galaxies with associated absorbers decreases monotonically to about 0 at  $\rho \sim 1500$  kpc. Similarly, about 50% of galaxy groups are found to have associated Ly $\alpha$  absorption.

(15 – see Sect. 5.3.6). At impact parameters  $< 350$  kpc associated O VI is detected for about 67% (4 of 6) of field galaxies with  $v_{gal} < 2500$  km s $^{-1}$  brighter than  $0.1 L_*$ . Only 8% (1 of 13) of such group galaxies are found to have associated O VI. Only one field galaxy has associated O VI at  $\rho > 300$  kpc, but the impact parameter for three of the five O VI lines associated with a bright group galaxy is 300–450 kpc.

(16 – see Sect. 5.4). Our sample includes four edge-on galaxies for which we know which side is approaching/receding and which have an intergalactic absorber with impact parameter  $< 350$  kpc that lies near the extended plane of the galaxies. We do not find a correlation between the difference in velocity between the absorber and the galaxy, suggesting that the

intergalactic gas does not know about the rotation of the underlying galaxy. However, we need to confirm this disconnect using more examples.

(17) We can combine conclusions (2), (3) and (15) to imply that many intergalactic O VI lines originate in photoionized gas within 500 kpc of bright ( $L > 0.1 L_*$ ) galaxies. As is the case in larger and more redshifted samples of O VI absorbers, there are cases in which the H I and O VI lines have similar widths, but also cases where broader H I lines are seen. It is not clear yet, however, whether these broad lines are single- or multi-component absorbers.

(18) Conclusions (3), (4) and (10) suggest that there is an increase in the temperature of the gas within a few hundred kpc of galaxies, although we cannot clearly exclude alternative explanations such as an increase in the amount line broadening caused by an increase in the amount of tidal material with high velocity gradients. However, heating inside gravitational wells is predicted in hydrodynamical simulations of structure formation in the universe (Cen & Ostriker 1999; Davé et al. 2001; Cen & Fang 2006).

(19) Combining conclusions (5)–(9) implies that intergalactic Ly $\alpha$ /Ly $\beta$  and O VI absorbers are associated with galaxies. For the parts of parameter space where our sample is complete, we show that an  $L > 0.1 L_*$  galaxy can be found within 1.5 Mpc of each absorber, while each  $L > 0.1 L_*$  field galaxy has an associated absorber within 350 kpc. About half of the  $L > 0.1 L_*$  group galaxies have an associated absorber within 350 kpc, while associated Ly $\alpha$  absorption is found for about 50% of the galaxy groups.

(20) Conclusions (11)–(14) show that weak lines are seen at all impact parameters, but strong lines above a given equivalent width limit only occur below a given impact parameter. Similarly, the strongest lines occur where the galaxy density is highest, although weak lines also occur in high-density regions. This suggests that denser patches of intergalactic gas are more often found closer to galaxies than at large impact parameter.

(21) All the arguments summarized above can be reconciled if galaxies have gaseous envelopes (“halos”) that are several hundred kpc in radius, smoothly connecting to intergalactic filaments. These halos consist of intergalactic gas that is in the process of falling in toward the galaxies and possibly heating up as it falls, but the gas has not yet taken on the kinematics of those galaxies. The baryonic content of this photoionized and warm collisionally ionized gas located within 400 kpc of galaxies exceeds by a factor  $\sim 2$ –4 the baryonic content of the galaxies. This gas likely plays a crucial role in the evolution of galaxies.

The data in this paper were obtained with the NASA-CNES-CSA *Far Ultraviolet Spectroscopic Explorer*, FUSE, operated for NASA by The Johns Hopkins University under NASA contract NAS5-32985 and with the NASA ESA *Hubble Space Telescope*, at the Space Tele-

scope Science Institute, which is operated by the Association of Universities for Research in Astronomy, Inc. under NASA contract NAS5-26555. Spectra were retrieved from the Multi-mission Archive (MAST) at STScI. The study made use of the NASA/IPAC Extragalactic Database (NED), which is operated by the Jet Propulsion Laboratory, California Institute of Technology, under contract with NASA. Over the course of this study, BPW was supported by NASA grants NNG04GA39G, NNG06GG39G (FUSE), GO-00754.01-A (STScI) and NNX07AH42G (ADP). BDS was supported by grants NAS5-31248 (NASA/FUSE) and MSN111587 from the University of Colorado (NASA Cosmic Origins Spectrograph).

## Appendix

Here we present notes on individual sightlines. We refer to Fig. 8 and Table 3 for even more details. The notes often give the parameters of a galaxy near the line of sight, in the format e.g.,  $(v_{gal}, D_{gal}, \rho=925, 13.4, 140)$ . These three numbers give the systemic velocity ( $v$ ) in  $\text{km s}^{-1}$ , diameter at 25th magnitude surface brightness ( $D$ ) in kpc, and impact parameter ( $\rho$ ) in kpc.

*1H 0419–577.* – Although there is just a FUSE spectrum of this target, and it has low S/N ( $\sim 5$ ), it is included in the sample because the impact parameter to NGC 1574 ( $v_{gal}, D_{gal}, \rho=925, 13.4, 140$ ) is low. A strong  $\text{Ly}\beta$  and a possible  $\text{Ly}\gamma$  line are seen at  $1112 \text{ km s}^{-1}$ . There is a hint of  $\text{O VI } \lambda 1031.926$  absorption, but only at the  $2\sigma$  level. The confirming  $\text{O VI } \lambda 1037.617$  line is hidden in geocoronal  $\text{OI}^*$  emission, and the orbital-night-only data have no signal. Table 3 lists NGC 1574 as the associated galaxy because it is the northernmost galaxy in the LGG 112 ( $\langle v \rangle = 1095 \text{ km s}^{-1}$ ) group, and 1H 0419–577 lies only 140 kpc from it (see filled square in Fig. 8(1)). However, the other group galaxies also have fairly low impact parameters, between 442 and 627 kpc, while a small galaxy (LSBG F157–081;  $v_{gal}, D_{gal}, \rho=1215, 3.7, 70$ ) is somewhat closer. We choose to list NGC 1574 as the associated galaxy, because it has smaller  $\rho/D_{gal}$  (10) than LSBG F157–081 (19), but we could also have interpreted the absorption as a general group detection.

Two more galaxy groups lie near the sightline, and like LGG 112 these groups are quite well-defined. Non-detections are listed for LGG 119 ( $v_{gal}=1095 \text{ kpc}$ , nearest galaxy ESO 118-G34 at 700 kpc) and LGG 114 ( $v_{gal}=1481 \text{ kpc}$ , nearest galaxy APMBGC157+016+068 at 317 kpc). A final non-detection entry is given Table 3 for NGC 1533 ( $v_{gal}, D_{gal}, \rho=790, 17.7, 396$ ), as it does not belong to any of the groups.

*1H 0707–495.* – The feature listed as  $\text{Ly}\beta$  at  $1302 \text{ km s}^{-1}$  is associated with ESO 207-G09 ( $v_{gal}, D_{gal}, \rho=1029, 8.0, 482$ ), but needs confirmation with an observation of  $\text{Ly}\alpha$ . The association is relatively unambiguous (see Fig. 8(2)). A galaxy with unknown velocity (ESO207-G31) could have  $\rho \sim 370 \text{ kpc}$ , if its velocity is similar to that of the  $\text{Ly}\beta$  line.

*1H 0717+714.* – This sightline passes close to several galaxies in the LGG 141 group ( $\langle v \rangle = 3001 \text{ km s}^{-1}$ ), with UGC 3804 being the closest at 199 kpc (filled square in Fig. 8(3)). UGC 3921, UGC 3940 and IC 2184 have velocities similar to those of the group galaxies (2475, 2462 and  $3605 \text{ km s}^{-1}$ , respectively), but lie outside the group on the sky, and are thus listed separately in Table 3.

No  $\text{Ly}\alpha$  data exist for this sightline, making the analysis more difficult. However, there is a feature that is likely to be  $\text{Ly}\beta$  at  $2888 \text{ km s}^{-1}$ . On the other hand, it is possible that this feature is a weak C II line at  $v_{\text{LSR}} = -200 \text{ km s}^{-1}$  associated with the nearby ( $< 1^\circ$ )



high-velocity cloud complex A. No 21-cm HI emission is detected at this velocity in the direction of 1H0717+714, but if we interpret the absorption as CII, its strength suggests  $N(\text{HI}) \sim 4 \times 10^{17} \text{ cm}^{-2}$ , which is below the 21-cm detection limit. An interpretation as CII is not supported by the higher Lyman lines, as there is no evidence for a component at  $-200 \text{ km s}^{-1}$ . Further, complex A has velocities of  $\sim -160 \text{ km s}^{-1}$  nearest 1H0717+714, while velocities of  $\sim -200 \text{ km s}^{-1}$  are seen only  $3^\circ$  or more away.

Further arguing in favor of interpreting the feature as  $\text{Ly}\beta$  is the clear  $66 \pm 15 \pm 9 \text{ m}\text{\AA}$  absorption feature at  $2914 \text{ km s}^{-1}$  on the O VI  $\lambda 1031.926$  velocity scale. In the combined orbital day plus orbital night data this is blended with geocoronal O I\* emission, but it is very clear in the orbital-night-only data. This feature could be  $\text{Ly}\beta$  at  $4750 \text{ km s}^{-1}$ , but there are no known galaxies near that velocity. It is more likely that it is redshifted O VI  $\lambda 1031.926$  matching the  $\text{Ly}\beta$  line. The only problem with this interpretation is that the corresponding O VI  $\lambda 1037.617$  line is not clearly visible. Considering the errors on the probable O VI  $\lambda 1031.926$  feature, the equivalent width of the other O VI line is expected to be between 25 and  $40 \text{ m}\text{\AA}$ . Since the detection limit is  $23 \text{ m}\text{\AA}$ , the apparent non-detection is not too problematic, but data with higher S/N ratio are sorely needed (they were approved, but not executed before FUSE was decommissioned).

*3C 232.* – With Mrk 205, this is one of two targets with good data that lies behind the disk of a nearby galaxy, NGC 3067 ( $v_{gal}$ ,  $D_{gal}$ ,  $\rho = 1476, 17.0, 14$ ) in the case of 3C 232. A very strong  $\text{Ly}\alpha$  line ( $N(\text{HI}) = 8 \times 10^{19} \text{ cm}^{-2}$ ) is detected in the *GHR*S spectra of 3C 232, as are many other ions (OI, CII, CIV, MgI, MgII, AlII, SiII, SiIII, SiIV, AlII, FeII). These lines were analyzed in detail by Tumlinson et al. (1999) and Keeney et al. (2005). Unfortunately, the FUV flux of 3C 232 is too low ( $0.5 \times 10^{-14} \text{ erg cm}^{-2} \text{ s}^{-1} \text{ \AA}^{-1}$ ) to obtain a useful FUSE spectrum.

In addition to NGC 3067, there are 16 other galaxies in the GH 50 ( $\langle v \rangle = 1442 \text{ km s}^{-1}$ ) group with impact parameter between 427 and 1000 Mpc. If any any of these have associated absorption, it will be hidden by the strong line originating in NGC 3067.

There are three galaxies with sufficiently different velocity to warrant separate entries in Table 3: UGC 5272 ( $v_{gal}$ ,  $D_{gal}$ ,  $\rho = 520, 6.5, 359$ ), UGC 5340 ( $v_{gal}$ ,  $D_{gal}$ ,  $\rho = 503, 8.3, 660$ ) and Mrk 412 ( $v_{gal}$ ,  $D_{gal}$ ,  $\rho = 4479, 11.7, 196$ ). These are not discussed by Tumlinson et al. (1999) and Keeney et al. (2005). Any  $\text{Ly}\alpha$  absorption near  $520 \text{ km s}^{-1}$  is obscured by the Galactic  $\text{Ly}\alpha$  line, however. There is a clear feature that is probably  $\text{Ly}\alpha$  at  $4526 \text{ km s}^{-1}$ , and that can be associated with Mrk 412, which is the only known galaxy with similar velocity; see filled symbol in Fig. 8(5).

*3C 249.1.* – One possible  $3\sigma$   $\text{Ly}\alpha$  line is found at  $1861 \text{ km s}^{-1}$ . There are four galaxies

with similar velocity and impact parameter near this velocity: UGC 5854 ( $v_{gal}$ ,  $D_{gal}$ ,  $\rho=1808$ , 7.7, 505), UGC 5841 ( $v_{gal}$ ,  $D_{gal}$ ,  $\rho=1766$ , 12.2, 538), NGC 3329 ( $v_{gal}$ ,  $D_{gal}$ ,  $\rho=1812$ , 14.3, 543) and UGC 5814 ( $v_{gal}$ ,  $D_{gal}$ ,  $\rho=1881$ , 13.3, 641); see Fig. 8(6). In Table 3 the absorption line is associated with the largest of these three (NGC 3329), but this is an arbitrary choice. For the other galaxies near this velocity non-detections are listed.

The velocity of the galaxy with the smallest angular distance (UGC 6065) has not yet been measured. It has an impact parameter of 238 ( $v_{gal}/4000$ ) kpc, and diameter of 25 ( $v_{gal}/4000$ ) kpc. So, if this galaxy had a velocity like that of the Ly $\alpha$  line at 1861 km s<sup>-1</sup>, its diameter would be similar to those of the other five galaxies near this velocity, but it would have an impact parameter of only  $\sim 107$  kpc, and it would be listed as the galaxy associated with the Ly $\alpha$  line.

*3C 263.* – As many as 17 galaxies with velocity near about 1100 km s<sup>-1</sup> lie within 1 Mpc of this sightline. For five of these the ratio  $\rho/D_{gal}$  is less than 125, and these are the ones listed in Table 3: NGC 3682 ( $v_{gal}$ ,  $D_{gal}$ ,  $\rho=1532$ , 11.8, 626), UGC 6448 ( $v_{gal}$ ,  $D_{gal}$ ,  $\rho=991$ , 5.1, 643), UGC 6390 ( $v_{gal}$ ,  $D_{gal}$ ,  $\rho=1008$ , 10.3, 634), NGC 3945 ( $v_{gal}$ ,  $D_{gal}$ ,  $\rho=1220$ , 15.6, 950) and UGC 6534 ( $v_{gal}$ ,  $D_{gal}$ ,  $\rho=1273$ , 15.2, 955). No absorption is seen near their velocities.

*3C 273.0.* – In this spectrum there are four Ly $\alpha$  lines with  $v < 6000$  km s<sup>-1</sup>. Two (at 1010 and 1580 km s<sup>-1</sup>) are strong, two (at 2160, 2274 km s<sup>-1</sup>) are weak. This sightline was analyzed in great detail by Sembach et al. (2001) and Tripp et al. (2002), and it was included in the sample of Penton et al. (2000). The equivalent widths and velocities all agree between these papers and Table 3. The two strong lines are associated with the Virgo cluster and assigning it to any individual galaxy (if any) would be very ambiguous. The LGG catalogue splits the galaxies near this sightline into two groups – LGG 287 ( $\langle v \rangle = 1655$  km s<sup>-1</sup>) and LGG 292 ( $\langle v \rangle = 938$  km s<sup>-1</sup>), see Fig. 8(7)/(8). The impact parameters (191 and 311 kpc) listed in Table 3 correspond to the nearest galaxy that has a velocity within  $\pm 200$  km s<sup>-1</sup> of the Ly $\alpha$  detection. The probable detection of O VI at 1008 km s<sup>-1</sup> was previously reported in three other papers. However, the three papers disagree on the value of the equivalent width. Sembach et al. (2001) reported  $26 \pm 10$  mÅ, Danforth et al. (2006) gave  $35 \pm 6$  mÅ, Tripp et al. (2008) listed  $31 \pm 7$  mÅ, while we find  $21 \pm 3 \pm 7$  mÅ. Our value is smaller than any of the others because we correct for the 5 mÅ contribution of H<sub>2</sub> L(6-0) P(4)  $\lambda 1035.181$  line, unlike the other authors. Taking this into account, we agree with Sembach et al. (2001).

Sembach et al. (2006) also reported an O VI  $\lambda 1037.617$  absorption to go with the 1580 km s<sup>-1</sup> Ly $\alpha$  line. However, the detailed modeling of the H<sub>2</sub> lines shows that this is actually Galactic H<sub>2</sub> L(5-0) R(3)  $\lambda 1041.158$ , as can be seen in Fig. 2.

For the two weak components, there are two galaxies with  $v_{gal}$  between 2000 and

2500 km s<sup>-1</sup>. UGC 7625 ( $v_{gal}$ ,  $D_{gal}$ ,  $\rho$ =2234, 9.6, 771) has a large impact parameter, while 2MASX J122815.85+024202.5 ( $v_{gal}$ ,  $D_{gal}$ ,  $\rho$ =2286, 5.0, 429) is closer to the AGN. Both galaxies have almost the same ratio of  $\rho/D_{gal}$ . In Table 3 the Ly $\alpha$  component at 2274 is (somewhat arbitrarily) associated with 2MASX J122815.85+024202.5, and the one at 2160 km s<sup>-1</sup> with UGC 7625. This results in  $\Delta v$ =−12 and +74 km s<sup>-1</sup> instead of −126 and −40 km s<sup>-1</sup>, respectively.

*3C 351.0.* – As there is a Lyman limit system at  $z$ =0.22 toward this sightline, there is no flux below 1112 Å, and the Ly $\beta$  and O VI lines cannot be checked. Good Ly $\alpha$  data exist, however. The intrinsic absorption system at  $z$ =0.3721 was studied by Yuan et al. (2002).

There are 12 galaxies with  $v_{gal}$  between 3012 and 3855 km s<sup>-1</sup> within 1 Mpc of this target (see Fig. 8(10)). Just four of these (NGC 6292, NGC 6306, NGC 6307, NGC 6310) are included in the RC3. Within 5 degrees (3 Mpc) of 3C 351.0 there are tens of galaxies whose velocities cluster around 3300 km s<sup>-1</sup>, with a range from 2500 to 4000 km s<sup>-1</sup>. Garcia (1993) did not define these galaxies as a group, probably because not all radial velocities had been measured at the time. However, there is clearly a group in this part of the sky, and we identify it as LGG179A in Table 3, as its right ascension lies between that of LGG179 and LGG180.

Two strong Ly $\alpha$  features are found near these velocities, at 3598 and 3465 km s<sup>-1</sup>. The velocities and impact parameters of the galaxies are such that Table 3 associates the detection at 3598 km s<sup>-1</sup> with Mrk 892 ( $v_{gal}$ ,  $D_{gal}$ ,  $\rho$ =3617, 10.2, 170, smaller filled square in Fig. 8(10)). The one at 3465 km s<sup>-1</sup> is listed as associated with NGC 6292 ( $v_{gal}$ ,  $D_{gal}$ ,  $\rho$ =3411, 22.1, 314), which has the smallest velocity difference (see larger filled square in Fig. 8(10)). NGC 6310 ( $v_{gal}$ ,  $D_{gal}$ ,  $\rho$ =3386, 28.5, 402, large open square with plus next to larger black square in Fig. 8(10)) has the same  $\rho/D_{gal}$  ratio as NGC 6292, but a non-detection is listed because of the larger impact parameter and larger velocity difference with the absorption. Of the other nine galaxies, six have velocity between 3012 and 3350 km s<sup>-1</sup>, and three lie between 3736 and 3855 km s<sup>-1</sup>. All are fairly large (>7 kpc) and a non-detection is given in Table 3 for each of these.

Two galaxies with different velocity have small impact parameters and are included separately in Table 3: UGC 10770 ( $v_{gal}$ ,  $D_{gal}$ ,  $\rho$ =1108, 5.9, 531) and SDSS J170349.45+601806.1 ( $v_{gal}$ ,  $D_{gal}$ ,  $\rho$ =5183, 6.6, 594). Ly $\alpha$  absorption at 5175 km s<sup>-1</sup> is associated with the SDSS galaxy (not shown in Fig. 8 because  $v$ >5000 km s<sup>-1</sup>).

*ESO 141-G55.* – Several galaxies have impact parameters between 400 kpc and 1 Mpc, concentrated around three velocities. IC 4824 and ESO 141-G42 have  $v_{gal}$ =953 and 935 km s<sup>-1</sup>, and lie close together at 769 and 790 kpc impact parameter. IC 4826 and IC 4819 have sim-

ilar velocity (1925 and 1841 km s<sup>-1</sup>), and similar impact parameter (865 and 868 kpc), but lie in opposite directions from ESO 141-G55, so separate entries are given in Table 3. This is also the case for ESO 141-G51 ( $v_{gal}$ ,  $D_{gal}$ ,  $\rho$ =3497, 14.2, 410) and IC 4843/ESO 141-G46 ( $v_{gal}$ =3975 and 4079 km s<sup>-1</sup>,  $\rho$ =662 and 878 kpc). No Ly $\alpha$  or O VI absorption is seen in the spectrum of ESO 141-G55. Penton et al. (2000) listed  $1.5\sigma$  ( $12\pm 8$  mÅ) features near 8449 and 9078 km s<sup>-1</sup>. However, these are likely to be spurious.

*ESO 185-IG13.* – This nearby galaxy ( $v_{gal}$ =5600 km s<sup>-1</sup>) is the only AGN in the sample with  $v_{gal}$ <7000 km s<sup>-1</sup>. In spite of this and in spite of its low S/N (4.1) FUSE spectrum it is included because the impact parameter to IC 4889 ( $v_{gal}$ =2528 km s<sup>-1</sup>) is just 62 kpc and very strong Ly $\beta$ , Ly $\gamma$ , C III and O VI are seen. Follow-up FUSE observations were approved twice, but never executed. Non-detections are listed for three other galaxies: IC 4888, 2MASXJ 194221.91–550627.5 and ESO 185-G03. The last two have large impact parameter (672 and 985 kpc) and  $v_{gal}$ ~3000 km s<sup>-1</sup>, and only ~90 mÅ O VI  $\lambda$ 1031.926 upper limits are given. Like IC 4889, IC 4888 has low impact parameter (123 kpc), and almost the same velocity, but it’s diameter is one-third that of IC 4889.

*ESO 438-G09.* – Only a *STIS*-G140M spectrum is available for this target. It lies behind the LGG 230 group, with nine galaxies clustering around 1425 km s<sup>-1</sup> (see Fig. 8(12)). ESO 438-G05 is the nearest, with an impact parameter of 173 kpc. A very strong Ly $\alpha$  line is seen at 1426 km s<sup>-1</sup>, which is associated with the group in Table 3. Bowen et al. (2002) previously listed this line, and associated it with UGCA 226 ( $v_{gal}$ ,  $D_{gal}$ ,  $\rho$ =1500, 19.9, 178). However, there are several other nearby group galaxies: ESO 437-G05 ( $v_{gal}$ ,  $D_{gal}$ ,  $\rho$ =1507, 19.2, 173), ESO 438-G12 ( $v_{gal}$ ,  $D_{gal}$ ,  $\rho$ =1322, 6.8, 245) and ESO 438-G10 ( $v_{gal}$ ,  $D_{gal}$ ,  $\rho$ =1487, 9.6, 248). There is no reason to prefer associating the absorption with any particular one of these.

An additional Ly $\alpha$  line at 2215 km s<sup>-1</sup> (also first listed by Bowen et al. 2002) is not considered as originating in the group, because of the large velocity difference and because the group galaxies have velocities ranging from 1230 to 1517 km s<sup>-1</sup>. Instead it is listed under 2MASX J111343.40–274328.8 ( $v_{gal}$ ,  $D_{gal}$ ,  $\rho$ =2100, 4.8, 577 kpc), which is the only candidate galaxy with  $\rho$ <900 kpc.

*Fairall 9.* – Although this sightline passes relatively close to the LGG 19 group ( $\langle v \rangle$ =5035 km s<sup>-1</sup>), the two nearest galaxies in that group (NGC 484, ESO 113-G35) have large impact parameters (735, 799 kpc), and no absorption is seen. Penton et al. (2000) reported on this sightline, and only list absorbers at  $v$ >5000 km s<sup>-1</sup>.

*H 1821+643.* – This sightline lies at relatively low galactic latitude (27°), and Galactic extinction clearly influences the number of bright galaxies that are visible near it. . Only four

small galaxies with  $v_{gal} < 6000 \text{ km s}^{-1}$  are known within 1.5 Mpc of the sightline, and two of these have  $\rho/D_{gal} > 125$ . That leaves NGC 6690 ( $v_{gal}$ ,  $D_{gal}$ ,  $\rho=488, 8.7, 858$ ), which is included in Table 3. Penton et al. (2000) list no absorption lines below  $6000 \text{ km s}^{-1}$ , mostly because their GHRS spectrum does not extend below  $4500 \text{ km s}^{-1}$ . The *STIS*-E140M spectrum shows two low redshift Ly $\alpha$  absorbers, at  $2836$  and  $4084 \text{ km s}^{-1}$  for which the nearest galaxies with similar velocities have  $\rho \sim 2.5$  Mpc. The line at  $2836 \text{ km s}^{-1}$  is the weakest line in our sample ( $17 \pm 5 \text{ m}\text{\AA}$ ). In addition, there is a Ly $\alpha$  line at  $5253 \text{ km s}^{-1}$ , but no galaxies with similar velocity are known with impact parameter  $< 3$  Mpc.

Low-redshift O VI absorbers (at  $z=0.22497$ ) were first discovered by Savage et al. (1998) and Tripp et al. (2000) in this sightline.

*HE 0226–4110*. – Lehner et al. (2006) analyzed the IGM absorption in this sightline. They listed the system at  $5235 \text{ km s}^{-1}$ , which includes Ly $\alpha$  and both O VI lines. However, the O VI  $\lambda 1031.926$  line is contaminated by interstellar H<sub>2</sub> L(4-0) R(1)  $\lambda 1049.960$ . Nevertheless, the very good H<sub>2</sub> model for this sightline (see Wakker 2006) shows that not all of this feature can be H<sub>2</sub>, and about half is likely to be O VI, centered at  $5240 \text{ km s}^{-1}$ . Unfortunately, the corresponding O VI  $\lambda 1037.617$  line is contaminated by O VI  $\lambda 787.711$  at  $z=0.3406$  (see Lehner et al. 2006). Aiding the interpretation is the possible detection of weak C III ( $23 \pm 9 \text{ m}\text{\AA}$ ) and C IV ( $39 \pm 11 \text{ m}\text{\AA}$ ) absorption. The lines can be associated with NGC 954 ( $v_{gal}=5353 \text{ km s}^{-1}$ ), which has impact parameter  $562 \text{ kpc}$ , and which belongs to the LGG 62 group. If this interpretation is correct, it is the O VI detection with the largest impact parameter. We note that the galaxy survey in this region of sky is relatively good: the RC3 include three galaxies with  $\rho < 1.5$  Mpc, and *NED* lists four more, including three low-surface brightness galaxies.

There may be a weak ( $\sim 2\sigma$ ) Ly $\alpha$  line at  $1413 \text{ km s}^{-1}$ , near the velocity of NGC 986A. This feature was not considered significant by Lehner et al. (2006), and we also list it as a non-detection in Table 3.

On the other hand, Danforth & Shull (2008) claimed an absorption line at  $3642 \text{ km s}^{-1}$  that was not found by Lehner et al. (2006). The nearest galaxy within  $400 \text{ km s}^{-1}$  has an impact parameter of  $1.5$  Mpc. We measured this feature as  $22 \pm 10 \text{ m}\text{\AA}$ , and decided that it is a noise fluctuation, just like some other similar-looking features near it.

*HE 0340–2703*. – The *STIS*-G140M spectrum of this target shows intrinsic Ly $\gamma$ , Ly $\delta$ , Ly $\epsilon$ , S VI  $\lambda\lambda 933.378, 944.523$  ( $z=0.2830$ ), as well as Ly $\beta$ , O VI  $\lambda 1031.926$  and O VI  $\lambda 1037.617$  at  $z=0.1655$ . In addition to these lines there are three features that are probably Ly $\alpha$  at  $1361, 1785$  and  $4100 \text{ km s}^{-1}$ , although there is a chance that they are Ly $\beta$  or Ly $\gamma$  at higher redshift.

Assuming that these are Ly $\alpha$ , we associate the feature at 1785 km s $^{-1}$  with NGC 1412 ( $v_{gal}$ ,  $D_{gal}$ ,  $\rho$ =1790, 12.3, 167), although ESO 483-G32 ( $v_{gal}$ ,  $D_{gal}$ ,  $\rho$ =1756, 9.8, 152) (for which we list a non-detection) is just as likely a candidate (see the adjacent filled and open circles in Fig. 8(17)). Several other galaxies with  $|\Delta v| < 400$  km s $^{-1}$  and  $\rho = 1$  Mpc can be found, but as Fig. 8(17) shows, NGC 1412 or ESO 483-G32 is the most likely associated galaxy. Table 3 lists a separate non-detection for 6dF J0342278–260243 ( $v_{gal}$ ,  $D_{gal}$ ,  $\rho$ =1738, 3.2, 325), the one remaining galaxy with  $\rho/D_{gal} < 125$ .

For the line at 4100 km s $^{-1}$  there are two candidates with large  $\rho$  (shown by a large filled circle and a smaller open overlapping circle in Fig. 8(18)): 2MASX J034134.24–27491.87 ( $v_{gal}$ ,  $D_{gal}$ ,  $\rho$ =4125, 10.9, 913) and ESO 419-G03 ( $v_{gal}$ ,  $D_{gal}$ ,  $\rho$ =4109, 26.9, 942). We choose the largest of these as the associated galaxy in Table 3, giving a non-detection for the other.

The Ly $\alpha$  line at 1361 km s $^{-1}$  can be associated with the large galaxy NGC 1398 ( $v_{gal}$ ,  $D_{gal}$ ,  $\rho$ =1407, 29.8, 244). The sightline passes near the LGG 97 group, whose center lies about 5° ( $\sim 1.6$  Mpc) to the west of the QSO. The 32 group members defined by Garcia (1993) include two galaxies with  $\rho < 1$  Mpc: NGC 1371 ( $v_{gal}$ ,  $D_{gal}$ ,  $\rho$ =1471, 30.6, 838) and NGC 1385 ( $v_{gal}$ ,  $D_{gal}$ ,  $\rho$ =1493, 18.4, 861). There are another five galaxies with  $\rho < 1$  Mpc to the west of the QSO which were not included in the group, but which have a velocity within 100 km s $^{-1}$  of that of the group galaxies: NGC 1398 ( $v_{gal}$ =1407 km s $^{-1}$ ,  $\rho$ =244 kpc), ESO 482-G46 ( $v_{gal}$ =1525 km s $^{-1}$ ,  $\rho$ =543 kpc), ESO 482-G39 ( $v_{gal}$ =1381 km s $^{-1}$ ,  $\rho$ =588 kpc), ESO 482-G11 ( $v_{gal}$ =1595 km s $^{-1}$ ,  $\rho$ =646 kpc), and ESO 482-G06 ( $v_{gal}$ =1535,  $\rho$ =705 kpc).

*HE 1029–1401.* – There are high S/N ( $\sim 28$ ) *STIS*-G140M data for this bright target, but no FUSE observation was done. Three Ly $\alpha$  lines are found, at 2004, 2457 and 4567 km s $^{-1}$ , as reported by Penton et al. (2004). The middle one of these can be associated with the galaxy 6dF J1033307–144736 ( $v_{gal}$ ,  $D_{gal}$ ,  $\rho$ =2475, 10.1, 427). For the other two the nearest galaxies have impact parameter  $> 1$  Mpc: MCG–2-27-1 ( $v_{gal}$ ,  $D_{gal}$ ,  $\rho$ =2028, 13.9, 1065) and MCG–2-27-9 ( $v_{gal}$ ,  $D_{gal}$ ,  $\rho$ =4529, 377, 1035) (triangles in Fig. 8(19)/(21)).

*HE 1143–1810.* – Several galaxies have impact parameter  $< 1$  Mpc, concentrating around three velocities. First there are ESO 571-G18 ( $v_{gal}$ ,  $D_{gal}$ ,  $\rho$ =1391, 7.5, 368), [KKS2000]25 ( $v_{gal}$ ,  $D_{gal}$ ,  $\rho$ =1227, 7.4, 437) and NGC 3887 ( $v_{gal}$ ,  $D_{gal}$ ,  $\rho$ =1209, 20.2, 596). A second group is formed by ESO 572-G06 ( $v_{gal}$ ,  $D_{gal}$ ,  $\rho$ =1737, 9.9, 811), ESO 572-G09 ( $v_{gal}$ ,  $D_{gal}$ ,  $\rho$ =1737, 12.9, 884 kpc), and ESO 572-G07 ( $v_{gal}$ ,  $D_{gal}$ ,  $\rho$ =1466, 9.3, 976) which are part of the LGG 263 group. Finally, there is ESO 571-G16 ( $v_{gal}$ ,  $D_{gal}$ ,  $\rho$ =3637, 26.8, 851). There is no Ly $\beta$  detected, so we list a non-detection for each of these galaxies in Table 3. There is no data allowing us to search for Ly $\alpha$  lines.

*HE 1228+0131.* – This is a sightline with low S/N *STIS*-E140M and FUSE data ( $\sim 5$ ),

that passes through the Virgo cluster. At velocities below  $2000 \text{ km s}^{-1}$ , galaxies in two groups lie near it. For  $v_{gal}=700\text{--}1200 \text{ km s}^{-1}$  the nearest galaxy is part of LGG 292: MCG0-32-16 with  $v_{gal}$ ,  $D_{gal}$ ,  $\rho=1105$ , 6.3, 131. Although five more small galaxies have smaller impact parameter, Table 3 lists NGC 4517 ( $v_{gal}$ ,  $D_{gal}$ ,  $\rho=1121$ , 53.8, 383), because it is so large. No absorption is found in the  $700\text{--}1200 \text{ km s}^{-1}$  velocity range.

There are 36 galaxies in the velocity range  $1250\text{--}1850 \text{ km s}^{-1}$ , which spans the velocities of the galaxies in the LGG 287 group ( $\langle v \rangle = 1655 \text{ km s}^{-1}$ ). Two large galaxies are among the five with the lowest impact parameters: NGC 4536 ( $v_{gal}$ ,  $D_{gal}$ ,  $\rho=1804$ , 32.9, 338) and NGC 4517A ( $v_{gal}$ ,  $D_{gal}$ ,  $\rho=1530$ , 32.3, 466). No other large galaxy has impact parameter  $<700 \text{ kpc}$  (see Fig. 8(22)). The two absorption lines at  $1482$  and  $1700 \text{ km s}^{-1}$  are listed as generic group absorption in Table 3. Both were previously reported by Penton et al. (2000). These authors actually listed three lines, at  $1666$ ,  $1745$  and  $1860 \text{ km s}^{-1}$ , but the spectrum is too noisy to support splitting the strong  $\text{Ly}\alpha$  line into separate components at  $1666$  and  $1745 \text{ km s}^{-1}$ , and the claimed  $1860 \text{ km s}^{-1}$  detection may well be noise. The latter system has a very strong  $\text{Ly}\alpha$  line, and  $\text{Ly}\gamma$  through at least  $\text{Ly}\zeta$  are seen, as are C III and C I, but not O VI, although that may be because of the low S/N ratio of the data. The  $\text{Ly}\beta$  line of this system is contaminated both by Milky Way O VI  $\lambda 1031.926$  and by intrinsic S VI absorption.

Rosenberg et al. (2003) discussed this sightline, analyzing the metal-line absorption and estimating absorber-sizes. They also considered the galaxies with the lowest impact parameters and concluded that it is more likely that they are associated with gaseous filaments than with individual galaxies.

There is a third  $\text{Ly}\alpha$  line at  $2306 \text{ km s}^{-1}$ , which can be associated with UGC 7625 ( $v_{gal}$ ,  $D_{gal}$ ,  $\rho=2234$ , 9.6, 339), one of eight galaxies with  $\rho < 1 \text{ Mpc}$  and  $v_{gal}=2100\text{--}2500 \text{ km s}^{-1}$ , but one of only two with  $\rho < 550 \text{ kpc}$ ).  $\text{Ly}\beta$  is also seen for this system. Formally, the dwarf [ISI96]1228+0116 ( $\rho=182 \text{ kpc}$ ) is the nearest galaxy.

*HS 0624+6907.* – Two galaxies are known near this relatively high extinction sightline: UGC 3580 ( $v_{gal}$ ,  $D_{gal}$ ,  $\rho=1201$ , 18.0, 729; to the north) and UGC 3403 ( $v_{gal}$ ,  $D_{gal}$ ,  $\rho=1264$ , 12.6 932; to the west). No detections are found below  $6000 \text{ km s}^{-1}$ , although the *STIS*-E140M data are relatively noisy.

Aracil et al. (2006) make a more extensive study of the spectrum of this target, listing just one detection with  $v < 6000 \text{ km s}^{-1}$ . However, we do not confirm that there is a line at  $5262 \text{ km s}^{-1}$ , for which Aracil et al. (2006) quoted an equivalent width of  $41 \pm 10 \text{ m}\text{\AA}$ .

*HS 1543+5921.* – This object is a  $z=0.807$  QSO lying directly behind the dwarf galaxy SBS 1543+593, which is a member of the GH152 (=LGG402) group ( $\langle v \rangle = 2828 \text{ km s}^{-1}$ ).

Several papers have been written on this pair, including Bowen et al. (2001) and Bowen et al. (2005), who reported on the absorption lines. Chengalur & Kanekar (2002) and Rosenberg et al. (2006) showed an HI map of SBS 1543+593. With  $\rho=0.3$  kpc, it is the closest coincidence in our sample.

*IRAS 09149–6206.* – Near this low galactic latitude sightline lie nine galaxies with velocities between 1900 and 3200  $\text{km s}^{-1}$ . For seven of these, the possible associated  $\text{Ly}\beta$  absorption is hidden by the Milky Way C II  $\lambda 1036.337$  or intrinsic C III  $\lambda 977.020$  absorption. Limits on O VI  $\lambda 1031.926$  can be set for five galaxies, but in two cases they require orbital-night-only data. No detections are found.

*IRAS F22456–5125.* – This sightline shows eight intrinsic systems, whose  $\text{Ly}\delta$  and  $\text{Ly}\epsilon$  lines fall between 1025 and 1045 Å. Fortunately, they are not located near the velocities of the only two known galaxies with  $\rho < 1$  Mpc: ESO 238-G05 ( $v_{gal}$ ,  $D_{gal}$ ,  $\rho=706$ , 5.9, 616) and ESO 149-G03 ( $v_{gal}$ ,  $D_{gal}$ ,  $\rho=594$ , 3.3, 895). No absorption is seen, and the  $\rho/D_{gal}$  ratio is high enough only for ESO 238-G05 to list it in Table 3.

*MCG+10-16-111.* – This is a relatively low redshift ( $v_{gal}=8124$   $\text{km s}^{-1}$ ) Seyfert galaxy that lies in the direction of several galaxy groups. Thus, *NED* includes 94 galaxies with  $v_{gal}$  between 400 and 6000  $\text{km s}^{-1}$  and impact parameter  $< 1$  Mpc (26 of which are listed in the RC3). For the discussion below, these are divided into several groupings, based on their group membership, velocity, and position relative to MCG+10-16-111. With nine  $\text{Ly}\alpha$  lines at  $v < 5500$   $\text{km s}^{-1}$ , this sightline is the most complicated in our sample. Bowen et al. (2002) originally observed the AGN and discussed the detections. They also included an image that shows several of the galaxies near MCG+10-16-111. However, our interpretation of the associations between the  $\text{Ly}\alpha$  absorptions and these galaxies differs in some details from that presented by Bowen et al. (2002).

Five of the galaxies have  $v_{gal}=400\text{--}900$   $\text{km s}^{-1}$ . One of these is the large galaxy NGC 3556 ( $v_{gal}$ ,  $D_{gal}$ ,  $\rho=695$ , 25.8, 462). This is the galaxy most likely associated with the  $\text{Ly}\alpha$  line at 942  $\text{km s}^{-1}$  (see first panel for MCG+10-16-111, Fig. 8(25)). We further list a non-detection for UGC 6249 ( $v_{gal}$ ,  $D_{gal}$ ,  $\rho=1058$ , 8.1, 620), the only other galaxy with  $v \sim 1000$  and  $\rho/D_{gal} < 125$ . We choose to associate the detection with NGC 3556 even though the difference in velocity between with the absorber is smaller for UGC 6249, because NGC 3556 is much larger and has much smaller impact parameter.

Twelve galaxies with velocities between 1000 and 1500  $\text{km s}^{-1}$  are members of the LGG 244 group ( $\langle v \rangle = 1230$   $\text{km s}^{-1}$ ) and have  $\rho < 1$  Mpc. The sightline does not pass between the galaxies of this group, however; the group galaxy with the smallest impact parameter is CGCG 291-76 ( $\rho=616$  kpc). There is no  $\text{Ly}\alpha$  line with  $v_{gal}$  in the velocity range spanned by



the galaxies in LGG 244, so a non-detection is listed for this group in Table 3.

The sightline also goes through the LGG 234 group ( $\langle v \rangle = 1692 \text{ km s}^{-1}$ ), which has thirty galaxies with  $\rho < 1 \text{ Mpc}$ . The ones included in the RC3 are shown by filled squares in the LGG 234 panel of Fig. 8(26). Most of these group galaxies are small. Bowen et al. (2002) associated the strong Ly $\alpha$  line seen at  $1654 \text{ km s}^{-1}$  with NGC 3619 ( $v_{gal}$ ,  $D_{gal}$ ,  $\rho = 1542, 21.2, 145$ , larger of the two filled squares at  $\rho < 200 \text{ kpc}$ ), which is the nearest large group galaxy. There are also seven dwarfs ( $D_{gal} < 5 \text{ kpc}$ ) near NGC 3619 with impact parameters ranging from 94 to 248 kpc, as well as UGC 6304 ( $v_{gal}$ ,  $D_{gal}$ ,  $\rho = 1762, 11.3, 163$ , smaller filled square with  $\rho < 200 \text{ kpc}$ ). NGC 3619 and UGC 6304 lie in opposite directions from MCG+10-16-111, and have velocity differences of 112 and  $-108 \text{ km s}^{-1}$  with the absorption lines, so there is no real reason to preferentially associate either galaxy with the absorption line. In Table 3 the Ly $\alpha$  line at  $1654 \text{ km s}^{-1}$  is listed as generally associated with the LGG 234 group.

The two absorption lines at  $2022$  and  $2136 \text{ km s}^{-1}$  are listed under NGC 3625 ( $v_{gal}$ ,  $D_{gal}$ ,  $\rho = 1966, 18.1, 190$ ) and NGC 3613 ( $v_{gal}$ ,  $D_{gal}$ ,  $\rho = 2054, 35.3, 41$ ). Both galaxies are members of the LGG 232 group. It is likely that at least one of the two lines is associated with NGC 3613, which has the fourth smallest impact parameter for any galaxy in our sample. It is quite possible that both lines originate in the NGC 3613 halo, but there is no a-priori reason to exclude associating one with NGC 3625. Other, smaller group members lie at  $203 \text{ kpc}$  (UGC 6344) and  $506 \text{ kpc}$  (NGC 3669). In addition there are many dwarfs with impact parameter  $< 1 \text{ Mpc}$ .

In addition to the three galaxy groups listed above, there are several more galaxies with velocities between  $2500$  and  $7000 \text{ km s}^{-1}$ . Table 3 includes UGC 6335 ( $v_{gal}$ ,  $D_{gal}$ ,  $\rho = 2927, 20.6, 957$ ), CGCG 291-61 ( $v_{gal}$ ,  $D_{gal}$ ,  $\rho = 3188, 14.4, 367$ ), and MCG+10-16-118 ( $v_{gal}$ ,  $D_{gal}$ ,  $\rho = 5357, 16.6, 208$ ). The last two of these can be associated with Ly $\alpha$  lines at  $3113$  and  $5363 \text{ km s}^{-1}$ , while the other one yields a non-detection. Figure 8 includes a panel for the  $3113 \text{ km s}^{-1}$  Ly $\alpha$  line (Fig. 8(28)), but not for the one at  $5363 \text{ km s}^{-1}$ , as it has  $v > 5000 \text{ km s}^{-1}$ .

Finally, there are three more features that might be Ly $\alpha$  at  $3541, 3792$  and  $4043 \text{ km s}^{-1}$ , even though there are no galaxies known with such velocities within  $2.5 \text{ Mpc}$ . These are  $3\text{--}5\sigma$  detections, but they seem secure, unless they are blueshifted absorption lines intrinsic to MCG+10-16-111 ( $v = 8124 \text{ km s}^{-1}$ ).

*MRC 2251–178.* – This target is surrounded by three galaxies with  $v_{gal} \sim 3270 \text{ km s}^{-1}$ , lying toward the south (ESO 603-G27,  $v_{gal}$ ,  $D_{gal}$ ,  $\rho = 3267, 15.6, 322$ ), north (ESO 603-IG23,  $v_{gal}$ ,  $D_{gal}$ ,  $\rho = 3282, 12.5, 412$ ), and east (MCG–3-58-13,  $v_{gal}$ ,  $D_{gal}$ ,  $\rho = 3271, 10.0, 846$ ). A two-component Ly $\alpha$  line is present at  $3212$  and  $3046 \text{ km s}^{-1}$ , previously listed by Penton et al. (2004). In Table 3 these are listed as associated with the nearest two galaxies, while an

upper limit is given for MCG–3-58-13. The two associations are shown in a single panel in Fig. 8(33), since it is not obvious which line should go with which galaxy. Danforth et al. (2006) claimed a  $29 \pm 16$  mÅ O VI absorber at  $3205 \text{ km s}^{-1}$ , but we cannot confirm this, instead setting an upper limit of 27 mÅ. As can be seen from Fig. 2, the wiggle in the spectrum that Danforth et al. (2006) probably identified as O VI  $\lambda 1031.926$  is more likely to be due to the FUSE detector flaw. We cannot actually check this, since Danforth et al. (2006) do not show their version of the data.

ESO 603-G31 ( $v_{gal}$ ,  $D_{gal}$ ,  $\rho=2271$ , 9.1, 422) has an associated Ly $\alpha$  line at  $2265 \text{ km s}^{-1}$ . This Ly $\alpha$  line was listed as two detections by Penton et al. (2004), though the rms is not high enough to justify splitting this absorption line. There is also a  $3\sigma$  feature that can be interpreted as O VI  $\lambda 1037.617$  at  $2283 \text{ km s}^{-1}$ . Unfortunately, the corresponding O VI  $\lambda 1031.926$  line is hidden by geocoronal O I\* emission, which is present even in the orbital-night only data. This feature cannot be Ly $\beta$  at higher velocity, as there is no corresponding Ly $\alpha$  line, so O VI is the most likely interpretation. Danforth et al. (2006) did not list this feature.

Finally, there is a feature (also listed by Penton et al. 2004) that is best interpreted as a weak Ly $\alpha$  line at  $4371 \text{ km s}^{-1}$ . The nearest galaxy with similar velocity (NGC 7381,  $v_{gal}=4521 \text{ km s}^{-1}$ , see Fig. 8(34)) has high impact parameter: 2470 kpc.

*Mrk 9.* – Several galaxies in the group LGG 143 ( $\langle v \rangle = 3420 \text{ km s}^{-1}$ ) lie within 1 Mpc of this sightline: UGC 3943 ( $v_{gal}$ ,  $D_{gal}$ ,  $\rho=3527$ , 24.8, 422), UGC 3897 ( $v_{gal}$ ,  $D_{gal}$ ,  $\rho=3529$ , 19.4, 877), UGC 3885 ( $v_{gal}$ ,  $D_{gal}$ ,  $\rho=3809$ , 15.3, 904) and UGC 3855 ( $v_{gal}$ ,  $D_{gal}$ ,  $\rho=3167$ , 29.2, 950). No absorption is identified, although no Ly $\alpha$  data is available and Ly $\beta$  at the velocities of these galaxies would be hidden by Galactic H<sub>2</sub>. Absorption is also absent near  $1092 \text{ km s}^{-1}$ , the velocity of UGC 4121 ( $\rho=895$  kpc).

*Mrk 106.* – This sightline passes within a few hundred kpc of the group GH 44 ( $\langle v \rangle = 619$ ). Table 3 includes UGC 4879 ( $v_{gal}$ ,  $D_{gal}$ ,  $\rho=600$ , 2.8, 266), and NGC 2841 ( $v_{gal}$ ,  $D_{gal}$ ,  $\rho=638$ , 13.9, 453), which is the nearest large galaxy in the group. The RC3 includes many other small ( $D_{gal} < 5$  kpc) group galaxies with  $\rho < 1$  Mpc. Unfortunately, any possible Ly $\beta$  absorption is hidden in Galactic O I\* emission, which is still present in the orbital-night-only data, while any O VI is hidden by what appears to be Ly $\beta$  at  $2407 \text{ km s}^{-1}$ .

If there are any H I, O VI and C III absorption lines associated with CGCG 265–14 ( $v_{gal}$ ,  $D_{gal}$ ,  $\rho=3334$ , 13.1, 772) or UGC 4984 ( $v_{gal}$ ,  $D_{gal}$ ,  $\rho=3386$ , 15.5, 881), they are invisible, as they are all hidden by Galactic lines.

A feature is seen at  $1033.94 \text{ \AA}$  that is best interpreted as intergalactic Ly $\beta$  at  $2407 \text{ km s}^{-1}$ , although it could possibly be O VI  $\lambda 1031.926$  at  $586 \text{ km s}^{-1}$ . A spectrum containing  $1220 \text{ \AA}$  is needed to resolve this issue. UGC 4800 ( $v_{gal}=2433 \text{ km s}^{-1}$ ) has similar velocity, and is

included in Table 3, even though its impact parameter is as large as 1030 kpc.

*Mrk 110.* – There is a FUSE spectrum for this target, but it has an S/N ratio of about 1, so it is not useful. The *STIS*-G140M spectrum shows two clear and one possible features. The clearest feature is almost certainly  $\text{Ly}\alpha$  at  $3579 \text{ km s}^{-1}$ . The nearest galaxy with similar velocity is UGC 4984 ( $v_{\text{gal}}=3386 \text{ km s}^{-1}$ ), but it has a very large impact parameter ( $\rho=1975 \text{ kpc}$ ). UGC 4934 could have smaller impact parameter ( $\sim 1400 \text{ kpc}$ ), if its velocity were like that of the absorber. There is also a feature at the wavelength where the corresponding Si III line is expected. However, this is more likely to be another  $\text{Ly}\alpha$  line at  $1297 \text{ km s}^{-1}$ . The nearest galaxy with known velocity within  $200 \text{ km s}^{-1}$  is UGC 5354, which has impact parameter 1700 kpc.

There is one further possible feature, which could be a broad, but shallow line at  $2247 \text{ km s}^{-1}$ . However, it is only  $2.5\sigma$  and we do not consider it to be real.

There is no detectable absorption near  $638 \text{ km s}^{-1}$ , the velocity of NGC 2841, which has an impact parameter of only 144 kpc. This was previously reported by Côté et al. (2005). However, the detection limit for this line is only  $108 \text{ m}\text{\AA}$ , because of the damping wings of the Galactic  $\text{Ly}\alpha$  absorption.

*Mrk 205.* – Mrk 205 lies behind the disk of the nearby galaxy NGC 4319 ( $v_{\text{gal}}=1357 \text{ km s}^{-1}$ ). A strong  $\text{Ly}\alpha$  line is detected at  $1289 \text{ km s}^{-1}$ . By itself the  $\text{Ly}\alpha$  spectrum suggests two components, but this must be due to some hot pixels near  $1260 \text{ km s}^{-1}$ , since the  $\text{Ly}\beta$  absorption shows a single saturated component. There is also absorption in many other high- and low-ionization species, including C IV, Si IV, C III, Si III, N II, S III, O I, Si II, C II, N I, Al II and Fe II, as well as  $\text{H}_2$ . O VI and N V are not detected, however, although the O VI  $\lambda 1031.926$  line would be hidden by Galactic C II, and the O VI  $\lambda 1037.617$  line is near geocoronal O I\* emission, so the  $37 \text{ m}\text{\AA}$  upper limit is derived from the night-only data. Bowen & Blades (1993) originally reported on the Mg II absorption from NGC 4319, but the full *STIS*-E140M and FUSE spectra of this sightline have not yet been analyzed in detail.

NGC 4319 is not the only galaxy with low impact parameter to Mrk 205, as can be seen from the open square in Fig. 8(38). For instance, three other large galaxies and two dwarfs have impact parameters  $<200 \text{ kpc}$ : NGC 4291 ( $v_{\text{gal}}=1757 \text{ km s}^{-1}$ ) is at 51 kpc, NGC 4386 at 136 kpc, NGC 4363 at 148 kpc, Mailyan 68 at 71 kpc and CGCG 352-27 at 78 kpc. Based on their velocities, the large galaxies with impact parameter  $<1 \text{ Mpc}$  can be divided into two groups: four galaxies with  $v_{\text{gal}}$  between  $1187$  and  $1357 \text{ km s}^{-1}$  and ten galaxies with  $v_{\text{gal}}=1570$  to  $1980 \text{ km s}^{-1}$ . The latter are all members of the GH 107 group, so a second entry for Mrk 205 is given in Table 3 for the velocity of NGC 4291, the group member with the lowest impact parameter. This velocity is sufficiently different from that of the  $\text{Ly}\alpha$

lines that any line associated with NGC 4291 would appear in the velocity range  $\sim 1500$  to  $2000 \text{ km s}^{-1}$ . Unfortunately, the only upper limits that can be set are for  $\text{Ly}\alpha$  and  $\text{O VI } \lambda 1031.926$ .

A third entry (an upper limit) for Mrk 205 is given in Table 3 for UGC 7226 ( $v_{gal}=2267 \text{ km s}^{-1}$ ), which is not part of the GH 107 group.

*Mrk 279.* – This is a sightline with very high S/N –  $\sim 20$  at  $\lambda < 1000$ ,  $\sim 40$  for  $1000$ – $1180 \text{ \AA}$ , and  $\sim 25$  at  $\lambda > 1200 \text{ \AA}$ . There are three large galaxies with  $v_{gal} < 6000 \text{ km s}^{-1}$ , but all have  $\rho > 600 \text{ kpc}$ : UGC 8737 ( $1873 \text{ km s}^{-1}$ ), NGC 5832 ( $453 \text{ km s}^{-1}$ ), FGC 1680 ( $3865 \text{ km s}^{-1}$ ). No  $\text{Ly}\alpha$  or  $\text{O VI}$  are detected at  $v_{gal} < 6000 \text{ km s}^{-1}$ . Penton et al. (2000) listed six significant and two  $< 3\sigma$  detections at  $v_{gal}=5000$ – $8000 \text{ km s}^{-1}$ , based on a *GHR*S spectrum. However, *STIS*-E140M data show that the claimed detections at  $6372$ ,  $6445$  and  $6925 \text{ km s}^{-1}$  are much more likely to be intrinsic Si III lines, as there are clear  $\text{Ly}\alpha$  and C III absorptions at the corresponding velocities. Their  $5631 \text{ km s}^{-1}$   $\text{Ly}\alpha$  line is really NV in complex C (see Fox et al. 2004), while the  $5246$  and  $5486 \text{ km s}^{-1}$  features are not seen in the *STIS* spectrum. This leaves just one confirmed  $\text{Ly}\alpha$ , at  $7779 \text{ km s}^{-1}$ .

*Mrk 290.* – This is a sightline with five groups of entries in Table 3. The galaxies with similar velocities usually lie in different directions, while in general their velocities differ by a few hundred  $\text{km s}^{-1}$ . Therefore, all galaxies are listed separately in Table 3.

To the north of Mrk 290 lie several galaxies with  $v_{gal} \sim 700 \text{ km s}^{-1}$ , which are in the LGG 396 group. NGC 5963 ( $v_{gal}$ ,  $D_{gal}$ ,  $\rho=656$ ,  $12.3$ ,  $307$ ) is the nearest. It is associated with a  $\text{Ly}\beta$  line seen at  $720 \text{ km s}^{-1}$  in the orbital-night-only data (see filled square in Fig. 8(39)). Four other large group galaxies with similar velocity are listed in Table 3, though all have impact parameters  $> 734 \text{ kpc}$  (NGC 5907, NGC 5879, NGC 5866B, NGC 5866; see open squares with plusses in Fig. 8(39)). Eight dwarfs (not listed in Table 3) have impact parameters between  $307$  and  $550 \text{ kpc}$ , but the association of the  $\text{Ly}\beta$  line with NGC 5963 is comparatively secure.

There is no  $\text{Ly}\alpha$  data for the velocity of NGC 5981 ( $v_{gal}$ ,  $D_{gal}$ ,  $\rho=1764$ ,  $22.5$ ,  $725$ ), while  $\text{Ly}\beta$ , and  $\text{O VI}$  are hidden by Galactic  $\text{O VI}$  and  $\text{H}_2$ , respectively,

This sightline also passes within  $0.5$  of the group GH 158 (also known as LGG 402), which has  $\langle v \rangle = 2882 \text{ km s}^{-1}$ . In the RC3 the nearest of these group galaxies is NGC 5987 at  $424 \text{ kpc}$ , which has a very large diameter ( $D_{gal}=52 \text{ kpc}$ ). *NED* includes nine more small galaxies lying next to the group having velocities between  $2900$  and  $3350 \text{ km s}^{-1}$ , and impact parameters  $< 1 \text{ Mpc}$ . 2MASX J153514.22+573052.9, CGCG 297-17 and SDSS J153733.02+583446.7 are large enough ( $\rho/D_{gal} < 80$ ) to merit separate entries in Table 3. Pisano et al. (2004) obtained VLA and DRAO HI 21-cm data for the field around Mrk 290, but failed to detect HI

emission from any of the group galaxies. They also discussed a FUSE spectrum of Mrk 290, based on the first 13 ks observation. After this paper was published, another 92 ks of data was taken toward Mrk 290, which turned out to be almost three times brighter as before during the longest (54 ks) individual exposure. With these much improved data, there appears to be O VI at  $3073 \text{ km s}^{-1}$ , seen in both the O VI  $\lambda 1031.926$  and the O VI  $\lambda 1037.617$  lines, although the O VI  $\lambda 1037.617$  line only shows up as a wing in Galactic Ar I. The equivalent width given in Table 3 is double the value measured using only the positive-velocity half of the line. Unfortunately, the corresponding Ly $\beta$  line is hidden in Galactic C II, while there is no data for Ly $\alpha$ . This O VI feature thus remains rather uncertain, but it is listed under the entry for NGC 5987 ( $\rho=424 \text{ kpc}$ ).

The velocity of SDSS J153802.76+573018.3 ( $v_{gal}=3525 \text{ km s}^{-1}$ ) is similar to that of the GH 158 galaxies, but sufficiently different that this galaxy is listed separately.

The *GHR*S spectrum of this target only allows a search for Ly $\alpha$  at velocities above  $4000 \text{ km s}^{-1}$ . One weak line is found at  $4638 \text{ km s}^{-1}$ , which was included by Penton et al. (2000). The nearest known galaxies with similar velocity are NGC 5971 ( $v_{gal}$ ,  $D_{gal}$ ,  $\rho=4306$ , 29.5, 1586, triangle in Fig. 8(41)) and SBS 1533+574B ( $v_{gal}$ ,  $D_{gal}$ ,  $\rho=4287$ , 9.1, 721, open circle in Fig. 8(41)).

*Mrk 335.* – There are three Ly $\alpha$  detections at  $v<6000 \text{ km s}^{-1}$  toward this target. The two at  $1954$  and  $2286 \text{ km s}^{-1}$  were previously reported by Penton et al. (2000), based on a *GHR*S-G140M spectrum. We observed this sightline with the *STIS*-E140M, finding a similar equivalent width for the feature at  $1954 \text{ km s}^{-1}$  ( $229\pm 12 \text{ m}\text{\AA}$  versus  $229\pm 30 \text{ m}\text{\AA}$  in Penton et al.), while for the other feature we find  $114\pm 17 \text{ m}\text{\AA}$ , whereas Penton et al. (2000) quoted  $81\pm 26 \text{ m}\text{\AA}$ . The stronger Ly $\alpha$  also shows a weak Ly $\beta$  absorption, adjacent to the strong Galactic L(6-0) R(4) H $_2$  line at  $1032.520 \text{ \AA}$ . The  $2\sigma$  feature at  $4268 \text{ km s}^{-1}$  that Penton et al. (2000) listed is not confirmed by the E140M spectrum, however.

The correspondence between Ly $\alpha$  absorptions and galaxies is complex for this sightline. The only simple association is for the component at  $2286 \text{ km s}^{-1}$ , which can be associated with NGC 7817 ( $v_{gal}$ ,  $D_{gal}$ ,  $\rho=2308$ , 30.4, 395, Fig. 8(44)).

For the (stronger) feature at  $1954 \text{ km s}^{-1}$ , the existence of better galaxy data than is usually the case makes the choice of association more complicated. On the other hand, as can be seen in Fig. 8(43), there are no large galaxies with low impact parameter near this velocity. This feature might be associated with NGC 7817 (see large plussed circle in Fig. 8(43)), although a  $\Delta v$  of  $355 \text{ km s}^{-1}$  would be much higher than is normally found. The only other non-dwarf galaxies with similar velocity within 1 Mpc are ESDO F538-2 ( $v_{gal}$ ,  $D_{gal}$ ,  $\rho=2175$ , 7.2, 320) and NGC 7798 ( $v_{gal}$ ,  $D_{gal}$ ,  $\rho=2404$ , 12.4, 915). For most sightlines

this is where the search would stop, and we would associate the absorption with ESDO F538-2, even though  $\Delta v=219 \text{ km s}^{-1}$ . However, van Gorkom et al. (1996) did a deep search for H I clouds near Mrk 335, and found the tiny ( $D_{gal}=0.7 \text{ kpc}$ ) dwarf [vCS96] 000254.9+195654.3 at a velocity of  $1950 \text{ km s}^{-1}$  and with impact parameter of only 78 kpc (see tiny black circle in Fig. 8(43)). As  $\rho/D_{gal}\sim 110$  for this galaxy, only a factor two larger than the value of 43 for ESO F538-2, but  $\Delta v=7 \text{ km s}^{-1}$ , Table 3 lists the absorption at  $1954 \text{ km s}^{-1}$  as being associated with [vCS96] 000254.9+195654.3, while non-detections are listed for ESDO F538-2 and NGC 7798.

In the velocity range 713 to  $1108 \text{ km s}^{-1}$  there are 17 known galaxies with impact parameter  $<1 \text{ Mpc}$ , 10 of which are included in the RC3. However, the two largest (NGC 100 and NGC 7814) have large impact parameter (814 kpc). For all other galaxies the ratio  $\rho/D_{gal}$  is larger than 90, and all have  $D_{gal}<7 \text{ kpc}$ . The smallest impact parameter (170 kpc) is for ESDO F538-1, a galaxy with  $D_{gal}=1.1 \text{ kpc}$ . UGC 47 ( $D_{gal}=3.3 \text{ kpc}$ ) has the next smallest  $\rho$  (447 kpc). No absorption feature is seen in the velocity range 700 to  $1150 \text{ km s}^{-1}$ , but there is a weak feature at  $1308 \text{ km s}^{-1}$  (lying outside the spectral range analyzed by Penton et al. 2000). However, there are no known galaxies within 1 Mpc with  $v_{gal}$  between 1150 and  $1970 \text{ km s}^{-1}$ . In Table 3 the galaxy listed for this feature is UGC 12893 ( $v_{gal}, D_{gal}, \rho=1108, 6.0, 697$ ), which has the smallest velocity difference. However, this is rather ambiguous assignment, as can be seen in Fig. 8(42).

Finally, UGC 44 is a large ( $D_{gal}=21.5 \text{ kpc}$ ) galaxy with  $v_{gal}=5936 \text{ km s}^{-1}$ , but there is no Ly $\alpha$  near that velocity, although there is a strong feature at  $6280 \text{ km s}^{-1}$ . Because of the relatively small velocity difference between this feature and the velocity of Mrk 335 itself ( $v_{gal}=7730 \text{ km s}^{-1}$ ), it is not listed in Table 3.

*Mrk 421.* – A weak but clear Ly $\alpha$  line is detected at  $3007 \text{ km s}^{-1}$  in this sightline. This detection was first reported by Penton et al. (2000). Savage et al. (2005a) showed that there is no O VI absorption at this velocity. They also studied in detail the galaxies in the field near this sightline, showing that there are no known galaxies with similar velocity within 1 Mpc, and just two dwarfs within 3.5 Mpc, one of which is HS 1059+3934 ( $v_{gal}, D_{gal}, \rho=3274, 3.8, 1041$ ).

*Mrk 477.* – Although the S/N ratio of this spectrum near O VI  $\lambda 1031.926$  is about 10, the continuum of this target shows strong fluctuations that are probably due to intrinsic emission lines, making the continuum fit uncertain. Furthermore, the SiC data are too noisy to be useful, and there is no Ly $\alpha$  data. The only measurements that generally can be made are  $\sim 40 \text{ m\AA}$  upper limits on Ly $\beta$  and O VI  $\lambda 1037.617$ .

The galaxies near this sightline come in three groups. At velocities between 750 and

950 km s<sup>-1</sup> there are many dwarfs and one substantial galaxy with large impact parameter (NGC 5866,  $v_{gal}$ ,  $D_{gal}$ ,  $\rho=769$ , 16.7, 930). The nearest dwarf (SDSS J144303.81+535457.5,  $v_{gal}$ ,  $D_{gal}$ ,  $\rho=838$ , 1.5, 138) has  $\rho/D_{gal} < 100$ , so it is included in Table 3. Six galaxies lie between 2056 and 2181 km s<sup>-1</sup> of which UGC 9452 ( $v_{gal}$ ,  $D_{gal}$ ,  $\rho=2173$ , 17.1, 278), NGC 5687 ( $v_{gal}$ ,  $D_{gal}$ ,  $\rho=2119$ , 23.1, 743) and KUG 1437+524 ( $v_{gal}$ ,  $D_{gal}$ ,  $\rho=2181$ , 9.6, 743) are included in Table 3. Finally, two of the three galaxies near 3300 km s<sup>-1</sup> are in Table 3: NGC 5751 ( $v_{gal}$ ,  $D_{gal}$ ,  $\rho=3242$ , 21.6, 419) and SBS 1436+529 ( $v_{gal}$ ,  $D_{gal}$ ,  $\rho=3389$ , 10.0, 761).

*Mrk 478.* – A strong Ly $\alpha$  line is seen at 1573 km s<sup>-1</sup> toward Mrk 478, which was included by Penton et al. (2004), although their reported equivalent width is smaller than our measurement ( $194 \pm 31$  mÅ vs  $254 \pm 14$  mÅ). Based on the equivalent and velocity width of the Ly $\alpha$  line, an  $\sim 100$  mÅ Ly $\beta$  line is expected. There indeed seems to be an 78 mÅ feature at the right place, except that it would just be a  $2\sigma$  detection. The nearest large galaxy is NGC 5727 ( $v_{gal}$ ,  $D_{gal}$ ,  $\rho=1491$ , 16.1, 645). As can be seen from the filled circle in Fig. 8(46), this is not the only possible galaxy that can be associated with the absorption line. However, it is by far the largest galaxy. Two of the smaller galaxies have  $\rho/D_{gal} < 125$  and are listed separately in Table 3: UGC 9519 ( $v_{gal}$ ,  $D_{gal}$ ,  $\rho=1692$ , 5.3, 624) and UGC 9562 ( $v_{gal}$ ,  $D_{gal}$ ,  $\rho=1253$ , 6.4, 748). However, SDSSJ144003.48+340559.6 ( $v_{gal}$ ,  $D_{gal}$ ,  $\rho=1492$ , 3.1, 605) is not included, as it is a dwarf close to NGC 5727.

A final galaxy for which a non-detection is listed in Table 3 is UGC 9540 ( $v_{gal}$ ,  $D_{gal}$ ,  $\rho=802$ , 4.3, 400). Two more similar sized galaxies with similar velocities are not listed because they have  $\rho/D_{gal} > 125$ .

*Mrk 501.* – There are two galaxies with similar velocity and impact parameter that may be associated with the Ly $\alpha$  line at 4593 km s<sup>-1</sup>: CGCG 225-6 ( $v_{gal}$ ,  $D_{gal}$ ,  $\rho=4648$ , 10.7, 517) and NGC 6257 ( $v_{gal}$ ,  $D_{gal}$ ,  $\rho=4692$ , 18.0, 521). The first of these lies to the north of Mrk 501, the second to the south. In Table 3 the Ly $\alpha$  line is listed under the larger galaxy, NGC 6257, while a non-detection is listed for CGCG 225-6. This choice is arbitrary, but it allows us to account for having one detection for two galaxies. Penton et al. (2000) also reported this absorption line. Four more galaxies have  $\rho < 1$  Mpc: UGC 10625 ( $v_{gal}$ ,  $D_{gal}$ ,  $\rho=2048$ , 11.7, 700), NGC 6239 ( $v_{gal}$ ,  $D_{gal}$ ,  $\rho=922$ , 11.3, 807), NGC 6255 ( $v_{gal}$ ,  $D_{gal}$ ,  $\rho=918$ , 15.2, 854) and NGC 6907 ( $v_{gal}$ ,  $D_{gal}$ ,  $\rho=850$ , 12.2, 895). Separate non-detection entries are given each of these.

*Mrk 509.* – A strong Ly $\alpha$  line is detected at 2545 km s<sup>-1</sup>, previously reported by Penton et al. (2000). The FUSE spectrum shows the corresponding Ly $\beta$  line. The nearest galaxy with known velocity between 2000 and 3000 km s<sup>-1</sup> is MCG-1-54-3 ( $v_{gal}=2231$  km s<sup>-1</sup>) at  $\rho=4834$  kpc, so this seems to be a clear case of an absorber in a void. However, there are five galaxies with unknown velocity that potentially could have impact parameter between

1400 and 2500 kpc, *if* their velocity is similar to that of the absorber: [RC3]A2052–1056, [RC3]A2030–0838, MCG–1-52-4, MCG–2-52-17 and MCG–2-53-13. On the other hand, the likelihood that this is actually the case is low.

*Mrk 586.* – Absorption is absent for NGC 851 ( $v_{gal}$ ,  $D_{gal}$ ,  $\rho=3111$ , 11.9, 967). On the other hand, what may be Ly $\beta$  is detected at 1464 km s<sup>−1</sup>. No Ly $\alpha$  data is available to confirm this identification, and the redshift of Mrk 586 is sufficiently high (0.1553) that it could be a higher-redshift ionic line, although the FUSE spectrum does not show evidence for a redshifted system. If it is Ly $\beta$ , the nearest galaxy with similar velocity has impact parameter >1 Mpc (NGC 864,  $v_{gal}=1560$  km s<sup>−1</sup>,  $\rho=1240$  kpc).

*Mrk 734.* – This is one of a few sightlines that passes near the center of a galaxy group with many galaxies, namely GH 78. Geller & Huchra (1983) include nine galaxies in this group, eight of which have velocities ranging from 628 to 1191 km s<sup>−1</sup>, with one standing out at 1726 km s<sup>−1</sup>. Without this last one, the average velocity of the group galaxies is 921 km s<sup>−1</sup>. The galaxy with the lowest impact parameter to Mrk 734 is NGC 3666 ( $v_{gal}$ ,  $D_{gal}$ ,  $\rho=1062$ , 12.7, 133), while the other seven original group galaxies have  $\rho=230$  to 603 kpc. *NED* includes another 13 small galaxies inside the GH 78 velocity range that can be considered part of the group.

Although the FUSE spectrum of this target has relatively low S/N ratio ( $\sim 5.5$ ), two Ly $\beta$  absorption lines are clearly detected, at 478 and 757 km s<sup>−1</sup>. Ly $\gamma$  may also be present at 745 km s<sup>−1</sup>. There is a  $2\sigma$  feature that may be OVI at  $\sim 720$  km s<sup>−1</sup>, but the S/N ratio of the spectrum is insufficient to confirm it. The two Ly $\alpha$  lines are listed as generic group detections in Table 3.

There are four other galaxies near Mrk 734 that are not in the GH 78 group for which non-detections are listed separately: 2MASX J112139.77+112924.2 ( $v_{gal}$ ,  $D_{gal}$ ,  $\rho=5944$ , 6.2, 388), SDSS J111938.66+112643.3 ( $v_{gal}$ ,  $D_{gal}$ ,  $\rho=3054$ , 5.3, 500), and IC 2763 ( $v_{gal}$ ,  $D_{gal}$ ,  $\rho=1574$ , 10.4, 617).

*Mrk 771.* – This sightline is included in the sample because the *STIS*-G140M data are good, although the FUSE spectrum has low S/N (4.6).

There are three similar-strength Ly $\alpha$  absorptions, at 1184, 1891 and 2557 km s<sup>−1</sup>. All three were reported by Penton et al. (2004). The 2557 km s<sup>−1</sup> line was also reported by Côté et al. (2005). It can clearly be associated with UGC 7697 ( $v_{gal}$ ,  $D_{gal}$ ,  $\rho=2536$ , 24.6, 139; see Côté et al. 2005), which is the only galaxy with velocity between 2000 and 3000 km s<sup>−1</sup> and impact parameter <1 Mpc (filled circle in Fig. 8(53)).

There are two galaxies with  $v_{gal}$  between 1700 and 2100 km s<sup>−1</sup> (see Fig. 8(52)). The



small galaxy KUG 1229+207 ( $v_{gal}$ ,  $D_{gal}$ ,  $\rho$ =1921, 6.5, 184) has small impact parameter, while the large galaxy NGC 4450 ( $v_{gal}$ ,  $D_{gal}$ ,  $\rho$ =1956, 23.4, 851) is more distant. Table 3 lists the Ly $\alpha$  absorption as associated with KUG 1229+207.

The most difficult to associate is the 1184 km s<sup>-1</sup> absorption. There are five large galaxies in the LGG 289 group that have  $v_{gal}$  within 250 km s<sup>-1</sup> from this detection ( $v_{gal}$ =1027–1403 km s<sup>-1</sup>, open symbols in Fig. 8(51)). They have  $\rho$ =502, 666, 807, 846 and 962 kpc. The nearest galaxy (with  $\Delta v_{gal}$ =259 km s<sup>-1</sup>), however, is IC 3436 ( $v_{gal}$ ,  $D_{gal}$ ,  $\rho$ =925, 1.8, 183), but this is a small dwarf not in the LGG 289 group. Table 3 lists the absorption line as associated with NGC 4561 (the  $\rho$ =502 kpc group galaxy), but this is one of the most uncertain associations in the table.

*Mrk 817.* – This sightline passes through the edge of the GH 144 group ( $\langle v \rangle$ =1967 km s<sup>-1</sup>), with the closest large galaxy being UGC 9391 ( $v_{gal}$ ,  $D_{gal}$ ,  $\rho$ =1921, 14.5, 308). Three other large galaxies are listed in the RC3 with velocities between 1900 and 2300 km s<sup>-1</sup> and  $\rho$ <1 Mpc (UGC 9477, NGC 5667 and NGC 5678). *NED* gives another six smaller such galaxies, two of which have impact parameter <308 kpc. The nearest is the dwarf PWWF J1437+5905 ( $v_{gal}$ ,  $D_{gal}$ ,  $\rho$ =2233, 1.0, 191) which was identified by Pisano et al. (2004) in a VLA HI map of the field around Mrk 817. A somewhat larger dwarf (SDSS J143903.89+544717.6,  $v_{gal}$ ,  $D_{gal}$ ,  $\rho$ =2134, 4.0, 202) has similar impact parameter.

We find four Ly $\alpha$  features in this sightline, at 1922, 2085, 4670 and 5081 km s<sup>-1</sup> (confirming the entries in the list of Penton et al. (2000)). The first two can be associated with the GH 144 group, and are listed under the entries for SDSS J143903.89+544717.6 and UGC 9391 (see Fig. 8(54)/(55)), with velocities of 1922 and 2085 km s<sup>-1</sup>. We find accompanying Ly $\beta$  absorption at 2081 km s<sup>-1</sup>.

For the feature at 4670 km s<sup>-1</sup> we cannot find any galaxies with similar velocity at impact parameter <5 Mpc. This feature is therefore listed as intergalactic in Table 3.

The feature at 5081 km s<sup>-1</sup> has extremely strong O VI associated with it, and it is likely to be gas expanding away from Mrk 817 at 4500 km s<sup>-1</sup>.

*Mrk 876.* – There are three Ly $\alpha$  features at  $v$ <6000 km s<sup>-1</sup> in this sightline. The strong one at 3481 km s<sup>-1</sup> is associated with UGC 10294 ( $v_{gal}$ ,  $D_{gal}$ ,  $\rho$ =3516, 27.6, 282; Fig. 8(58)). The corresponding Ly $\beta$  line contaminates Galactic O VI  $\lambda$ 1037.617, which is indicated by the fact that the  $N_a(v)$  profiles of the two Galactic O VI lines do not match (see Wakker et al. 2003). Ly $\gamma$  may be seen at the 2 $\sigma$  level. A 4 $\sigma$  (18 $\pm$ 4 $\pm$ 7 mÅ) feature is also present where redshifted O VI  $\lambda$ 1031.926 is expected, but the corresponding O VI  $\lambda$ 1037.617 line is hidden by H<sub>2</sub> absorption. Danforth et al. (2006) gave an upper limit of 16 mÅ for associated O VI absorption. There are only two other galaxies near this velocity: NGC 6135, and UGC 10376,

but they have impact parameters of 630 and 799 kpc. Note that the RC3 gives a velocity of  $822 \text{ km s}^{-1}$  for UGC 10376, but according to Schneider et al. (1992) it is  $3246 \text{ km s}^{-1}$ .

The other two  $\text{Ly}\alpha$  lines, at  $936$  and  $1109 \text{ km s}^{-1}$ , appear to be associated with NGC 6140 ( $v_{gal}, D_{gal}, \rho=910, 27.1, 206$ ) the only large galaxy with velocity between  $700$  and  $1375 \text{ km s}^{-1}$  within  $1 \text{ Mpc}$  (see Fig. 8(57)). The four dwarf galaxies in this velocity range all have much larger impact parameters: UGC 10369 ( $v_{gal}, D_{gal}, \rho=998, 5.9, 493$ ), UGC 10194 ( $v_{gal}, D_{gal}, \rho=870, 6.9, 573$ ), CGCG319-39 ( $v_{gal}, D_{gal}, \rho=933, 2.9, 763$ ) and IC 1218 ( $v_{gal}, D_{gal}, \rho=1109, 4.8, 767$ ). Non-detections are listed in Table 3 for the first of these two galaxies, as they have  $\rho/D_{gal}<125$ .

The line at  $1109 \text{ km s}^{-1}$  is unusually narrow ( $b=14 \text{ km s}^{-1}$ ,  $\text{FWHM}=23 \text{ km s}^{-1}$ ), but its identification as  $\text{Ly}\alpha$  is fairly secure, since there are no other known intergalactic absorber systems that would produce an ionic line at its wavelength.

Using a G140M *STIS* spectrum ( $30 \text{ km s}^{-1}$  resolution) Côté et al. (2005) reported a strength of  $390 \text{ m}\text{\AA}$  at  $935 \text{ km s}^{-1}$  for the  $\text{Ly}\alpha$  absorber, Shull et al. (2000) gave  $324\pm52 \text{ m}\text{\AA}$  at  $958 \text{ km s}^{-1}$ , whereas we find  $476\pm14 \text{ m}\text{\AA}$  at  $936 \text{ km s}^{-1}$  from our *STIS*-E140M data. The  $\text{Ly}\beta$  line corresponding to the  $\text{Ly}\alpha$  at  $936 \text{ km s}^{-1}$  is strongly contaminated by two-component  $\text{H}_2$  L(6-0) R(3)  $\lambda 1028.985$  absorption. However, the S/N ratio in this sightline is so high (33) that a good (two-component)  $\text{H}_2$  model can be made (see Wakker 2006), which fits all uncontaminated  $\text{H}_2$  lines extremely well. This shows that the feature contains  $79\pm6 \text{ m}\text{\AA}$  of  $\text{Ly}\beta$ , though the systematic error is large ( $33 \text{ m}\text{\AA}$ ). Shull et al. (2000) reported  $110\pm50 \text{ m}\text{\AA}$  for this line, but that clearly includes the  $\text{H}_2$  absorption.

In addition, there is O VI  $\lambda 1031.926$  absorption, centered at  $945 \text{ km s}^{-1}$ . This line is contaminated by  $\text{H}_2$  L(6-0) P(4) at  $1035.7830 \text{ \AA}$ , but the very good  $\text{H}_2$  model does not account for all the absorption near this wavelength, unlike what is the case for all other  $J=4$   $\text{H}_2$  lines. Danforth et al. (2006) reported this O VI absorption, but their  $\text{H}_2$  model is not as precise. Consequentially, they listed an equivalent width that is too high ( $26\pm7 \text{ m}\text{\AA}$ ). We measure it as  $17\pm4\pm8 \text{ m}\text{\AA}$ .

*Mrk 926.* – This is the only sightline in the sample with only one known galaxy with  $v_{gal}=400\text{--}6000 \text{ km s}^{-1}$  and impact parameter  $<1 \text{ Mpc}$ : the dwarf SDSS J230556.27–100257.0 ( $v_{gal}, D_{gal}, \rho=2304, 2.6, 697$ ). Because  $\rho/D>125$  this galaxy is not listed in Table 3. There are also no  $\text{Ly}\alpha$  lines with  $v<5000 \text{ km s}^{-1}$ , as was previously noted by Penton et al. (2004). The FUSE spectrum has low S/N and thus contributes no useful pathlength to the  $\text{Ly}\beta$  and O VI search.

*Mrk 1095.* – Few galaxies lie near this target. UGC 3303 ( $v_{gal}, D_{gal}, \rho=522, 6.4, 571$ ) has low velocity, but the only line for which a limit can be set is O VI  $\lambda 1031.926$ .

UGC 3258 ( $v_{gal}$ ,  $D_{gal}$ ,  $\rho$ =2821, 8.6, 999) has large impact parameter, and no absorption is found. The only probable Ly $\alpha$  feature is found at 4048 km s<sup>-1</sup>, and this was listed by Penton et al. (2000). There are some galaxies near 4000 km s<sup>-1</sup>, but they have large impact parameter. The smallest are 834 and 836 kpc for two tiny galaxies ([OHG88] 0510-0037, [OHG88] 0510-0036,  $D_{gal}$ =1.8 kpc). The nearest large galaxy with  $|\Delta v| < 300$  km s<sup>-1</sup> is UGC 3262 ( $v_{gal}$ =4285 km s<sup>-1</sup>) at 1306 kpc.

*Mrk 1383.* – This sightline is one of the few that passes between galaxies in a galaxy group (LGG 386 or GH 145). The group has  $\langle v \rangle = 1701$  km s<sup>-1</sup>, and 32 galaxies have impact parameter  $< 1$  Mpc. No absorption is seen near this velocity, however. The closest of nine group galaxies in the RC3 is UGC 9348, with  $\rho = 622$  kpc. *NED* includes seven small ( $D_{gal} < 3$  kpc) galaxies with smaller impact parameter (as low as 236 kpc for 2dF-GRS N413Z236), as well as the larger galaxy SDSS J143229.08+001734.4 ( $D_{gal}$ =15.4 kpc) at 602 kpc. Another 13 galaxies found only in *NED* have impact parameter  $> 622$  kpc.

*Mrk 1513.* – Like Penton et al. (2004), we find no Ly $\alpha$  absorption below 5000 km s<sup>-1</sup>. The only galaxy with impact parameter less than 1 Mpc is UGC 11782 at 412 kpc. This lack of galaxies is only partly the result of the target’s low galactic latitude – there are relatively few galaxies in this region of the sky, which is in the direction diametrically opposite to the Virgo cluster.

*MS 0700.7+6338.* – Like VII Zw 118, this sightline passes through the LGG 140 group ( $\langle v \rangle = 4404$  km s<sup>-1</sup>). The closest group galaxy is UGC 3660 ( $v_{gal}$ ,  $D_{gal}$ ,  $\rho$ =4262, 31.0, 356). Strong Ly $\beta$  and probable C III absorption is seen at 4322 km s<sup>-1</sup>, but O VI is absent. In Table 3 this system is listed as generally associated with the group. There is one other galaxy within 1 Mpc that is not in the group (UGC 3685,  $v_{gal}$ ,  $D_{gal}$ ,  $\rho$ =1797, 25.9, 941). However, near this velocity only O VI  $\lambda 1037.617$  is not blended with interstellar O VI, O I or H<sub>2</sub>.

*NGC 985.* – NGC 985 passes through the southern outskirts of the LGG 71 galaxy group, which has  $\langle v \rangle = 1406$  km s<sup>-1</sup>. Forty eight group galaxies have impact parameter less than 1 Mpc (see Fig. 8(61)). Eleven of these are included in the RC3, and eight of these have diameter  $> 10$  kpc. Their velocities range from 1145 to 1781 km s<sup>-1</sup>, although the velocity range for the large ( $D_{gal} > 10$  kpc) galaxies is smaller (1241–1534 km s<sup>-1</sup>). Of these, NGC 988 ( $v_{gal}$ =1504 km s<sup>-1</sup>) lies much closer than other group galaxies ( $\rho$ =175 kpc, vs  $> 394$  kpc for the rest, see large open square in Fig. 8(61)). No Ly $\alpha$  line is within the velocity range spanned by the velocities of the group galaxies, so Table 3 lists a generic group non-detection.

There are two galaxies with higher velocity: DDO 23 ( $v_{gal}$ ,  $D_{gal}$ ,  $\rho$ =2110, 15.3, 993) and Mrk 1042 ( $v_{gal}$ ,  $D_{gal}$ ,  $\rho$ =2133, 3.1, 996). Two weak (3.5 and 3.2 $\sigma$ ), broad absorption lines may be present at velocities of 1924 and 2183 km s<sup>-1</sup>. These were previously reported

by Bowen et al. (2002). Both are rather shallow (10% depth) and the one at  $1924 \text{ km s}^{-1}$  may not be real. It is hard to justify an association with NGC 988 or the LGG 71 group, as proposed by Bowen et al. (2002). NGC 988 has low impact parameter, but the velocity difference is large ( $420 \text{ km s}^{-1}$ ). This is much larger than in any other case with impact parameter  $<1 \text{ Mpc}$ , for which we can always find a galaxy within  $320 \text{ km s}^{-1}$ . The group galaxy with the velocity closest to that of the absorber is called NGC 1052-[PBF2005]GC47 ( $v_{gal}=1781 \text{ km s}^{-1}$ ) in *NED* but it is very small. The nearest (in velocity) substantial group galaxy is NGC 991 ( $v_{gal}, D_{gal}, \rho=1534, 12.9, 475$ ), for which  $\Delta v=390$  and  $649 \text{ km s}^{-1}$ . The velocities of the absorptions resemble those of DDO 23 better (differences 186 and  $78 \text{ km s}^{-1}$ ), but the impact parameter to this galaxy is large. In Table 3 both features are listed under DDO 23, but this is by no means a clear-cut association and may be the most debatable one in the table.

*PG 0804+761.* – Penton et al. (2004) and Côté et al. (2005) separately observed this sightline with the *STIS*-G140M. grating. Both reported the  $\text{Ly}\alpha$  line at  $1537 \text{ km s}^{-1}$ , though there is disagreement about the equivalent width. Integrating from 1420 to  $1680 \text{ km s}^{-1}$ , we find  $114 \pm 14 \text{ m}\text{\AA}$ . Côté et al. (2005) gave  $260 \text{ m}\text{\AA}$ , while Penton et al. (2004) split the line into two components, with a total equivalent width of  $139 \pm 35 \text{ m}\text{\AA}$ . The evidence for a two-component absorption line is weak, but if it is a single component, the line would have a large, but not extreme width ( $178 \text{ km s}^{-1}$ , see Sect. 3.2). This  $\text{Ly}\alpha$  line is associated with UGC 4238 ( $v_{gal}, D_{gal}, \rho=1544, 16.3, 155$ ; filled circle in Fig. 8(63)). Two other galaxies with similar velocity are included in Table 3, but they have much larger impact parameter (NGC 4466,  $v_{gal}, D_{gal}, \rho=1416, 8.4, 839$ ) and NGC 2591 ( $v_{gal}, D_{gal}, \rho=1323, 18.5, 907$ ).

A second  $\text{Ly}\alpha$  line is seen at  $1144 \text{ km s}^{-1}$ . Penton et al. (2004) also reported this feature. At the wavelength where the corresponding O VI  $\lambda 1031.926$  absorption is expected there is a  $47 \text{ m}\text{\AA}$  feature. Danforth et al. (2006) listed this as a  $36 \pm 10 \text{ m}\text{\AA}$  O VI  $\lambda 1031.926$  absorber. However, it is much more likely that this is Galactic C II at  $-140 \text{ km s}^{-1}$ , associated with HVC complex A, whose edge lies about 1 degree away (see Wakker 2001). The strength of the C II line would typically correspond to a total hydrogen column density of about  $2 \times 10^{17} \text{ cm}^{-2}$ . Weak H I absorption, on the order of a few  $10^{16} \text{ cm}^{-2}$  is seen in the FUSE spectrum, so this gas appears to be mostly ionized, as is expected at these column densities. An association between this component and a galaxy is somewhat uncertain, as can be seen from the symbols in Fig. 8(62). It could be associated with UGC 4238 ( $v_{gal}, D_{gal}, \rho=1544, 16.3, 155 \text{ kpc}$ ), but  $\Delta v$  is too large ( $400 \text{ km s}^{-1}$ ). For the same reason, we do not associate the  $\text{Ly}\alpha$  with UGC 4527 ( $v_{gal}, D_{gal}, \rho=721, 4.7, 438$ ), since  $\Delta v=423 \text{ km s}^{-1}$ . Instead, in Table 3 UGC 3909 ( $v_{gal}, D_{gal}, \rho=945, 11.3, 829, \Delta v=199 \text{ km s}^{-1}$ ) is listed as the associated galaxy, in spite of the large impact parameter. Within the range implied by all other associations. UGC 3909 is preferred over NGC 2591 ( $v_{gal}, D_{gal}, \rho=1323, 18.5, 907$ ), because it has slightly

smaller impact parameter. Furthermore, there are four galaxies with unknown velocity that could have smaller impact parameter (UGC 4360, UGC 4413 at  $\rho \sim 560$  kpc, UGC 4563, UGC 4194 at  $\rho \sim 800$  kpc). This is therefore one of the most uncertain associations in Table 3.

The weak  $\text{Ly}\alpha$  at  $2282 \text{ km s}^{-1}$  ( $28 \pm 7 \text{ m}\text{\AA}$ ) was not reported by Penton et al. (2004), but it can be seen in their spectra. In Table 3 it is associated with UGC 4202 ( $v_{gal}$ ,  $D_{gal}$ ,  $\rho=2296, 12.0, 875$ ), which is not listed in the RC3.

At  $5549 \text{ km s}^{-1}$  there is a very strong  $\text{Ly}\alpha$ , with accompanying  $\text{Ly}\beta$ , though no O VI. No galaxy is known within 3 Mpc with  $v_{gal}$  between 5000 and 6000  $\text{km s}^{-1}$ . This may be because no deep searches were made in this direction.

*PG 0838+770.* – A reasonably good FUSE spectrum exists for this target, which passes within 10 kpc of UGC 4527 ( $v_{gal}=721 \text{ km s}^{-1}$ ,  $D_{gal}=4.7$  kpc), a small irregular galaxy. A strong  $\text{Ly}\beta$  absorption line is seen centered at  $716 \text{ km s}^{-1}$ , but O VI is absent.

The sightline also passes through the LGG 165 group, which has 13 galaxies with velocities between 1257 and 1544  $\text{km s}^{-1}$  within 1 Mpc. NGC 2591 has the lowest impact parameter (444 kpc). No associated absorption is seen. UGC 4238 ( $v_{gal}$ ,  $D_{gal}$ ,  $\rho=1544, 16.3, 803$ ) has similar velocity as the group galaxies, but it is not a group member, and it lies in the opposite direction seen from PG 0838+770. It is therefore listed separately.

UGC 4623 ( $v_{gal}=2885 \text{ km s}^{-1}$ ) is the only known galaxy with  $v_{gal} > 2000 \text{ km s}^{-1}$ , and has impact parameter 467 kpc, but no absorption is seen near this velocity.

*PG 0844+349.* – No high-resolution *GHR*S or *STIS* spectrum exists for this sightline. The FUSE spectrum shows three features just redward of O VI  $\lambda 1031.926$ . Two of these are interpreted as  $\text{Ly}\beta$  at 2260 and 2326  $\text{km s}^{-1}$  and are associated with UGC 4621 ( $v_{gal}$ ,  $D_{gal}$ ,  $\rho=2306, 10.3, 372$ ), one of the few cases that we associate two lines with a single galaxy. Four galaxies other than UGC 4621 have similar velocities (see Fig. 8(67)): HS 0846+3522 ( $v_{gal}$ ,  $D_{gal}$ ,  $\rho=2481, 0.6, 387$ ), SDSS J084619.14+351858.2 ( $v_{gal}$ ,  $D_{gal}$ ,  $\rho=2368, 3.8, 391$ ), CG222 ( $v_{gal}$ ,  $D_{gal}$ ,  $\rho=2429, 1.1, 411$ ), and KUG 0847+350 ( $v_{gal}$ ,  $D_{gal}$ ,  $\rho=2354, 4.0, 421$ ), but all are dwarfs with larger impact parameter. A fourth galaxy with similar velocity (UGC 4660;  $v_{gal}$ ,  $D_{gal}$ ,  $\rho=2203, 11.6, 826$ ) is listed as a non-detection in Table 3.

The third feature just redward of O VI  $\lambda 1031.926$  seems to be O VI at 365  $\text{km s}^{-1}$  that can be associated with NGC 2683 ( $v_{gal}$ ,  $D_{gal}$ ,  $\rho=410, 23.0, 250$ ). This is supported by the apparent  $\text{Ly}\beta$  line detected at 351  $\text{km s}^{-1}$ , as well as by extra (though blended) absorption at the wavelength where O VI  $\lambda 1037.617$  would be. Three additional galaxies in Table 3 have  $v_{gal} \sim 400 \text{ km s}^{-1}$  (see Fig. 8(66)): [KK98]69 ( $v_{gal}$ ,  $D_{gal}$ ,  $\rho=463, 6.4, 228$ ), UGC 4787 ( $v_{gal}$ ,  $D_{gal}$ ,  $\rho=552, 6.6, 816$ ) and UGC 4704 ( $v_{gal}$ ,  $D_{gal}$ ,  $\rho=596, 13.2, 967$ ).

*PG 0953+414.* – Toward this sightline the RC3 includes just two galaxies with impact parameter less than 1 Mpc – NGC 3104 ( $v_{gal}$ ,  $D_{gal}$ ,  $\rho=612$ , 11.5, 296) and NGC 3184 ( $v_{gal}$ ,  $D_{gal}$ ,  $\rho=593$ , 23.4, 758). There is a weak feature in the damping wing of Galactic Ly $\alpha$  that is probably Ly $\alpha$  at 621 km s $^{-1}$  (see Fig. 8(68)). In addition, a  $5\sigma$  ( $39\pm 8\pm 7$  mÅ) feature at 637 km s $^{-1}$  seems to be O VI, as there are no higher redshift systems that produce absorption at that wavelength. Unfortunately, the corresponding O VI  $\lambda 1037.617$  line is only measureable in the lower S/N night-only data; the upper limit (22 mÅ) is compatible with the detection of the O VI  $\lambda 1031.926$  line, however.

*NED* lists twenty more galaxies with impact parameter below 1 Mpc near this sightline, most of which are small. Of the 13 with velocity  $\sim 600$  km s $^{-1}$ , 12 are KUG and SDSS galaxies with impact parameter  $>600$  kpc (i.e. much larger than the 296 kpc to NGC 3104), and with  $\rho/D_{gal} > 125$ , so none is listed in Table 3. However, the table does give upper limits on Ly $\alpha$  lines for two relatively small galaxies with  $\rho/D_{gal} < 125$  (KUG 0956+420 and Mrk 1427 at 332 and 390 kpc, respectively).

Also in *NED* is KUG 0952+418 ( $v_{gal}$ ,  $D_{gal}$ ,  $\rho=4695$ , 9.2, 449), whose velocity is similar to that of three closely-spaced Ly $\alpha$  absorption lines, at 4670, 4807 and 4961 km s $^{-1}$ . These three absorption lines were previously listed by Savage et al. (2002). At impact parameters larger than 1 Mpc, there are many galaxies with  $v_{gal} \sim 2000$  km s $^{-1}$ , as well as a few with  $v_{gal} \sim 4800$  km s $^{-1}$ , including some in the group GH 49 at 2.2 Mpc. Finally, UGC 5290 ( $v_{gal}$ ,  $D_{gal}$ ,  $\rho=5030$ , 20.8, 1292) lies about 1 Mpc away. No galaxies are known within 3 Mpc with  $v_{gal}$  between 2800 and 4600 km s $^{-1}$ , however. The most probable explanation for these Ly $\alpha$  absorbers thus seems to be an intergalactic filament that is associated with the galaxies near 4800 km s $^{-1}$ . Table 3 lists all three as associated with KUG 0952+418, but a deeper search for faint galaxies may turn up others.

*PG 1001+291.* – The situation for PG1001+291 is complicated. The *STIS*-E140M spectrum is of reasonably good quality (S/N $\sim 8$ ), but the FUSE spectrum only has S/N $\sim 4$ , making the upper limits to Ly $\beta$  and the O VI lines not very significant, and resulting in effectively useless C III data. There are several galaxies with  $v_{gal} \sim 500$  km s $^{-1}$ , with UGC 5427 being small ( $D_{gal}=3.6$  kpc), but having an impact parameter of only 84 kpc. A feature is seen in the Ly $\alpha$  line at 487 km s $^{-1}$ , but it is close to where the Galactic line completely saturates, so the line is noisy. Two other small galaxies have similar velocity: UGC 5340 ( $v_{gal}$ ,  $D_{gal}$ ,  $\rho=503$ , 8.3, 296) and UGC 5272 ( $v_{gal}$ ,  $D_{gal}$ ,  $\rho=520$ , 6.5, 731). Because of the small impact parameter, Table 3 lists the Ly $\alpha$  line at 487 km s $^{-1}$  as associated with UGC 5427, as well as non-detections for UGC 5340 and UGC 5227.

An additional Ly $\alpha$  feature is found at 1069 km s $^{-1}$ , but the nearest galaxies with similar velocities have large  $\rho$  and are small (Fig. 8(71)): MCG+5-24-11 (=UGCA 201,  $v_{gal}$ ,  $D_{gal}$ ,

$\rho=1363$ , 3.5, 188,  $\rho/D_{gal}=54$ ), UGC 5464 ( $v_{gal}$ ,  $D_{gal}$ ,  $\rho=1011$ , 7.2, 337,  $\rho/D_{gal}=47$ ) and UGC 5478 ( $v_{gal}$ ,  $D_{gal}$ ,  $\rho=1378$ , 11.2, 686). Table 3 chooses to associate the  $1069 \text{ km s}^{-1}$  absorption with UGC 5464 ( $\Delta v=-58 \text{ km s}^{-1}$ ), rather than with MCG+5-24-11 ( $\Delta v=294 \text{ km s}^{-1}$ ), even though the latter has smaller impact parameter. In contrast, Bowen et al. (1996) associated the  $1069 \text{ km s}^{-1}$  feature with MCG+5-24-11.

In addition to these lines, there is a Ly $\alpha$  line at  $4602 \text{ km s}^{-1}$ . The nearest galaxy with similar velocity is UGC 5461 at  $\rho=1249 \text{ kpc}$ .

*PG 1011–040.* – The RC3 includes three galaxies near this sightline: IC 600 ( $v_{gal}$ ,  $D_{gal}$ ,  $\rho=1309$ , 15.1, 417), MCG–1-26-12 ( $v_{gal}$ ,  $D_{gal}$ ,  $\rho=662$ , 10.4, 750), and NGC 3115 ( $v_{gal}$ ,  $D_{gal}$ ,  $\rho=658$ , 26.6, 900). Two additional large galaxies can be found in *NED*: LCRS B101019.9–032413 ( $v_{gal}$ ,  $D_{gal}$ ,  $\rho=3395$ , 9.8, 680) and 2MASX J101213.26–040226.2 ( $v_{gal}$ ,  $D_{gal}$ ,  $\rho=5619$ , 20.2, 852). No absorption features are found in any line near the velocities of these galaxies. It is possible that Ly $\alpha$  absorption is present, but there are no Ly $\alpha$  data. No previous paper has reported results for this sightline.

*PG 1049–005.* – Non-detections are listed for seven galaxies near this sightline: UGC 5922 ( $v_{gal}$ ,  $D_{gal}$ ,  $\rho=1846$ , 9.2, 391), IC 653 ( $v_{gal}$ ,  $D_{gal}$ ,  $\rho=5538$ , 45.2, 438), CGCG 10-41 ( $v_{gal}$ ,  $D_{gal}$ ,  $\rho=1810$ , 4.5, 475), UGC 6011 ( $v_{gal}$ ,  $D_{gal}$ ,  $\rho=5547$ , 33.5, 685), UGC 5943 ( $v_{gal}$ ,  $D_{gal}$ ,  $\rho=4544$ , 22.4, 689), NGC 3365 ( $v_{gal}$ ,  $D_{gal}$ ,  $\rho=986$ , 23.2, 943) and NGC 3521 ( $v_{gal}$ ,  $D_{gal}$ ,  $\rho=805$ , 49.2, 962). The S/N ratio of the *STIS*-G140M data is relatively low, however (7.2), and the detection limit is at best  $75 \text{ m}\text{\AA}$ . Côté et al. (2005) claimed an  $80 \text{ m}\text{\AA}$  line at  $5538 \text{ km s}^{-1}$ , but this is (a) near the limit of detection and (b) more likely to be Galactic NV  $\lambda 1238.821$ . There is a hint of an absorption line near  $2253 \text{ km s}^{-1}$ , but it measures as  $135 \pm 105 \text{ m}\text{\AA}$ , and this is probably not significant.

*PG 1116+215.* – This sightline has high S/N FUSE and *STIS*-E140M data (S/N $\sim 25$  and  $\sim 10$ , respectively). Both Penton et al. (2004) and Sembach et al. (2004) reported the Ly $\alpha$  lines at  $1479$  and  $4884 \text{ km s}^{-1}$ , with equivalent widths that are within  $1\sigma$  of the values in Table 3. The feature at  $1479 \text{ km s}^{-1}$  can be associated with UGC 6258 ( $v_{gal}$ ,  $D_{gal}$ ,  $\rho=1454$ , 14.4, 543 kpc; see Fig. 8(73)). Danforth et al. (2006) listed a corresponding OVI  $\lambda 1037.617$  feature. However, this can be shown to be Ly $\xi$  at  $z=0.138$ , at which redshift there is a Lyman-limit system in which 19 Lyman lines, from Ly $\alpha$  to Ly $\tau$ , can be identified.

There is another Ly $\alpha$  absorber at  $4884 \text{ km s}^{-1}$ . The only galaxy with  $\rho < 3000$  and  $|\Delta v| < 400 \text{ km s}^{-1}$  is NGC 3649 ( $v_{gal}$ ,  $D_{gal}$ ,  $\rho=4979$ , 26.9, 1742; triangle in Fig. 8(74)). There is a feature at the position of Ly $\beta$  that corresponds to this Ly $\alpha$  absorption, even though it is much narrower. The most likely explanation is that the Ly $\alpha$  is actually a two-component absorber. Danforth et al. (2006) list an upper limit for OVI at this velocity, but any OVI

absorption would be blended with Ly $\nu$  at  $z=0.138$  and their upper limit does not take this into account.

*PG 1149–110.* – There are eight galaxies at various velocities that lie close to this target. Unfortunately, the *STIS*-G140M spectrum has a relatively low S/N ratio of 5.2, and there is an unidentified emission feature near 1232 Å. Nevertheless, the following galaxies are listed in Table 3: NGC 3942 ( $v_{gal}$ ,  $D_{gal}$ ,  $\rho=3696$ , 232., 141), MCG–2-30-33 ( $v_{gal}$ ,  $D_{gal}$ ,  $\rho=1273$ , 5.1, 442), NGC 3892 ( $v_{gal}$ ,  $D_{gal}$ ,  $\rho=1697$ , 24.3, 529), MCG–2-30-39 ( $v_{gal}$ ,  $D_{gal}$ ,  $\rho=1483$ , 13.6, 541), LCRS B115151.0–113904 ( $v_{gal}$ ,  $D_{gal}$ ,  $\rho=3009$ , 20.4, 640), LCSB S1630P ( $v_{gal}$ ,  $D_{gal}$ ,  $\rho=1971$ , 11.2, 642), PGC 37027 ( $v_{gal}$ ,  $D_{gal}$ ,  $\rho=2379$ , 14.5, 812), and Mrk 1309 ( $v_{gal}$ ,  $D_{gal}$ ,  $\rho=1715$ , 13.2, 909). Ly $\alpha$  absorption lines are seen at 1665 and 3728 km s $^{-1}$ , and they are associated with NGC 3942 (Fig. 8(75)) and NGC 3892 (Fig. 8(76)), respectively. These lines were also reported by Bowen et al. (2005). However, Bowen et al. gave an equivalent width of  $1100\pm30$  mÅ for the feature at 1665 km s $^{-1}$ , which is clearly too strong, with too low an error. We find  $437\pm69$  mÅ.

*PG 1211+143.* – Together with 3C 273.0 and HE 1228+0131 this is one of three sightlines passing through the Virgo cluster. That means that many galaxies have impact parameter  $<1$  Mpc. A histogram of the velocities of these galaxies shows three groups:  $v_{gal}<400$  km s $^{-1}$ ,  $v_{gal}=450\text{--}1600$  km s $^{-1}$ , and  $v_{gal}=1650\text{--}2550$  km s $^{-1}$ . Together, the RC3 and *NED* include 55 galaxies in the first group, 91 in the second and 44 in the third. Many (but not all) of these galaxies were assigned to one of the LGG groups by Garcia (1993). The sightline passes between the galaxies of the LGG 285 and LGG 289 groups. So, Table 3 gives these two entries for PG 1211+143, with the impact parameter that of the nearest group galaxy with  $D_{gal}>9$  kpc. LGG 289 ( $\langle v \rangle=1282$  km s $^{-1}$ ) includes IC 3077 ( $v_{gal}$ ,  $D_{gal}$ ,  $\rho=1411$ , 9.3, 215), as well as NGC 4206 ( $v_{gal}$ ,  $D_{gal}$ ,  $\rho=702$ , 40.5, 418) and three more large galaxies with  $\rho>700$  kpc. LGG 285 ( $\langle v \rangle=1282$  km s $^{-1}$ ) includes IC 3061 ( $v_{gal}=2361$  km s $^{-1}$ ) at  $\rho=121$  kpc, NGC 4189 ( $v_{gal}=2113$  km s $^{-1}$ ) at 413 kpc and seven more galaxies with  $\rho=420\text{--}1000$  kpc.

Absorption near these velocities is only seen at 2110 km s $^{-1}$ , with equivalent width  $104\pm8$  mÅ. It is listed under the LGG 285 group in Table 3 (at  $\rho>121$  kpc). This line was previously reported by Penton et al. (2004), although they gave  $v=2130$  km s $^{-1}$ , and equivalent width  $186\pm19$  mÅ. This discrepancy may partly be because of differences in the continuum placement but also because Penton et al. (2004) included the  $<1\sigma$  noisy wings in the velocities over which they integrated. However, we only get 125 mÅ if we do that.

Danforth et al. (2006) mysteriously listed a  $45\pm14$  mÅ O VI  $\lambda 1037.617$  feature at 2130 km s $^{-1}$ . However, as can be seen in Fig. 2, there clearly is nothing significant within 200 km s $^{-1}$  of this velocity. We derive an upper limit of 19 mÅ. Since Danforth et al. (2006) did not show their data, it is not possible to determine which feature they had in mind.



Penton et al. (2004) also listed the two lines at 4932 and 5015 km s<sup>-1</sup>, with equivalent widths of 189±46 and 154±40 mÅ. We find 165±7±4 and 231±7±4 mÅ, respectively. Since the higher-velocity line is clearly stronger than the lower-velocity one (see Fig. 2), the Penton et al. (2004) result cannot be correct. The nearest galaxy with known velocity within ±400 km s<sup>-1</sup> of these absorption lines is CGCG 69-129 ( $v_{gal}$ ,  $D_{gal}$ ,  $\rho$ =4987, 10.0, 1919), which is the one listed in Table 3. Potentially, IC 3073 has much smaller impact parameter (670 kpc) if its velocity were ~5000 km s<sup>-1</sup>.

Tumlinson et al. (2005) analyzed two absorption systems at 19400 and 15300 km s<sup>-1</sup>, which have many HI lines, as well as O VI, C III and Si III.

*PG 1216+069.* – This sightline passes within 1 Mpc from a large number of galaxies (265 are known in *NED*), including galaxies in six LGG groups – LGG 288 ( $\langle v \rangle$ =505 km s<sup>-1</sup>), LGG 292 ( $\langle v \rangle$ =938 km s<sup>-1</sup>), LGG 289 ( $\langle v \rangle$ =1282 km s<sup>-1</sup>), LGG 287 ( $\langle v \rangle$ =1655), LGG 278 ( $\langle v \rangle$ =2078 km s<sup>-1</sup>) and LGG 281 ( $\langle v \rangle$ =2473 km s<sup>-1</sup>). There is a *STIS*-E140M spectrum with relatively low S/N (9 per 6.5 km s<sup>-1</sup> resolution element), and a low S/N (~5) FUSE spectrum, which makes the analysis difficult. Nevertheless, we can discern three Ly $\alpha$  absorption lines, at 1106, 1443 and 1895 km s<sup>-1</sup>. The third of these is a damped Ly $\alpha$  system, which was discussed in detail by Tripp et al. (2005). Bowen et al. (1996) first identified the damped Ly $\alpha$  absorber in a low S/N *GHR*S spectrum, listing a velocity of 1650 km s<sup>-1</sup>.

In Table 3 we associate the absorption at 1106 km s<sup>-1</sup> with LGG 292 (nearest galaxy NGC 4241 at  $\rho$ =104 kpc; Fig. 8(79)), that at 1443 km s<sup>-1</sup> with LGG 289 (nearest galaxy UGC 7423 at  $\rho$ =264 kpc; Fig. 8(80)), and that at 1895 km s<sup>-1</sup> with LGG 278 (nearest galaxy NGC 4223 at  $\rho$ =283 kpc; Fig. 8(81)), although the first two of these are certainly open for discussion.

In addition to the six galaxy groups at  $v_{gal}$ <2500 km s<sup>-1</sup>, the sightline passes within 1 Mpc from six galaxies that have  $v_{gal}$  between 2500 and 5600 km s<sup>-1</sup>: NGC 4257 ( $v_{gal}$ ,  $D_{gal}$ ,  $\rho$ =2756, 16.0, 689), NGC 4246 ( $v_{gal}$ ,  $D_{gal}$ ,  $\rho$ =3725, 40.1, 644), NGC 4247 ( $v_{gal}$ ,  $D_{gal}$ ,  $\rho$ =3810, 18.8, 742), NGC 4296 ( $v_{gal}$ ,  $D_{gal}$ ,  $\rho$ =4227, 25.4, 596), IC 771 ( $v_{gal}$ =5477, 26.9, 841), and IC 3136 ( $v_{gal}$ ,  $D_{gal}$ ,  $\rho$ =5594, 28.8, 684). There are two Ly $\alpha$  lines, at 3774 and 3808 km s<sup>-1</sup>, which, because of its low impact parameter are both associated with SDSS J121903.72+063343.0 ( $v_{gal}$ ,  $D_{gal}$ ,  $\rho$ =3833, 5.1, 103,  $\rho/D_{gal}$ =20.2). Non-detections are listed for NGC 4246 ( $v_{gal}$ ,  $D_{gal}$ ,  $\rho$ =3725, 40.1, 644,  $\rho/D_{gal}$ =16) and NGC 4247 ( $v_{gal}$ ,  $D_{gal}$ ,  $\rho$ =3838, 18.8, 742,  $\rho/D_{gal}$ =39), even though these are much larger galaxies and NGC 4246 has the lowest  $\rho/D_{gal}$  ratio. The associations are a bit ambiguous, however.

*PG 1259+593.* – PG 1259+593 is one of the few sightlines with both high S/N FUSE and high S/N *STIS*-E140M data. Richter et al. (2004) analyzed all IGM lines in detail,

listing the  $\text{Ly}\alpha$  and  $\text{Ly}\beta$  detections at 678 and 2275  $\text{km s}^{-1}$ , although they gave velocities of 686 and 2278  $\text{km s}^{-1}$ . Their listed equivalent widths are similar to ours within  $1\sigma$  for the 2275  $\text{km s}^{-1}$  component, but they differ for the 678  $\text{km s}^{-1}$  component. The difference in the  $\text{Ly}\alpha$  equivalent width ( $231\pm9$  mÅ in Table 3 vs  $190\pm24$  in Richter et al. (2004)) is probably caused by the fact that Richter et al. fitted a polynomial to the continuum around this line, while we model the Galactic damped  $\text{Ly}\alpha$  profile. In the case of  $\text{Ly}\beta$  ( $<15$  mÅ vs  $23\pm6$  mÅ in Richter et al. 2004) the difference is due to the different manner by which the  $\text{H}_2$  line is removed. Côté et al. (2005) also presented a plot of the *STIS*-G140M spectrum of the  $\text{Ly}\alpha$  line, measuring it as  $330\pm80$  mÅ. Our reduction of this spectrum gives  $245\pm70$  mÅ, more in line with the equivalent width found from the E140M data.

An apparently double O VI feature is seen, centered at 627  $\text{km s}^{-1}$ , surrounded by  $\text{Ly}\beta$  at 2269  $\text{km s}^{-1}$  and  $\text{Ly}\delta$  at  $z=0.0894$ . The two apparent features are centered at 627 and 689  $\text{km s}^{-1}$ . Even though this feature is offset in velocity from  $\text{Ly}\alpha$  by  $-50$   $\text{km s}^{-1}$ , the identification of the 627  $\text{km s}^{-1}$  feature as O VI is fairly secure, because a) there are no high redshift systems that produce absorption at this wavelength, and b) there is a corresponding feature for O VI  $\lambda 1037.617$  that is half the strength. The other feature does not have such a counterpart. We measure  $22\pm5$  mÅ for the 627  $\text{km s}^{-1}$  absorption, and  $14\pm5$  mÅ for the 689  $\text{km s}^{-1}$  absorption. We conclude that there is O VI  $\lambda 1031.926$  at 627  $\text{km s}^{-1}$ , while the 689  $\text{km s}^{-1}$  absorption is considered not significant.

These features were reported in three previous papers. Richter et al. (2004) gave an equivalent width of  $63\pm22$  mÅ, centered at 690  $\text{km s}^{-1}$ , but integrated from 580 to 710  $\text{km s}^{-1}$ . However, this would not only include the probable O VI, but also the  $\text{Ly}\delta$  line at  $z=0.0894$ ; further we find an equivalent width of  $50\pm10$  mÅ when integrating over this velocity range. Danforth et al. (2006) listed  $14\pm9$  mÅ at 687  $\text{km s}^{-1}$ ; apparently only measuring the least significant of the three features. Tripp et al. (2008) gave  $40\pm5$  mÅ at 630  $\text{km s}^{-1}$ . Using their integration range of 590 to 730  $\text{km s}^{-1}$  we find  $36\pm8$  mÅ, though a fit would give a central velocity of 644  $\text{km s}^{-1}$ . Clearly, different authors do not agree about the detailed interpretation and measurement of these two features, but they all agree that O VI  $\lambda 1031.926$  is present.

The impact parameter of UGC 8146 ( $v_{gal}=669$   $\text{km s}^{-1}$ ) is only 80 kpc, so the  $\text{Ly}\alpha$  and O VI absorptions can be confidently associated with that galaxy (see Fig. 8(83)). Two other small galaxies have similar velocity, but are not included in Table 3 because  $\rho/D_{gal}>100$ . NGC 4964 ( $v_{gal}$ ,  $D_{gal}$ ,  $\rho=755$ , 4.4, 672) has large impact parameter, while SDSS J130206.46+584142.9 ( $v_{gal}$ ,  $D_{gal}$ ,  $\rho=623$ , 1.8, 72), is a dwarf companion of UGC 8146.

A second  $\text{Ly}\alpha$  absorber is visible at 2275  $\text{km s}^{-1}$ . There are several large galaxies with diameter  $>10$  kpc and  $v_{gal}\sim 2500$   $\text{km s}^{-1}$  within 1 Mpc (Fig. 8(84)): UGC 8046 ( $v_{gal}$ ,  $D_{gal}$ ,

$\rho=2572, 11.8, 584$ ), UGC 8040 ( $v_{gal}, D_{gal}, \rho=2522, 16.8, 595$ ) and NGC 4814 ( $v_{gal}, D_{gal}, \rho=2513, 35.0, 694$ ). The feature is listed as associated with the edge-on galaxy UGC 8040, which is the largest of the two galaxies with  $\rho \sim 590$  kpc. Associating it with NGC 4814 instead would have been justifiable, however. Six more dwarfs with similar velocity and  $\rho < 1$  Mpc are listed in *NED*. *NED* also lists SDSS J125926.78+591735.0 ( $v_{gal}=2867, 6.5, 255$ ), which is included separately in Table 3.

Finally, a third Ly $\alpha$  feature at  $v < 5000$  km s $^{-1}$  is visible at 4501 km s $^{-1}$ . For this velocity neither the RC3 nor *NED* lists any galaxy closer than MCG+10-19-23 at impact parameter 1.8 Mpc, so this feature is classified as intergalactic in Table 3.

*PG 1302–102.* – The *STIS*-E140M spectrum of this sightline shows several absorption lines between 1216 and 1224 Å, but all but two of these can be identified as Ly $\beta$  at  $z=0.188$  to 0.192, or Ly $\gamma$  at  $z=0.254$ . The remaining lines are probably Ly $\alpha$  at 1045 and 1316 km s $^{-1}$ . The latter identification is secure, as Ly $\beta$  and C III absorption are also seen at this velocity, while the first is uncertain. Danforth et al. (2006) reached the same interpretation for these lines. In the RC3 and *NED* there are 22 galaxies with impact parameter  $< 1$  Mpc near this sightline. Separate entries are given in Table 3 for the seventeen of these for which the ratio  $\rho/D_{gal} < 125$ . For all except two these are upper limits, which is unsurprising since all but three of the galaxies have impact parameter  $> 650$  kpc.

The table includes the following galaxies. Toward the north lie NGC 4939 ( $v_{gal}, D_{gal}, \rho=3111, 24.6, 104$ ), DDO 163 ( $v_{gal}, D_{gal}, \rho=1123, 11.0, 930$ ), NGC 4818 ( $v_{gal}, D_{gal}, \rho=1065, 24.0, 987$ ), and NGC 4948A ( $v_{gal}, D_{gal}, \rho=1553, 10.5, 991$ ). Toward the east is MCG–2-34-6 ( $v_{gal}, D_{gal}, \rho=1213, 18.2, 391$ ), while toward the south lies NGC 5068 ( $v_{gal}, D_{gal}, \rho=672, 10.9, 995$ ). In a westerly direction lies the group LGG 307, of which NGC 4920 ( $v_{gal}, D_{gal}, \rho=1336, 6.8, 473$ ) is the nearest. Other listed group members are MCG–1-33-60 ( $v_{gal}, D_{gal}, \rho=1487, 20.1, 830$ ), MCG–2-33-85 ( $v_{gal}, D_{gal}, \rho=1582, 11.6, 863$ ), UGCA 312 ( $v_{gal}, D_{gal}, \rho=1307, 8.6, 900$ ), and UGCA 308 ( $v_{gal}, D_{gal}, \rho=1322, 9.4, 986$ ). Also toward the west are MCG–2-33-75 ( $v_{gal}, D_{gal}, \rho=1247, 6.8, 658$ ), MCG–2-33-95 ( $v_{gal}, D_{gal}, \rho=2753, 17.4, 657$ ), while in a southwesternly directly lie MCG–2-33-97 ( $v_{gal}, D_{gal}, \rho=2705, 14.9, 782$ ), NGC 4933 ( $v_{gal}, D_{gal}, \rho=2965, 34.9, 820$ ), UGCA 307 ( $v_{gal}, D_{gal}, \rho=824, 9.1, 882$ ), and NGC 4802 ( $v_{gal}, D_{gal}, \rho=1013, 12.8, 901$ ).

As Fig. 8(86) shows, two galaxies have considerably lower impact parameter than the rest. These are the two that we associate the two Ly $\alpha$  lines with. The line at 1045 km s $^{-1}$  is associated with MCG–2-34-6, while the one at 1316 km s $^{-1}$  is listed under NGC 4920. This assignment is chosen because it minimizes the velocity differences between absorption and galaxy ( $\Delta v = -168, 20$  km s $^{-1}$  for this choice, instead of  $\Delta v = -103, +291$  km s $^{-1}$  for the alternative). MCG–1-33-83 potentially has smaller impact parameter (308 kpc), but its

velocity is unknown.

The association of the Ly $\alpha$  line at 3909 km s<sup>-1</sup> with NGC 4939 is much less ambiguous, as can be seen in Fig. 8(87). NGC 4939 is the only galaxy near this velocity with low impact parameter.

*PG 1341+258.* – Bowen et al. (2002) claimed a 120±20 mÅ detection of Ly $\alpha$  at 1425 km s<sup>-1</sup>, but we do not see this line, and instead derive a 30 mÅ upper limit around this velocity. From the plot in the Bowen et al. (2002) paper it looks like there may be a feature, which we measure to be at 1454 km s<sup>-1</sup>, but with equivalent width 20±12 mÅ, i.e. not significant. The only other measurement from this sightline is a non-detection for CGCG 132-10 ( $v_{gal}$ ,  $D_{gal}$ ,  $\rho$ =3188, 6.9, 825).

*PG 1351+640.* – In this spectrum absorption is seen at 1771 and 1447 km s<sup>-1</sup>. The corresponding Ly $\beta$  lines are hidden by Galactic O VI and intrinsic Ly $\delta$  absorption, respectively. The O VI  $\lambda$ 1031.926 lines are hidden by strong H<sub>2</sub> lines, while an upper limit can be derived for the O VI  $\lambda$ 1037.617 line.

There are five galaxies with  $v_{gal}$  between 1247 and 1971 km s<sup>-1</sup> and with  $\rho$ <500 kpc: UGC 8894 ( $v_{gal}$ ,  $D_{gal}$ ,  $\rho$ =1771, 12.9, 274), UGCA 375 ( $v_{gal}$ ,  $D_{gal}$ ,  $\rho$ =1763, 7.3, 299; Mrk 277 in the RC3, lying in a direction on the sky opposite to UGC 8894), SDSS J134800.10+633120.8 ( $v_{gal}$ ,  $D_{gal}$ ,  $\rho$ =1665, 2.5, 284), and SDSS J134711.13+625006.3 ( $v_{gal}$ ,  $D_{gal}$ ,  $\rho$ =1496, 2.5, 482). Associating the Ly $\alpha$  at 1771 km s<sup>-1</sup> with UGC 8894 seems an obvious choice (see Fig. 8(89)). However, associating the 1447 km s<sup>-1</sup> absorption is more tricky. In Table 3 it is listed with UGCA 375 ( $\Delta v$ =316 km s<sup>-1</sup>, see Fig. 8(88)), but it is easy to argue that it should also be associated with UGC 8894 ( $\Delta v$ =324 km s<sup>-1</sup>) or even with SDSS J134711.13+625006.3 or SDSS J134800.10+6733120.8 ( $\Delta v$ =49 km s<sup>-1</sup> and 218 km s<sup>-1</sup>, open circles). However,  $\rho/D_{gal}$ =192 and 113 for these galaxies, which would be larger than is the case for any other association. Obviously, any association choice is dubious.

Penton et al. (2004) have this sightline in their sample, but surprisingly they did not list the two 3.5 $\sigma$  features at 1771 and 1447 km s<sup>-1</sup>, even though they can be seen in their figure of the spectrum and even though they sometimes listed 2 $\sigma$  features that do not seem to be real.

*PG 1444+407.* – This sightline has reasonable quality *STIS*-E140M data (S/N~9), but low-quality *FUSE* data (S/N~4). Therefore, the upper limits for Ly $\beta$  and O VI are not very significant, especially for velocities where only orbital-night data can be used. For Ly $\alpha$  the limits are about 50 mÅ. No Ly $\alpha$  appears associated with UGC 9497 ( $v_{gal}$ ,  $D_{gal}$ ,  $\rho$ =633, 4.0, 445), nor with SDSS J145001.59+402142.4 ( $v_{gal}$ ,  $D_{gal}$ ,  $\rho$ =4814, 8.0, 653). However, Ly $\alpha$  is clearly present at 5638 km s<sup>-1</sup>, and is associated with UGC 9502 ( $v_{gal}$ ,  $D_{gal}$ ,  $\rho$ =5672, 27.8,

637).

A line also appears at  $2630 \text{ km s}^{-1}$ , which in Table 3 is listed under SDSS J145045.59+413742.1 ( $v_{gal}$ ,  $D_{gal}$ ,  $\rho=2582$ , 4.2, 897; Fig. 8(90)), in spite of the large impact parameter. Several other galaxies with similar velocity are present with impact parameters of 1200 to 1800 kpc. A potential alternative candidate is UGC 9495, whose velocity is unknown. If it is similar to the velocity of the detected  $\text{Ly}\alpha$  line at  $2630 \text{ km s}^{-1}$ , its impact parameter would be 551 kpc, and its diameter 12.9 kpc, in which case we would associate it with the detection.

*PG 1553+113.* – There are few galaxies in the part of the sky near PG 1553+113. Only one can be found in the RC3 or *NED* with impact parameter  $<1$  Mpc: UGC 10014 ( $v_{gal}$ ,  $D_{gal}$ ,  $\rho=1121$ , 7.1, 916).

*PG 1626+554.* – There are just two galaxies with low impact parameter near this target: NGC 6182 ( $v_{gal}$ ,  $D_{gal}$ ,  $\rho=5138$ , 38.1, 338) and NGC 6143 ( $v_{gal}$ ,  $D_{gal}$ ,  $\rho=1595$ , 6.8, 403). No  $\text{Ly}\alpha$  data exist, and no  $\text{Ly}\beta$  absorption is seen.

*PHL 1811.* – PHL 1811 lies in a part of the sky where there are few nearby galaxies. In fact, only two galaxies with  $\rho < 1$  Mpc can be found in *NED*: SDSS J214451.59–084537.6 ( $v_{gal}$ ,  $D_{gal}$ ,  $\rho=1276$ , 0.2, 674) and SDSS J215446.45–084616.9 ( $v_{gal}$ ,  $D_{gal}$ ,  $\rho=5498$ , 12.0, 787), which is listed in Table 3. A very narrow feature (FWHM  $14 \text{ km s}^{-1}$ ) can be seen at  $5402 \text{ km s}^{-1}$ , which may be  $\text{Ly}\alpha$ . The sightline contains a Lyman limit system at  $z=0.08093$  which was discussed in detail by Jenkins et al. (2003, 2005).

Jenkins et al. (2003) listed possible  $\text{Ly}\alpha$  lines at  $3537$  and  $5202 \text{ km s}^{-1}$ . However these are actually O VI  $\lambda\lambda 1031.926$ ,  $1037.617$  at  $z=0.1919$ , which is confirmed by the fact that these lines have the same velocity structure, as well as by the presence of a corresponding (weak)  $\text{Ly}\alpha$  absorption. Danforth et al. (2006) gave a lower limit of  $63 \text{ m}\text{\AA}$  for the O VI line corresponding to the erroneously claimed  $3537 \text{ km s}^{-1}$   $\text{Ly}\alpha$ . This is not only inappropriate, since the line is redshifted O VI  $\lambda 1031.926$ , but also mysterious, since there is a strong redshifted ( $z=0.0735$ )  $\text{Ly}\gamma$  line at the corresponding wavelength.

*PKS 0405–12.* – Prochaska et al. (2004) and Williger et al. (2006) analyzed the FUSE and *STIS*-E140M spectra of this sightline in detail. Williger et al. (2006) listed seven  $\text{Ly}\alpha$  features at  $v < 5000 \text{ km s}^{-1}$ . Four of those are less than  $1.5\sigma$  and probably not real. Lehner et al. (2007) reidentified the features and concluded that the absorptions that are believable are at  $1220.605$ ,  $1227.359$ ,  $1230.136$ ,  $1233.808$  and  $1236.105 \text{ \AA}$ . The first two of these are best interpreted as O VI redshifted to  $z=0.1828$ , especially since a strong H I absorption system ( $\text{Ly}\alpha$  to  $\text{Ly}\zeta$ ) is seen at this redshift. The feature at  $1230.136 \text{ \AA}$  is probably  $\text{Ly}\alpha$  at  $3574 \text{ km s}^{-1}$ . The nearest galaxy with  $v_{gal} \sim 3500 \text{ km s}^{-1}$  is 2MASX J040607.61–102327.2 at  $\rho=1.5$  Mpc. The feature at  $1236.105 \text{ \AA}$  is listed as intergalactic  $\text{Ly}\alpha$  at  $v=5035 \text{ km s}^{-1}$  – no

galaxies with similar velocity are known within 3 Mpc. The feature at  $1233.808 \text{ \AA}$  was listed as a  $3\sigma$  detection by Lehner et al. (2007), but we decided that it is not significant.

*PKS 0558–504.* – Near this sightline lie ESO 205-G34, NGC 2104 and NGC 2101, all of which have impact parameter  $>500$  kpc and velocity  $\sim 1100 \text{ km s}^{-1}$ . In addition, there is NGC 2152, for which no velocity has been determined, but which potentially has a small impact parameter:  $\rho = 172 \times (v_{gal}/2000)$  kpc. Finally, there is ESO 205-G07 at  $v_{gal} = 2000 \text{ km s}^{-1}$ . No  $\text{Ly}\alpha$  data exist for PKS 0558–504, and no  $\text{Ly}\beta$  absorption with  $v < 5000 \text{ km s}^{-1}$  is seen.

*PKS 2005–489.* – For this sightline Penton et al. (2004) listed three  $\text{Ly}\alpha$  lines at velocities below  $5100 \text{ km s}^{-1}$ . Two of these are strong lines centered at  $4973$  and  $5071 \text{ km s}^{-1}$ , and for both  $\text{Ly}\beta$  absorption is also detected. The higher-velocity  $\text{Ly}\beta$  line is contaminated by the FUSE detector flaw near  $1043 \text{ \AA}$ , and its measured equivalent width is too large; however, we can’t correct for this. The nearest galaxies with similar velocity are ESO 233-G37 ( $v_{gal}$ ,  $D_{gal}$ ,  $\rho = 4950, 26.4, 599$ ) and 2MASX J200943.13–481105.2 ( $v_{gal}$ ,  $D_{gal}$ ,  $\rho = 5116, 16.6, 787$ ). The feature that Penton et al. (2004) identified as a third  $\text{Ly}\alpha$  at  $2752 \text{ km s}^{-1}$  is more likely to be Si III absorption at a velocity of  $5073 \text{ km s}^{-1}$ . It has an equivalent width of  $29 \pm 4 \text{ m\AA}$ . In this system  $\text{Ly}\alpha$ ,  $\text{Ly}\beta$  and C III are detected at velocities of  $5071$ ,  $5079$  and  $5065 \text{ km s}^{-1}$ , and the C III line is rather strong (see Table 4). Photoionization modeling using *CLOUDY* (Ferland et al. 1998) shows that the column densities of H I, C III and Si III can be explained with a  $2.8$  kpc thick feature having  $\log n = -4.0 \text{ cm}^{-3}$ , and metallicity  $0.1$  times solar. Running a *CLOUDY* model with just the H I and C III column densities leads to a prediction for the Si III equivalent width on the order of  $25 \text{ m\AA}$ , for gas densities  $\sim 10^{-4} \text{ cm}^{-3}$ .

The sightline passes through the group LGG 430, which is defined by 12 galaxies that have  $\langle v \rangle = 2955 \pm 213 \text{ km s}^{-1}$ , with velocities ranging from  $2504$  to  $3200 \text{ km s}^{-1}$ . Seven of the defining galaxies have impact parameter  $< 1$  Mpc to PKS 2005–489. The RC3 lists another 6 galaxies within the group’s defining velocity range, and *NED* includes another 10, for a total of 23 galaxies with  $v_{gal}$  in the range  $2504$  to  $3200 \text{ km s}^{-1}$  and  $\rho < 1$  Mpc. Since the feature at  $1226.916 \text{ \AA}$  is most likely Si III at  $5073 \text{ km s}^{-1}$ , there apparently is no  $\text{Ly}\alpha$  absorption associated with the group.

*PKS 2155–304.* – Penton et al. (2000) listed eight  $\text{Ly}\alpha$  lines at  $v = 2600$ – $5700 \text{ km s}^{-1}$  in this sightline, based on a *GHR*S spectrum ( $20 \text{ km s}^{-1}$  resolution), although the features at  $2632$ ,  $2785$ ,  $4031$ ,  $4709$ , and  $5618 \text{ km s}^{-1}$  are all less than  $2.5\sigma$ . Although Penton et al. (2000) listed them as having “significance level”  $> 4$ , none of these features are confirmed in the *STIS*-E140M spectrum of PKS 2155–304, with upper limits that are three times better than those derived from the *GHR*S spectrum. Only the feature at  $5618 \text{ km s}^{-1}$  is confirmed in the E140M data, but now has a velocity of  $5673 \text{ km s}^{-1}$ .

The three features that Penton et al. (2000) listed at velocities of 4951, 5013 and 5119 km s<sup>-1</sup> must have been mismeasured by them. Based on the *GHR*S data they gave equivalent widths of 64, 82 and 218 mÅ. We can reproduce these values by summing over the following velocity ranges: 4850–4970 km s<sup>-1</sup>, 4970–5040 km s<sup>-1</sup> and 5040–5230 km s<sup>-1</sup>. As can be seen in Fig. 2, the first of these would then cover half of the most-negative-velocity component, plus some velocities where no absorption is seen in the E140M data; although there appeared to be a hint of absorption in the G140M data. The second of the Penton et al. (2000) components would cover the other half of the leftmost absorber. The third component covers a velocity range that spans an asymmetrical absorption. None of these three components seem to be justifiable as-is. Even if the equivalent widths given by Penton et al. (2000) were based on gaussian fits, it is hard to see how they were derived.

We instead measure three different components in the *STIS*-E140M spectrum (which shows the same structure as the *GHR*S data), at velocities of 4990, 5101 and 5164 km s<sup>-1</sup>. We also find Lyβ absorption with similar component structure, although the absorption at the highest velocities is confused with the FUSE detector flaw near 1043 Å. We associate these absorbers with ESO 466-G32, a galaxy at  $v_{gal}=5153$  km s<sup>-1</sup> with impact parameter 306 kpc, which is not included in the RC3, but listed in *NED*.

The sightline also passes through the edge of the LGG 450 group ( $\langle v \rangle = 2601$  km s<sup>-1</sup>). The RC3 includes two group galaxies (ESO 466-G36 and NGC 7163), while *NED* lists five more large (ESO 466-G29, 2dF GRSS407Z162, MCG–5-51-2, ESO 466-G43 and 2dF GRSS408Z175) as well as three more small galaxies with velocity between 2380 and 2875 km s<sup>-1</sup>. However, no absorption is seen anywhere in this velocity range down to a limit of ~30 mÅ (in spite of the 2.5σ features claimed by Penton et al. (2000)).

*RX J0048.3+3941*. – For this sightline the impact parameter with M 31 is just 22 kpc. High-negative velocity O VI absorption (–300 km s<sup>-1</sup>) is present, as it is in many sightlines in the southern sky (see Wakker et al. 2003). A few other galaxies have impact parameter <1 Mpc. Five are included in the RC3, but four are small and have velocity similar to UGC 655 ( $v_{gal}$ ,  $D_{gal}$ ,  $\rho=829$ , 6.9, 602 kpc), the largest and the only one listed in Table 3. *NED* lists two more galaxies (UGC 578 and CGCG 535-25), having velocities of 1471 and 4001 km s<sup>-1</sup> and impact parameters of 499 and 810 kpc. No intergalactic lines are seen near any of these velocities, although in most cases the possible intergalactic line is blended with interstellar atomic or molecular absorption.

*RX J0100.4–5113*. – Near this target lies ESO 151-G19 ( $v_{gal}$ ,  $D_{gal}$ ,  $\rho=1386$ , 6.5, 902). There may be a 2σ associated Lyα feature in the *STIS* spectrum, at 1111 km s<sup>-1</sup>, but this is not a convincing detection and it is not listed in Table 3. There is another possible (3σ) Lyα feature at 4874 km s<sup>-1</sup>; the nearest galaxy is ESO 195-G17 ( $v_{gal}$ ,  $D_{gal}$ ,  $\rho=1189$ ,

18.6, 1189), although a galaxy with unknown velocity (ESO 195-G24) would have impact parameter  $\sim 800$  kpc if it were at  $v_{gal} \sim 4700$  km s $^{-1}$ .

*RX J1830.3+7312.* – As Bowen et al. (2002) reported, there are five Ly $\alpha$  lines seen toward this target in the *STIS*-G140M spectrum. The two absorptions at 1968 and 1549 km s $^{-1}$  can be associated with two galaxies lying close to the sightline: NGC 6645A ( $v_{gal}$ ,  $D_{gal}$ ,  $\rho=1558$ , 18.2, 308; Fig. 8(95)) and NGC 6654 ( $v_{gal}$ ,  $D_{gal}$ ,  $\rho=1821$ , 18.2, 186; Fig. 8(96)). There are five more galaxies with similar velocity and  $\rho < 1$  Mpc: MCG+12-17+27 ( $v_{gal}$ ,  $D_{gal}$ ,  $\rho=1404$ , 5.2, 262), UGC 11331 ( $v_{gal}$ ,  $D_{gal}$ ,  $\rho=1554$ , 10.5, 296), CGCG 340-51 ( $v_{gal}$ ,  $D_{gal}$ ,  $\rho=1469$ , 4.3, 337), NGC 6643 ( $v_{gal}$ ,  $D_{gal}$ ,  $\rho=1489$ , 26.4, 638), and UGC 11193 ( $v_{gal}$ ,  $D_{gal}$ ,  $\rho=1489$ , 8.9, 985). As Fig. 8(96) shows, the association between NGC 6654 and the 1968 km s $^{-1}$  Ly $\alpha$  absorber is easy to justify. For the other absorber, the large galaxy NGC 6654A is preferred over the smaller ones near it. These galaxies were not included as a group in the LGG list of Garcia (1993), because some redshifts were missing at the time. To account for this, a new group has been defined, using the galaxies above, excepting UGC 11193. The right ascension of this group would place it between LGG 420 and LGG 421, so it is identified as LGG 420A in Table 3.

For a third Ly $\alpha$  feature, at 2383 km s $^{-1}$ , the nearest galaxies are UGC 11295 and UGC 11382, which have impact parameters of 1307 and 1332 kpc (see triangle in Fig. 8(97)). Finally, there are lines at 4260 and 4770 km s $^{-1}$ , but the only galaxy near that velocity with  $\rho < 3000$  kpc is UGC 11334 ( $v_{gal}$ ,  $D_{gal}$ ,  $\rho=4582$ , 37.8, 1022 kpc; Fig. 8(98)/(99)).

*Ton S180.* – Two galaxies in the nearest galaxy group, the Sculptor Group, have low impact parameter: NGC 247 ( $v_{gal}$ ,  $D_{gal}$ ,  $\rho=159$ , 15.7, 125) and NGC 253 ( $v_{gal}$ ,  $D_{gal}$ ,  $\rho=251$ , 20.7, 166; closed and open symbol in Fig. 8(100)). There is a clear O VI pair at 260 km s $^{-1}$ , with an accompanying  $2.5\sigma$  detection of a C III line. Ly $\beta$  is confused with geocoronal O I\* emission, but seems absent, while any Ly $\alpha$  is completely hidden in the Galactic Ly $\alpha$  absorption. The O VI velocity lies below the nominal survey limit of 400 km s $^{-1}$ , but no positive-velocity Galactic high-velocity clouds are known in this part of the sky, so an association with NGC 247 or NGC 253 is likely. Three other Sculptor group galaxies (NGC 45, NGC 300 and NGC 24) have larger impact parameter (437, 534 and 876 kpc) and similar velocity (468, 142 and 554 km s $^{-1}$ ); no features are seen near those velocities.

Three weak but clear Ly $\alpha$  absorbers are found between 1500 and 5000 km s $^{-1}$ , all of which were listed by Penton et al. (2004). In Table 3 the absorber at 2792 km s $^{-1}$  is associated with the relatively small galaxy 2MASX J005700.66–232044.2 ( $v_{gal}$ ,  $D_{gal}$ ,  $\rho=2657$ , 4.9, 560; Fig. 8(102)), which is not in the RC3. The absorber at 1939 km s $^{-1}$  can be associated with either ESO 541-G05 ( $v_{gal}$ ,  $D_{gal}$ ,  $\rho=1958$ , 8.3, 774; included in the RC3) or ESO 474-G45 ( $v_{gal}$ ,  $D_{gal}$ ,  $\rho=1863$ , 7.2, 777; not in the RC3), both of which are small, but lie in opposite directions



from Ton S180 (see Fig. 8(101)). Table 3 includes both galaxies, but the Ly $\alpha$  is listed under ESO541-G05, while an upper limit is given for ESO 474-G45. The third Ly $\alpha$  feature is at 3001 km s $^{-1}$ , but the nearest galaxy with similar velocity is ESO 474-G25 ( $v_{gal}=2850$  km s $^{-1}$ ; Fig. 8(103)), which has  $\rho=1.5$  Mpc.

Finally, there is a strong Ly $\alpha$  and Ly $\beta$  line at 5519 km s $^{-1}$ , already reported by Penton et al. (2004). The nearest galaxy with similar velocity is 2MASX J010208.03–224559.7 ( $v_{gal}$ ,  $D_{gal}$ ,  $\rho=5611$ , 16.6, 1547).

*Ton S210.* – This sightline passes through the nearby Sculptor group (LGG 4). The galaxy with the smallest impact parameter is NGC 253 (374 kpc). Formally, its velocity of 251 km s $^{-1}$  excludes it from our sample. However, there is an O VI absorption line at 288 km s $^{-1}$ , which is very unlikely to be related to the Milky Way as Ton S210 lies near the South Galactic Pole. This feature is also unlikely to be related to the Magellanic Stream, as the Stream has velocities of  $\sim 0$  km s $^{-1}$  in this part of the sky. It is also unlikely that this is a high redshift line, as there are no strong intergalactic absorption-line systems in this sightline. The most likely association is with NGC 253, or possibly with the Local Group. Unfortunately, the possible corresponding Ly $\alpha$  absorption is hidden in the Galactic Ly $\alpha$  line, and Ly $\beta$  absorption is limited to  $<20$  mÅ, which still means Ly $\alpha$  could be as strong as 100 mÅ (see Table 3).

We also give non-detections for NGC 45 ( $v_{gal}$ ,  $D_{gal}$ ,  $\rho=468$ , 6.5, 702), NGC 613 ( $v_{gal}$ ,  $D_{gal}$ ,  $\rho=1475$ , 27.4, 872) and ESO 413-G02 ( $v_{gal}$ ,  $D_{gal}$ ,  $\rho=5588$ , 17.9, 942).

*VII Zw 118.* – This is one of two targets passing through the (large) group LGG 140 (the other sightline being MS 0700.7+6338). The nearest group galaxy is UGC 3648 ( $v_{gal}$ ,  $D_{gal}$ ,  $\rho=4530$ , 25.9, 620), with UGC 3642 ( $v_{gal}$ ,  $D_{gal}$ ,  $\rho=4498$ , 28.2, 738), and UGC 3660 ( $v_{gal}$ ,  $D_{gal}$ ,  $\rho=4252$ , 31.0, 845) also within 1 Mpc. UGC 3648 was not listed as a group galaxy by Garcia (1993), but only because its velocity was not yet known at the time. A weak Ly $\alpha$  absorption at 4613 km s $^{-1}$  is seen near the group’s velocity, and it is listed as associated with UGC 3648 in Table 3 (see Fig. 8(107)).

A much stronger Ly $\alpha$  line is found at 2438 km s $^{-1}$ , which can be associated with UGC 3748 ( $v_{gal}$ ,  $D_{gal}$ ,  $\rho=2479$ , 12.2, 753; Fig. 8(106)). Ly $\beta$  is also seen in this system. We find  $70 \pm 8$  mÅ for Ly $\beta$ , while Shull et al. (2000) reported  $110 \pm 50$  mÅ. Penton et al. (2004) listed both features, but split both of them into two components. Based on just the noisy line structure there is little evidence to support this, except that single lines would have relatively large (though not extraordinary so) FWHM (148 and 109 km s $^{-1}$ ), and that the Ly $\beta$  line has an FWHM of only 63 km s $^{-1}$ . The 2438 km s $^{-1}$  Ly $\alpha$  line also may be slightly asymmetric.

A weak ( $3\sigma$ )  $\text{Ly}\alpha$  feature is also seen at  $1697 \text{ km s}^{-1}$ . The nearest galaxy with similar velocity is UGC 3685 ( $v_{gal}=1797 \text{ km s}^{-1}$ ), at 1.4 Mpc (Fig. 8(105)). However, a galaxy with unknown velocity, UGCA 133, might have  $\rho=800 \text{ kpc}$  if its velocity were about  $1700 \text{ km s}^{-1}$ .

## Appendix B

We include a table of all galaxies in our sample that have velocity less than 7000 km/s and impact parameter less than 2 Mpc to one of the 76 extragalactic sightlines. A sample is included, but the full table can be found in the on-line version of this paper. It is important to note that this table is inhomogeneous. Near some sightlines deep searches for dwarf galaxies exist, near others they don't. The table should therefore not be used for statistical analyses for faint galaxies, except for galaxies with diameter  $>7.5$  kpc.

The values in the "Note" column give extra information. Notes starting with "GH" or "LGG" indicate the galaxy is a member of a GH or LGG group; this is (followed by the distance that would have been derived if the galaxy's velocity were used directly. Other notes can be "ASSUME", when the galaxy's velocity is unknown, "ASSUME-CHECKED" when the galaxy's velocity remained unknown after we checked NED, or "MINDIST", when we assumed the minimum distance of 2.9 Mpc to estimate the impact parameter. A plain number gives the velocity distance for galaxies for which a better distance estimate was instead taken from the literature.

## REFERENCES

- Aracil B., Tripp T.M., Bowen D.V., Prochaska J.X., Chen H.-W., Frye B.L, 2006, MNRAS, 367, 139
- Bahcall J.N., Jannuzzi B.T., Schneider D.P., Hartig G.F., Bohlin R., Junkkarinen V., 1991, ApJ, 377, L5
- Bergeron J., Boissé, P., 1991, A&A, 243, 344
- Blackman C.P., 1981, MNRAS, 195, 451
- Bosma A., 1981, AJ, 86, 1791
- Bosma A., van der Hulst J.M., Athanassoula E., 1988, A&A, 198, 100
- Bowen D.V., Blades J.C., 1993, ApJ, 403, 55
- Bowen D.V., Blades J.C., Pettini M., 1996, ApJ, 464, 141
- Bowen D.V., Tripp T.M., Jenkins E.B., 2001, AJ, 121, 1456
- Bowen D.V., Pettini M., Blades J.C., 2002, ApJ, 580, 169
- Bowen D.V., Jenkins E.B., Pettini M., Tripp T.M., 2005, ApJ, 635, 880
- Broeils A.H., van Woerden H., 1994, A&AS, 107, 129
- Carignan C., Puche D., 1990, AJ, 100, 641

Table 13. Galaxy-absorber coincidences<sup>1</sup>

AGN	Galaxy	type	$l$	$b$	$v_{\text{hel}}$	$D_{\text{gal}}$	$R_{\text{gal}}$	$\alpha$	$\rho$	Note
(1)	(2)	(3)	[°]	[°]	[km s <sup>-1</sup> ]	[Mpc]	[kpc]	[°]	[kpc]	(11)
1H0419–577	LSBGF157–081	.....	267.22	-41.78	1215	15.4	3.7	0.27	72	NED
1H0419–577	IC2039	.L..0*P	266.36	-44.58	250	2.9	0.8	2.62	132	MINDIST
1H0419–577	NGC1574	.LAS–*	266.89	-42.58	925	13.6	13.4	0.59	140	LGG112
1H0419–577	HIPASSJ0423–56	.....	265.95	-42.60	1345	17.2	0.0	0.97	291	NED
1H0419–577	APMBGC157+016+068	.....	265.87	-42.67	1350	17.3	4.7	1.05	317	NED
1H0419–577	IC2038	.S..7P*	266.34	-44.60	712	8.1	4.1	2.64	373	0
1H0419–577	ESO118–G19	.....	268.72	-42.59	1239	15.7	3.7	1.40	384	NED
1H0419–577	NGC1533	.LB.–..	266.45	-44.43	790	9.2	7.4	2.46	396	0
1H0419–577	NGC1533:[RMF2004]2	.....	266.52	-44.36	831	9.8	0.0	2.38	406	NED
1H0419–577	NGC1533:[RMF2004]1	.....	266.53	-44.36	846	10.0	0.0	2.38	415	NED

Note. — 1: Column (1) gives the name of the AGN target, Col. (2) the galaxies near the AGN sightline. Column (3) is the galaxy type, taken from the RC3 (de Vaucouleurs et al. 1991). Columns (4) and (5) give the Galactic longitude and latitude of the galaxy. Column (6), (7), and (8) are the galaxy’s heliocentric velocity, estimated distance and estimated diameter (with values of 0.0 meaning the diameter is unknown). Columns (9) and (10) are the angular and line-of-sight separation between target and galaxy (in degrees and kpc). Column (11) gives a note: group membership (followed by the distance that would have been derived if the galaxy’s velocity was used directly), whether the galaxy’s velocity is unknown (note=ASSUMEV), or unknown and checked in NED (note=ASSUME-CHECKED), or whether the minimum distance (2.9 Mpc) was assumed (note=MINDIST). A plain number gives the velocity distance for galaxies for which a better distance estimate was instead taken from the literature.

- Carilli C.L., van Gorkom J.H., 1992, *ApJ*, 399, 373
- Casertano S., van Gorkom J.H., 1991, *AJ*, 101, 1231
- Cen R., Tripp T.M., Ostriker J.P., Jenkins E.B., 2001, *ApJ*, 559, L5
- Cen R., Ostriker J.P., 1999, *ApJ*, 514, 1
- Cen R., Fang T., 2006, *ApJ*, 650, 573
- Chen H.-W., Lanzetta K.M., Webb J.K., Barcons X., 2001, *ApJ*, 559, 654
- Chengalur J.N., Kanekar N., 2002, *A&A*, 388, 383
- Chiappini C., Matteucci F., Romano D., 2001, *ApJ*, 554, 1044
- Churchill C.W., Kacprzak G.G., Steidel C.C., Evans J.L., 2007, *ApJ*, 661, 714
- Côté S., Wyse R.F.G., Carignan C., Freeman K.C., Broadhurst T., 2005, *ApJ*, 618, 178
- Danforth C.W., Shull J.M., 2005, *ApJ*, 624, 555
- Danforth C.W., Shull J.M., Rosenberg J.L., Stocke J.T., 2006, *ApJ*, 640, 716
- Danforth C.W., Shull J.M., 2008, *ApJ*, 679, 643
- Davé R., Cen R., Ostriker J.P., Bryan G.L., Hernquist L., Katz N., Weinberg D., Norman M.L., O’Shea B., 2001, *ApJ* 552, 473
- de Vaucouleurs G., de Vaucouleurs A., Corwin H.G., Buta R.J., Paturel G., Fouque, P., 1991, *Third Reference Catalogue of Bright Galaxies*, Springer Verlag, Berlin, Heidelberg, New York.
- Fang T., Bryan G.L., 2001, *ApJ*, 561, L31
- Ferland G.J., Korista K.T., Verner D.A., Ferguson J.W., Kingdon J.B., Verner E.M., 1998, *PASP*, 110, 761
- Fox A.J., Savage B.D., Wakker B.P., Richter P., Sembach K.R., Tripp T.M., 2004, *ApJ*, 602, 738
- Fox A.J., Wakker B.P., Savage B.D., Tripp T.M., Sembach K.R., Bland-Hawthorn J., 2005, *ApJ*, 630, 332
- Freedman W., Madore B.F., Gibson B.K., Ferrarese L., Kelson D.D., et al., 2001, *ApJ* 553, 47
- Fridman A.M., Afanasiev V.L., Dodonov S.N., Koruzhii O.V., Moiseev A.V., Sil’chenko O.K., Zasov A.V., 2005, *A&A*, 430, 67
- Fukugita M., Peebles P.J.E., 2004, *ApJ*, 616, 643
- Fukugita M., Peebles P.J.E., 2006, *ApJ*, 639, 590

- Furlanetto S.R., Philips L.A., Kamionkowski M., 2005, MNRAS, 359, 295
- Ganguly R., Cen R., Fang T., Sembach K.R., 2008, ApJ, 678, 89
- Garcia A.M., 1993, A&AS, 100, 47
- García-Ruiz I., Sancisi R., Kuijken K., 2002, A&A, 394, 769
- Garrido O., Marcelin M., Amram P., Balkowski C., Gach J.L., Boulesteix J., 2005, MNRAS, 362, 127
- Geller M.J., Huchra J.P., 1982, ApJ, 257, 423
- Geller M.J., Huchra J.P., 1983, ApJS, 52, 61
- Gopal-Krishna, Irwin J.A., 2000, A&A, 361, 888
- Impey C.D., Petry C.E., Flint K.P., 1999, ApJ 524, 536
- Jannuzi B.T., Bahcall J.N., Bergeron J., Boksenberg A., Hartig G.F., et al., 1998, ApJS, 118, 1
- Janknecht E., Reimers D., Lopez S., Tytler D., 2006, A&A, 458, 427
- Jarvis B.J., Dubath P., Martinet L., Bacon R., 1988, A&AS, 74, 513
- Jenkins E.B., Bowen D.V., Tripp T.M., Sembach K.R., Leighly K.M., Halpern J.P., Lauroesch J.T., 2003, AJ, 125, 2824
- Jenkins E.B., Bowen D.V., Tripp T.M., Sembach K.R., 2005, ApJ, 623, 767
- Kaasra J.S., Werner N., den Herder J.W.A., Paerels F.B.S., de Plaa J., Rasmussen A.P., de Vries C.P., 2006, ApJ, 652, 189
- Kacprzak G.G., Churchill C.W., Steidel C.C., Murphy M.T., 2008, ApJ, 135, 922
- Keeney B.A., Momjian E., Stocke J.T., Carilli C.L., Tumlinson J., 2005, ApJ, 622, 267
- Kim T.-S., Cristiani S., D’Odorico S., 2001, A&A, 373, 757
- Kim T.-S., Carswell R.F., Cristiani S., D’Odorico S., Giallongo E., 2002, MNRAS, 335, 555
- Kobulnicky H.A., Gebhardt, 2000, AJ, 119, 1608
- Krum N., Salpeter E.E., 1979, AJ, 84, 1138
- Lanzetta K.M., Bowen D.V., Tytler D., Webb J.K., 1995, ApJ, 442, 538
- Lehner N., Savage B.D., Wakker B.P., Sembach K.R., Tripp T.M., 2006, ApJS 164, 1
- Lehner N., Savage B.D., Richter P., Sembach K.R., Tripp T.M., Wakker B.P., 2007, ApJ, 658, 680
- Márquez I., Masegosa J., Moles M., Varela J., Bettoni D., Galletta G., 2002, A&A, 393, 389

- Marzke R.O., Huchra J.P., Geller M.J., 1994, *ApJ*, 428, 43
- Mathewson D.S., Ford V.K., Buchhorn M., 1992, *ApJS*, 81, 413
- Mateo M., 1998, *ARA&A*, 36, 435
- McLin K., Stocke J.T., Weymann R.J., Penton S.V., Shull J.M., 2002, *ApJ* 574, L115
- Morris S.L., Weymann R.J. Savage B.D., Gilliland R.L., 1991, *ApJ*, 377, L21
- Morris S.L., Weymann R.J., Dressler A., McCarthy P.J., Smith B.A., Terrile R.J., Giovanelli R., Irwin M., 1993, *ApJ* 419, 524
- Narayanan A., Wakker B.P., Savage B.D., 2008, *ApJ*, submitted
- Nicastro F., Mathur S., Elvis M., Drake J., Fiore F., et al., 2005, *ApJ*, 629, 700
- Noordermeer E., van der Hulst J.M., Sancisi R., Swaters R.A., van Albada T.S., 2005, *A&A*, 442, 137
- Oort J.H., 1970, *A&A* 7, 381
- Oosterloo T., Shostak S., 1993, *A&AS*, 99, 379
- Oppenheimer B.D., Davé R., 2008, *arXiv*, 0806-2866
- Pedersen K., Rasmussen J., Sommer-Larsen J., Toft S., Benson A.J., Bower R.G., 2006, *New Astronomy* 11, 465
- Penton S.V., Stocke J.T., Shull J.M., 2000a, *ApJS*, 130, 121
- Penton S.V., Stocke J.T., Shull J.M., 2000b, *ApJ*, 544, 150
- Penton S.V., Stocke J.T., Shull J.M., 2002, *ApJ*, 565, 720
- Penton S.V., Stocke J.T., Shull J.M., 2004, *ApJS*, 152, 29
- Pisano D.J., Wakker B.P., Wilcots E.M., Fabian D., 2004, *ApJ*, 127, 199
- Prochaska J.X., Chen H.-W., Howk J.C., Weiner B.J., Mulchaey J.S., 2004, *ApJ* 617, 718
- Prochaska J.X., Weiner B.J., Chen H.-W., Mulchaey J.S., 2006, *ApJ* 643, 680
- Puche D., Carignan C., van Gorkom J.H., 1991, *AJ*, 101, 456
- Putman M.E., Rosenberg J.L., Stocke J.T., McEntaffer R., 2006, *ApJ*, 131, 771
- Rasmussen A.P., Kahn S.M., Paerels F., den Herder J.W., Kaastra J., de Vries C., 2007, *ApJ*, 656, 129
- Rhee M.-H., van Albada T.S., 1996, *A&AS*, 115, 407
- Richter, P, Savage B.D., Tripp T.M., Sembach K.R., 2004, *ApJS* 153, 165
- Rosenberg J.L., Ganguly R., Giroux M., Stocke J.T., 2003, *ApJ* 591, 677

- Rosenberg J.L., Bowen D.V., Tripp T.M., Brinks E., 2006, *AJ*, 132, 478
- Sandage A., Tammann G., 1975, *ApJ*, 196, 313
- Sancisi R., 1976, *A&A*, 53, 159
- Sancisi R., Fraternali F., Oosterloo T., van der Hulst Th., 2008, *A&A Rev*, 15, 189
- Savage B.D., Tripp T.M., Lu L., 1998, *AJ*, 115, 436
- Savage B.D., Sembach K.R., Tripp T.M., Richter P., 2002, *ApJ*, 564, 631
- Savage B.D., Wakker B.P., Fox A.J., Sembach K.R., 2005a, *ApJ*, 619, 863
- Savage B.D., Lehner N., Wakker B.P., Sembach K.R., Tripp T.M., 2005b, *ApJ*, 626, 776
- Schaye J., 2001, *ApJ*, 559, 507
- Schneider S.E., Thuan T.X., Mangum J.G., Miller J., 1992, *ApJS*, 81, 5
- Sembach K.R., Savage B.D., 1992, *ApJS*, 83, 147
- Sembach K.R., Howk J.C., Savage B.D., Shull J.M., Oegerle W.R., 2001, *ApJ*, 561, 573
- Sembach K.R., Wakker B.P., Savage B.D., Richter P., Meade M., et al., 2003, *ApJS*, 146, 165
- Sembach K.R., Tripp T.M., Savage B.D., Richter P., 2004, *ApJS*, 155, 351
- Shull J.M., Stocke J.T., Penton S., 1996, *AJ*, 111, 728
- Shull J.M., Giroux M., et al. 2000, *ApJ*, 538, L13
- Sommer-Larsen J., 2006, *ApJ* 644, L1
- Steidel C.C., 1995, in “QSO Absorption Lines”, ed. G. Meylan (Berlin: Springer), 139
- Stil J.M., Israel F.P., 2002, *A&A*, 389, 42
- Stocke J.T., Shull J.M., Penton S., Donahue M., Carilli C., 1995, *ApJ*, 451, 24
- Stocke J.T., Penton S.V., Danforth C.W., Shull J.M., Tumlinson J., McLin K.M., 2006, *ApJ*, 641, 217
- Thom C., Chen H.-W., 2008, arXiv, 0801.2380
- Tripp T.M., Lu L., Savage B.D., 1998, *ApJ*, 508, 200
- Tripp T.M., Savage B.D., 2000, *ApJ*, 542, 42
- Tripp T.M., Savage B.D., Jenkins E.B., 2000, *ApJ*, 534, L1
- Tripp T.M., Giroux M.L., Stocke J.T., Tumlinson J., Oegerle W.R., 2001, *ApJ*, 563, 724
- Tripp T.M., Jenkins E.B., Williger G.M., Heap S.R., Bowers C.W., Danks A.C., et al., 2002, *ApJ*, 575, 697



- Tripp T.M., Jenkins E.B., Bowen D.V., Prochaska J.X., Aracil B., Ganguly R., 2005, *ApJ*, 619, 714
- Tripp T.M., Sembach K.R., Bowen D.V., Savage B.D., Jenkins E.B., Lehner N., Richter P., 2008, *ApJS*, 177, 39
- Tully R.B., Shaya E.J., Karachentsev I.D., Courtois H., Kocevski D.D., Rizzi L., Peel A., 2008, *ApJ*, 676, 184
- Tumlinson J., Giroux M.L., Shull J.M., Stocke J.T., 1999, *AJ*, 118, 2148
- Tumlinson J., Shull J.M., Giroux M.L., Stocke J.T., 2005, *ApJ*, 620, 95
- van Gorkom J.H., Carili C.L., Stocke J.T., Perlman E.S., Shull J.M., 1996, *AJ*, 112, 1397
- Wakker B.P., 2001, *ApJS*, 136, 463
- Wakker B.P., Savage B.D., Sembach K.R., Richter P., Meade M., et al., 2003, *ApJS* 146, 1
- Wakker B.P., 2006, *ApJS*, 163, 282
- Wakker B.P., York D.G., Howk J.C., Barentine J.C., Wilhelm R., Peletier R.F., van Woerden H., Beers T.C., Ivezić Ž, Richter P., Schwarz U.J., 2007, *ApJL*, 670, L113
- Wakker B.P., York D.G., Wilhelm R., Barentine J.C., Richter P., Beers T.C., Ivezić Ž, Howk J.C., 2008, *ApJ*, 672, 298
- Weymann R.J., Jannuzzi B.T., Lu L., Bahcall J.N., Bergeron J., et al., 1998, *ApJ*, 506, 1
- Whiteoak J.B., Gardner F.F., 1977, *Aust. J. Phys.*, 30, 187
- Williger G.M., Heap S.R., Davé R., Ellingson E., Carswell R.F., Tripp T.M., Jenkins E.B., 2006, *ApJ*, 636, 631
- Wilman R.J., Morris S.L., Jannuzi B.T., Davé R., Shone A.M., 2007, *MNRAS*, 375, 735
- Yao Y., Nowak M.A., Wang Q.D., Schulz N.S., Canizares C.R., 2008, *ApJ* 672, L21
- Yuan Q., Green R.F., Brotherton M., Tripp T.M., Kaiser M.E., Kriss G.A., 2002, *ApJ*, 575, 687